Allelic Variation and Multigenic Metabolic Activity of Cytochrome P450s Confer Insecticide Resistance in Field Populations of *Anopheles funestus s.s.*, a Major Malaria Vector in Africa

Thesis submitted in accordance with the requirements of the University of Liverpool for the degree of Doctor in Philosophy

by

Sulaiman Sadi Ibrahim

January 2015

DECLARATION

This work has not previously been accepted in substance for any degree and is not being currently submitted in candidature for any degree.

Signed .....(Candidate)

Date .....

Statement 1

This thesis is the result of my own investigation, except where otherwise stated. Other sources are acknowledged and bibliography appended.

Signed .....(Candidate)

Date .....

Statement 2

I hereby give my consent for this thesis, if accepted, to be available for photocopying and for inter-library loan, and for the title and summary to be made available to outside organisations.

Signed .....(Candidate)

Date .....

DEDICATION

This work is for all the individuals (teachers, parents, loved ones and friends) that have been there for me when I needed them most, and encourage me most when in doubt on the vicissitudes of life.

ABSTRACT

Malaria control relies heavily on the use of insecticides, especially the pyrethroids, for control interventions such as Long Lasting Insecticide Nets (LLINs) and Indoor Residual Spraying (ITNs). However, widespread resistance to insecticides in major malaria vectors, such as *An. funestus* is threatening to derail these control tools. To design and implement suitable resistance management strategies which will ensure the continued effectiveness of these control tools it is necessary to elucidate the molecular basis of the resistance. In *An. funestus,* resistance is mainly metabolic with the duplicated P450s *CYP6P9a* and *CYP6P9b* implicated as the major pyrethroid resistance genes. Despite the detection of these key resistance genes the detailed molecular mechanisms through which they confer pyrethroid resistance remain uncharacterised. Because *CYP6P9a* and *CYP6P9b* were shown to exhibit significant allelic variation between resistant and susceptible mosquitoes, we hypothesised that this allelic variation is potentially a key mechanism conferring pyrethroid resistance. Here, I characterised the role of these genes in the resistance to pyrethroids and identified other candidate genes which confer cross-resistance to non-pyrethroid insecticides. The role of allelic variation in pyrethroid resistance was investigated using polymorphism survery and *in silico* prediction of activity. Metabolic activities and efficiencies of allelic variants of *CYP6P9a* and *CYP6P9b* were investigated using fluorescent probes, metabolism assays and transgenic expression in *D. melanogaster* system. Pyrethroid resistance causative mutations were detected using the site-directed mutagenesis. Other candidate P450s that confer cross-resistance to pyrethroids carbamates and organochlorines were identified and characterised.

This study revealed that *CYP6P9a* and *CYP6P9b* from resistant populations of *An. funestus* are undergoing directional selection with reduced genetic diversity and beneficial mutations selected, compared to the alleles from susceptible strain (FANG), which exhibited high genetic variation. Modelling and docking simulations predicted the alleles of *CYP6P9a* and *CYP6P9b* from the resistant strains all across Africa to metabolise pyrethroids with high efficiency while the susceptible alleles *FANGCYP6P9a* and *FANGCYP6P9b* were predicted to have low activity toward pyrethroids. Validation of the docking predictions with probes and metabolism assays established that the resistant alleles of *CYP6P9a* and *CYP6P9b* possess high activities toward pyrethroids with kinetic profiles significantly different (high affinity and catalytic efficiency) from those obtained from the FANG, indicating that allelic variation is playing a major role in pyrethroid resistance. These findings were further strengthened by results from transgenic expression with GAL4/UAS technology showing that flies expressing the resistant alleles of both genes were significantly more resistant to pyrethroids than those expressing the susceptible alleles.

Using mutagenesis, three key residues (Val^{109}, Asp^{335} and Asn^{384}) from the resistant allele of *CYP6P9b* were established as the important amino acid changes responsible for resistance with impact on substrate channelling, possible enhancement of interaction with redox partners and inter-molecular hydrogen bonding interactions, respectively conferring high metabolic efficiency. The finding of these resistance markers make it possible to design a diagnostic tool that can allow detection and tracking of the resistant alleles in the field population of *An. funestus* across Africa.

Other up-regulated P450s in multiple resistant populations from southern Africa were also characterised, revealing that pyrethroid resistance is mediated by other P450s as well: *CYP6M7*, *CYP6Z1*, *CYP9J11* and *CYP6AA4* all of which metabolise pyrethroids. *CYP6Z1* and *CYP9J11* are cross-resistance genes which metabolise bendiocarb, while *CYP6Z1* metabolise DDT in addition.

In conclusion, allelic variation is a key mechanism conferring pyrethroid resistance in *An. funestus s.s.* from sub-Saharan Africa. Key amino acid changes control pyrethroid resistance factors and these molecular markers can be used to design DNA-based diagnostic tests which will allow tracking of the resistance alleles in the field. Pyrethroid resistance is multi-genic in the field populations of *An. funestus* with other P450s involved apart from *CYP6P9a* and *CYP6P9b*. The finding of cross-resistance P450s is of concern to resistance management and should be taken into account when designing resistance management strategies.

ACKNOWLEDGEMENTS

The list is endless, especially since the three years spent created more questions in my mind than answers. However, I must acknowledge the risky investment my Supervisor (Dr. Charles Wondji) and Prof. Hilary Ranson made in choosing me out of the potential applicants back in 2011 and the rarest chances for training offered by my secondary Supervisor (Dr. Mark Paine). I have learnt a lot more than I could possibly comprehend and hope that I have managed to connect few dots, in here. Charles has always been a source of inspiration, encouragement and opportunities, while Mark provides me with excellent openings to learn new techniques, all the time whipping my mind to reflect deeply on ramifications of things I ignorantly claimed or deliberately avoided.

In the beginning there was Jacob (Dr Riveron J.M.) and at the end there stood Jacob, guiding, explaining in Spang-lish even if frustrated, arguing and making sure things are *'all-or-none'* perfect. Thanks a lot Jacob, for your time and patience.

My deepest gratitude goes to Bibby Jaclyn who helped me with the modelling and molecular docking component of this research even at the eleventh hour and Michael Voice (along with the other staff of the Cypex BioDundee who helped me with some part of the P450 characterisation experiment), as well as my advisory panel supervisors (Dr. Alvaro Acosta-Serrano and Dr. Gareth Lycett).

Other individuals who have helped me one way or another on this journey and on the course of this research include Drs. Abdulsalami Yayo Manu, Hanafy M. Ismail, Eva Maria Hodel, Cristina Yunta Yanes, Rodolphe Poupardin, Clare Strode, Craig Wilding, Lee Haines, Lisa Stone, Ms Helen Irving, Mr. Michael Kusimo, Ms Kayla G. Barnes and the rest of staff members and students from the Vector Biology Department. I am grateful for your patience and help.

Finally, thanks to the management of Bayero University Kano, Nigeria, especially Prof. Hafiz Abubakar for making this possible.

TABLE OF CONTENTS

LIST OF TABLES

LIST OF FIGURES

LIST OF APPENDICES

LIST OF ABBREVIATIONS

ace-1 *acetylcholinesterase 1*

An. *Anopheles*

AChE *Acetylcholinesterase*

Ae. *Aedes*

BAC Bacterial artificial chromosome

BLAST Basic local alignment search tool

Bti *Bacillus thuringiensis*

cDNA complementary DNA

Chr *Chrysanthemum*

CYPED *Cytochrome P450 Engineering Database*

Cx. *Culex*

DDE 1,1,1-dichloro-2,2-bis(4-chlorophenyl)ethane

DDT 1,1,1-Trichloro-2,2-bis(4-chlorophenyl)ethane

dH_20 Distilled water

DNA Deoxyribonucleic acid

DNase Deoxyribonuclease

dNTP Deoxyribonucleoside triphosphate

DTT Dithiothreitol

FAD Flavin adenine dinucleotide

FANG *An. funestus* from Angola

FMN Flavin mononucleotide

FUMOZ-R *An. funestus* from Mozambique-Resistant

GABA	Gamma-aminobutyric acid
gDNA	genomic DNA
GSH	Glutathione
HMG-CoA	3-hydroxy-3-methylglutaryl-coenzyme A
IPTG	Isopropyl β-D-1-thiogalactopyranoside
ITNs	Insecticide treated nets
KPi	Potassium phosphate
LB	Lysogeny broth
LLINs	Long lasting insecticide treated nets
$MgCl_2$	Magnesium chloride
mRNA	Messenger RNA
MS	Mass spectrometry
nAChR	Nicotinic acetylcholine receptor
NAD	Nicotinamide adenine dinucleotide
NADP	Nicotinamide adenine dinucleotide phosphate
NCBI	National centre for biotechnology information
NMR	Nuclear magnetic resonance
PCR	Polymerase chain reaction
P.	*Plasmodium*
PMSF	phenylmethanesulfonylfluoride
qPCR	Quantitative polymerase chain reaction
qRT-PCR	Quantitative reverse transcriptase polymerase chain reaction
r.m.s.d.	root mean square deviation

Rdl	Resistance to dieldrin
RIS	Reductase interacting site
RNA	Ribonucleic acid
RNase	Ribonuclease
RPL11	*Ribosomal protein L11*
RTS,S	Repeat region for T-cell epitope surface antigen of free S protein
S.	*Sacchromyces*
s.l.	*sensu laso*
S.O.C.	Super optimal broth with catabolite repression
s.s.	*sensu stricto*
*sf*9	*Spodoptera frugiperda* 9 cells
SRS	Substrate recognition site
T.	*Tribolium*
TB	Terrific broth
TLC	Thin layer chromatography
Tm	Melting temperature
TSE	Tris-Sucrose –EDTA
vdW	van der Waals
VGSC	Voltage-gated sodium channel
δ-ALA	Lamdaaminolevulinic acid

1. LITERATURE REVIEW

1.1 Background

Despite the recent decrease in global rates of mortality (42%) due to malaria (WHO, 2013b), the disease steals 627,000 lives in 2012 alone, mostly children under the age of 5. Malaria is caused by infection with protozoan parasites belonging to the genus *Plasmodium,* which are transmitted by female *Anopheles* mosquitoes (Cox, 2010). The major mosquito vectors in sub-Saharan Africa are *An. gambiae*, *An. arabiensis* and *An. funestus* (Ranson et al., 2011). Impediments to malaria control and eradication include the absence of a licensed vaccine (Mwangoka et al., 2013), development of and spread of parasite resistance to anti-malarial drugs (Packard, 2014) and the mosquito resistance to insecticides used in public health as reviewed (Corbel and N'Guessan, 2013). Control of malarial vectors relies heavily on the use of insecticide formulations alone or in combination, for wide-coverage as in conventional Insecticide Treated Nets (ITNs) (WHO, 2013b), Long-Lasting Insecticide Treated Nets (LLINs) and indoor residual spraying (IRS) (Hemingway, 2014). Unfortunately, widespread emergence and increasing resistance to insecticides especially pyrethroids- the only class fully approved by WHO for LLINs and ITNs (WHO, 2013a), in one of the major malaria vector *An. funestus* (Riveron et al., 2014a, Mulamba et al., 2014b, Coetzee and Koekemoer, 2013) is threatening the success of these intervention tools (WHO, 2012). Within the Funestus complex, *An. funestus s.s.* is the most widely, geographically distributed across African continent (Dia et al., 2013) and the specie with high vectorial capacity conferred by its unusually high anthropophilic and endophilic behaviour (Coetzee and Fontenille, 2004, Gilles and De Meillon, 1968). To date *An. funestus* populations from different regions of Africa have been established to be resistant to three of the four major classes of insecticides: pyrethroids, carbamates and organochlorines widely utilized for control of malaria vectors (Brown, 1986, Coetzee and Koekemoer, 2013, Dia et al., 2013, Ranson et al., 2011, Wondji et al., 2012, Corbel and N'Guessan, 2013). With the knockdown resistance (*kdr*) type mutation in the

voltage-gated sodium channel not yet selected in *An. funestus s.l.,* (Hemingway, 2014, Djouaka et al., 2011, Morgan et al., 2010, Wondji et al., 2007b) pyrethroid resistance is mainly metabolic and mediated fully or partially by P450 monooxygenases (Coetzee and Koekemoer, 2013, Wondji et al., 2012, Okoye et al., 2008, Corbel and N'Guessan, 2013). In *An. funestus* resistance to insecticides is heterogeneous across Africa, with populations from different regions showing overlapping or contrasting resistance patterns (Djouaka et al., 2011, Morgan et al., 2010, Cuamba et al., 2010, Wondji et al., 2012). The duplicated *CYP450s CYP6P9a* and *CYP6P9b* and other candidate genes detected through genome-wide microarray and transcriptomic analysis have been implicated as the major pyrethroid resistance genes in *An. funestus* across Africa (Amenya et al., 2008, Riveron et al., 2013, Wondji et al., 2009, Wondji et al., 2012, Gregory et al., 2011). But, despite the remarkable progress so far made in detection of such candidate resistance genes in *An. funestus* and their functional characterisation in some cases (Riveron et al., 2013, Riveron et al., 2014b), the exact mechanisms of pyrethroid resistance still remains unknown, factors responsible for multiple resistance to different insecticide classes are yet to be elucidated and molecular markers are lacking to track resistance in the field. Therefore this study was carried out to attempt to fill these gaps. Here, I dissected and assessed the impact of allelic variation in two major pyrethroid resistance genes *CYP6P9a* and *CYP6P9b*, identified molecular markers of pyrethroid resistance and discovered cross-resistance genes.

1.2 Malaria Vectors

Malarial parasite is transmitted by mosquitoes from the *Anopheles* genus which comprises nearly 500 species of which around 70 have been established as vectors (http://seeg.zoo.ox.ac.uk /themes/vectors). The continent of Africa bears the brunt of malaria burden because it has the most effective and efficient dominant vector specie (DVS) of human malaria (Gillies, 1987, Sinka et al., 2010) *An. gambiae s.s.* (Guerra et al., 2008) with its sibling *An. arabiensis*, also of major importance (Gillies, 1987). The DVS members of the *An. gambiae* complex also include in addition the salt water tolerant, coastal species *An. melas* and *An. merus* (Harbach, 2004). Other members of the *An. gambiae* complex

are either highly restricted in their distribution (e.g. *An. bwambae*, known to occur only in some geothermal springs in western Uganda (White, 1985) or are zoophilic in behaviour and not considered vectors of human malaria (e.g. *An. quadriannulatus A* and *An. quadriannulatus B*) (Sinka et al., 2010). Recently, two species were added to the *An. gambiae* complex based on molecular and bionomic evidences: the *An. gambiae* molecular "M form" is now named *An. coluzzii* Coetzee & Wilkerson sp. n., while the "S form" retains the nominotypical name *An. gambiae* Giles (Coetzee et al., 2013). *An. quadriannulatus* is retained for the southern African populations of this species, while the Ethiopian species is named *An. amharicus* Hunt, Wilkerson & Coetzee sp. n., based on chromosomal, cross-mating and molecular evidences. Beside the *An. gambiae* s.*l.* complex, *An. funestus* s.s. also play a major role in malaria transmission and in some parts of the continent has a greater impact on malaria transmission than *An. gambiae* (Coetzee and Fontenille, 2004). Indeed *An. funestus* is considered to be one of the first species to have adapted to human hosts (Charlwood et al., 1995).

1.2.1 Anopheles funestus

An. funestus is one of the major African vectors of malaria. Its distributed across sub-Saharan Africa wherever suitable swampy breeding habitats are available (Coetzee and Koekemoer, 2013). *An. funestus* belongs to a group of thirteen species (Dia et al., 2013) that are morphologically very similar in the adult stage (Coetzee and Fontenille, 2004). Four species, *An. funestus*, *An. vaneedeni*, *An. parensis* and *An. aruni*, possess identical morphology at all life stages and (Gillies, 1987, Gilles and De Meillon, 1968) and together with *An. funestus*-like, *An. confusus* and *An. longipalpis* type C are known as the Funestus sub-group (Dia et al., 2013). The second subgroup is designated Minimus subgroup and is composed of *An. leesoni* and *An. longipalpis* type A. The third is the Rivulorum subgroup which comprise *An. rivulorum*, *An. rivulorum*-like, *An. brucei* and *An. fuscivenosus*. *An. leesoni* is the most distinct at both egg and larval stage, while *An. confusus* is easily identified on larval characteristics. *An. rivulorum* and *An. brucei* also have distinctive larvae although these two species are virtually indistinguishable from each other (Coetzee and Fontenille, 2004). Apart from *An. funestus*, which is

highly anthropophilic, the rest of the group are mainly zoophilic (Coetzee and Fontenille, 2004). Nevertheless, *An. rivulorum* has been implicated as a minor vector in a locality in Tanzania (Wilkes et al., 1996). The *An. Funestus* complex is tabulated below (Table 1.1).

Table 1.1 African *An. funestus* complex. Adapted from (Dia et al., 2013).

African species of the Funestus Group				
Subgroup	**Species**	**Geographical distribution**	**Host preference**	**Vector role**
Funestus	*An. funestus*	continental	anthropophilic	major
	An. funestus-like	local	unknown	unknown
	An. aruni	local	unknown	unknown
	An. confusus	regional	zoophilic	unknown
	An. parensis	regional	unknown	minor
	An. vaneedeni	local	unknown	unknown
	An. longipalpis type C	local	zoophilic	unknown
Minimus	*An. leesoni*	continental	zoophilic	minor
	An. longipalpis type A	local	zoophilic	unknown
Rivulorum	*An. rivulorum*	continental	zoophilic	minor
	An. rivulorum-like	local	unknown	unknown
	An. brucei	local	unknown	unknown
	An. fuscivenosus	local	unknown	unknown

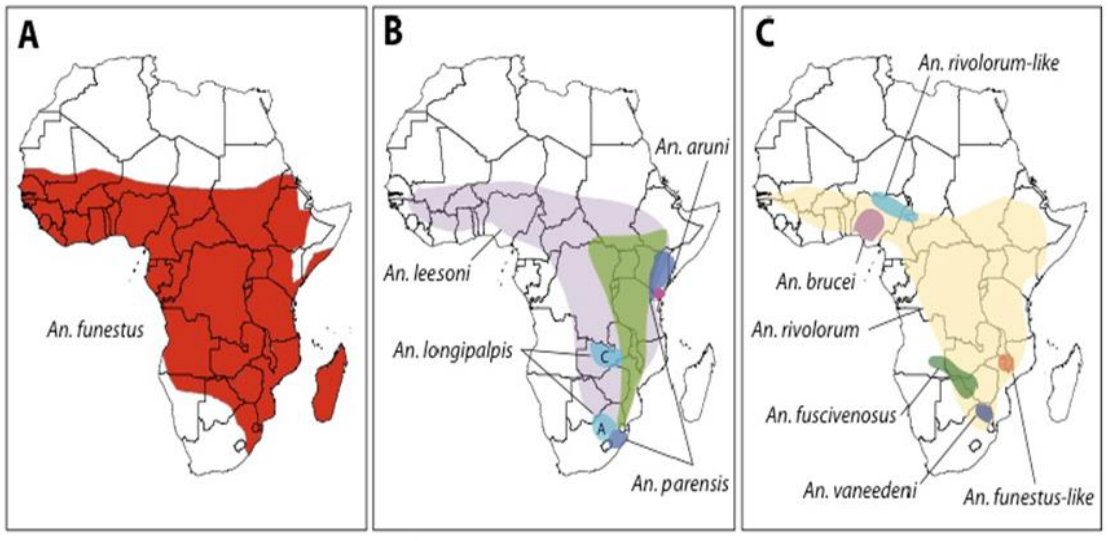

Figure 1. Distribution of the 13 species of the Funestus Group in Africa, A: *Anopheles funestus*, (modified from [37]); B: *An. leesoni*, *An. longipalpis* (type A and C), *An. aruni* and *An. parensis* (Courtesy of Dr. S. Manguin), C: *An. rivolorum*, *An. rivolorum-like*, *An. funestus-like*, *An. vaneedeni*, *An. fuscivenosus* and *An. brucei* (Courtesy of Dr. S. Manguin).

Figure 1.1: Distribution of species of Funestus complex. Adapted from (Dia et al., 2013).

An. funestus, *An. leesoni* and *An. rivulorum* exhibit the widest geographical distribution (Dia et al., 2013). They are traditionally represented throughout the entire sub-Saharan Africa (Gilles and De Meillon, 1968, Gillies, 1987). *An. funestus* is present everywhere across African continent (Figure 1.1), while the other species exhibit local distribution across the continent (Dia et al., 2013).

Whereas *An. gambiae* typically breeds in small temporary rain-dependent pools and puddles, *An. funestus* exploits large permanent or semi-permanent bodies of water containing emergent vegetation (Serazin et al., 2009). *An. funestus* reaches maximal abundance in the dry season after densities of *An. gambiae* and *An. arabiensis* have declined, thereby extending the period of malaria transmission (Gilles and De Meillon, 1968). *An. funestus* is the major vector responsible for malaria transmission in many places and has been implicated for malaria epidemics in some places (Fontenille et al., 1990, Hargreaves et al., 2003).

Despite its obvious importance as a vector, *An. funestus* has been neglected for almost half a century, with most of the research focusing on members of the *An. gambiae* complex (Coetzee and Fontenille, 2004). This neglect has been attributed to the difficulty of colonizing *An. funestus* in the laboratory setting and adaptability of the *An. gambiae* complex to laboratory conditions and the ease with which species in the group can be colonized.

1.3 Malaria Control

Malaria control has been described as too complex to be addressed by a single approach and as such attempt to describe it is fraught with danger (Shiff, 2002). An integrated approach to control using vector control strategies based on the biology of the mosquito, the epidemiology of the parasite, and human behaviour patterns is needed to prevent continued upsurge in malaria in the endemic areas (Mouchet and Carnevale, 1998). For theoretical purpose, malaria control can be considered from three major approaches: (i) treatment of infection caused by *Plasmodium*, (ii) control of the vector (mosquito) that spreads the malarial parasite, and (iii) antimalarial vaccines.

1.3.1 Treatment of Infection: Chemotherapy and Chemoprophylaxis

Malaria chemotherapy has relied largely on a comparatively small number of chemically related drugs belonging to four classes of compounds: 4-aminoquinolines (chloroquine, quinine, mefloquine, amodiaquine and halofantrine) or 8-aminoquinolines (primaquine), the antifolate compounds (pyrimethamine, proguanil, chlorcycloguanil, dapsone, and sulfadoxine), the artemisinin and derivatives (artemisinin, artesunate, artemether, arteether, dihydroartemisinin), and most recently, the hydroxynapthoquinone atovaquone (Schlitzer, 2008). Unfortunately, resistance to antimalarials usually develops within a few years (Ashley et al., 2014, White, 2014, Alker et al., 2008, Foote et al., 1990). Malaria chemoprophylaxis is the use of anti-malarial medication to prevent the occurrence of the symptoms of malaria (Schlagenhauf, 2010) especially in travellers (emigrants) from malaria-free regions journeying to endemic areas.

1.3.2 Malaria Vaccines

This is the idea of using vaccine against the malarial parasite *Plasmodium*. Presently, there are 38 *P. falciparum* and two *P. vivax* candidate malaria vaccines or vaccine components in preclinical or clinical progress (Karunamoorthi, 2014). But, the vaccine Repeat region for T-cell epitope surface antigen of free S protein (RTS,S) which targets the circumsporozoite stage of malarial parasite (Targett et al., 2013) has been described as the most promising. The RTS,S vaccine has already reached the Phase III clinical trials and its hoped that it could get licensed soon (Rts et al., 2012). However, the vaccine has been shown to reduce episodes of malaria by only 50%. Other challenges that need to be overcome is polymorphism in many key parasite antigens (Greenwood and Targett, 2011). It is likely vaccines that are effective enough to block transmission, will need to contain antigens from different stages of the parasite's life cycle.

1.3.3 Vector control

Various approaches are used to control vectors. This range from physical, environmental, biological and chemical measures, applied independently or in combination, to deter, reduce the number or eliminate mosquito vectors. Recent advances has also made it possible to apply a wide range of biotechnological techniques for these purposes.

1.3.3.1 Physical Methods

The physical approaches include drainage of stagnant water, frequent clearing of puddles, screening of windows and other apertures, and use of untreated bed nets. Larval source management (LSM) is one of the most important approaches to reducing malaria transmission which is largely forgotten (Fillinger and Lindsay, 2011); in the early twentieth century larviciding and environmental management were the only tools available to contain malaria. Screening of windows and other apertures can be very effective in keeping out mosquitoes, provided the screening is well fitted and without tears (Curtis, 1989). Bednets even untreated are also important and in some places have been associated with reduced prevalence (51%) of *P. falciparum* infection (Clarke et al., 2001b) Houses are the main places for contact between humans and night biting mosquitos (Gamage-Mendis et al., 1991). The impact of improved housing on reduction of indoor malaria vector densities and transmission is well established in several studies (Lwetoijera et al., 2013).

1.3.3.2 Biological Methods

Biological control methods refer to the use of natural enemies such as predatory fish, invertebrate predators and toxins produced by microbial agents such as *Bti* (Imbahale et al., 2011). *B. thuringiensis var. israelensis*, serotype H_{14} (*Bti*) has become the most commonly used microbial insecticide (biopesticide) to control pest and vector species (Rowe et al., 2003). *Bti* is non-toxic to humans, mammals, birds, fish, plants and most aquatic organisms and has been established to be a potent growth deterrant of the field population of *Cx. pipiens* (Altalhi, 2005). The active ingredient in

the Bt is the Cry protein which is activated in the gut of the mosquito larvae by proteolysis and binds to the receptors on the brush border membranes of epithelial cells, forming pores and disrupting movements of solutes (Sanahuja et al., 2011). This eventually leads to cell swelling and lysis.

The annual killifish (*Aphanius dispar dispar*) has also been demonstrated as a means of eradicating the aquatic stages of mosquitoes in transient pools (Matias and Adrias, 2010), because they can maintain permanent populations in such habitats by undergoing suspended animation or diapause during the embryonic stages, to survive periodic drought. Matias and colleagues have described the potential of annual killifish, *Nothorbronchius. guentheri*, for mosquito control because of its preference for mosquito larvae as prey, the successful demonstration of introducing the fish in the ponds in the form of diapausing eggs and the eradication of mosquito larval population in the ponds.

Another biological approach is introduction of Wolbachia symbionts into mosquito populations. For example, introduction of wMel strain of *Wolbachia* into field populations of *Ae. aegypti* resulted in a decreased dengue virus transmission (Hoffmann et al., 2011) with invasion almost reaching fixation in a few months following releases of wMel-infected *Ae. aegypti* adults. The wAlb strain of Wolbachia has also been established in the laboratory populations of *An. stephensi* and shown to confer resistance in mosquitoes to *P. falciparum* (Bian et al., 2013). Wolbachia spreads through cytoplasmic incompatibility rendering insects resistant to a variety of human pathogen.

1.3.3.3 Modern Biotechnological Approaches

Transgenic mosquitoes are a potential tool for the control or eradication of vectors of diseases like malaria (Boete et al., 2014). The idea behind this is to transform mosquitoes with genes that could render them refractory to infection by malaria, and then release them, thus making mosquito populations incapable of transmitting malaria. Sterile insect technique (SIT) is also increasingly utilised for control of malaria vectors. In this technique, reproductive cycles of mosquito vectors are interfered with using radiation-induced sterility, as described in the review (Oliva et al., 2014). The SIT conceived

by E.F. Knipling in 1937 relies on compromising the integrity of the hereditary machinery and fertility (Knipling, 1959) through mutagenic activity of irradiation, and mass release of the competitive, sterile insects into natural populations. In a review (Helinski et al., 2009), SIT was described as successfully used for the elimination of the New World screwworm *Cochliomyia hominivorax* from the USA and Central America, as well as the tsetse fly *Glossina austensi*. The technique had been tested in *An. arabiensis* Patton with negative correlation between insemination and dose (Helinski et al., 2006). However, in mosquitoes the technique is still in experimental phase with one of the major challenges being decreased mating competitiveness of the irradiated males (Helinski et al., 2009).

1.3.3.4 Chemical Methods

These are measures which include the use of chemicals in ITNs, LLINs, indoor residual sprays, pyrethroid-based coils or repellents, the letter which are applied topically to deter biting mosquitoes.

1.3.3.4.1 Indoor Residual Spray (IRS)

Many malaria vectors rest inside houses after taking a blood meal (endophily) and thus effective indoor residual spraying depends on whether mosquitoes rest indoors (Pates and Curtis, 2005). IRS involves spraying the walls and other surfaces of a house with a residual insecticide (http://apps.who.int/iris/bitstream/10665/80126/1/9789241505123_eng.pdf). For many months the insecticide will kill mosquitoes and other insects that come in contact with these surfaces. IRS kills mosquitoes after they have fed, when they come to rest on the sprayed surface. IRS prevents transmission of infection to other persons, has the advantage of being able to make use of a much wider range of insecticide products in comparison to LLINs and/or ITNs, for which pyrethroids are the only class of insecticide currently used (Pluess et al., 2010).

1.3.3.4.2 Insecticide Treated Bed Nets (ITNs)

ITNs are the most prominent malaria preventive measure for large-scale deployment in highly endemic areas (Lengeler, 2000). An ITN is a mosquito net that repels, disables and/or kills mosquitoes

coming into contact with insecticide on the netting material (World Health Organization, 2007). These are conventionally treated mosquito nets that have been treated by dipping in a WHO-recommended insecticide. To ensure its continued insecticidal effect, the nets are usually re-treated after three washes, or at least once a year. Relatively modest coverage with ITNs (around 60%) of all adults and children have been described as able to achieve equitable community-wide benefits (Killeen et al., 2007). ITNs have been shown to hinder around 50% of malaria cases, making its protective efficacy significantly higher than that of untreated nets which, under ideal conditions (such as those found in research settings), usually provide about half the protection of nets treated with an effective insecticide (World Health Organization, 2007, Clarke et al., 2001a).

1.3.3.4.3 Long-Lasting Insecticide Treated Bed Nets (LLINs)

Large-scale use of insecticide treated nets has a short-coming in that the impregnation and the re-impregnation needs technical skills and materials which may not be available (Lines, 1996), especially in remote areas. LLINs are developed because of these reasons and it is a factory-treated mosquito net made with netting material that has insecticide incorporated within or bound around the fibres (World Health Organization, 2007). The nets have been shown to retain its effective biological activity without re-treatment for at least 20 WHO standard washes under laboratory conditions and three years of recommended use under field conditions.

1.3.3.4.4 Repellents

Protection against arthropod bites is best achieved by avoiding infested habitats, wearing protective clothing, and applying insect repellent (Curtis, 1992). Commercially available insect repellents can be divided into two categories — synthetic chemicals and plant derived essential oils (Fradin and Day, 2002). The most widely marketed chemical-based insect repellent is *N, N*-diethyl-3-methyl-benzamide (DEET), which has been used worldwide (Fradin and Day, 2002, Karunamoorthi and Sabesan, 2009).

1.4 Insecticides

Insecticides are agents of chemical or biological origin that control insects (Ware and Whitacre, 2004). Insecticides may be natural or manmade and are applied to target pests in a myriad of formulations and delivery systems (sprays, baits, slow-release diffusion, etc). There are four major classes of insecticides used in public health sector: pyrethroids, organochlorines, carbamates and organophosphates (Krieger, 2010).

1.4.1 Pyrethroids

1.4.1.1 Introduction

The term "pyrethrum" refers to the dried and powdered flower heads of a daisy-like plant belonging to the *Chrysanthemum* genus (Schleier III and Peterson, 2011). Pyrethrins, the insecticidal ingredient occurring in the flowers of *Tanacetum cinerariaefolium* (also known as *Chr. cinerariaefolium* or *Pyr. cinerariaefolium*), have been used widely for human and animal health protection by controlling indoor pest insects such as cockroaches, houseflies, and mosquitoes since ancient times (Krieger, 2010). Pyrethrum extract contains six closely related insecticidal esters (Figure 1.2) collectively referred to as the pyrethrins, which differ only in the terminal substituents in the side chains of the acid and alcohol components. The acid is a substituted cyclopropanecarboxylic acid and the alcohol a substituted cyclopentenolone. The commercial limitations of pyrethrum extracts (pyrethrins), which are a mixture of six lipophilic esters were recognized because of their high rate of photodegradation and a short "knockdown" (rapid paralysis) effect (Schleier III and Peterson, 2011). After the discovery of the constituents of pyrethrins, researchers searched for derivatives of pyrethrins that had a higher resistance to photodegradation; this led to the synthesis of pyrethroids. The advantages of pyrethrins and pyrethroids are that they are highly lipophilic, have a short half-life in the environment, have low toxicity to terrestrial vertebrates and do not biomagnify like older chemical classes, such as organochlorines.

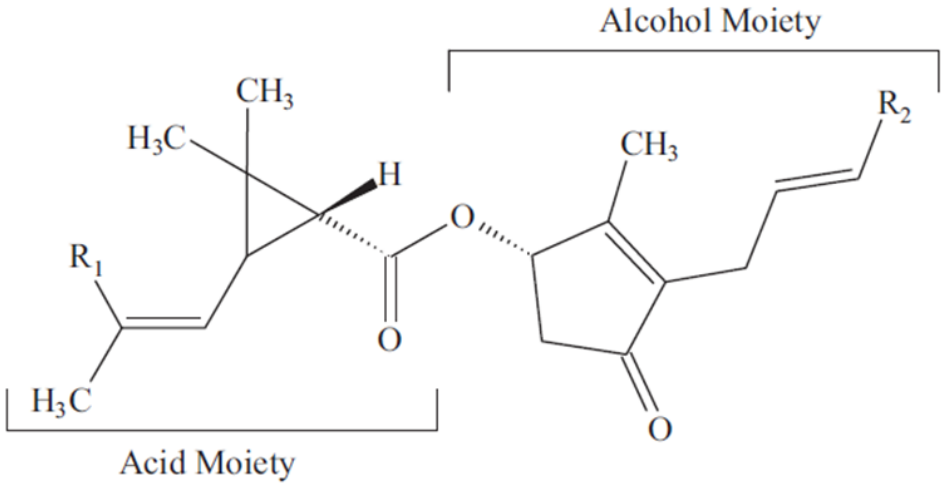

Esters of chrysanthemic acid			Esters of pyrethric acid		
	R_1	R_2		R_1	R_2
Pyrethrin I	CH_3	$CHCH_2$	Pyrethrin II	$CH_3OC(O)$	$CHCH_2$
Cinerin I	CH_3	CH_3	Cinerin II	$CH_3OC(O)$	CH_3
Jasmolin I	CH_3	CH_2CH_3	Jasmolin II	$CH_3OC(O)$	CH_2CH_3

Figure 1.2: The chemical structure of the six constituents of pyrethrum extracts which are collectively known as pyrethrins. Adapted from (Schleier III and Peterson, 2011).

Pyrethroids have wide application in agriculture and public health control of vectors, and have been described in a review by Gupta to account for approximately 25% of the world insecticide market (Gupta, 2014). For the public health market, they are used as indoor residual house sprays, to impregnate bednets, curtains and screens, and in coils, mats and aerosols (Hemingway et al., 2004). Synthetic pyrethroids can be classified into the first- and second-generation pyrethroids. First-generation pyrethroids, which are esters of chrysanthemic acid derivatives and alcohols having furan ring and terminal side chain moieties, are highly sensitive to light, air, and temperature (Krieger, 2010). Therefore, these pyrethroids have been used mainly for control of indoor pests, for example the chrysanthemates, resmethrin and phenothrin are used against household, veterinary, and stored-products pests, as reviewed in (Casida et al., 1983). The second-generation pyrethroids, which commonly have 3-phenoxybenzyl alcohol derivatives in the alcohol moiety, have excellent insecticidal

activity as well as sufficient stability in outdoor conditions conferred by substitution of photolabile moieties with dichlorovinyl, dibromovinyl substituent, and aromatic rings. Thus, the second-generation pyrethroids have been used worldwide for agricultural pests; for example permethrin and deltamethrin (Schleier III and Peterson, 2011). Pyrethroids are also grouped according to their structure (Figure 1.3) and toxicology, including those lacking α-cyano group (Type I, e.g. permethrin) and those with α-cyano group on the phenoxybenzyl moiety (Type II, e.g. deltamethrin) (Schleier III and Peterson, 2011). Type I pyrethroids differ from type II based on the distinct symptoms they evoke in insect targets and effects on sodium channel gating (Du et al., 2009).

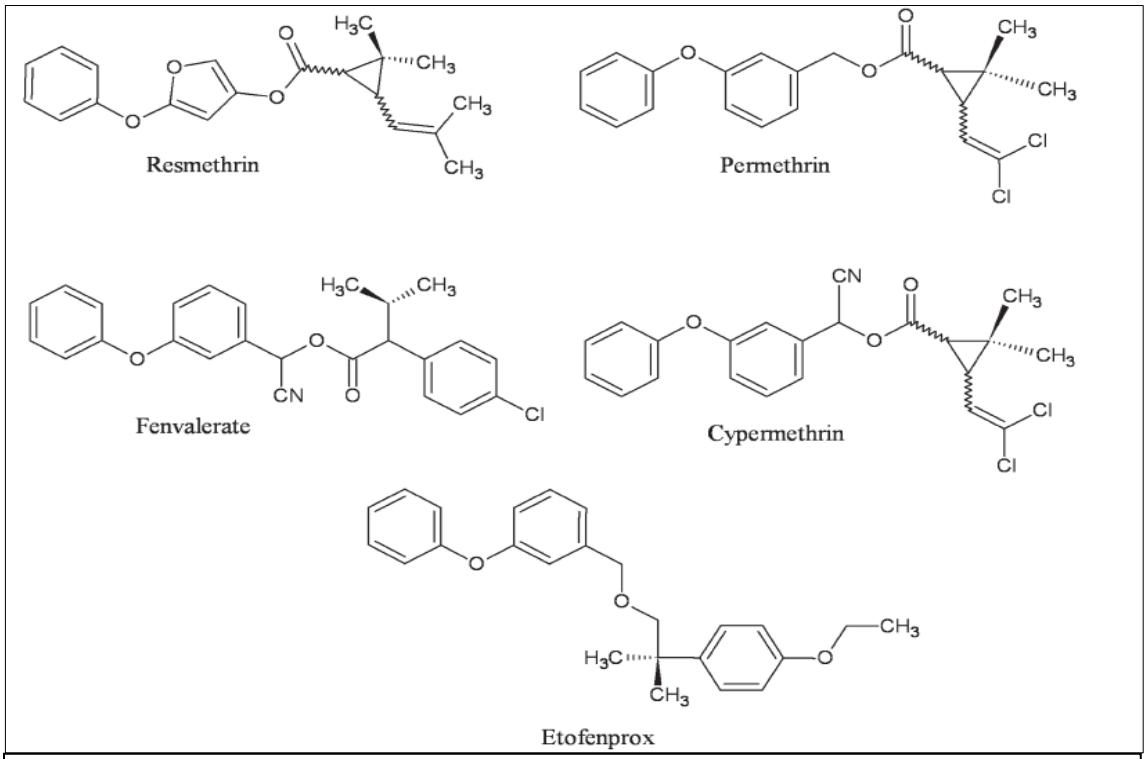

Figure 1.3: Chemical structure of type I (resmethrin and permethrin), type II (fenvalerate and cypermethrin) and pseudopyrethroid etofenprox. Adapted from (Schleier III and Peterson, 2011).

1.4.1.2 Mechanism of Action

The binding site of pyrethroid in voltage-gated sodium channel (VGSC) is located within a long, narrow hydrophobic cavity, delimited by the IIS4-S5 linker and the IIS5/IIIS6 helices (Figure 1.4), which

is accessible to lipid-soluble insecticides (Davies et al., 2007). During an action potential the sodium channel undergoes transitions between closed-resting, activated and inactivated functional states, and toxins binding to specific sites on the channel either alter the equilibrium between these functional states or block the channel pore (O'Reilly et al., 2006). The lipid soluble and pyrethroid insecticides preferentially target the open state of the voltage-gated sodium channel and their binding stabilize the open state, inhibiting the transition to the non-conducting deactivated or inactivated states. Consequently, the inward conductance of sodium is prolonged. The persistent depolarization of the plasma membrane resulting from the prolonged inward sodium conductance induces repetitive nerve firing and hyper-excitability, leading to paralysis and death of the insect.

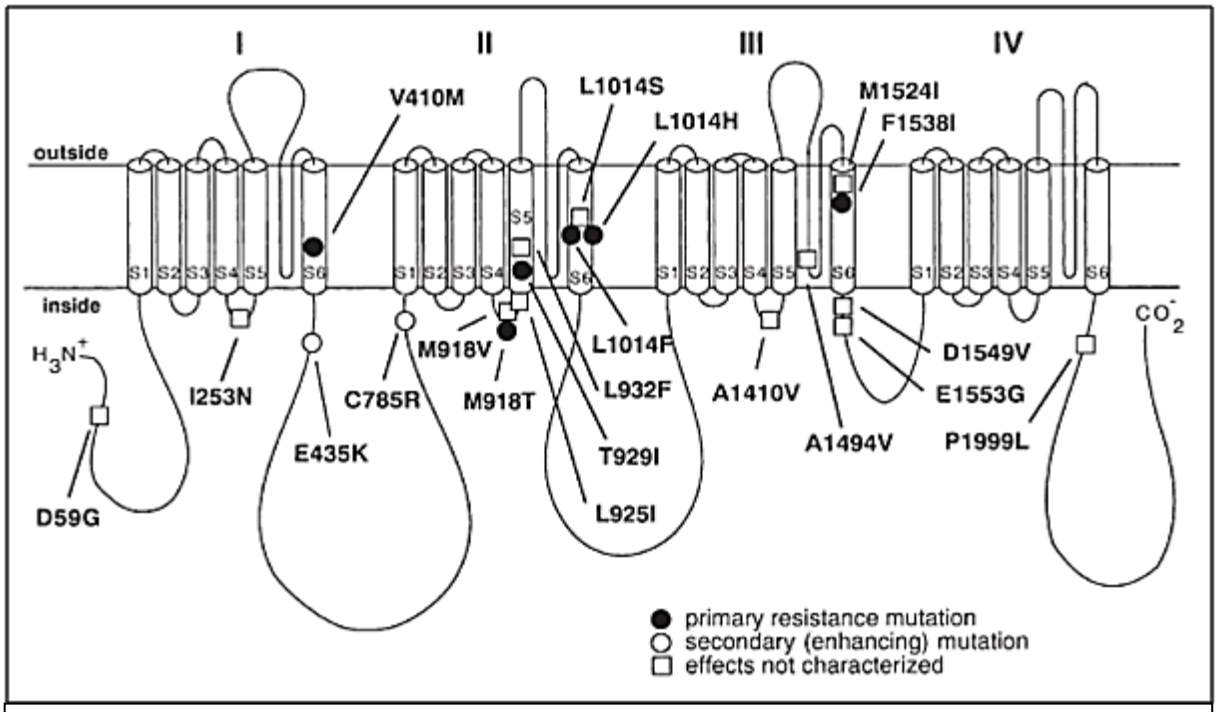

Figure 1.4: Diagram of the extended transmembrane structure of voltage-sensitive sodium channel a subunits showing the four internally homologous domains (labelled I–IV), each having six transmembrane helices (labelled S1–S6 in each homology domain), and the identities and locations of mutations associated with knockdown resistance. Adapted from (Soderlund and Knipple, 2003).

Type I pyrethroids (e.g., permethrin) are generally good knockdown agents due to their ability to induce repetitive firing in axons, resulting in restlessness, un-coordination and hyperactivity followed by prostration and paralysis. Type II pyrethroids significantly prolong channel open time (i.e.

sodium tail currents of 200 milliseconds to minutes), resulting in an increased resting membrane potential, inducing a depolarization dependent block of action potentials (Schleier III and Peterson, 2011) and causes a pronounced convulsive phase that results in better kill because depolarization of the nerve axons and terminals is irreversible (Bloomquist, 1996b).

1.4.1.3 Structure-Activity Relationships

Though there is no specific substructure, or reactive entity that can be identified as the toxophore that confers pyrethroid-like insecticidal activity (Krieger, 2010), there is a small group of essential features that pyrethroids require to possess high insecticidal activity, irrespective of the rest of the molecule or the nature of the target species (Schleier III and Peterson, 2011). The active esters of pyrethroids are 3-substituted cyclopropanecarboxylic acids which all have a 1R-configuration and a gem-dimethyl substitution at the C-2 of the cyclopropane ring (Schleier III and Peterson, 2011). Pyrethroids have three asymmetric carbon atoms and therefore could have as many as eight possible stereoisomers. The presence of two chiral centers in the cyclopropane ring of chrysanthemic acid produces two pairs of diastereomers as well, designated *cis* and *trans* on the basis of orientation of the C-1 and C-3 substitutions in relation to the plane of the cyclopropane ring; however, only isomers with the R configuration at the cyclopropane C-1 are insecticidally active (Schleier III and Peterson, 2011, Soderlund et al., 2002) (Figure 1.5).

In permethrin the methyl groups of the acid side chain was replaced with chlorine atoms, which block photochemical degradation on the adjacent double bond (Elliott et al., 1973). After the discovery of permethrin, researchers searched for compounds with a higher insecticidal activity and this led to the discovery of the cyano substitute at the benzylic carbon of the 3-phenoxybenzyl group.

Stereoisomerism is a less common feature of pyrethroid alcohol moieties. Nevertheless, when a chiral centre is present in the alcohol moiety at the carbon bearing the hydroxyl group, as in esters of α-cyano-3-phenoxybenzyl alcohol (e.g., deltamethrin), only one epimer has high insecticidal activity even when esterified to an acid moiety that contains the appropriate stereochemical configuration for

high insecticidal activity. In deltamethrin with 2 rings (3-phenoxybenzyl alcohol) the 1R-*cis* isomers are generally more active than the *trans* isomers (Gilbert and Gill, 2010). With alcohol moieties that contain only a single ring (e.g. pentafluorobenzyl group of fenfluthrin and cyclopentenone of allethrin) the *trans* isomers are more active. Also, contrary to the generalization for pyrethroids containing 3-phenoxybenzyl alcohol, theta-cypermethrin (*trans* isomer) is more potent in control of Lepidopteran than the *cis* isomer. In essence, the selective potency of pyrethroid isomers on insects depends on several factors one of which is the selective metabolic processes. For example, Pap and colleagues (Pap et al., 1996) tested pure optical isomers of phenothrin, permethin and cypermethrin on a wide spectrum of insects (*Blattella germanica, Leptinotarsa decemlineata, T. confusum, Oncopeltus fasciatus, Musca domestica, Ae. aegypti*) and discovered that the S isomer was more effective than R in all species. However, in the presence of metabolic inhibitors, the R isomer had comparable activity to the S towards mosquitoes but not the other species (Gilbert and Gill, 2010).

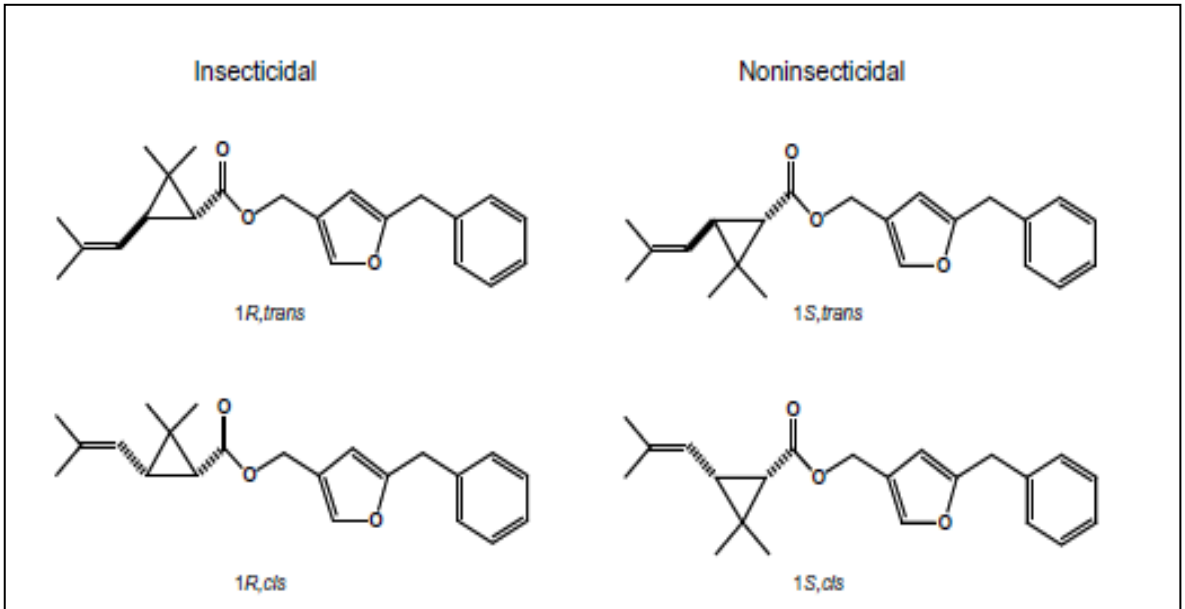

Figure 1.5: Structure-Activity Relationship in pyrethroids: (A) insecticidal and non-insecticidal isomers of resmethrin. Adapted from (Krieger, 2010).

1.4.1.4 Metabolism of Pyrethroids

The pyrethroids are detoxified by through attack by either esterases at the central ester bond, or by P450 monooxygenases at one or more of the acid or alcohol moieties (Schleier III and Peterson,

2011). However, presence of a *cis*-substituted acid moiety and a secondary alcohol moiety makes hydrolytic metabolism of pyrethroids limited (Soderlund and Knipple, 2003).

Analysis of the metabolic pathways of pyrethroid degradation in insects, including cockroach, housefly and cabbage looper (Shono et al., 1978) identified forty-two metabolites (including conjugates) from permethrin metabolism which occurred by ester cleavage to 3-phenoxybenzyl alcohol (3-PBA) and 3-(2,2-dichlorovinyl)-2,2-dimethylcyclopropanecarboxylic acid (DCVA). Hydroxylation has also been described to occurr at the 4'- and 6- positions of the phenoxybenzyl moiety and the *cis* or *trans* methyl groups of the DCVA (Gilbert and Gill, 2010).

In mosquitoes, metabolism of Type II pyrethroids may involve the oxidation of phenoxybenzyl ring as reported for *An. gambiae* CYP6M2 (Stevenson et al., 2011). CYP6M2 metabolised deltamethrin into 4'-hydroxydeltamethrin and incubation of HPLC-purified 4'-hydroxydeltamethrin (M4) with CYP6M2 produced cyano(3-hydroxyphenyl) methyl deltamethrate (M2), which in turn was found to be metabolized by the same enzyme to deltamethric acid (M1) (Figure 1.6). CYP6M2 thus, predominantly metabolizes deltamethrin by hydroxylation of the 4' position, cleavage of the ether bond between the aromatic rings, and hydrolysis into deltamethric acid.

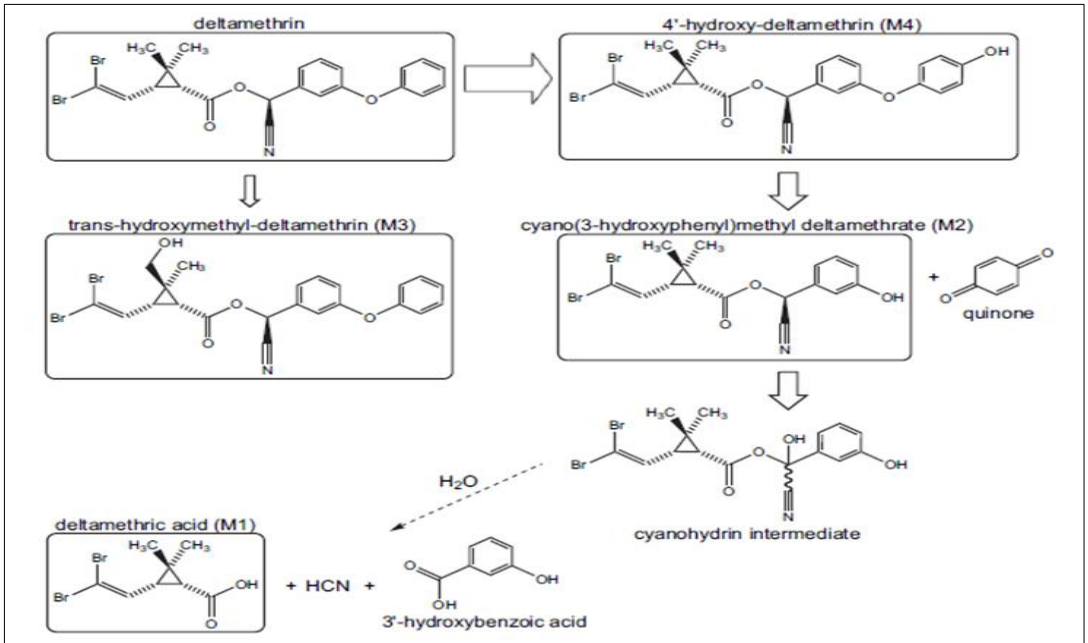

Figure 1.6: Metabolism of deltamethrin by recombinant *An. gambiae* CYP6M2.
Adapted from (Stevenson et al., 2011).

1.4.2 Organophosphates (OPs)

The toxicity of insecticidally active organophosphorus and carbamate esters to animals is attributed to their ability to inhibit acetylcholinesterase (*AChE*), a class of enzymes which catalyzes the hydrolysis of the neurotransmitter acetylcholine (ACh) (Fukuto, 1990). The binding of OPs to *AChE* results in disruption of nerve impulses, killing the insect or interfering with normal activities. OPs are normally esters, amides, or thiol derivatives of phosphoric, phosphonic, phosphorothioic, or phosphonothioic acids (Singh, 2012). The OPs are a very important group of compounds that vary tremendously in chemical structure and chemical properties (Bloomquist, 1996a). The OP compounds can be miscible with water, but more typically are miscible in organic solvents. Generally, OPs react with a serine hydroxyl group within the enzyme active site, phosphorylating the serine hydroxyl group and yielding a hydroxylated "leaving group". This process inactivates the enzyme and blocks the degradation of the neurotransmitter, acetylcholine. There are at least about 13 types of OPs (Gupta, 2011); of these malathion belongs to phosphorodithioates, sarin belongs to phosphornofluoridates, diazinon, parathrion and pirimiphos-methyl belong to phosphorothioates, and dichlorvos belongs to phosphonates. OPs used in mosquito control programmes include: fenthion (bytex), temephos (abate), chloropyrifos (dursban), fenithrothion (sumithion), pirimiphos-methyl (actelic), malathion, etc.

1.4.3 Carbamate

Carbamates are *N*-substituted esters of carbamic acid (Gupta, 2011). The inhibition of *AChE* by a carbamate insecticide occurs by a mechanism identical to that described for an organophosphates (Fukuto, 1990). The first step in the inhibition process involves the formation of the enzyme-inhibitor complex with subsequent carbamylation of the serine hydroxyl group and inhibition of the enzyme (Metcalf, 1971). Examples of carbamates are carbaryl (SEVIN), oxamyl (VYDATE), carbofuran (FURADAN), thiodicarb (LARVIN) (Singh, 2012), bendiocarb (Turcam), propoxur (BAYGON), etc.

1.4.4 Organochlorines (OCs)

Organochlorine pesticides are chlorinated hydrocarbons used extensively from the 1940s through the 1960s (Matsumura, 1985). Representative compounds in this group include DDT, methoxychlor, dieldrin, chlordane, toxaphene, mirex, kepone, lindane, and benzene hexachloride. Since the 1970s, DDT and most other chlorinated hydrocarbon compounds have been restricted or banned for agricultural use in most countries, due in part to their unacceptably long persistence in the environment and also because of increased concerns arising from their fat solubility (having a high partition coefficient in lipids versus water) and resultant long-term accumulation in fatty tissues of non-target organisms (Mellanby, 1992). However, DDT continues to be used in limited quantities in the control of insect vectors for public health purposes, as its approved by WHO in 2006 for IRS (Sadasivaiah et al., 2007). DDT affects the peripheral nervous system; initial contact with the insecticide causing neurons to fire spontaneously causing muscles twitch, with resulting tremors throughout the body and appendages, the so-called 'DDT jitters' (Davies et al., 2007). Over the course of a few hours or days, DDT exposure leads to excitatory paralysis and consequent death of the insect.

1.4.5 Other insecticides

Other compounds with insecticidal activities used for control of insect pests include neonicotinoids and ryanoids. Neonicotinoids, possess either a nitromethylene, nitroimine or cyanoimine group (Matsuda et al., 2001) and important neonicotinoids, such as imidacloprid, nitenpyram and acetamiprid, all contain a 6-chloro-3-pyridyl moiety and therefore resemble nicotine and epibatidine, both of which are potent agonists of nicotine acetylcholine receptors (nAChRs). Imidacloprid and other nitromethylene compounds like 1-(pyridine-3-yl-methyl)-2-nitromethylene-imidazoline (PMNI) are increasingly used worldwide as an insecticides (Bai et al., 1991).

Ryania insecticide is the powdered stem wood of *Ryania speciosa Vahl.*, a small shrub growing extensively in South America, and noted for its pest control properties (Crosby, 1971). The major

insecticidal and toxic constituents are ryanodine (Jefferies et al., 1992) and 9,12-didehydroryanodine (Waterhouse et al., 1984), which have attracted much attention as natural but expensive insecticides and for their action on the Ca^{2+}-ryanodine receptor complex of muscle (Lai and Meissner, 1989). Ryanodine has been described from several studies to induce paralysis in insects and vertebrates by causing a sustained contracture of skeletal muscle without depolarizing the muscle membrane (Bloomquist, 1996a).

1.5 Insecticide Resistance

1.5.1 Introduction

The term resistance is defined as the ability of an insect (population) to withstand the effects of an insecticide by becoming resistant to its toxic effects by means of natural selection and mutations (Davidson, 1957). Repeated exposure to insecticides can select individuals possessing biochemical machineries that can detoxify the insecticides more rapidly or are less sensitive to it (Gilbert and Gill, 2010). These individual survivors could then pass the resistance traits to the succeeding generations resulting in pest populations more resistant, until ultimately a situation is reached whereby the pests become completely resistant to the insecticide. In a recent review (Corbel and N'Guessan, 2013) resistance has been described to be present in more than 500 insect species worldwide and that to date malaria vectors have developed resistance to the main chemical classes used in public health, the pyrethroids, organochlroines, carbamates and organophosphates.

1.5.2 Types of Insecticides Resistance Mechanisms

The various mechanisms that enable insects to resist insecticides can be grouped into four distinct categories including metabolic resistance, target-site resistance, reduced penetration and behavioural avoidance, as aptly reviewed in (Corbel and N'Guessan, 2013) (see Figure 1.7). However, increased excretion of the insecticides by some pests is also termed another mechanism of resistance.

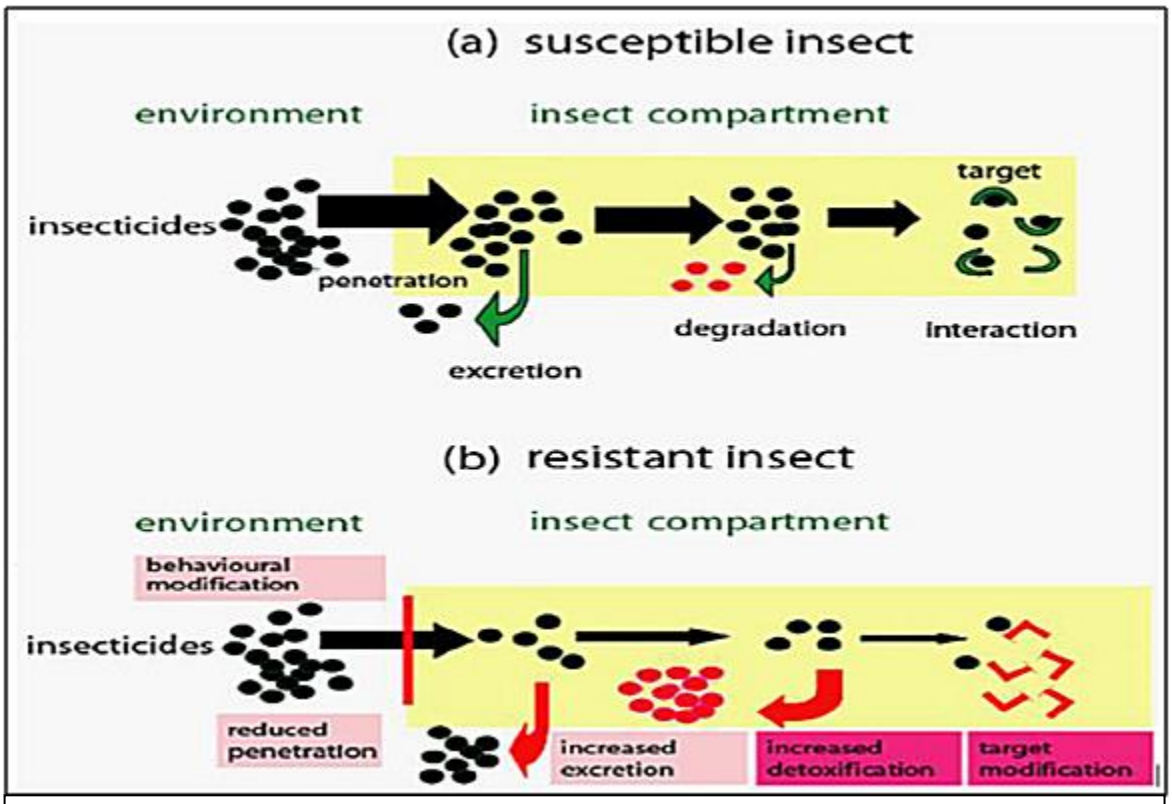

Figure 1.7: Scheme of potential behavioural and physiological changes associated with insecticide resistance in malaria vectors; (a) susceptible insect; (b) resistant insect. Adapted from (Corbel and N'Guessan, 2013).

1.5.2.1 Behavioural Resistance

Continues exposure to an insecticide may trigger changes in behavioural response of insect pests (Corbel and N'Guessan, 2013) leading to the avoidance of lethal doses of an insecticide (Chandre et al., 2000). This type of response can be divided into direct contact excitation (sometimes referred to as 'irritancy') and non-contact spatial repellency that is used when insects move away from the insecticide-treated area before making direct contact (Roberts et al., 1997). Behaviouristic resistance has been established in *An. funestus*; a shift from indoor to outdoor biting preferences in Tanzania in relation to increasing coverage of pyrethroid-impregnated net (Russell et al., 2011b) as well as significant changes in the host-seeking behaviour of the *An. funestus* population from Benin (West Africa) where scaling up of LLINs at community level induced a change from night biting to early-morning biting behaviour (Moiroux et al., 2012).

1.5.2.2 Penetration Resistance (Reduced penetration)

Modifications in the insect cuticle or digestive tracts can prevent, slow the absorption or reduce penetration of insecticides (Corbel and N'Guessan, 2013). Reduced uptake of insecticide (cuticular resistance) has been observed in some insect pests especially ones where the major route of exposure is through ingestion. For mosquito control, where insecticides are applied onto bed nets or on wall surfaces, uptake is primarily through the appendages. Therefore, increase in the thickness of the tarsal cuticle, or a reduction in its permeability to lipophilic insecticides, could have a major impact on the bioavailability of an insecticide *in vivo* (Corbel and N'Guessan, 2013). Decreased penetration of insecticides would allow sufficient time for detoxifying enzymes to metabolize the chemical and therefore make it less effective (Plapp, 1976). Microarrays studies have identified two genes encoding cuticular proteins that were upregulated in pyrethroid resistant strains of *An. stephensi* (Vontas et al., 2007) and *An. gambiae* (Awolola et al., 2009b). Also, it has been established using scanning electron microscopy that in a laboratory strain of *An. funestus* the mean cuticle thickness was significantly greater in pyrethroid tolerant mosquitoes than their susceptible counterparts (Wood et al., 2010).

1.5.2.3 Increased excretion

This is one of the mechanisms of resistance developed by insects. It was shown that larvae of Trinidad resistant strain of *Ae. aegypti* respond to DDT by excreting the insecticide into the perithrophic matrix, the production of which was sometime increased so much that it protruded from the anus (Abedi and Brown, 1961). This behaviour was more evident in some resistant strains than others and occurred to a much lesser extent in larvae of strain that are susceptible. It appeared to constitute a resistance mechanism for removing DDT from the alimentary canal.

1.5.2.4 Biochemical Resistance

Biochemical resistance mechanisms are divided into metabolic (alterations in the levels or activities of detoxification proteins) and target site (mutations in the sodium channel, *AChE* and gamma-aminobutyric receptor (GABA) genes, etc). Alone or in combination these mechanisms confer resistance, sometimes at an extremely high level, to all of the available classes of insecticides.

1.5.2.4.1 Metabolic-Based Resistance

Several reviews defined metabolic resistant (Corbel and N'Guessan, 2013, Russell et al., 2011a) as a resistance which is based on the detoxification enzymes which all insects possess and which help them to clear naturally occurring xenobiotics. As reviewed by Schuler and Berenbaum (Schuler and Berenbaum, 2013) overexpression of enzymes capable of detoxifying insecticides or amino acid substitutions within these enzymes, which alter the affinity/activity of the enzyme for the insecticide, can result in high levels of insecticide resistance. Overexpression of detoxification enzymes can occur as the result of gene amplification (e.g. duplication), or due to changes in either *trans*-acting regulatory elements or in the promoter region of the gene. The consequence is a significant increase of enzyme production/activity in resistant insects that enables them to metabolize or degrade insecticide before it exerts its toxic effect. Three major enzyme groups esterases, cytochrome P450s (*CYP450s*) and glutathione S-transferases (*GSTs*) have been described as being responsible for metabolically-based resistance to organochlorines, organophosphates, carbamates and pyrethroids (Hemingway and Ranson, 2000, Brooke et al., 2001, Aizoun et al., 2013).

1.5.2.4.1.1 Esterases-Based Metabolic Resistance

Over-production of non-specific carboxylesterases as an evolutionary response to organophosphate and carbamate insecticide selection pressure has been documented in numerous arthropod species including mosquitoes, cattle ticks, aphids and cockroaches (Hemingway et al., 2004). Several reviews have described esterases as responsible for hydrolysis of ester bonds of

insecticides or sequesteration (Corbel and N'Guessan, 2013) with the most widely studied mosquito species demonstrating this resistance mechanism are members of the *Culex* genus (Prato et al., 2012). In organophosphate-susceptible insects, the active oxon analogues of the insecticides act as esterase inhibitors, because they are poor substrates with a high affinity for the enzymes (Karunaratne et al., 1995). Esterases from susceptible insects exhibited lower activity towards xenobiotics (including insecticides) than their counterparts from resistant insects, which sequester the oxon analogues and thus protect the *AChE* target site. Enhanced esterase activities have been described in mosquitoes, for example, in permethrin resistant *An. gambiae* and in resistant *Ae. aegypti* (Hemingway et al., 2004, Vulule et al., 1999, Mourya et al., 1993)

In contrast to the situation in *Culex,* several reviews (Corbel and N'Guessan, 2013, Hemingway et al., 2004) reported a number of *Anopheles* species (ie *An. culicifacies*, *An. stephensi* and *An. arabiensis*) having a non-elevated esterase mechanism which confers resistance specifically to malathion through increased rates of metabolism. Malathion resistance in *Anopheles* had been associated with an altered form of esterase that specifically metabolizes the molecule at a much faster rate than that in susceptible counterparts (Herath et al., 1981, Hemingway, 1983). Recently, $Gly^{137}Asp$ and $Try^{251}Leu$ mutations in the active site of the Cotton Bollworm *Helicoverpa armigera* esterase have been shown to increase the OP-hydrolase activity of the enzyme 14- and 6-folds, respectively (Li et al., 2013). In multiple resistant populations of *An. funestus* from southern Africa, genome-wide microarray analysis have identified candidate carboxylesterases overexpressed (Riveron et al., 2014a). However, the role of these esterases in hydrolysis of OPs, carbamates or pyrethroid insecticides have not been validated.

1.5.2.4.1.2 Glutathione S-Transferases (GSTs)-Mediated Resistance

GSTs are dimeric, multifunctional enzymes that play a role in detoxification of a large range of xenobiotics by catalyzing the nucleophilic attack of reduced glutathione (GSH) on the electrophilic centres of lipophilic compounds (Sherratt and Hayes, 2001). Conjugation of glutathione (GSH) to

organic molecules enhances solubility, thus facilitating their eventual elimination (Corbel and N'Guessan, 2013). Elevated GST activity has been implicated in resistance to at least four classes of insecticides in insects (Hemingway et al., 2004). Higher enzyme activity is usually due to an increase in the amount of one or more GST enzymes, either as a result of gene amplification or more commonly through increase in transcriptional rate, rather than qualitative changes in enzyme structures until recent findings, e.g. see (Riveron et al., 2014b). At least six classes of insect *GSTs* have been identified in *An. gambiae* (Ranson et al., 2000), found in several large clusters on all three chromosomes. The Delta and Epsilon classes found exclusively in insects are the largest classes of insect GSTs. Members of both these classes have been implicated in resistance to all the major classes of insecticide.

It has been suggested that GSTs may play a role in pyrethroid resistance by detoxifying lipid peroxidation products induced by pyrethroids and/or by protecting from insecticide exposure induced oxidative stress rather than direct metabolism of the pyrethroids (Vontas et al., 2001).

However, in the case of *An. funestus* overexpression and qualitative changes in the amino acid sequence have been described as the reasons behind extreme DDT resistance and cross-resistance to permethrin (Riveron et al., 2014b). A single mutation in *GSTe2* gene ($Leu^{119}Phe$) was found to confer both high resistance to DDT and a cross resistance to pyrethroid permethrin in mosquito populations from Benin, West Africa.

1.5.2.4.1.3 P450-Monooxygenases-Mediated Resistance

Cytochrome P450 monooxygenases (*CYP450s*) are diverse family of hydrophobic, heme containing enzymes involved in the metabolism of numerous endogenous and exogenous compounds (Sridhar et al., 2012). P450s are important in adaptation of insects to toxic chemicals in their host plants and have been shown to be involved in the metabolism of virtually all insecticides (Hemingway and Ranson, 2000). The action of P450 monooxygenases usually result in the detoxification of the substrate, although the OP insecticides from the phosphorothionate are also activated to the more toxic oxon form (Bharate et al., 2010).

Insect P450s belong to four major clans: CYP3, CYP4, CYP2 and the mitochondrial clan (Feyereisen, 2012) and increased transcription of genes belonging to the CYP4 (from CYP4 clan), CYP6 and CYP9 families (both from CYP3 clan) has been observed in various insecticide-resistant species from different taxa (Feyereisen, 2005). Elevated monooxygenase activity is associated with pyrethroid resistance in *An. stephensi*, *An. gambiae*, *Cx. quinquefasciatus, Ae. aegypti* and *An. funestus* (Brogdon and McAllister, 1998, Vulule et al., 1994, Kasai et al., 1998, Stevenson et al., 2012, Cuamba et al., 2010, Djouaka et al., 2011). However, higher activity of enzymes and/or expression of detoxification genes in insecticide resistant populations do not necessarily correlate with resistance (Corbel and N'Guessan, 2013); for example elevated transcript levels of an adult-specific P450 gene, *CYP6Z1*, in pyrethroid-resistant strain *of An. gambiae* was reported (Nikou et al., 2003), though the enzyme does not metabolise pyrethroids (Chiu et al., 2008).

1.5.2.4.2 Target-site insensitivity

Insecticides generally act at a specific site within the insect, typically within the nervous system (e.g. OPs, carbamates, DDT and pyrethroid insecticides) (Corbel and N'Guessan, 2013) and modification in resistant strains of insects of such targets result in insecticide no longer binding effectively, rendering it ineffective (Ranson et al., 2000). Reduced sensitivity of the target receptors to insecticide results from non-synonymous point mutations in the gene encoding the protein.

1.5.2.4.2.1 Knockdown Resistance (kdr)

Mutations in the amino acid sequence in VGSC channels of nerve cell membranes leads to a reduction in the sensitivity of the channel to the binding of DDT and pyrethroids (Davies et al., 2007). Alterations in the target site that cause resistance to insecticides are often referred to as *kdr* in reference to the ability of insects with these alleles to withstand prolonged exposure to insecticides without being 'knocked-down" (Corbel and N'Guessan, 2013)(see Figure 1.4).

kdr was first recognised in houseflies by Busvine in 1951 (Busvine, 1951) and the *kdr* factor is now known to be a recessive allele conferring cross resistance to the entire class of pyrethroids as well as to DDT and its analogues (Davies et al., 2007). More than 20 unique sodium channel sequence polymorphisms have been identified in association with pyrethroid resistance. *kdr* has been reported in many important pest species and in many cases is accompanied by a second recessive resistance trait designated super-*kdr* which confers much greater resistance to pyrethroids (Farnham et al., 1987)

One of the most common amino acid replacements associated with pyrethroid resistance in malaria vectors especially *An. coluzzii*, *An. gambiae* Giles and *An. arabiensis* is a substitution of the leucine residue found at codon 1014 with either phenylalanine (1014F) (Martinez-Torres et al., 1998) or serine (1014S) (Ranson et al., 2000) in the sodium channel. To date, no *kdr* mutation has been discovered in the VGSC of *An. funestus* and associated with insecticide resistance.

1.5.2.4.2.2 Insensitive Acetylcholinesterase

Several mutations in the gene encoding *AChE* have been found in insects (Fournier, 2005) and the mutations result in reduced sensitivity to inhibition by insecticides (Weill et al., 2003). $Gly^{119}Ser$ mutation responsible for carbamate and OP resistance has been reported in *An. gambiae* and *Cx. pipiens* (Weill et al., 2004). Elevated expression of the *AChE* gene, due in part from gene duplication of $Gly^{119}Ser$ copies confer carbamate resistance in *An. gambiae* from West Africa (Edi et al., 2014).

1.5.2.4.2.3 GABA Receptor Rdl Mutation

The insect *GABA* receptor is implicated as a site of action for cyclodienes (Hemingway and Ranson, 2000). Several mutations in this receptor which lead to resistance have been described for insects (Corbel and N'Guessan, 2013). In *An. gambiae* substitution of conserved Ala^{302} in the *Rdl* locus with serine or glycine have been associated with resistance to dieldrin (Du et al., 2005).

Dieldrin resistance was detected in *An. funestus* populations from West (Burkina Faso) and Central (Cameroon) Africa (Wondji et al., 2011). The $Ala^{296}Ser$ mutation in *An. funestus* has been

associated with dieldrin resistance and is largely distributed in West and Central Africa (Wondji et al 2011) but absent in southern African populations. East (Uganda) and Southern (Malawi and Mozambique) populations were fully susceptible to dieldrin.

1.5.3 Interaction of Resistance Mechanisms

The co-presence of multiple resistance mechanisms exist in various insect species such as the house fly (Liu and Yue, 2000) and the mosquitoes *Cx. quinquefasciatus* (Xu et al., 2005), etc, and can confer onto some insect species high levels of resistance. **Cross-resistance** occurs when a resistance mechanism which allows insects to resist one insecticide, also confers resistance to another insecticide. Cross-resistance can occur between insecticides from different chemical classes (Ranson et al., 2011). **Multiple resistance** is a situation which occurs when insects develop resistance to several compounds by expressing multiple resistance mechanisms. The different resistance mechanisms can combine to provide resistance to multiple classes of insecticide products.

Multiple resistance in *Anopheles* mosquitoes have been described in several studies. For example, co-occurrence of metabolic resistance mechanisms and *kdr* in a population of *An. gambiae* s.s. from Nigeria was established by Awolola and colleagues (Awolola et al., 2009a). For cross-resistance, the gene *CYP6M2* from resistant strain of *An. gambiae* was found to metabolize Type I and Type II pyrethroids as well as organochlorine, DDT (Stevenson et al., 2011, Mitchell et al., 2012). Cross-resistance mechanism conferred by P450s (*CYP6P3* and *CYP6M2*) and *ace-1* duplication have been described in multiple resistant population of *An. gambiae* from Côte d'Ivoire (Edi et al., 2014). In *An. funestus* we (Riveron et al., 2014b) have dissected the mechanism of cross-resistance to DDT and Type I pyrethroid (permethrin) in multiple resistance populations from Benin Republic, and established that the *GSTe2* gene can confer cross-resistance between these insecticides.

1.6 Cytochrome P450-Dependent Monooxygenases (P450s)

1.6.1 Introduction

P450s are ubiquitous, heme-thiolate, 45- to 55-kDa enzymes (Feyereisen, 2012) important in oxidative, peroxidative and reductive metabolism of numerous and diverse endogenous compounds such as steroids, bile acids, fatty acids, prostaglandins, leukotrienes, biogenic amines, retinoids and phytoalexins (Nelson et al., 1996, Bergé et al., 1998). They embody one of the largest family of genes that are found in all organisms in all domains of life (Munro et al., 2013). The proteins, named for the absorption band of their Fe^{II}-CO complex (carbon-monoxide bound form) at 450nm (Omura and Sato, 1964), are one of the largest superfamilies of enzyme proteins. The P450 genes (also called *CYP*) are found in the genomes of virtually all organisms (Werck-Reichhart and Feyereisen, 2000), from bacteria to protists, plants, fungi, and animals (Feyereisen, 2012). Human genome carries about 57 CYP genes and insect genomes can carry from 48 as in honeybee *Apis mellifera* (Scott, 2008) to 170 as found in mosquito *Cx. quinquifasciatus* (Arensburger et al., 2010).

As mixed function monooygenases, P450s catalyse the transfer of one atom of molecular oxygen to a substrate, reducing the other to water (Equation 1.1), but they also show activity as oxidases, reductases, desaturases, isomerases, etc., and collectively are known to catalyse at least 60 chemically distinct reactions (Feyereisen, 2012, De Montellano, 2005).

$$RH + O_2 + NADPH + H^+ \rightarrow ROH + H_2O + NADP^+ \qquad \text{Equation 1.1}$$

There are soluble forms of P450 (in bacteria), and membrane-bound forms (in microsomes and mitochondria of eukaryotes) (Feyereisen, 2012). Most animal P450s are dependent on redox partners for their supply of reducing equivalents (NADPH cytochrome P450 reductase and cytochrome b_5 in microsomes; a ferredoxin and a ferredoxin reductase in mitochondria).

1.6.2 Classes and Structural Features of P450s

P450s can be divided into four classes depending on how electrons from NAD(P)H are delivered to the catalytic site (Werck-Reichhart and Feyereisen, 2000): Class I proteins require both an FAD-containing reductase and an iron sulphur redoxin; Class II proteins require only an FAD/FMN-containing P450 reductase for transfer of electrons; Class III enzymes are self-sufficient and require no electron donor; while P450s from Class IV receive electrons directly from NAD(P)H. This classification of the interactions with redox partners is unrelated to P450 evolutionary history.

Sequence identity among P450 proteins is often extremely low and there is only one absolutely conserved amino acid (Feyereisen, 2012). Highest conservation in the structure of P450s is found in the core of the protein around the heme and reflects a common mechanism of electron and proton transfer and oxygen activation. The conserved core is formed of a four-helix (D, E, I and L) bundle, helices J and K, two sets of β sheets, and a coil called the '*meander*'. These regions comprise: motif WxxxR located in the C-helix and easily discernible in multiple alignments; the Arg is thought to form a charge pair with the propionate of the heme (Feyereisen, 2012); the heme-binding loop, containing the most characteristic P450 consensus sequence (Phe-X-X-Gly-X-Arg-X-Cys-X-Gly), located on the proximal face of the heme just before the L helix, with the absolutely conserved cysteine that serves as fifth ligand to the heme iron; the conserved Glu-X-X-Arg motif in helix K, also on the proximal side of heme and probably needed to stabilize the core structure through a set of salt bridge interactions (E–R–R) with the fourth conserved motif, PxxFxPE/DRF (often PERF, but R is sometimes replaced by H or N), which is located after the K' helix in the "meander" facing the ExxR motif; and finally, the central part of the I helix, containing another consensus sequence considered as P450 signature (Ala/Gly-Gly-X-Asp/Glu-Thr-Thr/Ser), which corresponds to the proton transfer groove on the distal side of the heme (Werck-Reichhart and Feyereisen, 2000). This final conserved motif surrounds a conserved threonine in the middle of the long helix I that runs on top of the plane of the heme, over pyrrole ring (Feyereisen, 2012). The description of the structure essentially follows the

nomenclature of the P450cam protein, the camphor hydroxylase of *Pseudomonas putida* (Poulos et al., 1985) and typical outline of structural arrangement is given in Figure 1.8.

The most variable regions of P450s are associated with either amino-terminal anchoring or targeting of membrane-bound proteins, or substrate binding and recognition; the latter regions are located near the substrate-access channel and catalytic site and are often referred to as substrate-recognition sites (SRSs) as described by Gotoh (Gotoh, 1992). SRSs are described as flexible, moving upon binding of substrate so as to favour the catalytic reaction. Other variations reflect differences in electron donors, reaction catalysed or membrane localization. Most eukaryotic P450s are associated with microsomal membranes, and very frequently have a cluster of prolines (Pro-Pro-X-Pro) that form a hinge, preceded by a cluster of basic residues (the halt-transfer signal) between the hydrophobic amino-terminal membrane anchoring segment and the globular part of the protein (Werck-Reichhart and Feyereisen, 2000). The hinge slaps the globular domain of the P450s onto membrane surface and is important for heme incorporation and assembly. Additional membrane interaction seems to be mediated essentially by a region, located between the F and G helices that shows increased hydrophobicity (Williams et al., 2000). This region is thought to create a hydrophobic environment through which substrate can enter the active site.

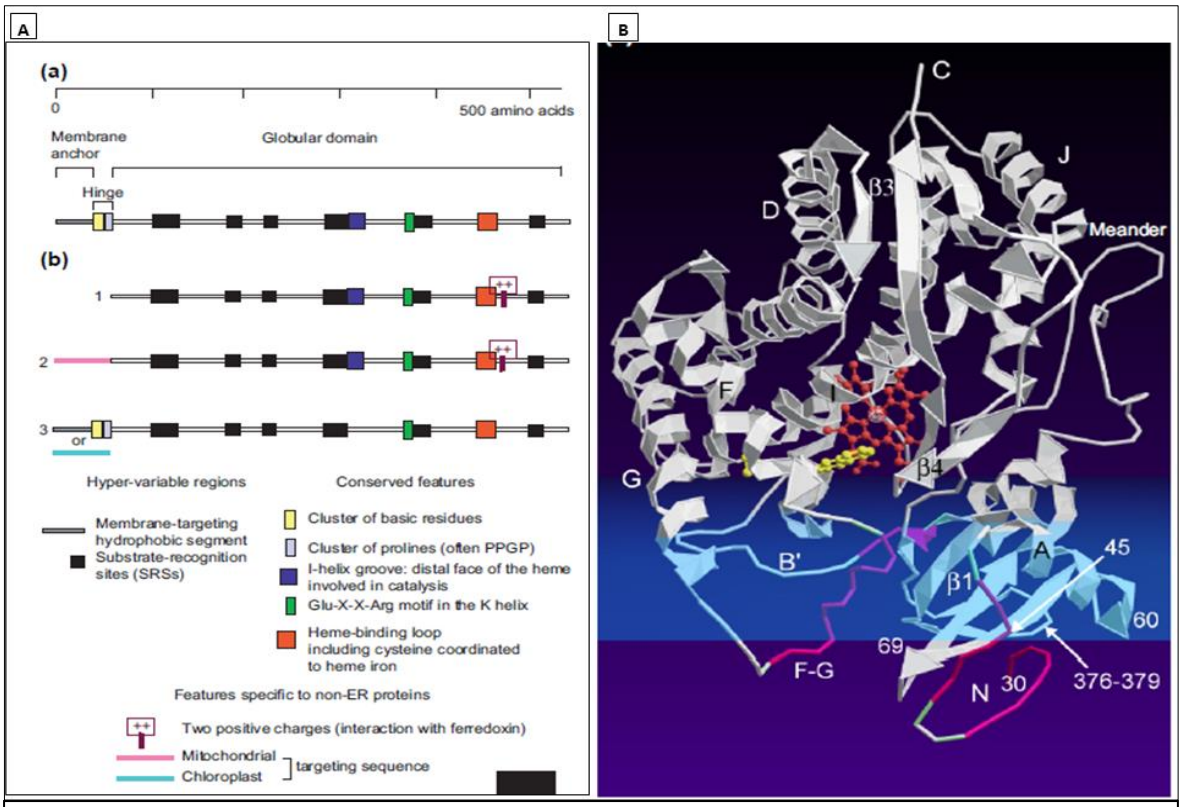

Figure 1.8: (A) Primary structures of P450 proteins. (a) Typical features of an ER-bound P450 protein (class II enzyme), (b) Variants of this canonical structure most commonly found: 1, soluble class I, 2, mitochondrial class I; 3, membrane-bound or plastidial class III: **(B) A ribbon representation of the distal face of the folded CYP2C5 showing its putative association with the ER membrane (purple), helices and sheets.** Heme is in orange and the substrate in yellow. Adapted from (Feyereisen, 2012).

1.6.3 Insects Cytochrome P450s

The first insect P450s cloned and sequenced were *CYP6A1* from *Musca domestica* (Feyereisen et al., 1989). Since then progress has been made in identification of insect P450s especially boosted with the successful sequencing of insect genomes including those of the fruit fly *D. melanogaster* and *An. gambiae* (Feyereisen, 2006, Claudianos et al., 2006, Feyereisen, 2012). Insect genome sequencing projects, starting with that of *D. melanogaster* in 2000, finally revealed the cast of P450 characters in insects (Tijet et al., 2001, Feyereisen, 2012). The cytochrome P450 complement size of an insect genome is not a definite number (Feyereisen, 2011); insects can survive with small genomic P450 complement even in toxic environments and larger number of P450s does not necessarily mean ability

to resist insecticides. However, insects do have large number of P450s due possibly to one of these two reasons (Scott, 2008): (i) detoxification of the numerous environmental and dietary toxins which constitutes the primary selective force for presence of P450s in each specie and maintenance of its diversity between species; (ii) or alternatively, the majority of P450s in insect are not involved in detoxification of xenobiotics, but rather in the metabolism of other compounds.

Insect CYP genes fall into four major clans (Feyereisen, 2006), named after the founding family in vertebrates (CYP3, CYP4, CYP2 clans) or their subcellular location (mitochondrial CYP clan) (Feyereisen, 2012). This classification is given in brief in Table 1.2. Though insect P450s are distributed across 48 major CYP families (Amenya et al., 2008) majority of the P450 genes implicated in resistance to insecticides are from three main families: CYP4, 6 and 9 (Feyereisen et al., 1989). Insect monooxygenases can be detected in a wide range of tissues. Highest activities are usually associated with the midgut, fat bodies and Malpighian tubules (Hodgson, 1983) but the expression of individual P450s can vary between these tissues (Scott et al., 1998a). Also, dramatic variation in monooxygenase activities and P450 levels occur during the development of most insects (Scott, 2008). In general, total P450 levels are undetectable in eggs, rise and fall in each larval instar, are undetectable in pupae and are expressed at high levels in adults.

Table 1.2 Four clans of CYP genes in insects, with CYP family numbers. Numbers as in 2010. Adapted from (Feyereisen, 2012).

CYP2 Clan	*Mitochondrial CYP Clan*	*CYP3 Clan*	*CYP4 Clan*
15	12	6	4
18	49	9	311-313
303-307	301-302	28	316
343	314-315	308-310	318
359	333-334	317	325
369	339	321	340-341
	353	324	349-352
	366	329	380
		332	367
		336-338	405
		345-348	411-412
		354	
		357-358	
		365	
		395-400	
		408	
		413	

1.6.4 Genomic Variation of Insects P450s

1.6.4.1 Allelic Variants, Copy Number Variation and Alternative Splicing

Allelic variants of cloned P450 cDNAs and genes are very frequent and were described in the earliest studies of insect P450 (Cohen et al., 1994). Examples of this variation were most striking in *An. gambiae* genome found to be highly polymorphic, with a single nucleotide polymorphism (SNP) frequency of 1 every 26bp in CYP genes (Wilding et al., 2009) and *An. funestus* in which, on average 7 SNPs per kilobase were observed in DNA fragments from 50 genes (Wondji et al., 2007a). In *An. funestus* CYP gene duplications have been reported in mosquitoes (Wondji et al., 2009, Irving et al., 2012). Using positional cloning technique, Wondji and colleagues have established that the *An. funestus CYP6P9* is duplicated into *CYP6P9a* and *CYP6P9b* while *CYP6M1* is triplicated into *CYP6M1a*, *CYP6M1b* and *CYP6M1c*.

Allelic variants of P450s were also described for *P. polyxenes* (Wen et al., 2006). Of the two paralogous genes *CYP6B1* and *CYP6B3*, the former has three variants (*CYP6B1v1*, *CYP6B1v2* and *CYP6B1v3*) which differ significantly in their linear and angular-furanocoumarin metabolising properties compared to the two variants from the *CYP6B3*.

There is little evidence for alternative splicing of insect P450 transcripts as additional means of generating diversity (Feyereisen, 2012). But, a typical example is the *Cyp4d1* gene from *D. melanogaster* which utilizes two alternate first exons, and expressed sequence tags (ESTs) for each transcript. The first cDNA cloned (Gandhi et al., 1992) uses a proximal first exon and corresponds to transcript *Cyp4d1*-PA, whereas several ESTs of transcript *Cyp4d1*-PB use a more distal first exon instead.

1.6.5 Mechanism of Action of CYP450s

CYP450s occupy central position in biological system for their ability to activate inert C-H bonds (Shaik et al., 2005). The ability to catalyse regiospecific and stereospecific oxidative attack on

non-activated hydrocarbons at physiologic temperatures make these enzymes to be compared to a nature's '*blowtorch*' (Werck-Reichhart and Feyereisen, 2000). As a nanomachine P450 uses dioxygen and two reducing equivalents to catalyse a variety of stereospecific and regioselective oxygen insertion into diverse organic compounds (Shaik et al., 2005, De Montellano, 2005). There are some structural features that are common to all P450 isoforms. The active species of the enzyme is an iron ion ligated to a protoporphyrin IX macrocycle and two additional axial ligands: one, called proximal, is a thiolate from a cysteinate side residue of the protein, and the other, called distal, is a variable ligand which changes during the catalytic cycle of the enzyme and thereby activates the enzyme's main function (Shaik et al., 2005).

The oxidized P450 is a mixture of a low spin (Fe^{III}) form with water as the sixth coordinated ligand on the opposite side of the Cys thiolate ligand and a high spin (Fe^{II}) pentacoordinated form (Feyereisen, 2012). P450 cylce has a multi-step and cyclical nature comparable to a ticking clock (Munro et al., 2013). In a resting state (Figure 1.9, 12 o'clock) the ferric form has distal water ligand. Substrate binding displaces water from the sixth liganding position, leading to a shift to high spin (1:00h-1:30h). This shift can be observed at 390-435nm (Type I spectrum) and is accompanied by a decrease in the redox potential of P450. The P450–substrate complex receives a first electron from a redox partner (P450 reductase or adrenodoxin at 2:00h), and the ferrous P450 (Fe^{II}) then binds O_2 (3:30h) to form ferric superoxo intermediate (4:30h). At this step carbonmonoxide can compete with O_2 for binding to P450; its binding leads to a stable complex, with an absorption maximum at 450nm which is catalytically inactive. The P450–O_2–substrate complex then accepts a second electron (from P450 reductase or in some cases cytochrome b_5, or from adrenodoxin) to form a ferric peroxide anion (6:00h). This second reduction is believed to be, though not always, the rate-determining step in the catalytic cycle (Shaik et al., 2005).

After consecutive protonation, a ferric hydroperoxo complex (the so-called Compound 0 specie, 7:30h) then leads to the activated oxygen form(s) of the enzyme (Feyereisen, 2012). Compound 0 is a good Lewis base and can abstract an additional proton to generate Compound I

(Shaik et al., 2005). This intermediate (Compound I, 9:00h) is an iron (IV) oxo species with a delocalized oxidizing equivalent. Hydroxylation of an un-activated C–H bond therefore follows a "rebound" mechanism, where hydrogen is abstracted from the substrate forming an iron (IV) hydroxide that then recombines quickly with the substrate radical (Feyereisen, 2012). This species then transfers an oxygen atom to the substrate; in this case the alkane is converted thereby to an alcohol (11:00h). After this catalytic reaction the alcohol exits the pocket, water molecules enters and the enzyme is restored to the resting state by binding a water molecule (12 o'clock).

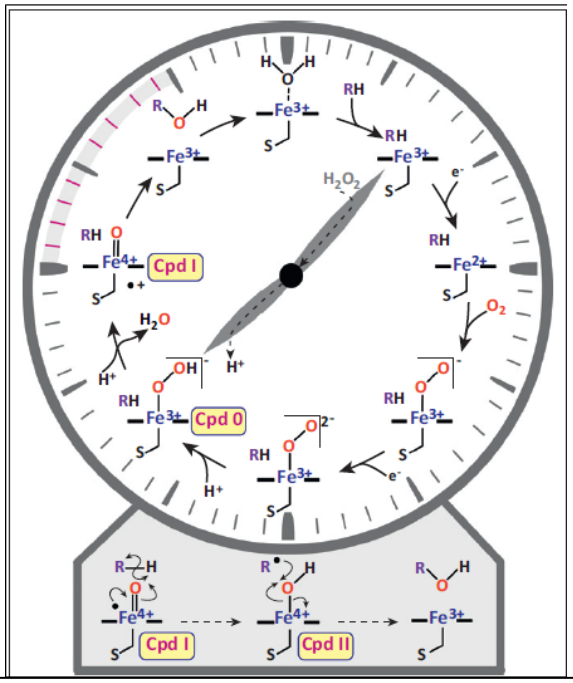

Figure 1.9: The P450 catalytic cycle clock and peroxide shunt pathway. The peroxide shunt pathway is depicted by the clock hands and uses H_2O_2 or related oxygen donors to directly generate compound 0 (7:30h) from the ferric substrate-bound form (1:30h). The oxygen rebound mechanism is in the base of the clock. This is an expansion of the highlighted portion between 9:00h (compound I) and 11:00h (hydroxylated product formation and release), and shows hydrogen abstraction from the substrate by compound I to form compound II (central image), prior to rebound of the hydroxyl to the substrate radical to form the hydroxylated product. Adapted from (Munro et al., 2013).

The efficiency of the catalytic cycle is dominated by a few key factors (Shaik et al., 2005). First is the donor ability of the thiolate ligand, which is referred to as the "push" effect (Dawson et al., 1976), and which seems to be crucial for the operation of the catalytic cycle. Second is the protonation and hydrogen-bonding machinery of the distal side that converts Cpd 0 into Cpd I and prevents the

generation of hydrogen peroxide and other oxygen wasting species ("uncoupling" processes that result in a loss of the reducing equivalents, NADH or NADPH) (Shaik et al., 2005). Third is the access of water molecules into the pocket, which needs to be well controlled. On one hand, water molecules seem to be important for protonation (Vidakovic et al., 1998), but on the other hand, too much of it leads to uncoupling (Raag et al., 1991). Finally, interaction of amino residues within the active site with the sulphur atom of the distal cysteinate ligand may enhance stability and activity (Shaik et al., 2005).

1.6.6 Redox Partners of Cytochrome P450s

The monooxygenation catalysed by P450s reaction requires a coupled and stepwise supply of electrons, which are derived from NAD(P)H and supplied via a redox partner (Paine et al., 2005). P450s can be divided into two major families (Class I and Class II) according to the different types of electron transfer systems they utilise (Figure 1.10). P450s in the Class I include bacterial and mitochondrial P450s, which use a two-component shuttle system consisting of an iron-sulfur protein (ferredoxin) and ferredoxin reductase. The Class II enzymes (microsomal P450s) receive electrons from a single membrane-bound enzyme, NADPH cytochrome P450 reductase (CPR), which contains FAD and FMN cofactors. Cytochrome b_5 may also couple with some members of the Class II P450s family to enhance the rate of catalysis. Although P450 redox partners are usually expressed independently, "self-sufficient" P450 systems have also evolved through the fusion of P450 and CPR genes. These fusion molecules are found in bacteria and fungi, e.g., the P450 *BM3*, a fatty acid ω-2 hydroxylase from *Bacillus megaterium,* which comprises a soluble P450 with a fused carboxyl terminal CPR module.

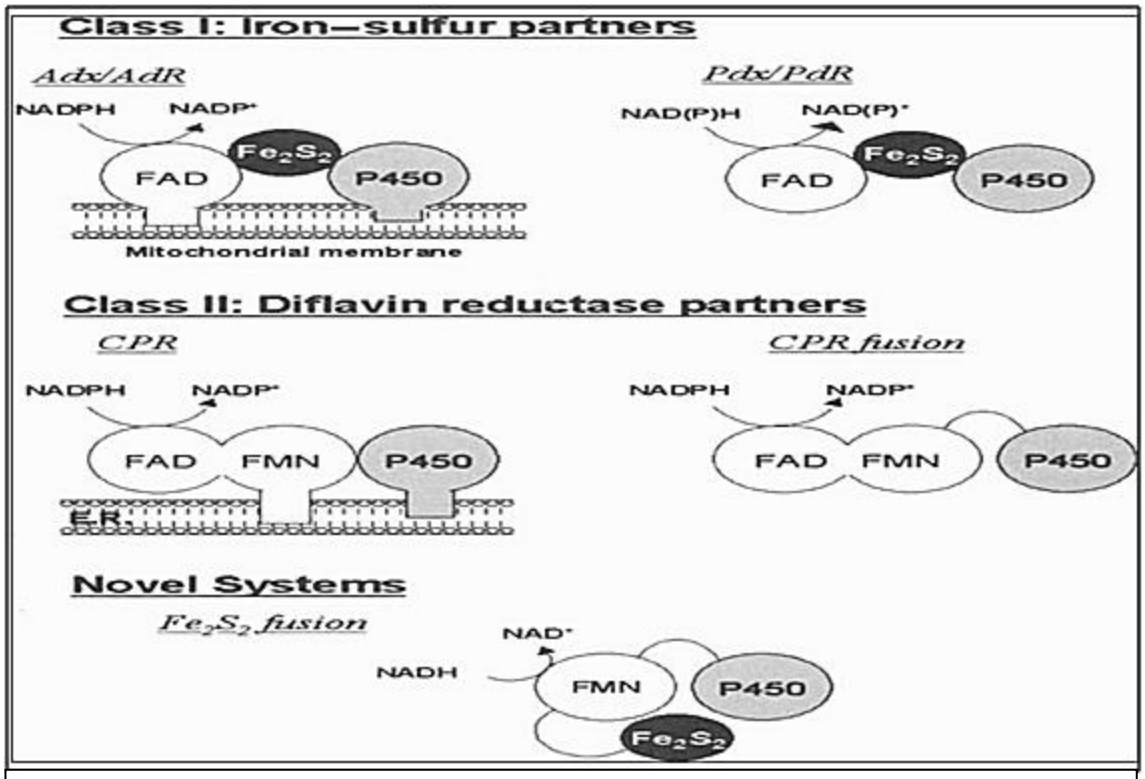

Figure 1.10: Electron transfer partners of cytochrome P450. In Class I systems, electrons are shuttled from NAD(P)H through an FAD-containing ferredoxin reductase and an iron-sulfur containing ferredoxin to P450; in prokaryotes these are typified by putidoredoxin reductase (PdR) and putidoredoxin (Pdx), and in eukaryotes by mitochondrial membrane associated adrenodoxin reductase (AdR) and adrenodoxin (Adx). Class II systems are driven by electrons delivered from NADPH through diflavin (FMN- and FAD-containing) reductases. In eukaryotes these are bound to the endoplasmic reticulum, while fused systems such as P450 BM3 exist in bacteria and fungi. Novel systems now include P450RhF, which contains an FMN-containing reductase fused with a ferredoxin-like centre and a P450. Adapted from (De Montellano, 2005, Paine et al., 2005).

1.6.6.1 NADPH Cytochrome P450 Oxidoreductase (CPR)

P450 reductase (EC 1.6.2.4) belongs to a family of flavoproteins utilizing both FAD and FMN as cofactors (Feyereisen, 2012). The P450 diflavin reductases emerged from the ancestral fusion of a gene coding for a ferredoxin reductase with its NADP(H) and FAD binding domains, with a gene coding for a flavodoxin with its FMN domain. The insect P450 reductases sequenced to date are orthologous to the mammalian P450 reductases, with an overall amino acid sequence identity of 54% for the house fly P450 reductase, first cloned and sequenced in 1993 (Koener et al., 1993).

Apart from plants, which contain multiple CPR genes (Benveniste et al., 1991) most organisms contain a single CPR gene (Urban et al., 1997). There is a single CPR gene in insect genomes, although

there are other diflavin reductases (Feyereisen, 2012). The housefly CPR gene codes for a protein of 671 amino acids and mapped to chromosome III and is 82% identical to the *D. melanogaster* CPR (Hovemann et al., 1997) and 75% identical to the CPR from *An. gambiae* (Nikou et al., 2003), which in turn is 96% identical to *An. funestus* CPR.

The insect, mammalian, and yeast enzymes are functionally interchangeable in reconstituted systems of the purified proteins or in heterologous expression systems (Feyereisen, 2012). CPR is responsible for transferring electrons to many naturally occurring electron acceptors, including P450 enzymes and cytochrome b_5 (Murataliev et al., 2004), as well as other redox proteins including cytochrome *c* (Williams and Kamin, 1962), heme oxygenase (Schacter et al., 1972), etc.

The microsomal P450 monooxygenase complex is localized to the endoplasmic reticulum membrane. Like P450, CPR contains an N-terminal hydrophobic region that spans the lipid membrane and anchors it to the surface (Paine et al., 2005). On membrane surface it is thought that CPR lies in such an orientation so that both the FMN and FAD/NADPH domains lie close to the membrane surface, which would allow optimal communication between the FMN and the P450 heme (Wang et al., 1997). Transient monooxygenase complexes are formed on the membrane surface as a result of collisions between P450s and CPR as each moves within the endoplasmic reticulum membrane with the phospholipid component of the membrane affecting intermolecular interactions of the monooxygenase complex and influencing substrate binding (Paine et al., 2005). Protein-protein interactions are also essential to enable electron transfer from the reduced FMN of the flavoprotein to the substrate-bound ferric form of the P450. Electrons are transferred from NADPH through the FAD and FMN coenzymes of CPR to the iron atom in the prosthetic heme group of the CYPs (Vermilion et al., 1981). The enzymes of diflavin reductases family have two tightly bound cofactors, FAD and FMN (Murataliev et al., 2004). These flavins participate in the transfer of the reducing equivalents from NADPH to the terminal electron acceptor (Figure 1.11). Two reducing equivalents are transferred from NADPH as a hydride ion, with FAD serving as the acceptor. Electrons are then transferred from FAD hydroquinone to the isoalloxazine ring of FMN, which in turn serves as a donor for one-electron

terminal acceptors. Diflavin reductases therefore serve to couple a two-electron donor (NADPH) with one-electron acceptors.

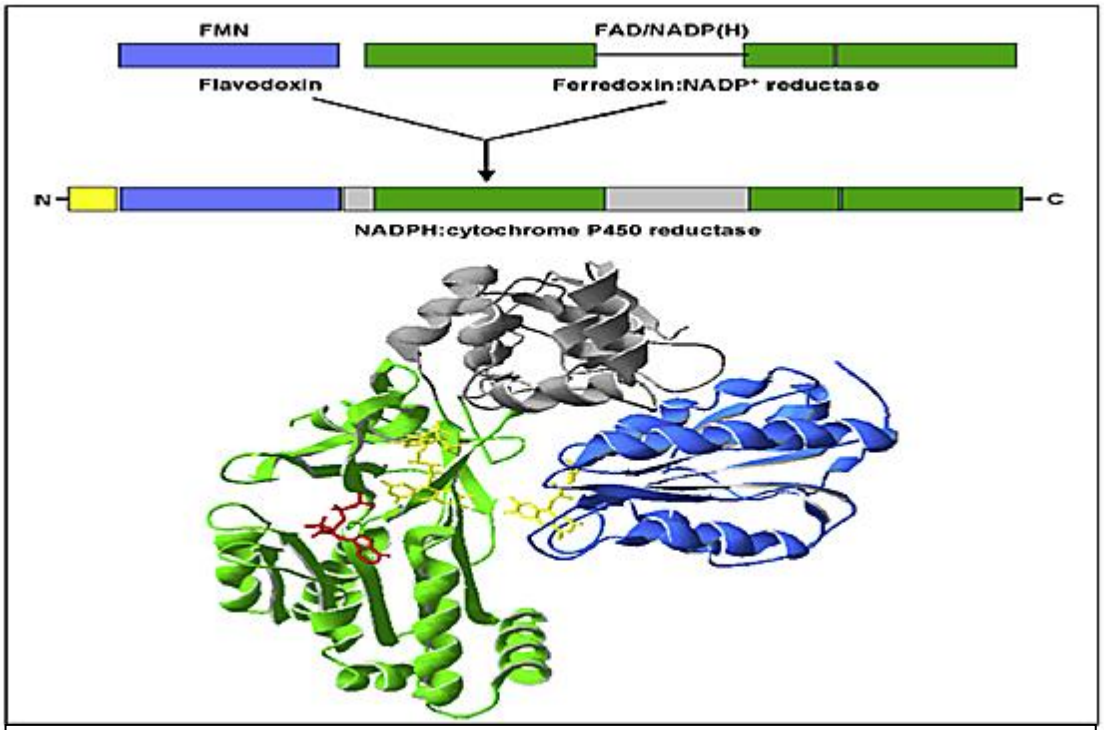

Figure 1.11: Domain architecture of microsomal P450 reductase. Top: Fusion of the genes of flavodoxin and ferredoxin reductase led to a flavoprotein containing both FAD and FMN cofactors bound to a single polypeptide chain. The N-terminal membrane anchor of P450 reductase is shown in yellow. Bottom: Domains of P450 reductase in the 3D structure. FAD/NADPH domain, green; FMN domain, blue; connecting domain, grey. Flavin cofactors are shown in yellow, $NADP^+$ in red. Adapted from (Murataliev et al., 2004, Feyereisen, 2012).

Since P450 is present in a 10-25-fold molar excess over CPR in the liver microsome (Estabrook et al., 1971, Paine et al., 2005, Backes and Kelley, 2003) and CPR orchestrates the recognition and reduction of not only multiple P450 isoforms but cytochrome b_5, cytochrome *c* and heme oxygenase as well (Kenaan et al., 2011), rapid association and dissociation of P450:CPR complexes is important for the system to work effectively (Paine et al., 2005). Several studies have found electrostatic interactions being the driving force behind the binding of P450 with CPR. Charge-pairing interactions between a small cluster of positively charged amino acid residues located on the surface of the side at which the prosthetic heme ligated to the P450 (proximal) and another cluster of negatively charged

amino acid residues located on the FMN domain of CPR is thought to drive the interaction between the P450s and CPR (Kenaan et al., 2011). A number of studies have established critical amino acid residues important for coupling of P450 with the CPR and transfer of electrons (Murataliev et al., 2004, Im and Waskell, 2011, Kenaan et al., 2011, Feyereisen, 2012).

1.6.6.2 Cytochrome b_5 (b_5)

Originally called cytochrome *m* (for microsomes) (Strittmatter and Ball, 1954) cytochrome b_5 was shown very early to be present in microsomes (Schenkman and Jansson, 2003), to contain protoporphyrin IX, not to bind CO, and to possibly serve as an electron transfer link between NADH and cytochrome *c* (Strittmatter and Ball, 1952). Cytochrome b_5 was originally discovered in *cecropia* silkworm larvae by Sanborn and Williams (Paine et al., 2005, Sanborn and Williams, 1950). b_5 is a small polypeptide (~17kDa) containing 129-134 residues, which are divided into an amino-terminal hydrophilic heme domain and a carboxyl-terminal hydrophobic membrane-binding region (Paine et al., 2005, Hlavica and Lewis, 2001, Mitoma and Ito, 1992). Like cytochromes P450 and CPR, b_5 is an integral membrane protein located on the cytosolic side of the endoplasmic reticulum where it is principally involved in lipid biosynthesis (Figure 1.12). It functions along with another ubiquitous electron transport protein cytochrome b_5 reductase (b_5R) as the electron donor to microsomal desaturases that synthesize unsaturated fatty acids, plasmalogens, and sterols (Vergeres and Waskell, 1995). b_5R is responsible for transferring electrons from NADH to b_5 in these reactions although NADPH can also be used as the electron donor in some cases (Gan et al., 2009); for b_5 can also accept electrons from an alternative reductase, CPR (Guengerich, 2005).

There is a single cytochrome b_5 gene in insect genomes (Feyereisen, 2012). *An. gambiae* cytochrome b_5 gene encodes 129 amino acids (Nikou et al., 2003) and its sequence is 58.1%, 53.5% and 94% identical with amino acid sequences of *D. melanogaster* (Kula et al., 1995), *Musca domestica* (Guzov et al., 1996) and *An. funestus* (Matambo et al., 2010) cytochrome b_5. In the endoplasmic reticulum, P450 and b_5 are found in approximately equal amounts (Dürr et al., 2007).

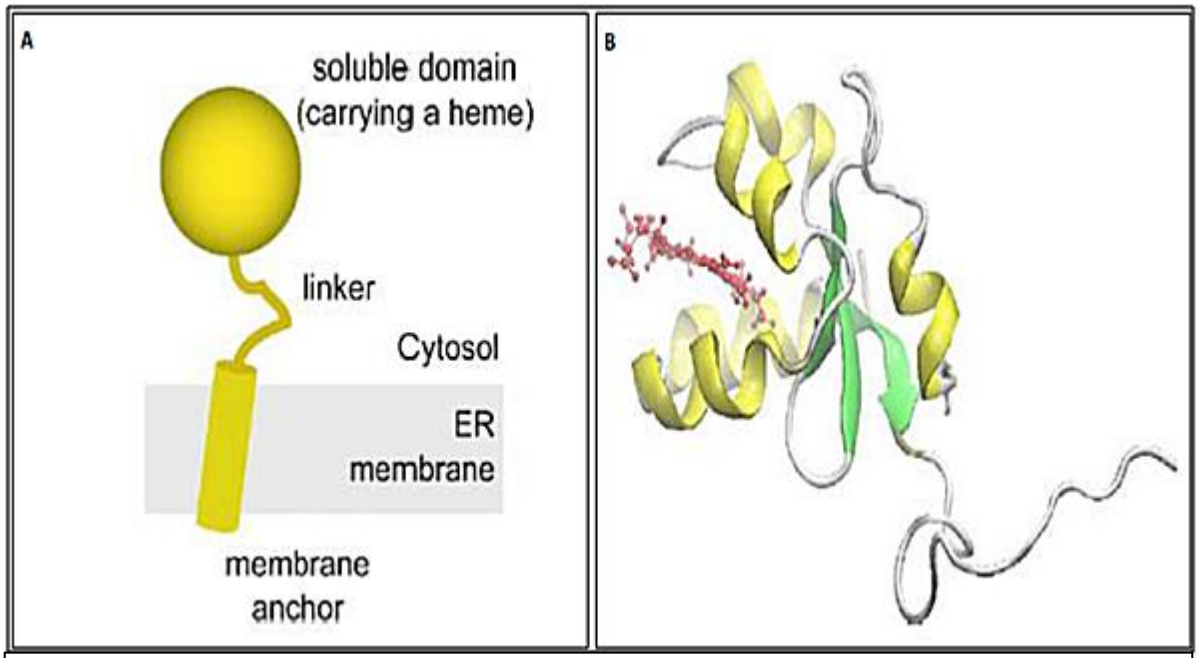

Figure 1.12: Topology and structure of *b_5*. (A) Topology of full-length *b_5*. (B) Structural elements of the soluble form of rabbit b_5, as seen in the solution-state NMR structure determination 1DO9. Shown in red is the heme prosthetic group which is held in the cleft between two helix–turn–helix motifs. These are 'tied together' by a three-stranded β-sheet (green). The C-terminal residues (lower right) are disordered in this structure; in full-length b_5 they form the link to the transmembrane anchor domain. Adapted from (Dürr et al., 2007).

b_5 is important for P450 catalysis. After binding oxygen, the oxyferrous protein of CYP2B4 accepts a second electron which is provided by either CPR or b_5. When the second electron is donated by b_5 product formation is ~10 to 100-fold faster (Im and Waskell, 2011) (Figure 1.13). Presence of b_5 allows less time for side products formation (hydrogen peroxide and superoxide) and improves by ~15% the coupling of NADPH consumption to product formation. Cytochrome b_5 thus acts as obligate electron donor (Schenkman and Jansson, 2003).

However, depending on the P450 enzyme and on the reaction catalysed, b_5 may be inhibitory, or without effect, or its presence may be obligatory (Feyereisen, 2012). Cytochrome b_5 can have a quantitative effect on overall reaction rates, and/or a qualitative role on the type of reaction catalysed and the ratio of the reaction products.

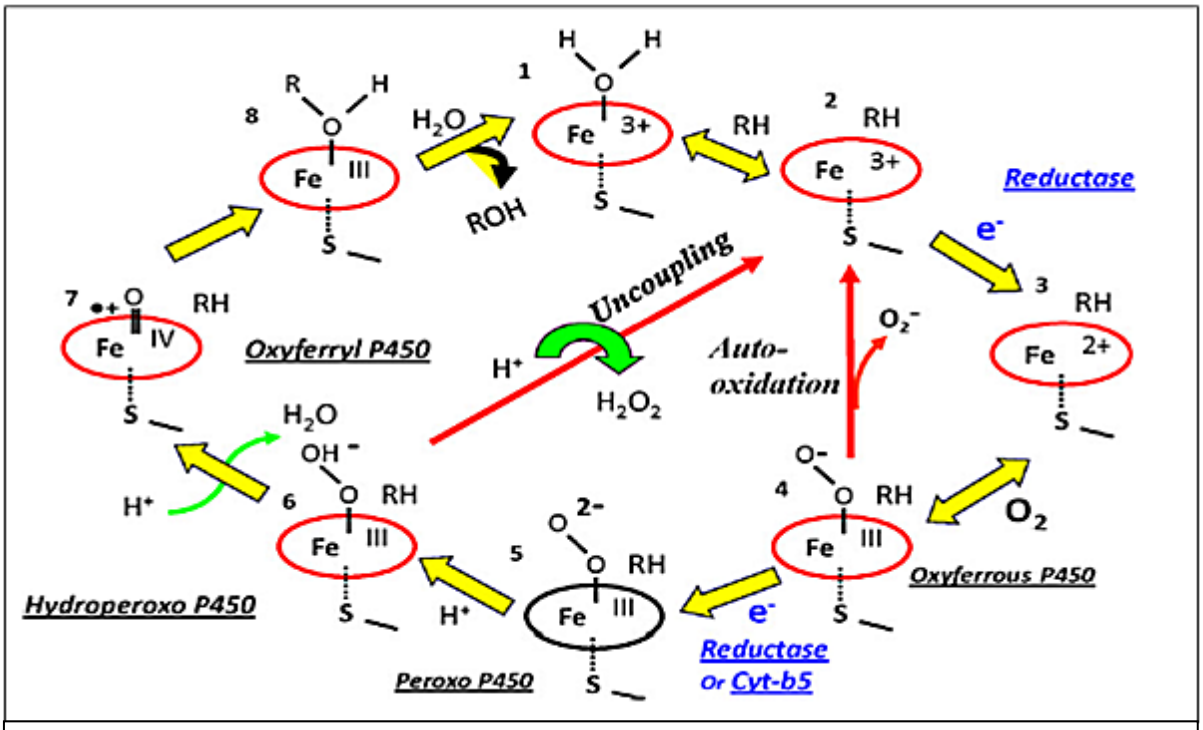

Figure 1.13: Catalytic cycle of P450s; role of CPR and b_5. Adapted from (Im and Waskell, 2011).

The role of b_5 may or may not depend on its electron transfer properties. It can influence the overall stoichiometry of the P450 reaction, in particular the "coupling rate" (the utilisation and fate of electrons from the NADPH). b_5 has been shown to compete with the CPR for the binding site on the proximal face of CYP2B4 (Im and Waskell, 2011). In this respect, at low molar ratios (<1) of b_5 to CPR, the more rapid catalysis results in enhanced substrate metabolism. In contrast, at high molar ratios (>1) of b_5 to CPR, b_5 inhibits activity by binding to the proximal surface of the P450s, preventing the reductase from reducing ferric cytochrome P450 to the ferrous protein effectively.

Cytochrome b_5 can also have effector role in the cytochrome P450 monooxygenase reaction (Imai and Sato, 1977, Hlavica, 1984). The b_5 binds and causes structural changes to human CYP3A4 which impact upon the redox changes of the P450 (Schenkman and Jansson, 2003). In reconstituted system, in the presence of testosterone or nifedipine, input of the first electron from NADPH to the monooxygenase (ferric to ferrous state) and product formation were negligible in the absence of b_5 (Yamazaki et al., 1995). Also, apo-b_5 was as effective as the holoprotein in supporting reduction of

CYP3A4 and product formation indicating that the role of b_5 did not require it to undergo redox changes or to transfer an electron to the P450 (Yamazaki et al., 1996). Like CPR, it is generally accepted that charge-pair interactions drive the formation of P450:b_5 complexes (Paine et al., 2005). Indeed, b_5 and CPR were discovered to bind to the basic, positively-charged residues on the proximal surface of CYP2B4 on unique but overlapping sites (Im and Waskell, 2011).

1.7 Molecular Basis of Monooxygenase-mediated Insecticide Resistance

1.7.1 Introduction

Metabolic resistance like moonoxygenase-mediated ones is more important than target-site insensitivity, for the detoxification has the potential to confer cross-resistance to toxins independent of their target sites (Scott, 1999, Dadd et al., 1985). Overexpression of a particular P450 is not necessarily an indicator of the involvement of same P450 in resistance. A typical P450 should only be considered to be involved in resistance if the following two criteria are met (Scott et al., 1998b): (1) the P450 must be shown to detoxify (or sequester) the compound to which the strain has resistance to, and (2) the resistant strain should have a greater amount of this P450, or the protein coded for by the resistant strain allele should be shown to have a greater catalytic activity (i.e. detoxification) compared to the protein coded for by the susceptible strain allele. In essence, there should be overexpression of the protein and increased detoxification of the insecticide (Liu and Scott, 1998) which can occur by *cis*- and *trans*- regulation of the transcription process. Thus, it is possible that insecticide resistance as a trait could map to a location in the genome that is different from the P450, which is involved in the detoxification (Scott, 1999). It is also noteworthy that the factor(s) responsible for *trans*- regulation of the P450(s) involved in resistance also appear capable of regulating the expression of other P450s that are not necessarily involved in resistance (at least in house flies). Knowing which subsets of P450s are elevated by the same regulatory factor(s) may help to understand cross-resistance patterns.

P450s operate in concert with redox partners, CPR and b_5 and thus enhancement of metabolism can potentially be acquired via multiple pathways (Schuler and Berenbaum, 2013). Schuler and Berenbaum summarised different resistance mechanism that could function at the transcriptional level: (i) higher constitutive production of transcripts due primarily to mutations in promoter sequences, (ii) higher inducible expression of transcripts due primarily to mutations in *trans*-acting factors or their signalling cascades (iii) and/or greater responsiveness to transcriptional inducers in food sources and/or environment; at the protein level: (iv) mutations in catalytic site residues which affect the range or rate of substrate metabolism, (v) mutations in the substrate access channel residues that affect substrate entry, (vi) mutations in the proximal surface residues that affect electron transfer from CPR and/or b_5, (vii) mutations in these interacting partners that affect coupling and electron delivery.

1.7.2 Distribution of Insecticide Resistance in *An. funestus* across Africa

To date, *An. funestus* has been shown resistant to major insecticides used in public health across Africa (Dia et al., 2013, Brown, 1986, Ranson et al., 2011, Coetzee and Koekemoer, 2013, Wondji et al., 2009, Wondji et al., 2012) (See Table 1.3 and Figure 1.14). However, pattern of resistance to insecticides differ across regions of Africa and this may have impact on insecticide resistance management strategies, because variation in the resistance pattern makes extrapolation from one locality to another, one region to another,or one country to another not feasible.

1.7.2.1 Southern Africa:

First report of pyrethroid resistance in *An. funestus* was in South Africa. After ~40 years of annual spray with DDT and eradication of *An. funestus* from South Africa, a switch to pyrethroid deltamethrin in Kwazulu/Natal (KZN) Province of South Africa in 1996 resulted in six-fold increase in malaria incidence by 1999 (Hargreaves et al., 2000). The surge in malaria incidence in KZN was due to a highly endophilic *An. funestus,* established to be resistant to pyrethroid insecticides. Thereafter, in

2001 Brooke (Brooke et al., 2001) reported high Type II pyrethroids and propoxur resistance in *An. funestus* from southern Mozambique, and in 2006 *An. funestus* highly resistant to Type II pyrethroids deltamethrin and ʎ-cyahalothrin were described from southern Mozambique (Casimiro et al., 2006). The population from Mozambique were also resistant to permethrin and marginally resistant to bendiocarb and propoxur, but fully susceptible to malathion and DDT.

Since then rapidly growing resistance to pyrethroids insecticides (Coetzee et al., 2013) as well as multiple resistant populations of *An. funestus* have been continuously reported in southern Africa. For example, Cuamba and colleagues in 2010 reported highly pyrethroid resistant populations of *An. funestus* from Chokwe, Mozambique (Cuamba et al., 2010), a region from which pyrethroid susceptibility have been described by Casimiro (Casimiro et al., 2006). In Malawi, high and multiple resistance to pyrethroids permethrin and deltamethrin as well as carbamates bendiocarb and propoxur were reported in 2010 (Hunt et al., 2010) in *An. funestus* population that are in turn fully susceptible to malathion, fenitrothion, pirimiphos methyl, dieldrin and DDT. A contrasting pattern of resistance was observed in Zambian populations of *An. funestus* (Chanda et al., 2011) that were found to be pyrethroid and DDT-resistant but susceptible to malathion consistent with other southern African populations. The Zambian population were also susceptible to bendiocarb in contrast to the Malawian and Mozambican populations described above.

The increase in pyrethroid resistance in *An. funestus* became finally selected: “pyrethroid resistance has been selected in Malawi over the last 3 years in the two major malaria vectors *An. gambiae* and *An. funestus*, with a higher frequency of resistance in the latter” (Wondji et al., 2012). Wondji and colleagues found that *An. funestus* from the Chikwawa, Malawi are resistant to the carbamate, bendiocarb and three pyrethroids (permethrin, deltamethrin and λ-cyhalothrin) and susceptible to DDT and pirimiphos methyl. This pattern of pyrethroid resistance for permethrin and deltamethrin was further confirmed in *An. funestus* population from Malawi and Mozambique, with Mozambican population exhibiting higher resistance with no mortality recorded after 1h, 30 minutes exposure to discriminating dose of pyrethroids (Riveron et al., 2013).

Table 1.3 Mechanism of resistance in *An. funestus* to main insecticide used in public health

Country	Insecticides	Resistance Mechanism	Reference
South Africa	Pyrethroids, Type II	N.D.	(Hargreaves et al., 2000)
Mozambique	Pyrethroids, Type I and II, propoxur	Mixed function oxidases	(Brooke et al., 2001)
Mozambique	Pyrethroids, Type I and II, bendiocarb, propoxur	Mixed function oxidases	(Casimiro et al., 2006)
Mozambique	Pyrethroids, Type I and II	P450 monoxygenases: *CYP6P9a*, *CYP6P9b*	(Cuamba et al., 2010)
Malawi	Pyrethroids, Type I and II, bendiocarb, propoxur	N.D.	(Hunt et al., 2010)
Zambia	Pyrethroids, Type I and II, DDT	N.D.	(Chanda et al., 2011)
Malawi	Pyrethroids, Type I and II, bendiocarb	P450 monoxygenases: *CYP6P9a*, *CYP6P9b*	(Wondji et al., 2012)
Uganda	Pyrethroids, Type I and II, DDT	P450 monoxygenases: *CYP6P9a*, *CYP6P9b*	(Morgan et al., 2010)
Kenya	Pyrethroids, Type I and II, DDT	Mixed function oxidases	(McCann et al., 2014), (Kawada et al., 2011)
Uganda	Pyrethroids, Type I and II, DDT	P450 monoxygenases: *CYP6P9a*, *CYP6P9b*	(Mulamba et al., 2014b)
Ghana	Pyrethroids, Type I, DDT	Mixed function oxidases	(Okoye et al., 2008)
Ghana	Bendiocarb, DDT	N.D.	(Hunt et al., 2011)
Burkina Faso	Dieldrin	Rdl mutation	(Dabire et al., 2007), (Wondji et al., 2011)
Benin	Pyrethroids, Type I and II, DDT, bendiocarb	P450 monoxygenases: *CYP6P9a*, *CYP6P9b, CYP6Z1; GSTs: GSTδ1_5, GSTe2*	(Djouaka et al., 2011)
Benin	Pyrethroids, Type I, DDT	*GSTe2*	(Riveron et al., 2014b)

N.D. Resistance mechanism not determined.

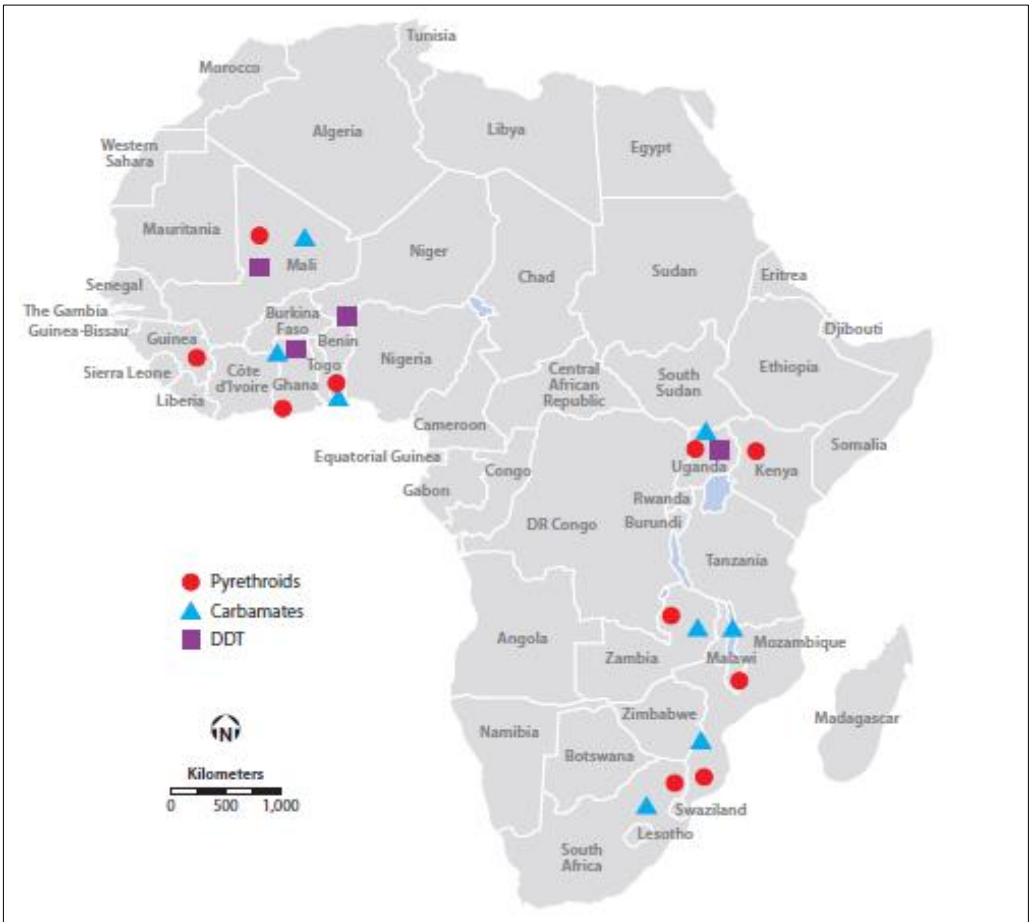

Figure 1.14: Insecticide resistance in *An. funestus* in Africa. Symbols indicate the presence of resistance in a country, and their position is not representative of actual geographical sites. Abbreviation: DDT, dichlorodiphenyltrichloroethane; DR Congo, Democratic Republic of the Congo. Adapted from (Coetzee and Koekemoer, 2013).

These and other studies not cited established that southern African *An. funestus* (from Malawi, Mozambique and Zambia) are resistant to pyrethroids and the resistance had been steeply increasing. While Malawian and Mozambican populations were resistant to carbamates bendiocarb and propoxur but susceptible to DDT, in contrast, Zambian population were resistant to DDT but susceptible to bendiocarb (Coetzee and Koekemoer, 2013). And all populations from these three countries were fully sensitive to organophosphate malathion and organochlorine dieldrin.

1.7.2.2 East Africa

Prior to 2010 there was no in-depth report on the resistance status of *An. funestus* to major insecticides used in public health in Uganda. In 2010, pyrethroid resistance was described in *An. funestus* from Uganda (Morgan et al., 2010). The population from Tororo was highly resistant to pyrethroids, marginally resistant to DDT, but fully susceptible to carbamate bendiocarb and organophosphates malathion and organochlorine dieldrin. Pyrethroids (permethrin and deltamethrin) and DDT resistance was reported as well in some populations of *An. funestus* from Masindi, north-western Uganda (Mulamba et al., 2014a) confirming the observations of Morgan and colleagues. This pattern of resistance was confirmed as increasing across Uganda and in Kisumu, western Kenya. Widespread resistance to Type I and Type II pyrethroids and DDT was recently confirmed by Mulamba and colleagues (Mulamba et al., 2014b) in *An. funestus* from several localities across Uganda, as well as populations from Kisumu, Kenya. However, as observed in the previous studies full susceptibility to bendiocarb, malathion and dieldrin was reported in these Ugandan and Kenyan populations.

After long term implementation of insecticide treated bed nets in western Kenya, *An. funestus* re-emerged as a major malarial vector in 2008 (McCann et al., 2014) with high infection rate and resistance to permethrin and deltamethrin, with mortalities lower than obtained with *An. gambiae* from the same locality.

1.7.2.3 West and Central Africa

Reliable literature on resistance status of *An. funestus* from West and Central Africa is only published from studies carried out in Benin, Ghana, Burkina Faso and Cameroon (Coetzee and Koekemoer, 2013).

In Ghana, in 2006 *An. funestu*s and *An. gambiae* were described as the major vector species in Obuasi gold mine (Coetzee et al., 2006) with the *An. funestus* from the study resistant to DDT and bendiocarb but susceptible to pyrethroids and malathion. A follow up study in this locality (Okoye et al., 2008) confirmed DDT resistance and discovered in addition resistance to permethrin. Further studies documented pyrethroid resistance in other regions of Ghana including Kassena-Nankana district (Anto et al., 2009) and four other localities were resistance to bendiocarb and DDT was discovered (Hunt et al., 2011). However, the populations tested from all localities by Hunt and colleagues were 100% susceptible to deltamethrin and malathion.

In contrast, in Burkina Faso study carried out in three sites confirmed that *An. funestus* populations were resistant to dieldrin but susceptible to pyrethroids and DDT (Dabire et al., 2007). Few years later another study published a result in agreement with the previous observation. In *An. funestus* populations from Burkina Faso and Cameroon, Wondji and colleagues (Wondji et al., 2011) reported high dieldrin resistance while Southern (Malawi and Mozambique) and East African (Ugandan) populations were fully susceptible to this insecticide. However, within the last few decades few researches have been conducted in Burkina Faso, Cameroon and other neighbouring West African countries to establish resistance status of *An. funestus* populations toward pyrethroids and other insecticides used in public health.

In 2011 multiple resistant populations of *An. funestus* were reported in Pahou, southern Benin, West Africa (Djouaka et al., 2011). In contrast with the findings in most southern African populations (susceptibility to DDT and high resistance to Type I and Type II pyrethroids), the

population from Benin were highly resistant to DDT with no mortality in females at all after one hour exposure. The population were also resistant to permethrin and deltamethrin (moderate), as well as bendiocarb. In line with the observations from Burkina Faso and Cameroon, the population from Benin exhibited moderate resistance to dieldrin as well. Full susceptibility to malathion was observed in line with the observation all across Africa. Further study in population of *An. funestus* from Kpome, Benin Republic and Gounougou, Cameroon confirmed that the populations from Kpome were highly resistant to DDT (just like in Pahou), and revealed moderate resistance to the organochlorine in the population from Gounougou, Cameroon (Riveron et al., 2014b).

In essence, across Africa, insecticide resistance in *An. funestus* show contrasting pattern and is increasing (Nkya et al., 2013), possibly due to selection pressure from agricultural practices and escalated usage of insecticides used in public health related vector controls.

1.7.3 Role of Cytochrome P450s in Insecticide Resistance in *An. funestus*

To date no *kdr* mutation has been detected in *An. funestus* (Hemingway, 2014, Coetzee and Koekemoer, 2013); rather, metabolic resistance caused by increased activity of P450s appears to be the major resistance mechanism both in laboratory and field populations of *An. funestus* (Corbel and N'Guessan, 2013, Coetzee and Koekemoer, 2013). In the beginning synergist assays and biochemical analyses were used to identify involvement of P450 resistance mechanisms (see Table 1.3); however, within the last ten years molecular analyses are increasingly used for identification and confirmation of P450 involvement in resistance especially to pyrethroids, in addition to other mechanisms.

In Southern Africa (Mozambique), synergist assays with piperonyl butoxide (PBO) and biochemical analysis suggested elevated levels of mixed function oxidases in *An. funestus* from Mozambique that are highly resistant to Type II pyrethroids and propoxur (Brooke et al., 2001). Thereafter, biochemical analysis revealed high levels of mixed function oxidases in multiple resistant populations of *An. funestus* from southern Mozambique (Casimiro et al., 2006). Since the population studied by Casimiro and colleagues were highly resistant to pyrethroids and marginally resistant to

bendiocarb and propoxur, monooxygenases were suspected to confer cross resistance to more than one class of insecticide. Further studies linked pyrethroid resistance to elevated levels of monooxygenases in Mozambique a year later (Casimiro et al., 2007).

Molecular tools were also applied to unveil the mechanism of pyrethroid resistance in *An. funestus* populations. Quantitative trait locus (QTL) mapping using resistant (FUMOZ-R) and pyrethroid susceptible (FANG) strains identified three pyrethroid resistance locus on chromosomes 2R, 2L and 3L (Wondji et al., 2007b) with the major one named *rp1* (resistance to permethrin 1) spanning a cluster of CYP6 genes. The *rp1* locus explained the bulk of pyrethroid resistance phenotype in FUMOZ-R *An. funestus* (Wondji et al., 2007a, Amenya et al., 2008). In 2009, Wondji and colleagues reported that the *rp1* QTL compose of 14 proteins coding genes of which 10 are P450s from CYP6 family and four of these genes (*CYP6P9*, *CYP6P4*, *CYP6AA4* and *CYP6P1*) are overexpressed in pyrethroid resistant *An. funestus* in comparison with the fully susceptible laboratory strain, FANG (Wondji et al., 2009). These findings suggested that P450 genes and their duplication could contribute to pyrethroid resistance in *An. funestus* adding another twist to the already complex pyrethroid resistance pattern in *An. funestus*. Another positional cloning approach was used by Wondji and colleagues (Irving et al., 2012) to identify genes conferring resistance in the uncharacterised *rp2* (resistance to pyrethroids 2) QTL in *An. funestus*. Apart from high number of SNP and triplication of *CYP6M1* observed in the *rp2* locus, gene expression profiling and validation indicated significant overexpression in the resistant FUMOZ-R strain of P450s *CYP6Z1*, *CYP6Z3* and *CYP6M7*.

Using *An. gambiae* 'detox chip' Christian and colleagues (Christian et al., 2011) investigated the genes up-regulated in male and female pyrethroid resistant *An. funestus* from southern Africa (Mozambique) and discovered three genes *CYP6P9*, *cytochrome oxidase* I (*CO*I) and *CYP6M7* as significantly, differentially overexpressed compared with FANG. This confirmed the observations made by Wondji and colleagues.

Meanwhile in 2010 Cuamba and colleagues reported involvement of *CYP6P9a* and *CYP6P9b* in resistance in a highly pyrethroid resistant populations of *An. funestus* from Chokwe, Mozambique

(Cuamba et al., 2010). Transcription profiling revealed *CYP6P9a* and *CYP6P9b* as overexpressed compared with the susceptible laboratory colony KELA from Mali. The same year in Uganda (East Africa) biochemical and transcriptional analysis of the Tororo *Anophele funestus* revealed the P450 *CYP6P9b* 12 times overexpressed compared with the FANG (Morgan et al., 2010). The Tororo population studied were highly resistant to pyrethroids but fully susceptible to carbamate bendiocarb and malathion and dieldrin. Still in Uganda, recently (Mulamba et al., 2014b) synergist assays and transcriptional analysis implicated metabolic resistance through elevated P450 monooxygenases in play, with *CYP6P9a* and *CYP6P9b* overexpressed in *An. funestus* resistant to Type I and Type II pyrethroids as well as DDT, compared with the FANG. In neighbouring Kenya (Kawada et al., 2011) widespread pyrethroid resistance was also reported in *An. funestus* with the involvement of metabolic resistance suspected from synergy assay with PBO.

In West Africa biochemical and transcriptional analysis of *An. funestus* from Benin (Djouaka et al., 2011) implicated *CYP6P9a*, *CYP6P9b* as well as *CYP6Z1* from resistant individuals as overexpressed compared with the laboratory susceptible strain, FANG. The *CYP6P9a* and *CYP6P9b* were found to be overexpressed in pyrethroid and DDT resistant mosquitoes compared with FANG, but with lesser overexpression compared with resistant populations from Southern Africa.

In 2012, Wondji and colleagues (Wondji et al., 2012) reported multiple resistance to pyrethroids and bendiocarb in *An. funestus* from Malawi and described the pyrethroid resistance in Malawi and Mozambique as metabolically-based. Biochemical assays in these resistant mosquitoes revealed that the pyrethroid resistance was metabolically-based and together with the transcription analysis implicated *CYP6P9a* and *CYP6P9b* overexpressed, as the major pyrethroid resistance genes in *An. funestus* from Southern Africa.

Further studies using genome-wide transcription analysis (microarrays) established consistent overexpression of duplicated P450s *CYP6P9a* and *CYP6P9b* in southern African (Malawi and Mozambique) populations of *An. funestus* compared with FANG (Riveron et al., 2013). The involvement of these P450s in pyrethroid resistance was validated via *in vitro* and *in vivo* functional

characterisation (Riveron et al., 2013, Riveron et al., 2014a). Analysis of sequences of *CYP6P9a* and *CYP6P9b* cDNA sequences Malawi and Mozambique revealed that the southern African alleles possessed significantly lower polymorphisms with reduced nucleotides substitutions compared with sequences from FANG which are highly polymorphic. Haplotypes from the southern African alleles formed clade together excluding sequences from FANG. The resistant alleles from southern Africa were described as undergoing directional selection with beneficial mutations selected and as such Malawi and Mozambique sequences of *CYP6P9a* and *CYP6P9b* share a group of intra-allelic amino acid substitutions in common which makes them different from FANG. Thus, in addition to overexpression and duplication, allelic variations in the coding regions of these major pyrethroid resistance genes could also impact on pattern of resistance in *An. funestus* populations from Africa.

Even though DDT and carbamate resistance observed across Africa is suspected to be monooxygenase mediated, in *An. Funestus,* to date, no single P450 has been characterised and validated as responsible for the resistance to either of these insecticides. For carbamate resistance PBO synergist assays have been used to show the potential role of monoxygenase, and for DDT resistance as well, no P450 has been confirmed as responsible for it, though *CYP6P9a*, *CYP6P9b* and *CYP6Z1* has been shown to be overexpressed in Benin populations that are resistant to DDT, carbamates as well as pyrethroids (Djouaka et al., 2011).

1.8 Hypothesis

The duplicated P450s *CYP6P9a* and *CYP6P9b* are overexpressed in resistant strains of *An. funestus* across Africa compared to the corresponding genes from the insecticide-susceptible strain, FANG. The two genes from southern African populations of *An. funestus* exhibited extensive allelic polymorphism in their coding regions compared with the FANG. The significant polymorphism patterns observed suggests that allelic variation in both genes could be one of the main mechanisms conferring resistance in these populations. Our hypothesis is that such allelic variations, in addition to overexpression is one of the main factors driving pyrethroid resistance. Specifically, variation in the

amino acid sequences in the coding regions of these genes may confer higher pyrethroids metabolizing efficiency. A handful of candidate P450s from the other well characterised QTLs, were also suspected to be able to metabolise pyrethroids and possibly confer cross-resistance to other classes of insecticides, especially DDT and bendiocarb. These include *CYP6M7* from *rp2* QTL in the light of its being overexpressed in multiple resistant *An. funestus s.s.* from southern Africa and *CYP6Z1* overexpressed in southern and West African populations. Other genes commonly overexpressed in southern African populations that are resistant to pyrethroids, carbamate and organochlorine insecticides include *CYP9J11* from *rp3* and *CYP6AA4* from the *rp1* QTLs. The potential role of these genes in pyrethroid metabolism and cross resistance to other insecticides used in public health will be elucidated in this study.

1.9 Aim and Objectives

The main aim of this study is to elucidate the molecular mechanisms through which P450 genes confer pyrethroid resistance or cross resistance to other insecticides, in the major malaria vector *An. funestus s.s.,* using functional characterisation approaches.

More specifically, the objectives of this study were:

(i) to investigate the impact of allelic variation in two genes (*CYP6P9a* and *CYP6P9b*) on pattern of pyrethroid resistance in *An. funestus* through polymorphism survey and *in silico* prediction of activity; (ii) to assess the metabolic efficiency of the alleles of *CYP6P9a* and *CYP6P9b* using heterologous expression and functional characterisation in order to find out if allelic variation is impacting their metabolic activities; (iii) to detect causative mutation(s) linked with pyrethroid resistance, with the aim to design a DNA-based diagnostic tools that will allow detection of the mutation(s) in the field population of *An. funestus,* and (iv) to identify candidate cross-resistance detoxification genes that can metabolize Type I and Type II pyrethroids as well as other non-pyrethroid insecticides, for example carbamates (bendiocarb and propoxur) and organochlorine (DDT).

2. POLYMORPHISM SURVEY AND PREDICTION OF IMPACT BY MODELLING AND DOCKING SIMULATIONS

2.1 Background

With the *kdr* type mutation in the VGSC not yet selected in *An. funestus s.s.* (Amenya et al., 2008, Hemingway, 2014), resistance to pyrethroids is mainly metabolic and mediated by detoxification enzymes-P450 monoxoygenases (Coetzee and Koekemoer, 2013, Wondji et al., 2012). QTL mapping (Wondji et al., 2007b) identified a major pyrethroid resistance locus on chromosome arm 2R which coincides with cluster of *CYP6* genes (Amenya et al., 2008). This *rp1* QTL which explained 87% of genetic variance in pyrethroid susceptibility in two families from reciprocal crosses between susceptible and resistant strains (Wondji et al., 2009), encoded 14 protein coding genes, 10 of which are cytochrome P450s. Two of these P450s *CYP6P9* and *CYP6P4,* which were found to be 25 and 51 times overexpressed in resistant females *An. funestus s.s.,* were also found to be tandemly duplicated in the BAC clone as well as laboratory and field samples, suggesting that this P450 duplication could contribute to pyrethroid resistance. Since then, the duplicated *CYP6P9* (*CYP6P9a* and *CYP6P9b*) were found to be highly overexpressed in resistant populations of *An. funestus s.s.* compared with the fully insecticide susceptible population (FANG), in southern Africa: including Mozambique (Cuamba et al., 2010, Christian et al., 2011, Riveron et al., 2013); Malawi (Wondji et al., 2012, Riveron et al., 2013) and Zambia (Riveron et al., 2014a). The genes were also found to be overexpressed in resistant populations of *An. funestus s.s*. from Benin, West Africa (Djouaka et al., 2011) and Uganda, East Africa (Morgan et al., 2010), compared with FANG, though with lower fold change. Overexpression of *CYP6P9a* and *CYP6P9b* was described as the major mechanism driving pyrethroid resistance in southern Africa (Riveron et al., 2013). The two genes from resistance strains were discovered to be undergoing directional selection in the southern African population of *An. funestus s.s.* (Riveron et al., 2013, Wondji et al., 2012) and exhibited extensive allelic polymorphisms (Riveron et al., 2013). The copy number variation in the coding regions of *CYP6P9a* and *CYP6P9b* could be impacting metabolic activity of the genes toward pyrethroid insecticides, augmenting resistance. Pyrethroid resistance

profiles in *An. funestus s.s.* varied across African continent (Cuamba et al., 2010, Djouaka et al., 2011, Riveron et al., 2013, Morgan et al., 2010) and it possibly mirrors the polymorphism variation in the major resistance genes *CYP6P9a* and *CYP6P9b*.

In silico homology modelling and docking simulations could be utilised to predict the potential impact of such polymorphisms in the activity of these P450s. This is because three-dimensional (3D) structure prediction using modelling and molecular docking of ligand insecticides into the active site of the models can help elucidate potential binding sites (Zhou and Johnson, 1999) and predict substrate specificity (De Rienzo et al., 2000), as well as key amino acid residues within contact distance of the substrate. Narrowing down the potential amino acid replacements that could impact on pyrethroid activity can help tailor the next set of experiments (e.g. functional characterisation and site-directed mutagenesis) to be done for fast validation and facilitate design of proper diagnostic tools that could allow for the detection of such mutations in the field. In terms of structure-activity relationship predictions modelling and docking simulations have been applied to predict interaction of pyrethroid insecticides with the insect P450s, including *An. gambiae CYP6M2* (Stevenson et al., 2011), *An. minimus CYP6AA3*, *CYP6AA7* and *CYP6AA8* (Lertkiatmongkol et al., 2011), as well as *Ae. aegypti CYP6Z8* (Chandor-Proust et al., 2013).

2.2 Objectives

This chapter aims at describing sequence characterisation of *CYP6P9a* and *CYP6P9b* and to map across Africa the polymorphisms and mutations that make the *CYP6P9a* and *CYP6P9b* genes from resistant and susceptible strain of *An. funestus* different. It also aims at predicting the potential impact of such polymorphism in the ability of these genes to confer pyrethroid resistance using homology models of these genes, molecular docking simulations and prediction of substrate access/products egress channels.

2.3 Methods

2.3.1 Mosquito Strains

Mosquito strains from different regions of Africa with different resistance profiles and the fully susceptible, laboratory strain, FANG (*An. funestus* from Angola) were used in this study. The FANG strain originated from Calueque, southern Angola: 16˚45'S, 15˚7'E and had been colonised in laboratory since 2002 (Hunt et al., 2005, Wondji et al., 2005). The field strains were collected from Pahou (6˚23'N, 2˚13'E), southern Benin Republic (Djouaka et al., 2011), Tororo district (0˚45'N, 34˚5'E), eastern Uganda (Morgan et al., 2010), Tihuquine, Chokwe district (24˚33'S, 33˚01'E), in southern Mozambique (Cuamba et al., 2010), Chikwawa (12˚19'S, 34˚01'E), Malawi (Wondji et al., 2012) and Katete (14˚11'S, 31˚52'E), Zambia (Riveron et al., 2014a). Details of resistance profile of these mosquitoes and transcriptional analysis of *CYP6P9a* and *CYP6P9b* alleles were already established in the studies cited above. The field populations from southern Africa were resistant to pyrethroids and carbamate insecticides, while those from East Africa were pyrethroid- and DDT-resistant, but susceptible to carbamates. West African populations were resistant to pyrethroids and carbamates and highly resistant to DDT, several magnitude compared with the levels observed in East Africa. Levels of pyrethroids resistance has been consistently higher in southern African populations of *An. funestus* compared to populations from other regions of Africa, with the highest resistance observed in populations from Mozambique (no mortality observed up to 1.5 hours). The variations in resistance profile could be due to differences in the underlying mechanisms or the same type of resistance mechanisms subtly changed; for example, polymorphism in the alleles of *CYP6P9a* and *CYP6P9b* could be impacting the pyrethroid resistance. Also, other candidate P450 genes, GSTs and carboxylesterases could independently or in concert with *CYP6P9a* and *CYP6P9b* be responsible for this widespread resistance to the three major classes of insecticides used in public health. No resistance to organophosphorus malathion was observed in all the field populations *of An. funestus* across Africa consistent with the reported absence of $Gly^{119}Ser$ mutations in the acetylcholinesterase gene.

2.3.2 Amplification of full length *CYP6P9a* and *CYP6P9b* Alleles

2.3.2.1 RNA Extraction

All mosquitoes used for RNA extraction were previously confirmed to be *An. funestus s.s.* using cocktail PCR (Koekemoer et al., 2002). Total RNA was extracted from pools of 10 females from resistant populations, as well as from FANG using the PicoPure RNA Extraction Kit from Arcturus (Life Technologies, CA, USA) according to manufacturer's protocol. RNA was extracted using Extraction Buffer (XB) and Conditioning Buffer (CB); isolated using 70% methanol, Wash Buffers W1 and W2 and eluted using Elution Buffer (EB). To enhance quality, RNA was DNase-treated following washing with W1. Quantity and quality of isolated RNA were determined with NanoDrop ND1000 Spectrophotometer (Thermo Fisher) and Agilent 2100 Bioanalyzer.

2.3.2.2 cDNA Synthesis (RT-PCR)

1µg of total RNA from resistant and susceptible (FANG) mosquitoes was used as a template for cDNA synthesis using the SuperScript® III First Strand Synthesis Kit (Invitrogen) according to the manufacturer's instructions. 13µl reaction mix consisting of 1µl (1µg) RNA diluted in 8µl DEPC-treated water, 1µl of Oligo(dT)20 (50mM), 3µl DEPC-treated water and 1µl of 10mM dNTP mix was initially incubated for 5 mins at 65^0C. 4µl of 5X first strand buffer, 1µl of 0.1M DTT, 1µl of RNase Out (40U/µl) and 1.5µl of SuperScript® III Reverse Transcriptase (200U/µl) was added to make the total volume to 20.5µl. The mix was then incubated at 25^0C for 5 mins, and then 50^0C for 60 mins, followed by 70^0C for 15 mins. 1µl of *E. coli* RNase H was added to the newly synthesized cDNA and incubated at 37^0C for 20 mins to remove residual RNA. Quantity and quality of the DNA was finally assessed using NanoDrop ND1000 Spectrophotometer (Thermo Fisher).

2.3.2.3 Cloning and Sequencing of An. funestus CYP6P9a and CYP6P9b full-length from cDNA

(i) Amplification of CYP6P9a and CYP6P9b alleles

The full length coding sequences of *CYP6P9a* and *CYP6P9b* alleles were amplified from cDNA sets from Benin, Uganda, Malawi, Mozambique, Zambia, and the FANG, using the primers listed in Table 2.1. To 14µl PCR mix made up of 3µl 5X Phusion HF Buffer (with 1.5mM $MgCl_2$ in final reaction), 0.12µl dNTP mix (85.7µM), 0.51µl each of forward and reverse primers (0.34µM), 0.15µl (0.015U) of Phusion High-Fidelity DNA Polymerase (Fermentas) and 10.71µl of dH_20, 1µl cDNA was added. Amplification was carried out using the following conditions: one cycle at 95°C for 5 mins; 35 cycles of 94°C for 20s (denaturation), 57°C for 30s (annealing), and extension at 72°C for 90s; and one cycle at 72°C for 5mins (final elongation). 3µl PCR products were separated on 1.5% agarose gel stained with ethidium bromide (0.5µg/µl) and visualised using transilluminator to confirm products size.

Table 2.1: Primers used for gene amplification and plasmid sequencing

Primer	Forward Sequence	Reverse Sequence	Size (bp)
*CYP6P9a*_Full	ATGGAGCTCATTAACGTGGTGTTGGC	TCA CAA TTT TTC CAC CTT CAA GTA ATT ACC CGC	1527
*CYP6P9b*_Full	ATGGAGCTCATTAACGTGGTGTTGGC	TTA CAC CTT TTC TAC CTT CAA GTA ATT ACC CGC	1527
pJET1.2	CGACTCACTATAGGGAGAGCGGC	AAGAACATCGATTTTCCATGGCAG	~1727
pJET725	CCGAAAAGTGCCACCTGAACGTCTAA	TCCTGTCTCAGTTTCCTGAAGCTTGCTC	~2277

(ii) Purification of PCR Product Ligation into pJET1.2 Blunt Vector

PCR products were cleaned individually with QIAquick® PCR Purification Kit (Qiagen) according to the manufacturer's instructions and cloned into pJET1.2/blunt cloning vector using the CloneJET PCR Cloning Kit (Fermentas) as described in Table 2.2.

Table 2.2: pJET1.2/Blunt ligation protocol

Component	Volume (µl) = 10
Blunting Reaction	
2X Reaction Buffer	5
Purified PCR Product	3.5
DNA Blunting Enzyme	0.5
Vortex briefly and microfuge for 5 seconds	-
Incubate blunting mix at 70°C for 5 mins	-
Chill on ice	-
Ligation Reaction	
pJET1.2/Blunt Cloning Vector (50ng/ µl)	0.5
T_4 DNA Ligase	0.5
Vortex briefly and microfuge for 5 seconds	-
Incubate mix at 22°C for 30 mins	-

(iii) Transformation and small-scale plasmids isolation

4µl (~5-10ng) of ligation product was added to 40µl Subcloning Efficiency™ *DH5α* Competent Cell (Invitrogen), chilled in sterile 1.5ml microcentrifuge tube. Reaction was mixed by gently flicking the bottom of the tube and left on ice for 30 mins. The cells were shocked for 45s at 42°C and then chilled immediately on ice for 2 mins. 950µl of pre-warmed S.O.C. medium was added and the tubes incubated at 37°C and 200 rpm for 1 hour. 50-100µl of transformants were spread onto LB plates containing 100mg/ml ampicillin and allowed to grow overnight at 37°C. Colonies were suspended separately in 20µl dH_20 and screened for presence of the gene in a PCR reaction using Kappa Taq DNA Polymerase (KAPABIOSYSTEMS) and the pJET1.2 primers listed in Table 2.1. 1.5µl of 10X Taq Buffer A, 0.75µl of $MgCl_2$ (25mM), 0.12µl of dNTP mix (10mM), 0.4µl each of forward and reverse primers, 0.12µl of 5U/µl KAPA Taq DNA Polymerase and 10.71µl dH_20 were mixed in total volume of 14µl, to which 1µl of colony was added. PCR was conducted using the following conditions: one cycle of 95°C for 3 mins; 25 cycles each of initial denaturation (94°C for 30 seconds), annealing (57-60°C for 30 seconds) and extension (72°C for 90 seconds); one cycle of final extension for 90 seconds at 72°C. PCR product was run on 1.5% agarose gel stained with ethidium bromide to confirm products size.

4µl of positive colonies were grown (miniprep) at 37°C for 16 hours in a 6ml LB medium containing 3µl ampicillin (100mg/ml), with shaking at 200 rpm. Plasmids were isolated using the

QIAprep® Spin Miniprep Kit (QIAGEN) according to the manufacturer's protocol. Quantity and quality of plasmid DNA was determined using NanoDrop ND1000 Spectrophotometer (Thermo Fisher).
The isolated plasmids were sequenced on both strands using the pJET725 primers (Table 2.1).

2.3.3 Sequence Analysis and Mapping of Polymorphisms

Analysis of sequences was conducted by detection of polymorphic positions through manual examination of sequence traces using BioEdit version 7.2.3.0 (Hall, 1999) and nucleotides differences in multiple alignments using CLC Sequence Viewer 6.8 (http://www.clcbio.com/).

DnaSP 5.10.01 (Librado and Rozas, 2009) was used to analyse intra-allelic genetic variation such as nucleotides and haplotypes diversity. Phylogenetic neighbour-joining trees of all haplotypes of *CYP6P9a* and *CYP6P9b* alleles were constructed using MEGA 6.0 (Tamura et al., 2013). After sequence analyses, the predominant haplotype of each gene from each country was selected for further analysis. Amino acids sequences were generated *in silico* using the *CLC* Sequence Viewer nucleotides analysis module and used for further analyses and identification of mutations.

2.3.4 Modelling of *CYP6P9a* and *CYP6P9b* alleles by Satisfaction of Spatial Restraints

Homology modelling (HMM) is simply a computational approach for 3D prediction of protein structure. It involves construction of an atomic-resolution model of the "*target*" protein (query) from its amino acid sequence using experimental, 3D structure of a related homologous protein ("*template*" also referred to as a *reference*). The profound success of HMM is because the 3D structure of proteins from the same family is more conserved than their primary sequences (Lesk and Chothia, 1980) and proteins that share low sequence similarity often possess similar structures (Fiser and Sali, 2003).

(i) Template Selection

The program BLASTp (Altschul et al., 1990) from NCBI (http://blast.ncbi.nlm.nih.gov/Blast.cgi) was used to search for the best template structure available in the protein data bank (PDB) database (Berman et al., 2002). A pairwise sequence alignment with the query protein sequences of CYP6P9a

and CYP6P9b recovered as top hit a crystal structure of human microsomal 450 *CYP3A4* (PDB:1TQN), with sequence similarities of 33% and 32% and lowest expectation value (*E*-value) of 1.0e-^{67} and 6.0^{-69} respectively for CYP6P9a and CYP6P9b. 1TQN is a crystal structure of *CYP3A4* resolved to 2.05Å without the *N*-terminal transmembrane leader sequence amino acids 3-23 (Yano et al., 2004) and deposited in protein database (http://www.rcsb.org/pdb/).

(ii) Template-Target Alignment

In order to maximise the alignment score between the template and the queries, pair-wise alignment of protein sequences (FASTA format) was done using T-Coffee (Notredame et al., 2000). The 3D-Coffee Expresso (http://tcoffee.crg.cat/apps/tcoffee/do:expresso) algorithm (Armougom et al., 2006) using sequence-structure threading (Fugue) generated a multisequence alignment by identifying template structure using a BLAST and substitution matrix of scores for each aligned pair of residues minus the penalties assigned to gaps, as explained elsewhere (Pierri et al., 2010). Residues present in the template and absent in the query were deleted, because misalignment of even a single residue can result in an error of about 4.0Å in the final model generated (Fiser and Sali, 2003).

(iii) Model Building

MODELLER is a standalone computer program that models 3D structures of proteins and their assemblies by satisfaction of spatial restraints (Sali and Blundell, 1993). The alignment files of a sequence to be modelled with known related structures is used by the MODELLER to automatically calculate a model with all non-hydrogen atoms. The input to the program are restraints on the spatial structure of the amino acid sequence(s) and ligands to be modelled and the output is a 3D structure that satisfies these restraints as well as possible. CYP6P9a and CYP6P9b models were created using the MODELLER 9.0*v2* (https://salilab.org/modeller/) and human *CYP3A4* (PDB:1TQN) as a template. MODELLER uses its SALIGN3D module to carry out template-query alignments and then extract spatial restraints from two sources: (i) homology-derived restraints on the distances and dihedral angles in

the target sequence extracted from its alignment with template structure (Sali and Blundell, 1993); (ii) stereochemical restraints such as bond length and bond angle preferences are obtained from the molecular mechanics force field of CHARMM-22 (MacKerell et al., 1998). Statistical preferences of main chain dihedral angles and non-bonded atomic distances are calculated by comparing the sequences of the target to the template, and a model calculated by optimisation employing methods of conjugate gradients and molecular dynamics (Braun and Go, 1985) with simulated annealing in Cartesian space. The loop-module in the MODELLER automatically models all the loops in the query by energy optimisation approach as well (Fiser et al., 2000). The software refines the models by tuning alignments and side chains automatically and then relaxes the backbone. The script used for template-query alignments and model building is given in Appendix 2.1B.

2.3.5 Models Assessment (Validation)

Models generated using the MODELLER were assessed by comparing the PROSAII *Z* score of the models and the template structure(s) (Sippl, 1993). The PROSAII *Z* score (scoring function) of a model is a measure of compatibility between its sequences and the structure and ideally the *Z* score of the model should be comparable to that of the template. One of the shortcomings of the *Z* score is that it is an internal evaluation between the modelled structure and the template to determine whether or not the model satisfies the spatial restraints imposed. Because of this an independent assessment tool, Errat was used to further validate the models.

2.3.5.1 Errat

For each query sequence 50 models were iteratively generated and externally assessed individually using Errat v2.0 (http://nihserver.mbi.ucla.edu/ERRAT/) in order to determine incorrectly determined structures. Errat analyses the statistical patterns of non-bonded interactions between different atom types (Colovos and Yeates, 1993). A single output plot is produced that gives the value of the error function *vs* position of a 9-residue sliding window of 96 reliable, high-resolution protein

structures. Regions of candidate protein structures that are mis-traced or mis-registered were then identified by analysis of the pattern of non-bonded interactions from each window. Out of 50 models generated from each query sequence, one model is selected based on Errat scores for molecular docking. Errat scores for the all the models with the lowest incorrectly folded regions selected for further analysis, as well as the score of the template (1QTN) could be found in Appendix 2.2.

2.3.6 Ligand Structures

Virtual datasets of ligand insecticides: permethrin (ZINC01850374), bifenthrin (ZINC02516821), deltamethrin (ZINC01997854), λ-cyhalothrin (ZINC01843672), etofenprox (ZINC02558051), DDT (ZINC01530011) and bendiocarb (ZINC02015426) were retrieved from the library of ZINC[12] (https://zinc.docking.org/) database in *MOL2* format (Irwin and Shoichet, 2005).

2.3.7 Preparation of Receptors (Models) and Ligands for Molecular Docking

MODELLER generates a model of main chain and side chain atoms devoid of hydrogen atoms and before docking simulation models were prepared by adding hydrogen atoms. This was done using using the Molegro Molecular Viewer 2.5 (MMV) software from *CLC bio* (http://www.clcbio.com/) and both receptor and ligands were prepared in PDB format following the assigning of chirality to some of the insecticide ligands, e.g. permethrin.

2.3.8 Molecular Docking with GOLD

Molecular docking is basically a conformational sampling procedure in which various docked conformations are explored to attempt to predict the potential right one (Wang et al., 2003). Conformational sampling must be guided by a scoring or energy function (Warren et al., 2006) that is used to evaluate the fitness between the protein and the ligand. The final docked conformations are usually selected according to their scores and/or productive poses. The accepted hypothesis is that lower energy scores represent better protein-ligand bindings compared to higher energy values. A number of approaches for the choice of scoring functions have been reported and can be roughly

grouped into three approaches: force field methods (Goodsell et al., 1996), empirical scoring functions (Wang et al., 2007) and knowledge-based potentials (Gohlke et al., 2000).

Genetic algorithm for ligand docking (GOLD) is an automated ligand docking program which uses genetic algorithm to perform protein docking (Jones et al., 1997). GOLD utilises evolutionary strategy to explore the conformational variability of a flexible ligand while simultaneously sampling available binding modes of the ligand into a partially flexible protein active site. Hydrogen bond motifs have been encoded into the GOLD algorithm in order to search the spaces of available binding modes efficiently. Also, a simple scoring function is used to rank generated binding modes. The program has been documented to achieve up to 71% success rate of predicting correct binding mode of a ligand onto a protein when compared with the results from X-ray crystals of protein-ligand complexes (Jones et al., 1997, Verdonk et al., 2003). GOLD employs artificial mimicry to simulate nature (CCDC, 2011); each potential docking mode (solution) is considered as a chromosome and is assigned a specific score. The chromosome contains information about the mapping of a ligand H-bond atom onto (complementary) protein H-bond atoms, mapping of hydrophobic points on the ligand onto protein hydrophobic point and the conformation around flexible ligand bonds and protein -OH groups. Sets of solutions are termed a population and corresponding chromosomes ranked according to fitness. Two individual chromosomes share the same niche if the r.m.s.d. between the coordinate of their donor and acceptor is less than 1.0Å (1.0Å = 0.1nm) apart. The population of chromosomes is iteratively optimised so that at each step of the run, a point mutation may occur in the chromosome, or two chromosomes may mate to produce a child (crossover) and migration of a population member from one island to another can take place. The optimised chromosome then becomes a parent and selection of parent chromosome is biased towards the fitter members of the population (ligand dockings with better fitness score).

For docking with GOLD*v3.2*, ChemScore fitness function was chosen for it has been trained by regression against binding affinities data (Eldridge et al., 1997). The function was derived empirically

from a set of 82 protein-ligand complexes for which measured binding affinities were available (Baxter et al., 1998). ChemScore estimates the total free energy change as the ligand binds to its respective receptor. Docking was performed using the genetic algorithm (GA) protocol as implemented on the user-friendly Hermes graphical user interface of GOLD. The active site of the protein was defined as a binding cavity (sphere) of 20Å radius centred on the heme-iron atom. 50 docking solutions (poses) of each ligand with respective receptor protein ranked according to their ChemScore fitness were generated. Solutions with the highest scores (best-ranked docking poses) which are in potentially productive orientations were selected for further analysis. Visualisation and preparation of figures from the docking were carried out using the PyMOL 1.7 and MMV.

2.3.9 *In silico* Analysis of Protein Pockets and Cavities

To investigate how the pyrethroid ligand could enter the active site of two models each from *CYP6P9a* (*MALCYP6P9a* and *FANGCYP6P9a*) and *CYP6P9b* (*MOZCYP6P9b* and *FANGCYP6P9b*) and how product could egress, a search of channels leading into and out of the the active site to the surface of the protein (bulk solvent) was conducted using the algorithm tool CAVER 3.1 (Petrek et al., 2006). CAVER models protein body on a discrete 3-dimensional grid space with all grid nodes clustered into two classes: inside nodes (inside atomic vdW radii) and outside nodes (nodes located outside the protein body). CAVER then spans the grid nodes avoiding nodes that are located in the convex hull in its calculation and then find channels by evaluating a cost-function every time a new grid node is reached (Cojocaru et al., 2007). Settings were set as described in CAVER PyMOL plugin v3.0 (http://www.caver.cz/fil/download/manual/caver_plugin_userguide.pdf): (i) maximum Java heap size ~6000; (ii) maximum probe radius which species the minimum radius a tunnel must have to be identified was set as 0.9; (iii) shell depth (the maximal depth of a surface region) was set as 4; (iv) shell radius (the radius of the shell probe which will be used to define which parts of the Voronoi diagram represent the bulk solvent) was set as 3; (v) clustering threshold which specify the level of detail at which the tree hierarchy of tunnel clusters will be cut was set as 3.5; (vi) number of approximating

balls which specify the number of balls that will be placed right under the surface of each larger atom to represent individual atoms in the input structure was set as 12. Starting points were set as x (-16.4), y (-22.6) and z (-9.6) using the input PDB file with search centre above the heme iron, and with a maximum distance of calculation starting point set as 3.0Å and desired radius of 5.0Å.

2.4 Results

2.4.1 Sequence Characterisation of *CYP6P9a* and *CYP6P9b* Alleles

To establish the genetic distances between African populations of *An. funestus* based on *CYP6P9a* and *CYP6P9b* DNA sequences, phylogenetic trees of predominant haplotypes of *CYP6P9a* and *CYP6P9b* alleles were constructed using MEGA 6.06. A best-fit substitution model was tested based on Bayesian information criteria using four haplotypes each of *CYP6P9a* and *CYP6P9b* and Kimura-2 model best described the haplotypes dataset. The model was then used with 500 bootstrap replicates and a maximum likelihood tree generated (Appendix 2.1A). Haplotypes from the same country form clade with one another. However, in both *CYP6P9a* and *CYP6P9b* haplotypes from Uganda clustered closer to southern African haplotypes followed by haplotypes from FANG. Benin haplotypes were the most distant from southern African haplotypes and the closest to the haplotypes of the susceptible FANG.

2.4.1.1 CYP6P9a Alleles

Thirty one cDNA sequences of *CYP6P9a* from across Africa were analysed for nucleotide variations and haplotypes diversity. *CYP6P9a* has 17 haplotypes (Appendix 2.8) and 71 polymorphic sites of which 21 were established as non-synonymous (Table 2.3). Highest polymorphism was observed with Benin alleles and the susceptible strain FANG, both of which show high nucleotides diversity with 34 and 23 polymorphic sites respectively of which 32 and 19 were synonymous. Uganda and Zambia alleles portrayed lowest diversity with only 2 haplotypes and one non-synonymous mutation each. Malawi and Mozambique also portrayed reduced nucleotides variations (4 and 5 nucleotides substitution respectively) of which 3 and 5 led to amino acids mutation respetively. This established that the East and southern African alleles of *CYP6P9a* with reduced diversity and high

number of amino acids mutations per substitution site were undergoing directional selection as documented for Malawi and Mozambique alleles of *CYP6P9a* and *CYP6P9b* (Riveron et al., 2013).

Table 2.3: Summary statistics for polymorphism of *CYP6P9a* between FANG and the resistant strains from Malawi and Mozambique, Zambia, Uganda and Benin

Samples	N	h	S	Syn	NonSyn	π (k)	D (Tajima)	D* (Fu and Li)
Malawi	5	4	4	1	3	0.010 (1.60)	-1.09^{ns}	-1.09^{ns}
Mozambique	5	4	5	0	5	0.0013 (2.0)	-1.12^{ns}	-1.12^{ns}
Zambia	5	2	1	0	1	0.00039 (0.60)	1.22^{ns}	1.22^{ns}
Fang	6	3	23	19	4	0.0053 (8.13)	-1.209^{ns}	-1.25^{ns}
Uganda	5	2	1	0	1	0.00026 (0.4)	-0.816^{ns}	-0.816^{ns}
Benin	5	3	34	32	2	0.0090 (13.80)	-1.157^{ns}	-1.157^{ns}
Total	31	17	71	50	21	0.0142 (21.80)	0.853^{ns}	0.140^{ns}

N= number of sequences (n); h = number of haplotypes; S = number of polymorphic sites; Syn = synonymous mutations; Nsyn = non-synonymous mutations; π = nucleotide diversity; k = mean number of nucleotide differences; D and D* = Tajima's and Fu and Li's statistics; ns = not significant; s = significant ($p<0.05$).

With amino acid sequences, alleles from different regions formed clades unique to their origins; however the predominant alleles of FANG cluster between the East (Uganda) and southern African alleles reflecting its distance from West African alleles (Figure 2.1A and B) and closer coding sequences similarity to East and southern African alleles.

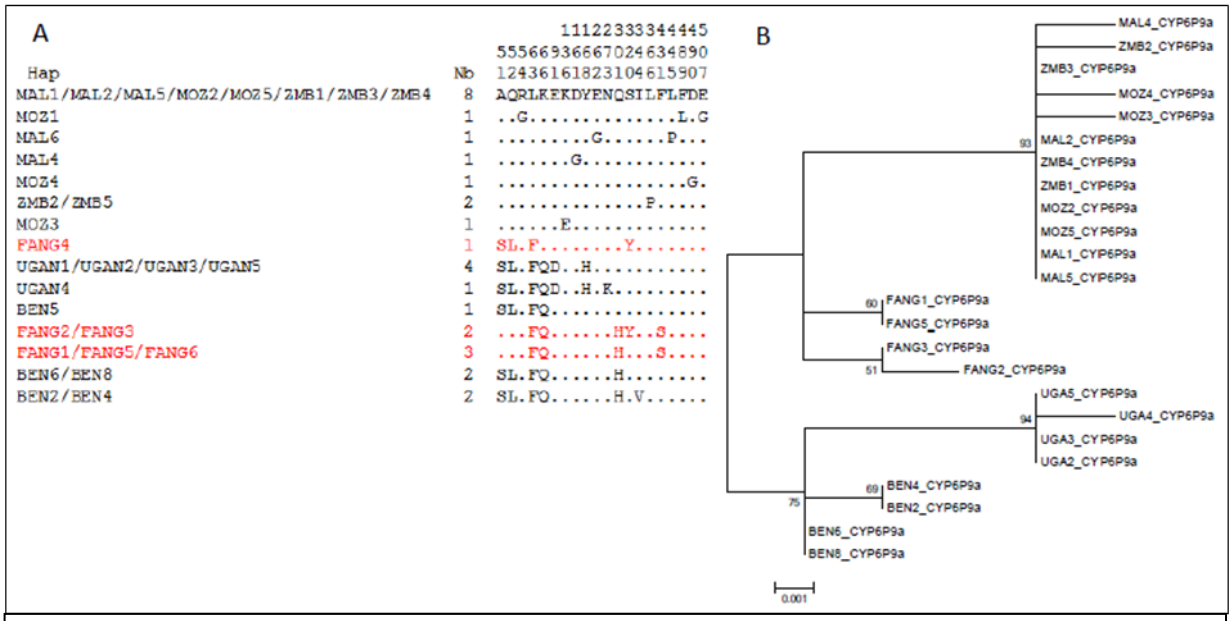

Figure 2.1: Schematic representation of haplotypes of *CYP6P9a* genes between the resistant mosquitoes from Malawi, Mozambique, Zambia, Uganda, Benin and the susceptible FANG. (A) The polymorphic amino acid positions with the column Nb indicating the number of individuals sharing the haplotype, **(B)** Neighbor-joining tree of *CYP6P9a* showing clades specific to each phenotype and origin (region). A number has been given to each haplotype preceded by MAL, MOZ, ZMB, UGA, BEN or FANG if it is unique to Malawi, Mozambique, Zambia, Uganda, Benin or FANG strains, respectively.

However, three mutations were found to be shared by resistant alleles from two or more regions across Africa compared with the susceptible FANG (Table 2.4). Polymorphic positions of these important mutations in DNA sequences of *CYP6P9a*, country of origin, amino acid changes, its location in the protein sequence and possible impact on enzyme activity are outlined in the Table below.

Table 2.4: Nucleotide polymorphism and amino acid substitutions between resistant alleles of *CYP6P9a* and *CYP6P9b* compared with FANG

Amino acid substitution	Mutation	Countries	Location and potential Impact
		CYP6P9a	
Ala^{51}Ser	151:G->T	Benin and Uganda	Possibly located within the hydrophobic domain targeting the endoplasmic reticulum membrane
Gln^{52}Leu	153: C->T	Benin and Uganda	Possibly located within the hydrophobic domain targeting the endoplasmic reticulum membrane
Phe^{63}Leu	189: T->G	Malawi, Mozambique, Zambia	Within the highly variable αA region
Gln^{66}Lys	196: C->A	Malawi, Mozambique, Zambia	Within the highly variable αA region
His^{301}Gln	903: A->C	Uganda, Malawi, Mozambique, Zambia	Two residues upstream the substrate recognition site 4 (SRS4)
Tyr^{320}Ser	959: A->C	Benin, Uganda, Malawi, Mozambique, Zambia	Middle of the αI helix and within SRS-4; one residue downstream the oxygen binding pocket (AGFETS) in *CYP6P9a*
Ser^{431}Phe	1292: T->C	Benin, Uganda, Malawi, Mozambique, Zambia	Within the loop joining the meander with the cysteine pocket; the loop is purported to house the reductase interaction site 2 (RIS-2)
		CYP6P9b	
Ser^{32}Asn	95: G->A	Benin, Uganda, Malawi, Mozambique, Zambia	Within the hydrophobic residues anchoring the protein to membrane. May impact on protein stability
Ile^{109}Val	325: A->G	Benin, Uganda, Malawi, Mozambique, Zambia	Within the SRS-1 and the B'C loop purported to be involved in substrate access and channelling
His^{169}Arg	506: A->G	Benin, Uganda, Malawi, Mozambique, Zambia	C-terminus of D helix
Gln^{171}Pro	512: A->C	Benin, Uganda, Malawi, Mozambique, Zambia	N-terminus of the E helix
Glu^{172}Asp	516: G->T	Benin, Uganda, Malawi, Mozambique, Zambia	N-terminus of the E helix
Glu^{335}Asp	1005: A->C	Benin, Uganda, Malawi, Mozambique, Zambia	In the –COOH terminus of the αI helix, possible impact as RIS-1 residues mediating interaction with P450 reductase
Ser^{384}Asn	1151: G->A	Uganda, Malawi, Mozambique, Zambia	In the β1_4 (αK') and within the highly conserved SRS5, with possible impact on substrate recognition
Ala^{401}Pro	12001: G->C	Benin, Uganda, Malawi, Mozambique, Zambia	Within the β2_2 domain; pyrrolidine ring can restrict conformational space

2.4.1.2 CYP6P9b Alleles

CYP6P9b has 15 haplotypes (Appendix 2.9) and 138 polymorphic sites (Table 2.5) the bulk of which were contributed from variations of Benin and FANG alleles compared with Uganda and

southern African alleles. Nucleotide diversities between all alleles of *CYP6P9b* were statistically significant ($p<0.05$; D* Fu and Li). Highest diversity was observed with FANG which has 38 polymorphic sites compared with 1 polymorphic site each for Uganda and Zambia alleles. Malawi, Mozambique and Benin alleles have 5, 2 and 3 polymorphic sites, respectively. 49 of the 138 polymorphisms in *CYP6P9b* alleles were non-synonymous with FANG alleles having only 7 non-synonymous mutations out of its 38 polymorphic positions. Unlike *BENCYP6P9a*, the *CYP6P9b* allele from Benin (*BENCYP6P9b*) exhibited reduced polymorphism and seems to be undergoing directional selection (3 polymorphic positions all of which are non-synonymous) just like the Uganda and southern African alleles of *CYP6P9b*.

Table 2.5: Summary statistics for polymorphism of *CYP6P9b* between FANG and the resistant strains from Malawi and Mozambique, Zambia, Uganda and Benin

Samples	N	h	S	Syn	NonSyn	π (k)	D (Tajima)	D* (Fu and Li)
Malawi	5	4	5	4	1	0.0013 (2.00)	-1.123^{ns}	-1.123^{ns}
Mozambique	5	3	2	1	1	0.0006 (1.00)	0.243^{ns}	0.243^{ns}
Zambia	5	2	1	0	1	0.00039 (0.6)	1.224^{ns}	1.224^{ns}
Fang	5	3	38	31	7	0.010(15.40)	-1.169^{ns}	-1.169^{ns}
Uganda	5	2	1	0	1	0.00039(0.60)	1.224^{ns}	1.224^{ns}
Benin	6	2	3	0	3	0.00065(1.00)	-1.233^{ns}	-1.260^{ns}
Total	31	15	138	89	49	0.029(44.625)	0.945^{ns}	1.424^{s}

N= number of sequences (n); h = number of haplotypes; S = number of polymorphic sites; Syn = synonymous mutations; Nsyn = non-synonymous mutations; π = nucleotide diversity; k = mean number of nucleotide differences; D and D* = Tajima's and Fu and Li's statistics; ns = not significant; s = significant ($p<0.05$)

As in *CYP6P9a* alleles of *CYP6P9b* (amino acid sequences from different regions) formed clades unique to their origins; however, alleles of FANG cluster between the East (Uganda) and West (Benin) African alleles and away from the Malawi, Mozambique and Zambia (Figure 2.2A and B). Up to eight amino acids shared by the haplotypes from resistant alleles make them different from the alleles from the major haplotypes of FANG. Countries sharing such polymorphism, polymorphic positions in cDNA and amino acid sequences, as well as location on the protein sequence and potential impact on functional activity are summarised in Table 2.4.

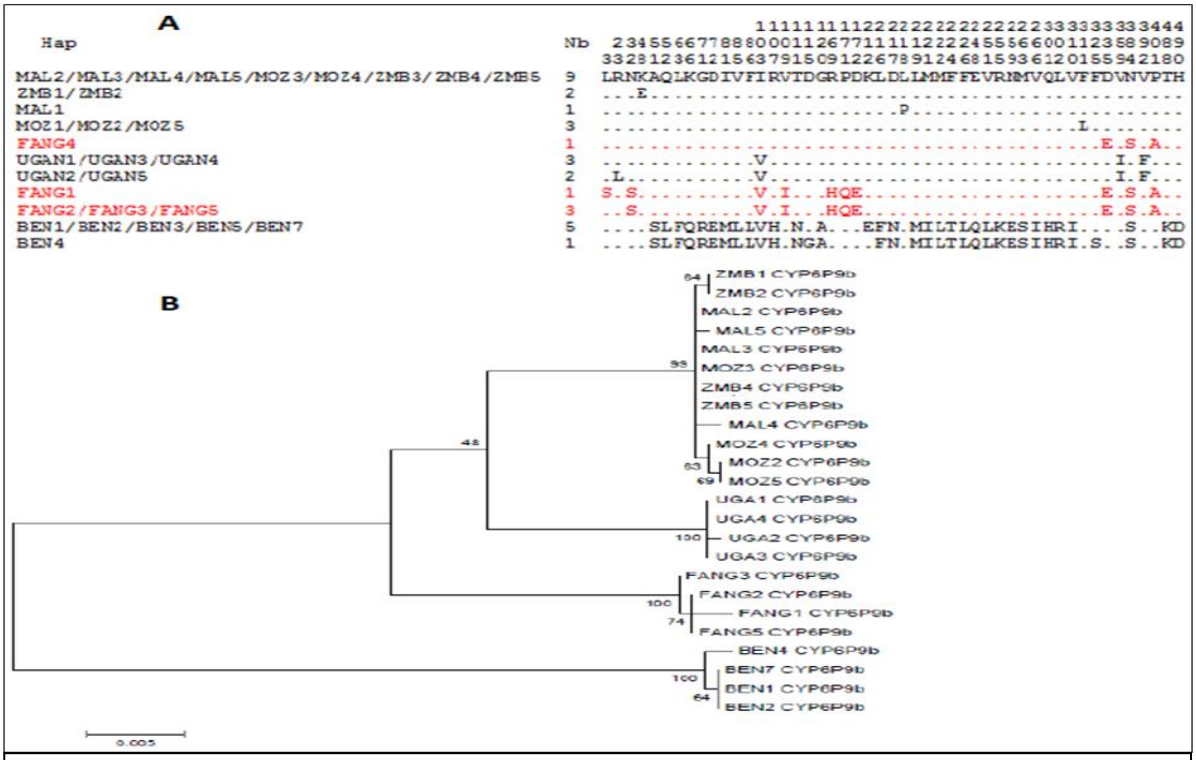

Figure 2.2: Schematic representation of haplotypes of *CYP6P9b* genes between the resistant mosquitoes from Malawi, Mozambique, Zambia, Uganda, Benin and FANG. (**A)** The polymorphic amino acid positions with the column Nb indicating the number of individuals sharing the haplotype **(B)** Neighbor-joining tree of *CYP6P9b* showing clades specific to each phenotype and origin (region).

2.4.1.3 Candidate Resistance Mutations

2.4.1.3.1 CYP6P9a

Comparison of the sequences of predominant haplotypes of *CYP6P9a* from FANG with those of the resistant strains revealed that only two substitutions Ser^{431}Phe and Tyr^{320}Ser are relatively fixed all across Africa (see Figure 2.1 and Figure 2.3). His^{301}Gln present in southern African and Ugandan alleles is absent in alleles from Benin. The Tyr^{320}Ser mutation replaces a bulky, polar, aromatic side chain with a smaller, polar, neutral serine. Prediction of structurally conserved regions of CYP6P9a using CYPED (Sirim et al., 2010) placed this mutation within the well-conserved αI helix that forms the heme-binding structural core and one residue downstream the oxygen-binding pocket of CYP6P9a. The mutation also mapped to the substrate recognition site number 4 (SRS4) determined by comparing the CYP6P9a amino acid sequences with that of the CYP101A from *Pseudomonas putida*

($P450_{cam}$), whose substrate-binding residues have been identified by x-ray crystallography of a substrate-bound form (Gotoh, 1992). In Ser^{431}Phe mutation polar, neutral serine is replaced with non-polar, aromatic phenylalanine. This substitution occured within the loop joining the meander (position 421-429) to the cysteine pocket (position 446-456). This loop consisting of 16 residues in CYP6P9a has been previously proposed to house the reductase interacting site 2 (RIS2) of the P450s (Hasemann et al., 1995) in three crystal structures of P450s ($P450_{cam}$, $P450_{terp}$ and $P450_{BM-3}$). In His^{301}Gln polar positive (basic) side chain of histidine is replaced with polar, neutral, amido side chain of glutamine. This mutation in the αI helix is located two residues from the putative SRS4. Other substitutions of particular interest include Ala^{51}Ser and Gln^{52}Leu observed in Benin and Uganda alleles and Phe^{63}Leu and Gln^{66}Lys (αA region) present in southern African alleles. However, analysis of *CYP6P9a* and also *CYP6P9b* sequences using DAS (Dense Alignment Surface) transmembrane prediction server (http://www.sbc.su.se/~miklos/DAS/) revealed that residues around these regions are not involved in contact with the membrane (Appendices 2.3 and 2.4 respectively).

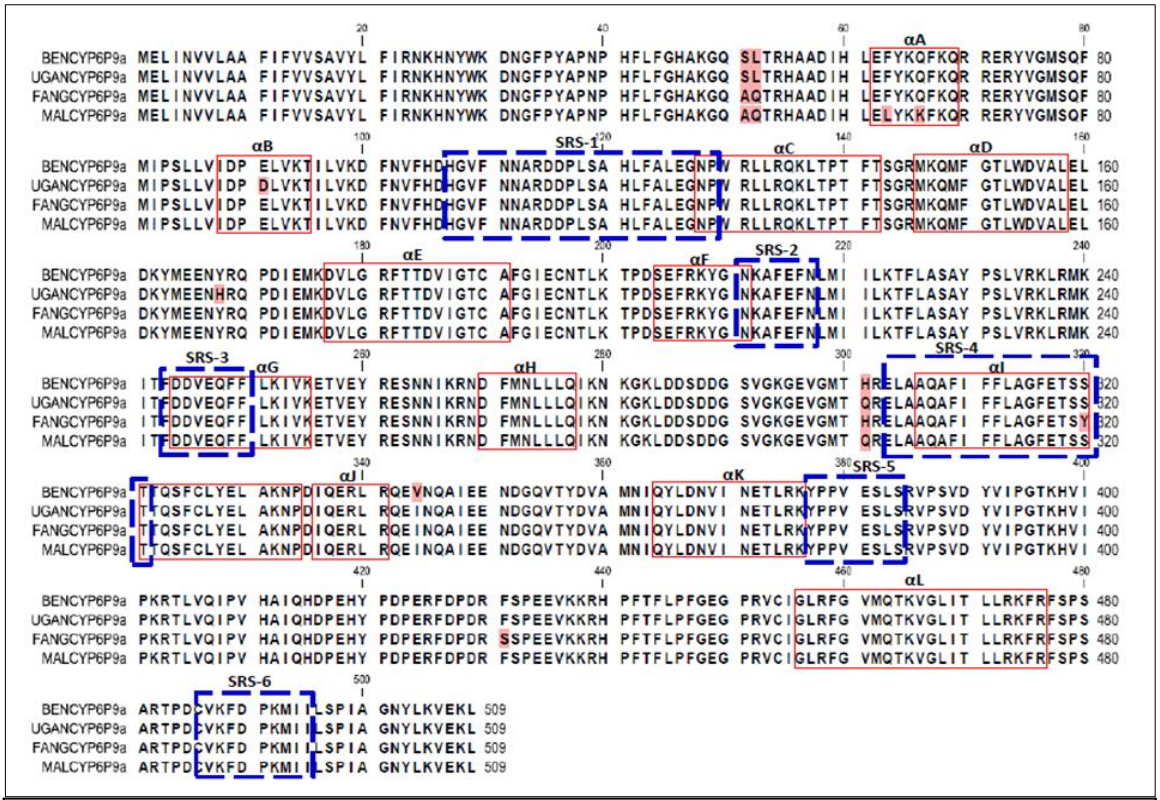

Figure 2.3: Comparison *An. funestus* CYP6P9a amino acid sequences from resistant and susceptible strains. Red solid lines represent helices A-L, while blue dashed lines correspond with the substrate recognition sites 1-6. Different residues are highlighted in pink.

2.4.1.3.2 CYP6P9b

CYP6P9a from southern Africa was described as more polymorphic than *CYP6P9b* with more DNA haplotypes (9 vs 5) and amino acid sequences of 11 vs 5 (Riveron et al., 2013) compared with FANG. Here, its confirmed with more sequences from Benin (West) and Uganda (East) Africa. *CYP6P9a* with 17 haplotypes has 15 different sequences across Africa, while *CYP6P9b* with 15 haplotypes possess only 11 different sequences (Figure 2.2). The $His^{301}Gln$ mutation absent in BENCYP6P9a appears in CYP6P9b in addition to the $Ala^{51}Ser$, $Gln^{52}Leu$, $Phe^{63}Leu$ and $Gln^{66}Lys$ replacement (Figure 2.4). With the exception of BENCY6P9b all the haplotypes of CYP6P9b possess $Ser^{384}Asn$ mutation, a replacement of a polar neutral amino acid, serine with another (asparaine). This mutation present in the *N*-terminus of the highly-conserved *β1-4* domain of CYP6P9b in FANGCYP6P9b mapped to the SRS5.

Seven amino acid substitutions ($Ser^{32}Asn$, $Ile^{109}Val$, $His^{169}Arg$, $Gln^{171}Pro$, $Glu^{172}Asp$ $Glu^{335}Asp$ and $Ala^{401}Pro$) (Table 2.4) are fixed in all the dominant haplotypes of CYP6P9b alleles from resistant individuals across Africa compared with the FANG. The $Ile^{109}Val$ mutation replaced nonpolar, larger side chain of isoleucine with a corresponding non-polar, hydrophobic side chain of smaller valine. This mutation is within the B'-C loop described as being highly variable (Sirim et al., 2010) and can result in an increase in the radius of the binding cavity and/or enhanced substrate access or product egress. In all CYP6P9b sequences the mutations $His^{169}Arg$ (C-terminus of D helix), $Gln^{171}Pro$ and $Glu^{172}Asp$ (the N-terminus of the E helix) are linked. In position 169 basic imidazole containing side chain of histidine was replaced with a basic side chain of arginine possessing guanidinium moiety. In position 171, polar, neutral glutamine was replaced with non-polar, aliphatic proline with its secondary imino group that could be held in rigid conformation which can reduce structural flexibility. The $Glu^{335}Asp$ replacement occurred in the last residue in the C-terminus of the αI helix downstream SRS4. The $Ala^{401}Pro$ mutation in β*2-2* domain resulted in replacement of non-polar alanine with non-polar proline. The bulky pyrrolidine ring of proline can restrict the conformational space and affect backbone dihedral angles and side chain rotations (MacArthur and Thornton, 1991).

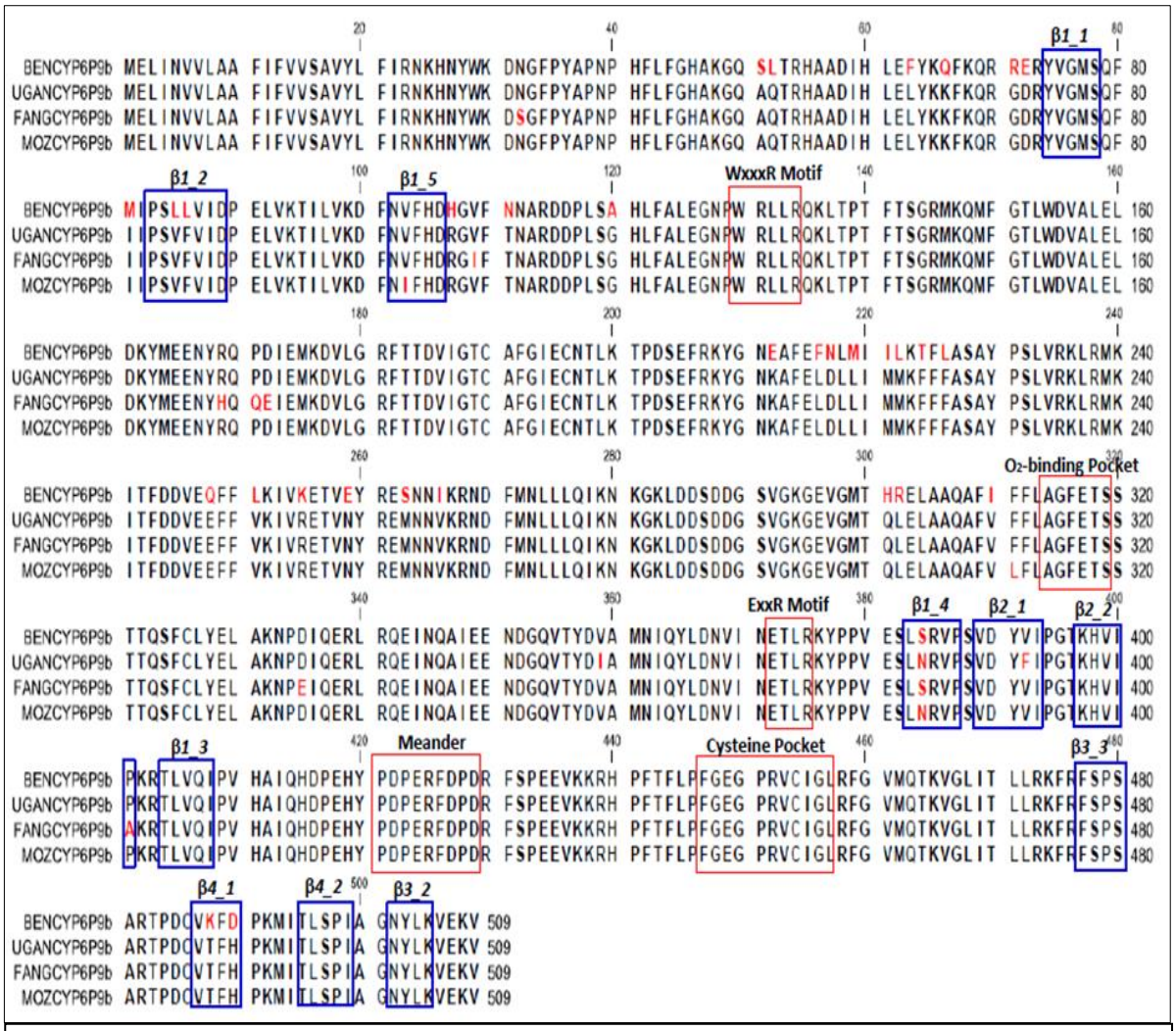

Figure 2.4: Structurally-conserved regions of *An. funestus* CYP6P9b sequences from resistant and susceptible strains. Red solid lines represent WxxxR motif, O_2-binding pocket/proton transfer group, ExxR motif, meander and cysteine pocket/heme-binding region; blue solid lines correspond with the protein *β*-sheets. Amino acids substitution is highlighted in pink.

2.4.2 Modelling and Molecular Docking Simulation Analyses

2.4.2.1 Models Production and Assessment

CYP6P9a and CYP6P9b models were generated with heme already in place and verifications with Errat v2.0 indicated that the models have reasonably good scores with highest overall quality factor obtained from UGANCYP6P9b and FANGCYP6P9b models (Appendix 2.2). For CYP6P9a models, regions with high disorderliness (backbone deviation from the crystal structure of the template used) shown in

black (Figure 2.5A and B) include amino acids 20-40 corresponding to the hydrophobic terminal domains that anchor the P450 to the surface of the membrane and residues preceding the αA helix, amino acids 60-120 encapsulating αA helix, *β1-1*, *β1-2,* αB helix and *β1-5* containing the putative SRS1, amino acids 280-300 corresponding to the loop joining the *C*-terminus of αH to the *N*-terminus of αI.

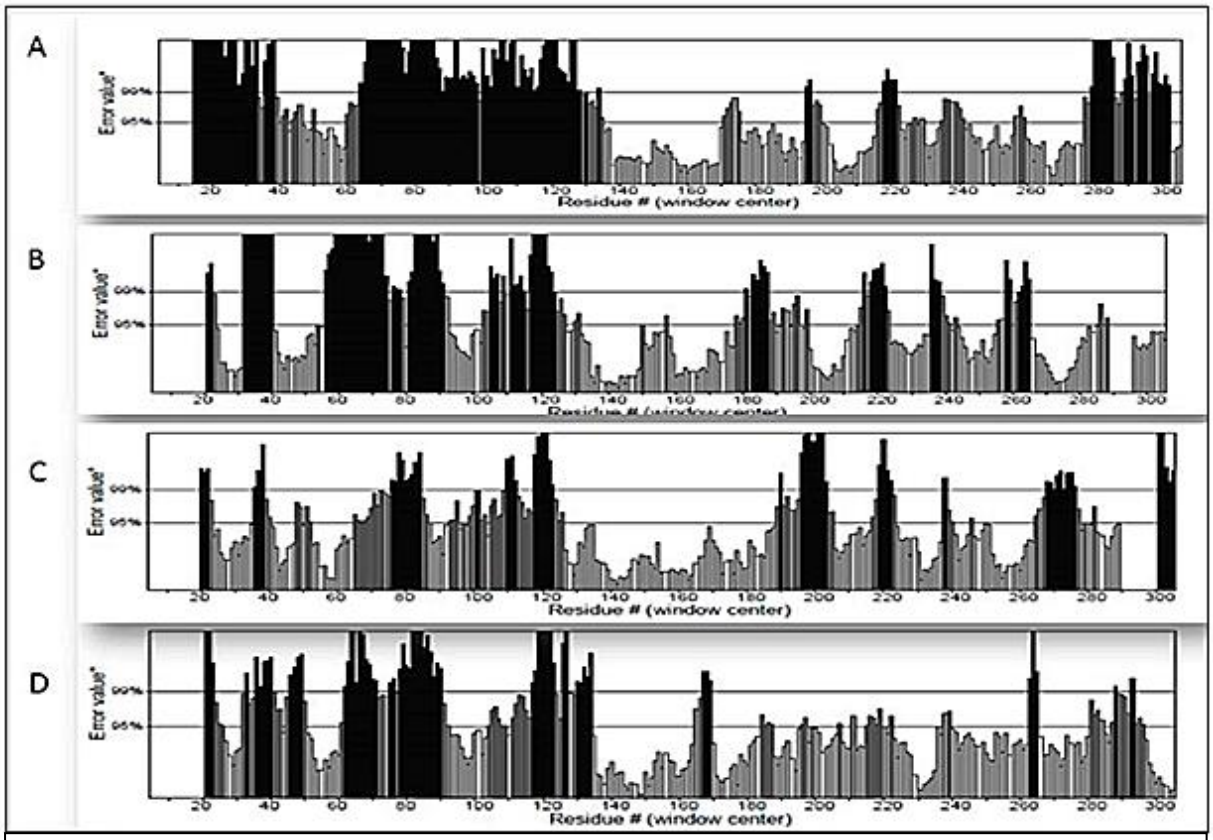

Figure 2.5: Errat plot for the lowest energy model. Disordered regions are identified on the error axis*, where 2 lines are drawn to indicate the confidence with which it's possible to reject regions that exceed the error value. The Overall Quality Factor represents the percentage of the protein within which the error value is below 95% rejection limit as given in Appendix 2.2. A and B are plots from MALCYP6P9a and FANGCYP6P9a models, while C and D represent plots of models of MOZCYP6P9b and FANGCYP6P9b respectively.

Regions with high disorder (backbone deviation from the folding pattern of the template) in CYP6P9b models (Figure 2.5C and D) include amino acids 10-40 corresponding to the sequences that constitute the hydrophobic membrane anchor, amino acids 70-90 corresponding to *β1-1* and *β1-2*, amino acids 110-120 mapped to *β1-5* containing the putative SRS1, as well as amino acids 195-220 which corresponds to the part of the F-G loop.

CYP6P9b models exhibited lesser backbone deviation compared with CYP6P9a models, though the models were created from the same 1TQN template which shares 32% and 33% identity respectively.

2.4.2.2 Molecular Docking Simulations

Binding energy of a ligand is defined as the difference in free energy of the protein plus the unbound ligand, and their complex; ChemScore estimates the total free energy change that occurs on ligand binding (Jones et al., 1997). Docking scores along with other relevant regression terms for binding of insecticide structure to CYP6P9a and CYP6P9b models are given in Tables 2.6 to 2.10 respectively. The general atom type parameters assigned to both atoms of ligand and that of receptor in contact with the ligand include S_{lipo} (lipophilic term: chlorine, bromine and iodine atoms which are not ions; sulphurs which are not acceptor or polar types; carbons which are not polar type); H_{bond} (*H bond donor:* nitrogens with hydrogens attached, hydrogens attached to N or O; *H-bond donor/acceptor:* oxygens attached to hydrogens, imine nitrogen; *H-bond acceptor:* oxygens not attached to hydrogens, N with no hydrogens and one or two connections, halogens that are ions, sulphurs with one connection); S_{Polar}(*non-H bond*: nitrogens with no hydrogens attached and more than two connections, phosphorus, sulphurs attached to one or more polar atoms (including H-bonding atoms and not including polar carbon atoms or fluorine atoms), carbons attached to two or more polar atoms (including H-bonding atoms and not including polar carbon atoms or fluorine atoms), carbons in nitriles or carbonyls, nitrogen atoms with no hydrogens and four connections, fluorine atoms); ΔE_{clash} (clash penalties between ligand atoms and receptor heavy atoms); S_{Metal} (contact between acceptor and/or donor atom in the receptor with the metal atom of the ligand, if any)(Verdonk et al., 2003, Eldridge et al., 1997, Baxter et al., 1998).

Detoxification of pyrethroids in insects follow two principal routes: ester hydrolysis catalysed by esterases and P450s, and hydroxylation of aromatic rings or methyl groups by P450s (Gilbert and Gill, 2010). Infra-red and NMR spectroscopy and TLC analysis established that housefly P450s preferentially hydroxylate permethrin isomers at position 4’ or 6 of the phenoxybenzyl ring and the

trans-methyl group (Shono et al., 1979), while *trans*-permethrin can be hydroxylated in position 6 of the benzyl ring and *cis*-permethrin in *cis*-methyl group as well as hydroxylation at 2' position. Other spectroscopic analysis, for example an LC-MS determined metabolism of deltamethrin by *An. gambiae* CYP6M2 to proceed preferentially via 4' hydroxylation (Stevenson et al., 2011).

Docking solutions obtained from this study were manually analysed, and productive poses with highest scores and lowest free binding energy selected for further analysis.

Docking of Permethrin: Permethrin docked in BENCYP6P9a with 2' position exposed for hydroxylation at a distance of 4.2Å (Figure 2.6A). In UGANCYP6P9a, FANGCYP6P9a and MALCYP6P9a, permethrin docked with the *trans* methyl group oriented toward the heme at a distance of 2.6Å, 5.7Å and 3.6Å respectively (Figure 2.6B, C and D) indicating that with the exception of BENCYP6P9a permethrin metabolism is predicted to proceed via *trans* methyl group hydroxylation. However, the pose with resistant models has the lower clash penalty and higher score (Table 2.6) indicating that the resistant alleles possibly possess the higher activity, compared with *FANGCYP6P9a* allele whose model produced lowest score and highest clash penalty.

Table 2.6: ChemScores of the productive binding of permethrin in CYP6P9a and CYP6P9b models

Models	Rank	ChemScore (kJ/mol)	ΔG (kJ/mol)	S(hbond)	S(metal)	S(lipo)	ΔE(clash)	ΔE (int)
BENCYP6P9a	2nd	44.14	-45.60	0.00	0.00	374.66	0.24	1.22
UGANCYP6P9a	1st	45.77	-47.54	0.00	0.00	391.27	0.50	0.27
FANGCYP6P9a	1st	37.91	-38.91	0.00	0.00	317.47	0.90	0.19
MALCYP6P9a	2nd	40.79	-43.49	0.00	0.00	356.63	0.15	2.55
BENCYP6P9b	1st	43.44	-44.22	1.01	0.00	362.91	0.22	0.57
UGANCYP6P9b	1st	43.32	-44.04	0.21	0.00	332.92	0.23	0.50
FANGCYP6P9b	1st	41.25	-42.88	1.00	0.00	346.85	1.94	1.68
MOZCYP6P9b	1st	46.07	-47.82	0.76	0.00	393.69	0.81	0.94

ΔG = free energy of binding, S(hbond) = contribution from hydrogen bonds, S(lipho) = lipophilic term, ΔE(clash) = clash penalties between ligand and receptors heavy atoms, and ΔE(int) = internal energy of the ligand or receptor.

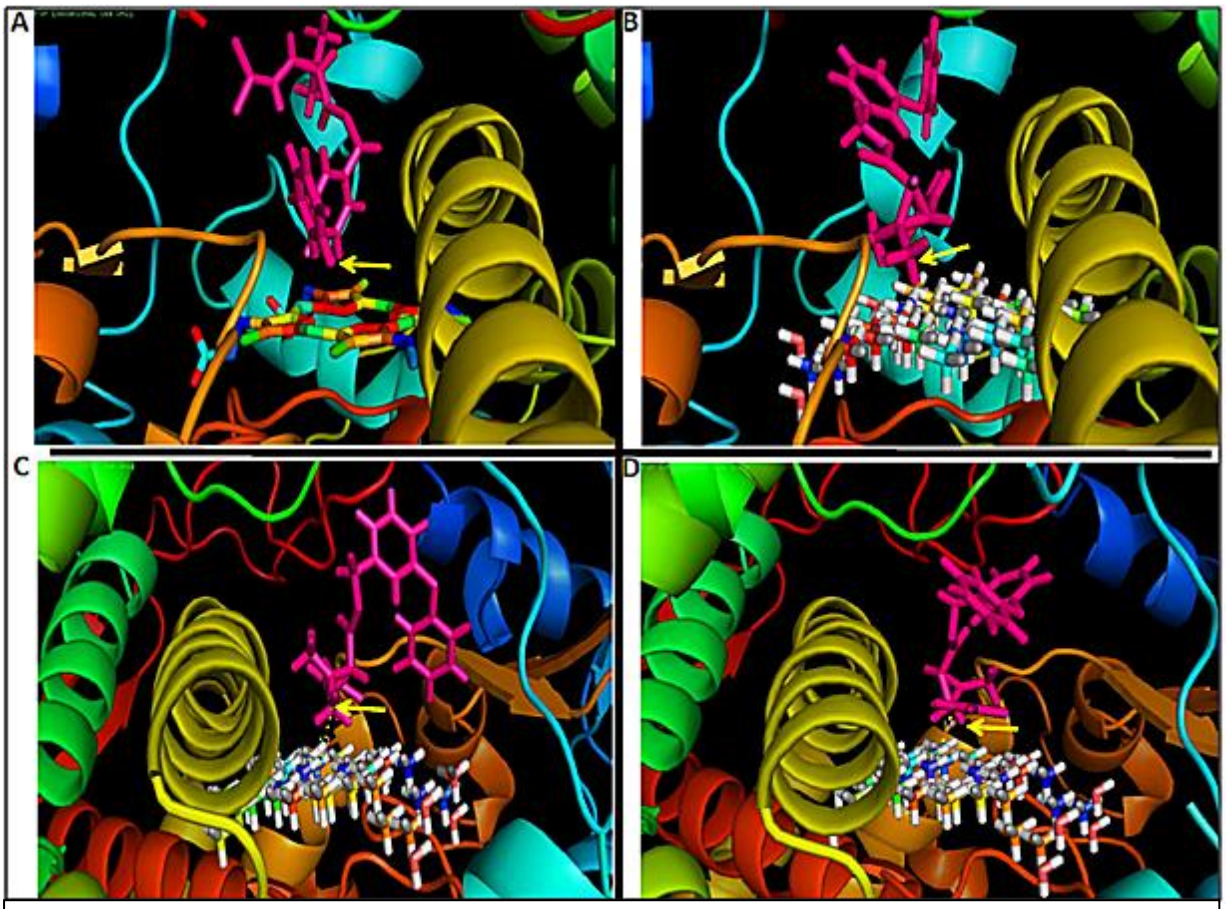

Figure 2.6: Binding modes of permethrin in (A) BENIN, (B) UGANDA, (C) FANG and (D) MALAWI CYP6P9a models. Permethrin is in stick format and hot pink. Heme atoms are in spectrum. Possible sites of metabolism are indicated with yellow arrows.

In BENCYP6P9b permethrin docked productively with the 4' spot of the phenoxy ring oriented above the heme at a distance of 3.3Å (Figure 2.7A), while in the active site of UGANCYP6P9b the insecticide docked with the 6 position of the phenyl ring at a distance of 3.7Å (Figure 2.7B). Permethrin docked to the active site of FANGCYP6P9b with dihalovinyl groups approaching the heme and the possible sites of attack away from the catalytic centre; *trans*-methyl group located 9.1Å from heme iron (Figure 2.7C) and 2' spot of phenyl ring at a 11.8Å distance. This unproductive conformation is the only pose in the ten top ranked solutions which exhibited a very high clash penalty.

In MOZCYP6P9b model the pyrethroid approached the heme with 4' spot of the phenoxy group docked above the heme iron, at a respectful distance of 3.1Å (Figure 2.7D). This binding mode

has the highest score and lowest free energy of binding, and thus *MOZCYP6P9b* was predicted to have highest activity for permethrin compared with all the other *CYP6P9a* and *CYP6P9b* alleles.

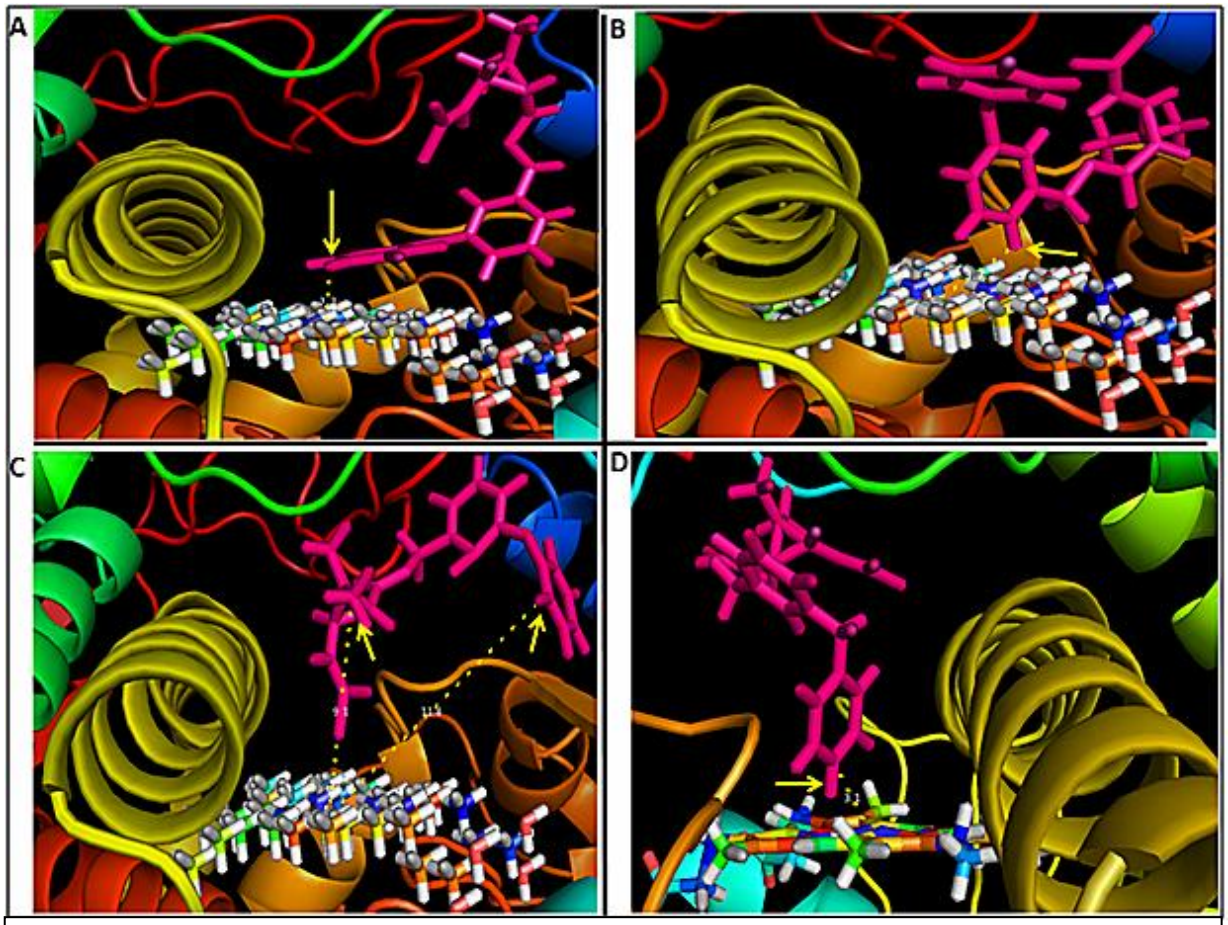

Figure 2.7: Binding modes of permethrin in (A) BENIN, (B) UGANDA, (C) FANG and (D) MOZAMBIQUE CYP6P9b models. Permethrin is in stick format and hot pink. Heme atoms are in stick format and spectrum. Possible sites of metabolism are indicated with red arrows.

Docking of Deltamethrin: P450-mediated biotransformation of deltamethrin possessing an α-cyano group have been shown to proceed via ester cleaved products and the 4'-hydroxy metabolites in the bulb mite *Rhizoglyphus robini* (Ruzo et al., 1988). Sequential metabolism of deltamethrin by *An. gambiae* CYP6M2 was revealed (Stevenson et al., 2011). Using *in silico* modelling and docking, LC-MS and NMR spectroscopy, Stevenson and colleagues have shown that CYP6M2 preferentially hydrolyses deltamethrin to initial product at 4' position, with trans-methyl hydroxylation being a minor route.

Analysis of the binding conformation of BENCYP6P9a and UGANCYP6P9a docked with deltamethrin revealed that the insecticide docked with the 2' position at a distance of 1.7Å and 4.0Å

respectively from the heme iron, with high score, very low binding energy and low clash penalties (Table 2.7, Figure 2.8A and B). The 4' spot however pointed away from the heme iron in both these solutions.

In contrast, in FANGCYP6P9a and MALCYP6P9a deltamethrin docked with the *trans* methyl group above the heme at a distance of 6.4Å and 3.4Å respectively (Figure 2.8C and D). These binding modes shared by these two alleles make them different from Benin and Uganda models in that *cis* and/or *trans* methyl hydroxylation is predicted in the top ranked poses for Malawi and FANG alleles. However, the *trans* methyl group in MALCYP6P9a was positioned closer to the heme compared with the situation in FANGCYP6P9a in which the deltamethrin is away for productive contact. Also, FANGCYP6P9a exhibited the highest clash penalty and MALCYP6P9a exhibited the lowest penalty compared with the other alleles. The high clash score for FANG may reflect steric hindrance/clashes with heavy atoms of the protein, restricting access to the catalytic hotspot and reducing catalysis.

Table 2.7: ChemScores of the productive binding of deltamethrin in CYP6P9a and CYP6P9b models

Models	Rank	ChemScore (kJ/mol)	ΔG (kJ/mol)	S(hbond)	S(metal)	S(lipo)	ΔE(clash)	ΔE (int)
BENCYP6P9a	1st	43.31	-46.31	0.00	0.00	384.88	0.79	2.03
UGANCYP6P9a	3rd	42.82	-44.14	0.00	0.00	366.31	0.76	0.75
FANGCYP6P9a	5th	41.01	-42.47	0.00	0.00	333.00	1.69	0.77
MALCYP6P9a	2nd	43.21	-45.81	0.00	0.00	380.88	0.32	3.87
BENCYP6P9b	1st	44.02	-45.31	0.00	0.00	347.54	0.25	0.74
UGANCYP6P9b	1st	42.90	-44.47	0.00	0.00	369.16	0.09	1.49
FANGCYP6P9b	1st	39.77	-41.38	1.97	0.00	307.33	0.98	0.69
MOZCYP6P9b	1st	45.90	-49.76	0.49	0.97	364.36	0.23	1.43

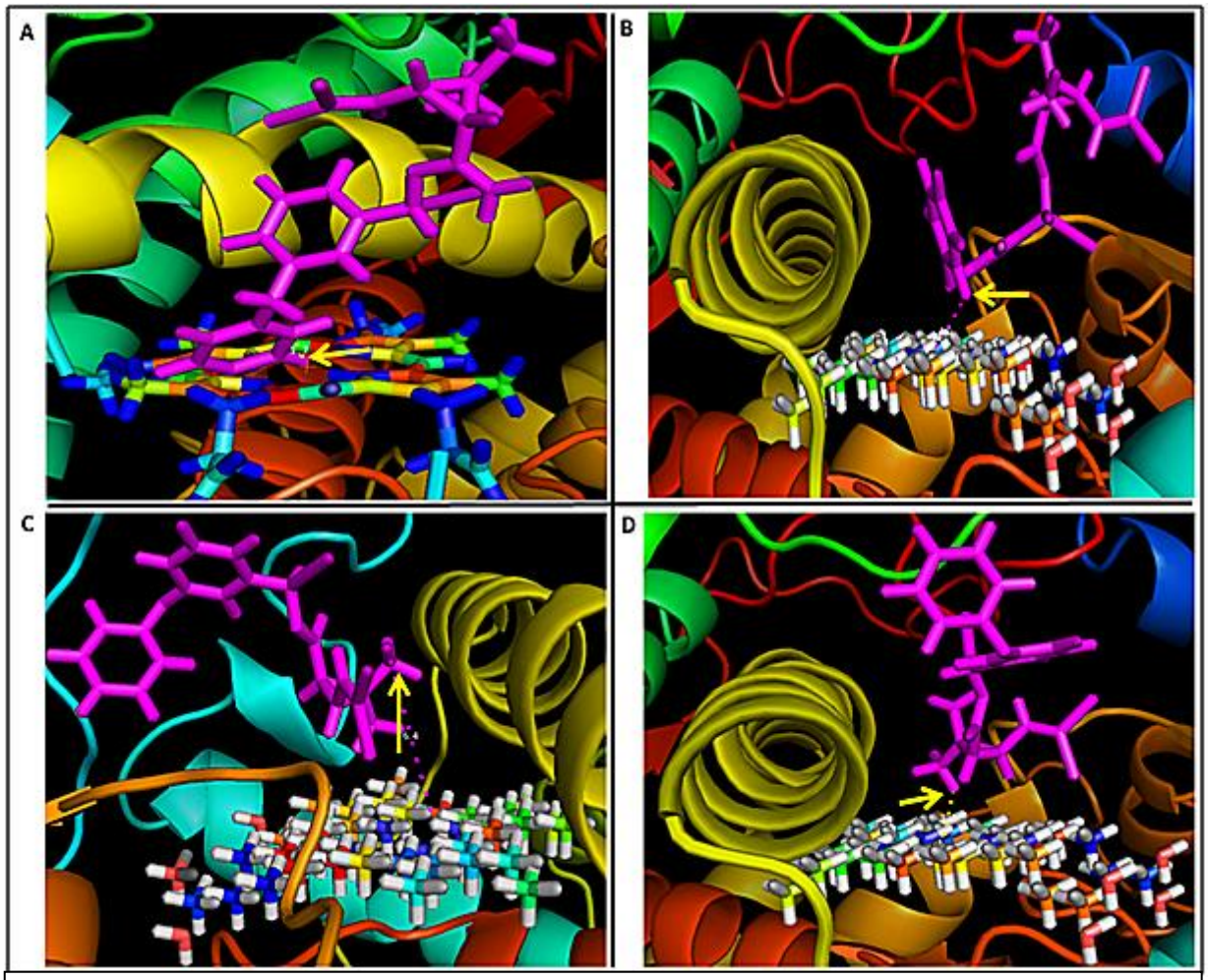

Figure 2.8: Binding modes of deltamethrin in (A) BENIN, (B) UGANDA, (C) FANG and (D) MALAWI CYP6P9a models. Deltamethrin is in stick format and magenta. Heme atoms are in spectrum. Possible sites of metabolism are indicated with yellow arrows.

With BENCYP6P9b and UGANCYP6P9b deltamethrin docked productively with 4' spot above the heme iron at a distance of 3.5Å and 4.1Å respectively (Figure 2.9A and B), with UGANCYP6P9b exhibiting low clash penalty (Table 2.7). Though, the insecticide docked in the active site of FANGCYP6P9b productively but in contrast the target 4' spot of the phenoxy ring is 8.9Å from heme iron catalytic hotspot (Figure 2.9C) with lower chances of optimal metabolism. Equally also, the binding mode of this model has the lowest scores and portrayed a very high contribution of hydrogen bonds than obtained with the other models.

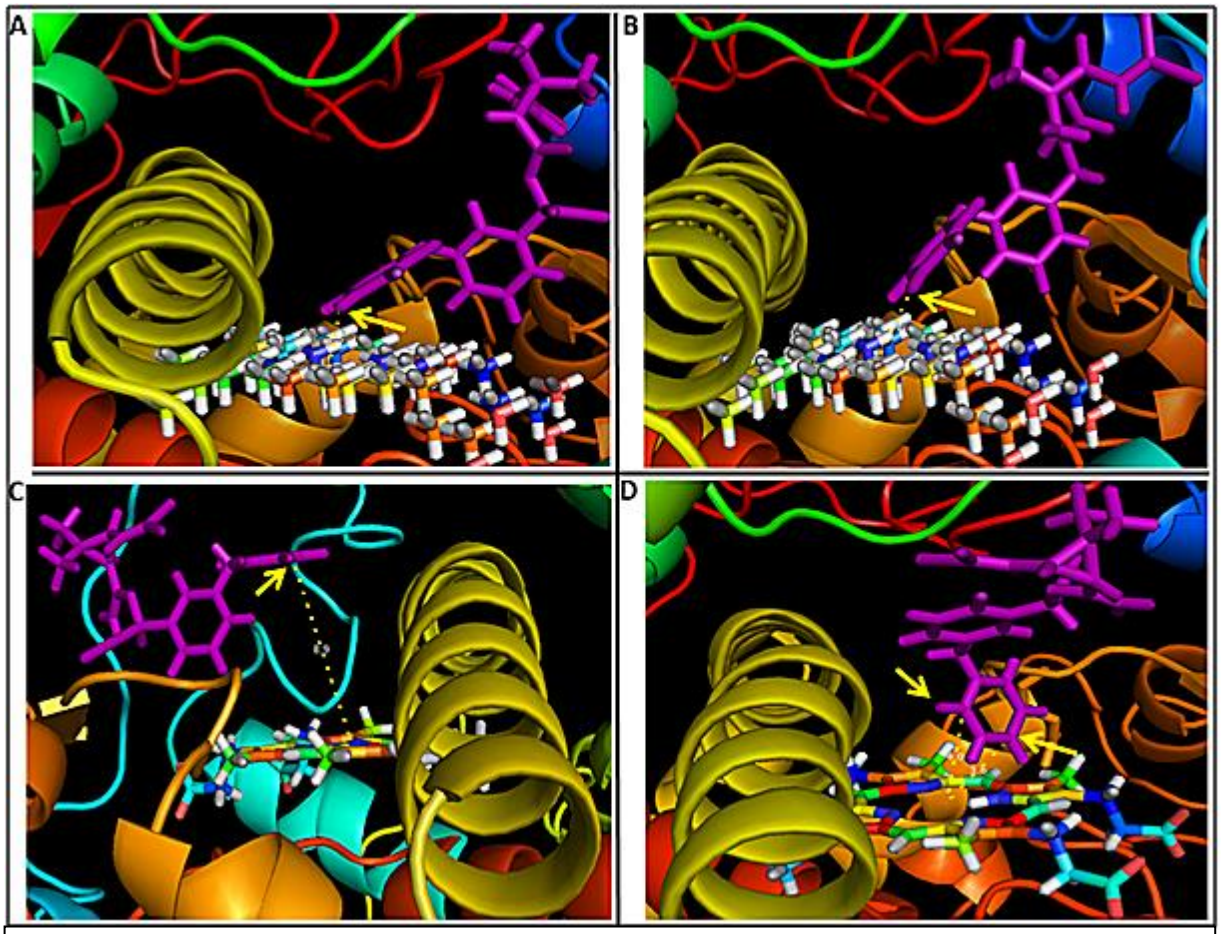

Figure 2.9: Binding modes of deltamethrin in (A) BENIN, (B) UGANDA, (C) FANG and (D) MOZAMBIQUE CYP6P9b models. Deltamethrin is in stick format and purple. Heme atoms are in spectrum. Possible sites of metabolism are indicated with yellow arrows.

The insecticide docked into MOZCYP6P9b in a perfect pose with the 4' position exposed for hydroxylation at reasonable distance of 3.6Å from the heme iron and 2' position, 4.0Å away (Figure 2.9D). This mode has the highest score of all the CYP6P9b models and lowest binding energy predicting highest activity toward deltamethrin compared with the results from models from FANG, and other models from resistant alleles. The fifth and sixth ranked solution with CYP6P9b model has the gem dimethyl moiety close to the heme at a distance of about 4-5Å (figure not provided). Thus *cis*/*trans*-methyl hydroxylation is predicted to occur from MOZCYP6P9b-mediated metabolism of deltamethrin, leading to multiple primary metabolites.

Docking of Etofenprox: Docking scores with etofenprox were comparable to values obtained with permethrin and deltamethrin (Table 2.8) with BENCYP6P9a having highest score, while FANGCYP6P9a exhibited lowest scores and largest clash penalty. In BENCYP6P9a, UGANCYP6P9a and MALCYP6P9a etofenprox docked in the top ranked solutions with aromatic groups above the heme and 2′ spot of phenoxy ring 3.3Å, 3.1Å and 2.2Å respectively from the heme (Appendix 2.5). In contrast, the insecticide docked in FANGCYP6P9a with ethoxy group positioned 5.7Å above the heme. In this posture sites of attack are predicted as the ether group or methyl groups (the closest being 3.5Å from heme iron), but etofenprox has been shown to be metabolised through aromatic ring hydroxylation, specifically in rats and dogs via 4′ hydroxylation (Hawkins, 1985) and these postures may not support optimal metabolism. Etofenprox is thus predicted to be metabolised by all the resistant alleles of CYP6P9a but not by FANGCYP6P9a.

In BENCYP6P9b and MOZCYP6P9b etofenprox docked possibly productively with 2′ spot of phenoxy ring oriented above the heme catalytic center at a distance of 3.4Å and 3.7Å respectively (Appendix 2.5). Though the insecticide docked in the same productive fashion in FANGCYP6P9b the 2′ spot is 6.6Å from the heme and this placed the insecticide away from the catalytic center and possibly reflect lower activity compared with the alleles from resistant strains. In UGANCYP6P9b the insecticide docked with 6 position of the benzyl ring at a distance of 5.5Å from the heme in all the top ranked solutions. A characteristic feature of docking with etofenprox is the unusually high clash penalty obtained from all models of CYP6P9b, indicating that this insecticide may not fit optimally in the active site of *CYP6P9b* for metabolism compared with the prediction the software made for the other pyrethroids.

Table 2.8: ChemScores of the productive binding of etofenprox in the CYP6P9a and CYP6P9b models

Models	Rank	ChemScore (kJ/mol)	ΔG (kJ/mol)	S(hbond)	S(metal)	S(lipo)	ΔE(clash)	ΔE (int)
BENCYP6P9a	1st	51.73	-54.38	0.00	0.00	449.12	0.65	0.74
UGANCYP6P9a	1st	50.84	-52.15	0.19	0.00	430.07	0.42	0.89
FANGCYP6P9a	1st	47.60	-49.88	0.83	0.00	386.99	0.95	1.32
MALCYP6P9a	1st	49.13	-50.93	0.00	0.00	419.62	0.06	1.73
BENCYP6P9b	5th	46.18	-47.34	0.89	0.00	363.42	1.36	0.98
UGANCYP6P9b	1st	51.07	-53.21	0.91	0.00	413.30	1.24	0.90
FANGCYP6P9b	1st	48.49	-49.51	0.00	0.00	407.52	1.38	0.64
MOZCYP6P9b	1st	52.41	-55.41	0.00	0.00	457.95	1.61	1.61

Docking of DDT: DDT is converted to dichlorodiphenyldicholoroethane (DDD) by reductive dechlorination in insects and higher animals (Kitamura et al., 2002), for example the reaction effected by *CYP6G1* in *D. melanogaster* (Joussen et al., 2008). However, DDT is mainly converted to DDE by dehydrochlorination in mammals and insects (Gold and Brunk, 1983, Smith, 2012) though dicofol (kelthane) is also generated. Mitchell and colleagues (Mitchell et al., 2012) have reported *An. gambiae* CYP6M2 capable of metabolizing DDT to dicofol, in presence of solubilising factor sodium cholate.

DDT exhibited good but lower docking scores with CYP6P9a and CYP6P9b models compared with values obtained from docking with pyrethroids (Table 2.9). But in all alleles of CYP6P9a *p,p'*-DDT docked away from heme iron for productive metabolism to take place. In the case of BENCYP6P9a, UGANCYP6P9a and FANGCYP6P9a the best ranked poses have target C-2 at a distance of 10.1Å, 8.5Å and 9.2Å respectively from heme (Appendix 2.6), away for metabolism to be effected. The second ranked DDT pose in MALCYP6P9a has chlorine group of the benzyl ring pointing unproductively at the heme and the C-4' at a distance of 4.5Å.

In BENCYP6P9b and UGANCYP6P9b DDT docked unproductively, away from the heme with C-2 at a distance of 8.7Å and 5.5Å respectively from heme iron. In Benin model the second benzyl ring of DDT clashes with the heme ring while in Uganda model its the trichloroethyl group that clashes with

the heme ring with a high penalty. The second ranked pose in FANGCYP6P9b has C-2 of DDT positioned at 9.8Å from heme iron, while in MOZCYP6P9b DDT docked away from heme iron with C-2 at 16.6Å distance.

The potentially unproductive binding conformation of DDT in all CYP6P9a and CYP6P9b models from field resistant populations, as well as the susceptible strain (FANG) suggests that these P450s are poor binders and/or poor metabolizers of this organochlorine insecticide.

Table 2.9: ChemScores of the productive binding of DDT in CYP6P9a and CYP6P9b models

Models	Rank	ChemScore (kJ/mol)	ΔG (kJ/mol)	S(hbond)	S(metal)	S(lipo)	ΔE(clash)	ΔE (int)
BENCYP6P9a	1st	36.20	-37.47	0.00	0.00	295.30	0.33	0.95
UGANCYP6P9a	2nd	38.36	-39.71	0.00	0.00	314.43	0.24	0.61
FANGCYP6P9a	2nd	35.46	-36.43	0.00	0.00	286.40	0.78	0.18
MALCYP6P9a	2nd	35.59	-39.20	0.00	0.00	284.48	2.55	0.19
BENCYP6P9b	1st	31.89	-32.91	0.00	0.00	256.36	0.65	0.37
UGANCYP6P9b	1st	29.23	-31.03	0.00	0.00	240.24	1.67	0.13
FANGCYP6P9b	2nd	33.20	-33.40	0.00	0.00	260.55	0.17	0.03
MOZCYP6P9b	1st	29.20	-31.75	0.00	0.00	246.38	0.85	1.69

Docking of Bendiocarb: In animals including man, rats and insects bendiocarb can be metabolised in several ways; these include hydrolytic cleavage to generate benzodioxol-4-ol, hydroxylation of the phenyl ring and hydroxylation of the *N*-methyl moiety (Roberts and Hutson, 1999). Ester hydrolysis to generate bendiocarb phenol has been described as the major pathway of metabolism of bendiocarb in the maize pest *D. undecimpunctata howardi* (Hsin and Coats, 1987). Recently Edi and colleagues (Edi et al., 2014) have reported a recombinant CYP6P3 from *An. gambiae* able to metabolise bendiocarb *in vitro* but more needs to be done to functionally characterise the mechanism of bendiocarb metabolism in Anopheline mosquitoes, especially *An. funestus*.

Binding scores of bendiocarb in CYP6P9a and CYP6P9b models were the lowest of all the insecticides screened. The insecticide docked in BENCYP6P9a and BENCYP6P9b in unproductive mode, in a tight embrace with heme in BENCYP6P9a and the phenyl ring clashing with the heme ring in

BENCYP6P9b (Appendix 2.7). The insecticide docked in UGANCYP6P9a with the C-5 of the phenyl ring pointing towards the heme iron at a distance of 5.4Å. In this mode, metabolism is possible through aromatic ring hydroxylation but the Chemscore as in the rest of docked poses with all alleles is very low (Table 2.10). In FANGCYP6P9a bendiocarb docked away with the C-5 of the phenyl ring 12.9Å from heme iron, while in MALCYP6P9a it docked with 2,2-dimethyl carbon atom pointing to the heme iron at a distance of 7.6Å. This potentially productive pose makes it possible for *N*-methyl hydroxylation were it not for the very low scores obtained.

Bendiocarb docked to UGANCYP6P9b unproductively with phenyl ring and *N*-methyl moiety clashing with the heme ring. For FANGCYP6P9b only the 10th ranked pose did not clash with the heme ring. In this pose the phenyl ring is located 14.7Å from heme iron and thus away for catalysis to take place. The insecticide docked unproductively, way from the heme in MOZCYP6P9b with 2,2-methyl group positioned 8.7Å from heme iron. Thus, the software predicted that *CYP6P9a* and *CYP6P9b* from both resistant and susceptible alleles do not bind bendiocarb and possibly have no activity towards the representative carbamate insecticide.

Table 2.10: ChemScores of the productive binding of bendiocarb in CYP6P9a and CYP6P9b models

Models	Rank	ChemScore (kJ/mol)	ΔG (kJ/mol)	S(hbond)	S(metal)	S(lipo)	ΔE(clash)	ΔE (int)
BENCYP6P9a	1st	22.49	-23.37	1.73	0.00	132.91	0.82	0.05
UGANCYP6P9a	1st	21.13	-22.17	0.98	0.00	144.16	0.53	0.52
FANGCYP6P9a	8th	13.57	-14.03	0.88	0.00	77.50	0.22	0.24
MALCYP6P9a	1st	21.02	-21.19	0.99	0.00	135.48	0.00	0.16
BENCYP6P9b	1st	20.53	-20.97	2.16	0.00	100.29	0.07	0.38
UGANCYP6P9b	1st	23.20	-23.34	1.95	0.00	126.39	0.00	0.13
FANGCYP6P9b	10th	11.53	-11.91	0.93	0.00	57.89	0.00	0.37
MOZCYP6P9b	1st	21.74	-22.04	1.81	0.00	119.45	0.07	0.23

2.4.3 Active Site Residues and Enzymes-Substrates Interactions

The majority of enzymes combine several strategies to enhance the rate of catalysis (Nelson et al., 2012). These include (1) covalent catalysis: acid-base catalysis involving key active sites amino acid residues, catalysis involving side chain(s)/cofactor(s) nucleophile, as well as the metal ion catalysis (metal taken up from the solution or tightly bound to the enzyme); (2) weak, non-covalent interactions: hydrophobic interactions, hydrogen bonds, vdW forces and electrostatic attractions. Evidences have shown that P450-mediated metabolism is carried out using the weak, non-covalent intra- and inter-molecular/atomic interactions to boost up the binding energy several orders of magnitude (Kenaan et al., 2011, Szklarz and Paulsen, 2002, Yoshioka et al., 2002, Paine et al., 2003).

To understand the key amino acid residues lining the active/binding sites of CYP6P9a and CYP6P9b models pattern of non-bonded interaction in the binding cavities were compared between southern African alleles and FANG using the productive poses of pyrethroids in the binding cavity of the models. The southern African alleles were chosen because highest resistance to pyrethroids were observed in southern Africa, where the two genes *CYP6P9a* and *CYP6P9b* are highly overexpressed compared with same genes from Benin (West Africa) and Uganda (East Africa), because of the highest signature of selection from them, and because the docking with pyrethroids predicted the southern African alleles of *CYP6P9a* and especially *CYP6P9b* to possess the highest activities compared with the *FANGCYP6P9a* and *FANGCYP6P9b*.

2.4.3.1 Deltamethrin

2.4.3.1.1 Active site residues of **CYP6P9a** *models*

Within MALCYP6P9a deltamethrin is surrounded by eleven nonpolar, aliphatic side chains notably from SRS1 (Ala^{113}, Leu^{118}, Ala^{124} and Leu^{125}) and Ile^{310}, Leu^{313} and Ala^{314} all from SRS4. Bulky, hydrophobic residue within 5.0Å of deltamethrin include Phe^{110} of the SRS1 which π-stack in T-shaped fashion with the phenoxy ring of deltamethrin at a distance of 4.31Å, Phe^{123} of SRS-1 which π-stack

face to face with the benzyl ring of deltamethrin at 3.7Å distance, Phe[216] (SRS2), which π-stack in T-fashion with the phenoxy ring, as well as Phe[309] positioned at a distance of 4.6Å from the phenoxy ring, two histidine residues, His[107] and His[121] both from SRS1 (Figure 2.10A). This cluster of phenylalanine forms a roof above the active site maximizing hydrophobicity and together with the large number of nonpolar, aliphatic side chains, make the binding site of deltamethrin highly hydrophobic. The aromatic residues may also contribute to catalysis via resonance stabilisation of aromatic rings of deltamethrin as it approached the heme.

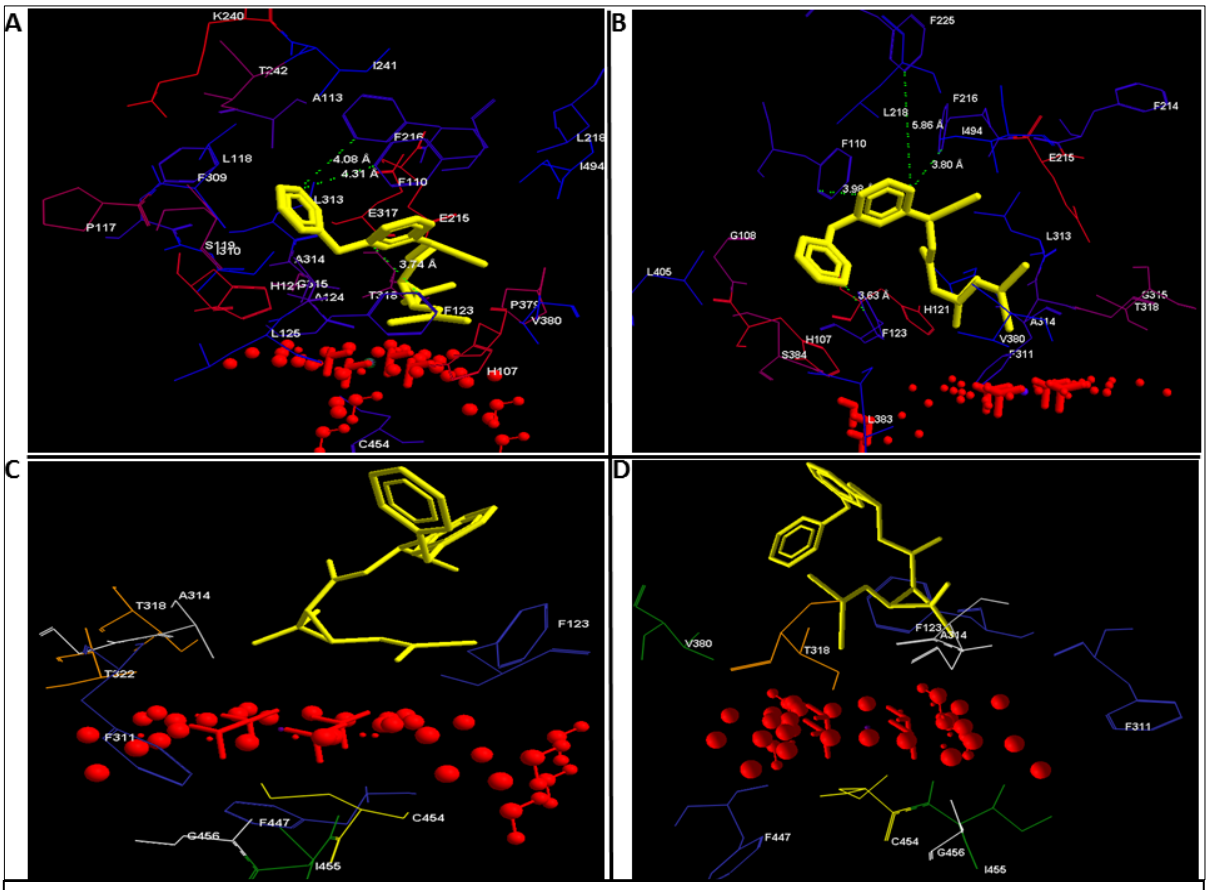

Figure 2.10: Binding modes of deltamethrin in MALCYP6P9a (A) and (C) and FANGCYP6P9a (B) and (D) models, showing residues involved in hydrophic contact, within 5.0Å radius (A and B) and residues from the predicted inter-molecular hydrogen bonds (C and D). Amino acid residues are annotated with numbers and heme atoms in red.

Though the cavity contains polar side chains including Ser[119] of SRS1, Glu[215] of SRS2, Thr[242] and Thr[318] of SRS4 (oxygen binding pocket) all of which could participate in a network of hydrogen bonding, MMV analysis predicted no hydrogen bonds between deltamethrin and amino acid residues

of MALCYP69a (Figure 2.10C) in agreement with the docking parameters with deltamethrin. This suggests that distal residues are not fully exploited in hydrogern bonding machinery to optimise conversion of Cpd O into Cpd I. For CYP6P9a, hydrogen bonds and ionic interactions might be secondary in importance compared with hydrophic and aromatic group interaction and π-anchorage.

In FANGCYP6P9a deltamethrin is surrounded within 5.0Å radius by seven nonpolar, aliphatic residues notably from SRS4 (Leu^{313} and Ala^{314}) and SRS5 (Val^{380} and Leu^{383}) (Figure 2.10B). This is in sharp contrast to the nonpolar residues in the binding site of deltamethrin within MALCYP6P9a the majority of which belong to SRS1. However, six phenylalanine residues surrounded deltamethrin in FANGCYP6P9a, four of which are less than 6.0Å from the aromatic rings. These include Phe^{110} (SRS1) which is in face to face π-stacking with benzyl ring (3.98Å), Phe^{123} (SRS1) which π-stack in sandwich fashion with phenoxy ring (distance of 3.63Å), as well as Phe^{216} (SRS2) and Phe^{225} both of which π-stack in a T-fashion with the benzyl ring (distances of 3.80Å and 5.86Å, respectively). The presence of large number of aromatic residues surrounding the insecticide indicated that FANGCYP6P9a employs hydrophobic interactions and resonance stabilisation as well, to effect catalysis.

Though the binding site harbors residues that could be involved in hydrogen bonding with deltamethrin (e.g. Glu^{215} (SRS2), Thr^{318} (SRS4) and Ser^{384} (SRS5), as obtained from analysis with MALCYP6P9a, no inter-molecular hydrogen bond was predicted between FANGCYP6P9a and deltamethrin (Figure 2.10D).

The absence of hydrogen bonding in the docking of deltamethrin these allele models is in line with the docking parameters obtained (no hydrogen bonding score for CYP6P9a with pyrethroids) and further strengthen the assumption that hydrophobic contacts, resonance stabilisation and π-π interactions are the major mechanisms for catalysis in CYP6P9a. However, from this analysis, no clue was found to substantiate the differences in the other binding parameters (ChemScore and free energy of binding) obtained from the resistant MALCYP6P9a and susceptible FANGCYP6P9a models.

2.4.3.1.2 Active site residues of CYP6P9b *models*

Deltamethrin in MOZCYP6P9b is surrounded within 5.0Å radius by eight nonpolar, aliphatic side chains (Figure 2.11A). There are only three bulky, hydrophobic side chains from Phe^{316} located 3.27Å from phenoxy ring, Phe^{226} and Phe^{312}. However, the insecticide is surrounded by a network of polar, neutral side chains of Ser^{119}, Thr^{111} , Asn^{112}, Ser^{319} and Ser^{320} (all residues from SRS1). These amino acids together with Arg^{114} (SRS1) and Glu^{247} (SRS3) could create a hydrogen bonding network that could bind the acid group allowing the alcohol group to approach the heme. They can also be involved in ionic interactions, enhancing catalysis. A hydrogen bond is predicted to be donated by the alcohol side chain of Thr^{111} to the acyl group of the acid moiety of deltamethrin (acceptor) with a distance of 2.95Å and a maximum binding energy of -2.5kJ/mol (Figure 2.11C).

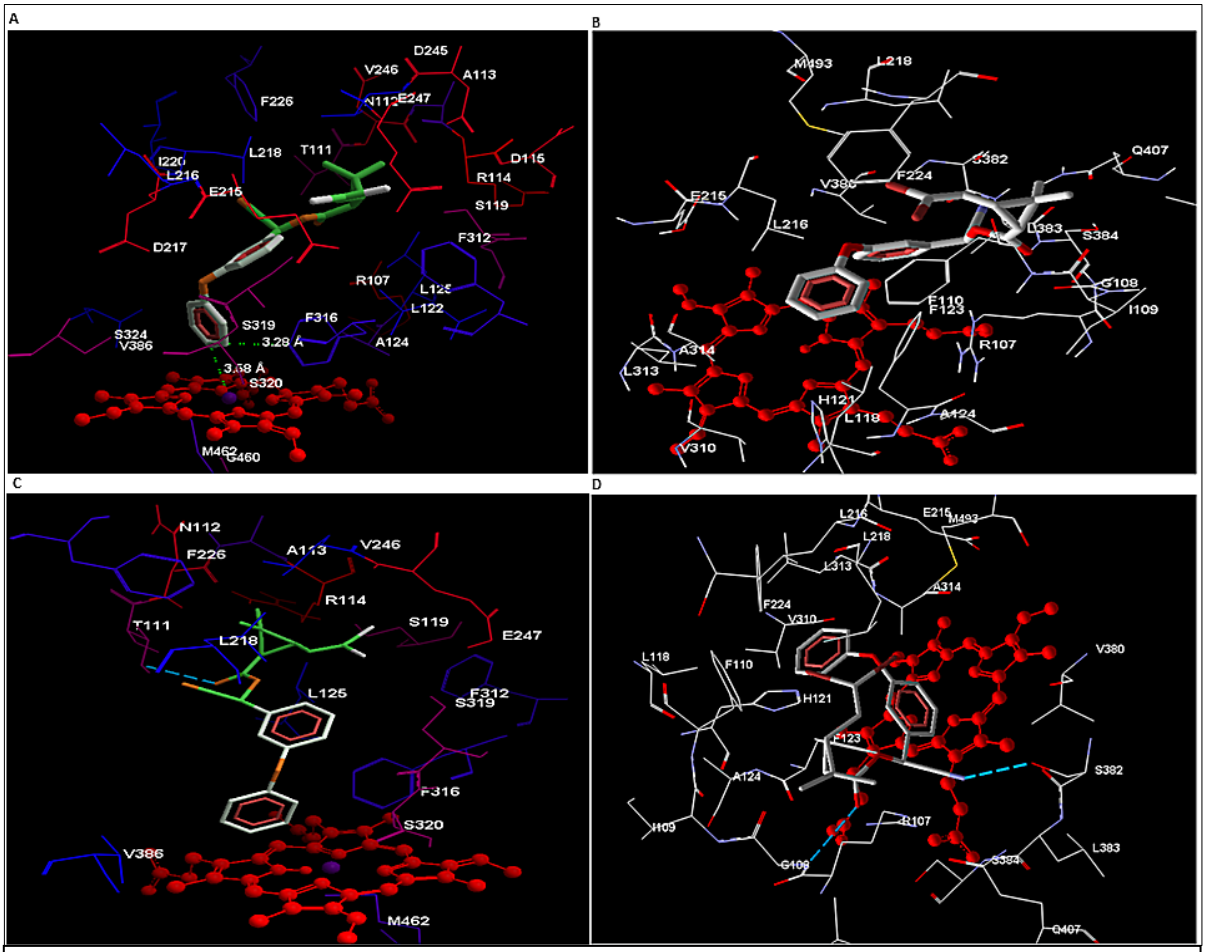

Figure 2.11: **Binding mode of deltamethrin in MOZCYP6P9b (A) and (C) and FANGCYP6P9b (B) and (D) with residues involved in hydrophobic contact (5.0Å radius) (A and B) and residues involved in intermolecular hydrogen bonds (C and D).** Amino acid residues are annotated with numbers and heme atoms in red. Inter-molecular hydrogen bondings are depicted in broken blue lines.

This distal hydrogen –bonding machinery are thought to accelerate formation of Cpd I from Cpd O, reducing generation of H_2O_2 and other O_2-wasting species (Shaik et al., 2005), as well as regulating the redox potential of the heme. The negatively charged side chain of Glu^{247} and the positive, guanidinium moiety of Arg^{114} are thought to be involved in ionic interaction stabilizing the ligand through electrostatic interactions. In contrast with the MALCYP6P9a and FANGCYP6P9a models, the MOZCYP6P9b binding cavity is not crowded with bulky aromatic side chains or proline residues. This property is predicted to increase the active site volume of *MOZCYP6P9b* and the access of pyrethroid insecticides to the heme catalytic center, enhancing catalysis.

In FANGCYP6P9b deltamethrin is surrounded within 5.0Å radius by eleven aliphatic, hydrophobic side chains (Figure 2.11B) and three bulky, aromatic rings: Phe^{224}, Phe^{110} (located 3.40Å from phenoxy ring with a possibility of parallel displaced π-stacking) and Phe^{123} which is positioned at 3.37Å distance from the phenoxy ring and could π-stack in a T-shape fashion. These two aromatic rings are also very close to each and could π-stack with each other to increase resonance stability of the phenoxy-benzyl moiety of deltamethrin. Thus, the topology of the binding site of deltamethrin in FANGCYP6P9b reflects a highly hydrophobic environment and extensive hydrogen bond networks.

Two intermolecular hydrogen bonds were predicted (Figure 2.11D): (i) between the alcohol side chain of Ser^{382} (SRS5) and the α-cyano group of the deltamethrin; within a distance of 2.96Å and contributed a maximum of -2.5kJ/mol binding energy; (ii) between the acyl oxygen of the acid group and the peptide bond between Arg^{107} and Gly^{108} (3.06Å and -1.86kJ/mol energy). In addition the binding site contains the His^{121} of SRS1, the Glu^{215} of SRS2 as well as Met^{493} which maps to SRS6 which could also be involved in hydrogen bonding network and ionic interactions enhancing catalysis. Though additivity of hydrogen bonds is beneficial, presence of so many hydrogen bonding interactions could be one of the mechanism which stabilised the insecticide a considerable distance (8.9Å away) from the heme catalytic center and possibly resulted in lower ChemScore towards deltamethrin as compared with the docking solutions from the resistant models, especially of MOZCYP6P9b.

2.4.4 Identification of Substrate Access Channel *pw2a*

Substrate access/product egress channels have been described as one of the most important factors that determine P450 activity toward substrates (Wade et al., 2004). Possible routes through which substrate can enter the active site or product egresses were searched in two models each from resistant (MALCYP6P9a and MOZCYP6P9b) and susceptible (FANGCYP6P9a and FANGCYP6P9b) strains.

For *MOZCYP6P9b* model a total of 30 substrates access and/or products egress tunnels were predicted from the interior active site of the protein to the bulk solvent. Of these channels the first ranked with highest throughput (0.86) (Figure 2.12A), lowest energy cost (0.27), and which is longest (21.42Å) has its gorge lined with about 41 residues. These tunnel-lining residues of which none is more than 3.0Å from the tunnel include those from the SRS1 (Arg^{107}, Gly^{108}, Val^{109}, Thr^{111}, Ser^{119}, Leu^{122}, Phe^{123}, Leu^{125}), those from SRS2 (Phe^{214}, Glu^{215}, Leu^{216}, and Asp^{217}), residues from SRS3 (Asp^{245}, Val^{246} and Glu^{247}), residues from SRS4 and O_2-binding pocket (Phe^{316}, Ser^{319}, Ser^{320} and Ser^{324}), residues from SRS5 including Arg^{385}, Val^{386}, Val^{387}, Ser^{388}, Asp^{390}, Tyr^{391} and residues from heme-binding region including Arg^{452}, Val^{453}, Cys^{454}. These tunnel-lining residues from BC loop, F/G loop, *β1_4* (SRS5), αI helix (SRS4) correspond to the channel *pw2a* described for many P450s (Wade et al., 2004, Cojocaru et al., 2007). Channel *pw2a* has been found to be common to many proteins studied by simulation; has been established to be the most energetically favourable of all the pathways observed in *CYP101* (Wade et al., 2004) and is proposed to be common to all P450s. It was also established as a product egress route for CYP101 and CYP2B4. This later property was described as possible because the *pw2a* is a holey channel, made possible due to the potential motion in the FG loop and/or the BC loop.

CAVER computed 23 possible tunnels for *FANGCYP6P9b* of which the first ranked (Figure 2.12B) with lower throughput (0.74) and higher cost (0.30) than the one from MOZCYP6P9b, is almost half short in length (13.91Å). Only 24 amino acid residues lined the tunnel gorge including those from SRS1 (Arg^{107}, Phe^{110}, Thr^{111}, Leu^{118}, His^{121}, Phe^{123} and Ala^{124}); residues from the SRS2 (Phe^{214}, Glu^{215}, Leu^{216}), residues from FG loop (Phe^{224}, Lys^{240}, Ile^{241}); one residue from SRS3 (Phe^{243}); residues from

SRS4 (including Gly^{315} and Thr^{318}, Phe^{309}, Val^{310} and Leu^{313}); Val^{380} of the SRS5 as well as Cys^{454} of the cysteine pocket. The corresponding Ile^{109} of FANGCYP6P9b is not part of any of the channels predicted for FANGCYP6P9b model. Another important difference observed is that deltamethrin docked in active site of MOZCYP6P9b is surrounded by this tunnel, the same insecticide in the model of FANGCYP6P9b is not enshrouded by the substrate access channel.

CAVER computed 27 channels for MALCYP6P9a and 22 channels for FANGCYP6P9a; however the first five top ranked tunnels for two alleles were not different in their composition and parameters.

These findings suggest that substrate access maybe playing a great role in the resistant alleles from *CYP6P9b* with tunnel lining residues for example the Val^{109} playing a critical role in proper positioning and affinity/specificity toward pyrethroids.

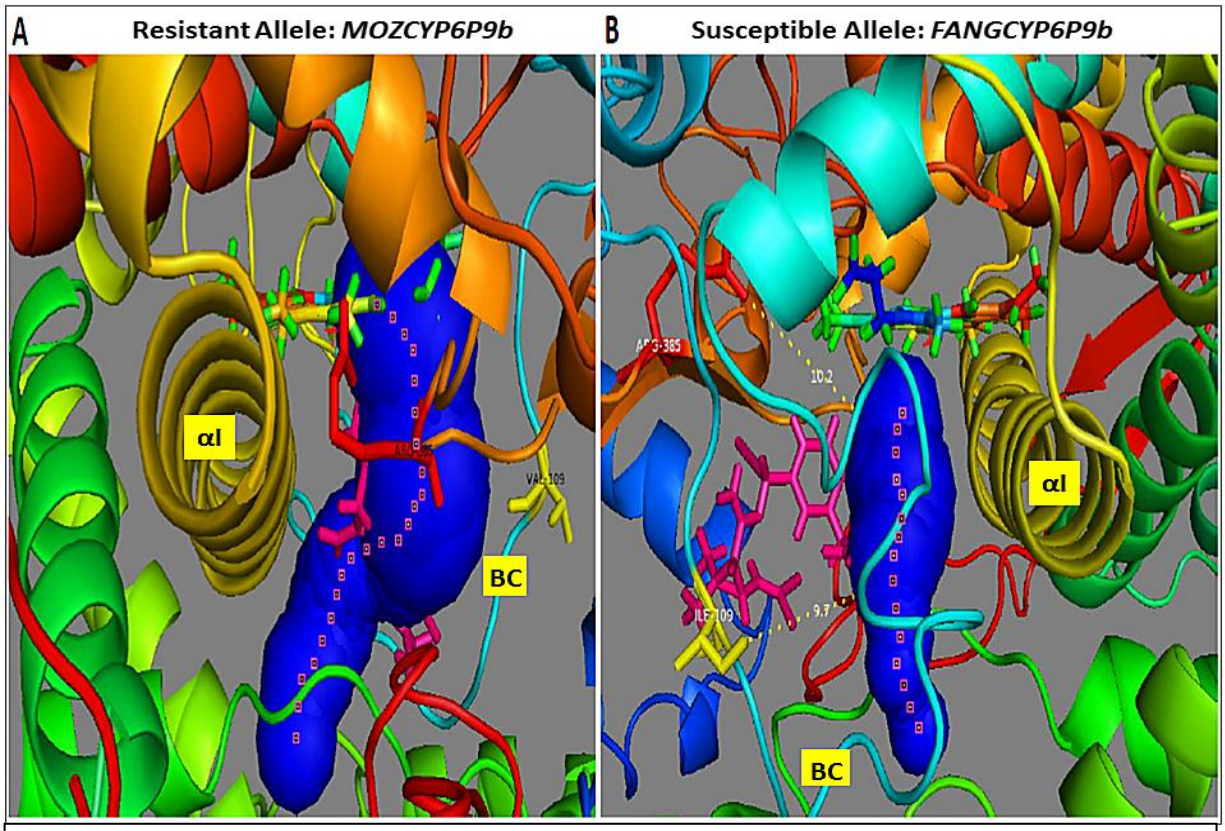

Figure 2.12: Trajectory of the substrates access channel *pw2a* in (A) MOZCYP6P9b and (B) FANGCYP6P9b models docked with deltamethrin. Helix I and BC loops are annotated; *pw2a* is in blue; deltamethrin is in stick format and pink; heme atoms are presented in stick format and spectrum. Val^{109} and Ile^{109} are annotated respectively.

2.5 Discussion and Conclusion

CYP6P9a with 17 haplotypes across Africa and 15 amino acid sequences is more polymorphic than *CYP6P9b* which posseses only 15 haplotypes and 11 different sequences. This is as observed in previous studies with alleles of *CYP6P9a* and *CYP6P9b* from southern Africa (Malawi and Mozambique) compared with the susceptible strain, FANG (Riveron et al., 2013). The East and southern African alleles of *CYP6P9a* exhibited reduced nucleotide variatins and seem to be undergoing directional selection while the West African *BENCYP6P9a* and the susceptible *FANGCYP6P9a* show high nucleotide diversity and are not undergoing directional selection.

CYP6P9b from FANG portrayed high polymorphic variations compared with the resistant alleles all across Africa (East, West and southern Africa). However, in contrast to West African *CYP6P9a*, *BENCYP6P9b* allele which portrayed extensive inter-allelic variation compared with the other resistant alleles of *CYP6P9b* is undergoing intra-allelic directional selection in its unique way. This phenomenon suggests a central importance of *CYP6P9b* over *CYP6P9a* within the context of directional selection and possibly pyrethroid resistance in general.

Comparison of the predominant haplotypes of *CYP6P9a* and *CYP6P9b* from resistant strains with corresponding sequences from *FANG* revealed that *CYP6P9a* has only two amino acids replacement that seem to be relatively fixed, while *CYP6P9b* possess seven mutations that are fixed in all the resistant strains compared with *FANG*. These 7 mutations in addition to $Ser^{384}Asn$ substitution (absent in *BENCYP6P9b*) map to catalytically important domains of *CYP6P9b* and are predicted to impact on the catalytic property of *CYP6P9b* from resistant alleles, making it possibly different from *FANGCYP6P9b* in terms of metabolic activity.

ChemScore of less than -30 was described as a predictor of tight binding ligands (Marechal et al., 2006), and based on this, pyrethroids etofenprox, permethrin and deltamethrin were predicted to be the tightest binders in order of listing. Docking analyses revealed dramatic differences in regio-

selectivity of different CYP6P9a and CYP6P9b models toward pyrethroid insecticides. The southern African models have the highest scores on average and all the models from resistant strains exhibited productive poses with pyrethroids, consistent with the established docking solution with other P450s. The FANG models have lower scores, docked away from the heme catalytic centre for optimal metabolism, or unproductively as observed with permethrin in FANGCYP6P9b (dihalovinyl group approaching the heme) and etofenprox in FANGCYP6P9a (ethoxy group above the heme).

While etofenprox docked into the active site of both CYP6P9a and CYP6P9b from resistant alleles with 2' spot of phenoxy ring oriented for attack (suggesting that these two genes may not differ in their activities toward etofenprox and primary product generated), remarkable differences were observed in the conformations of permethrin and deltamethrin within the active site of CYP6P9a and CYP6P9b. For example, the top ranked solutions of permethrin in UGANCYP6P9a, FANGCYP6P9a, MALCYP6P9a and deltamethrin in FANGCYP6P9a and MALCYP6P9a predicted *trans* methyl hydroxylation as the preferential mode of metabolism, while in BENCYP6P9b and MOZCYP6P9b with permethrin, as well as all CYP6P9b models (BEN-, UGAN-, FANG- and MOZCYP6P9b) with deltamethrin it's the 4' spot of the phenoxy ring which is oriented for metabolism. This established that CYP6P9a and CYP6P9b differ in their regio-selectivity toward permethrin and deltamethrin, with gem dimethyl attack favoured by CYP6P9a while 4' spot of phenoxy is the most preferred site of attack by CYP6P9b. The only exception is MOZCYP6P9b which produced multiple bound conformations with permethrin and deltamethrin (*trans* methyl group oriented for attack in some top ranked solutions) indicative of more than one primary metabolite.

The 4' spot has been described as the major site of attack on deltamethrin by insect P450s (Stevenson et al., 2011) and this productive pose is the one obtained especially with CYP6P9b from resistant alleles, and was predicted to have high activity towards pyrethroids. Its possible that *CYP6P9b* alleles are more efficient in pyrethroid metabolism compared with their *CYP6P9a* counterparts.

CYP6P9a and CYP6P9b models were also discovered to differ considerably in the composition of their pyrethroid binding sites, and this is reflected in the topology and geometry of their respective active sites. While the binding site of pyrethroids in CYP6P9a contains large number of aromatic (bulky) residues and possibly utilizes hydrophobic interactions, π-stacking, vdW interactions and resonance stabilization to drive catalysis, the active site of CYP6P9b especially from southern Africa contains few bulky residues and thus hydrophobic interaction is secondary in importance to ionic interactions and hydrogen bonding. The active site of CYP6P9b is rich in polar charged and neutral side chains with possibility of ionic attractions and hydrogen bonds driving catalysis. Ionic interactions have been described as the important non-bonded phenomena through which residues Glu^{216} and Asp^{301} exert substrate specificity and product region-selectivity in CYP2D6 (Paine et al., 2003). Thus, hydrogen bondings are predicted to be the most important factor for non-bonded interactions within the active site of both resistant MOZCYP6P9b and susceptible FANGCYP6P9b models, while its predicted to be of secondary importance in MALCYP6P9a and FANGCYP6P9a which showed no intermolecular hydrogen bonds with both permethrin and deltamethrin.

Analysis of the substrate access channels predicted that MOZCYP6P9b differs considerably in its topology compared with FANGCYP6P9b. The MOZCYP6P9b possesses a wide open channel *pw2a* which may enhance access of pyrethroids to the binding site and catalysis. The MOZCYP6P9b channel *pw2a* housed the Val^{109} residue predicted to be involved in affinity/specificity toward pyrethroids.

Analysis of nucleotide diversities and amino acid sequences of alleles of *CYP6P9a* and *CYP6P9b* coupled with modelling and docking simulations predicted that allelic variation is impacting on the activity of *CYP6P9a* and *CYP6P9b* toward pyrethroid insecticides with the alleles from resistant strains (especially from southern Africa) having high activity compared with alleles from susceptible strain (*FANG*) which were predicted to have lowest activity.

Allelic variation has been shown to impact on the catalytic activity of other P450s. For example, comparison of allelic variants *CYP6AB3v1* and *CYP6AB3v2* (a difference of only five amino

acid residues) of *D. pastinacella* (parsnip webworm) established that only a single amino acid difference Val^{92} in CYP6AB3v1 and Ala^{92} in CYP6AB3v2 makes the latter able to metabolize imperatorin, a toxic furanocoumarin with a high rate (Mao et al., 2007). It was also recently shown that a single mutation in the *GSTe2* gene (Leu^{119}Phe substitution) from resistant strain of *An. funestus* from Benin resulted in an increased binding cavity making the Phe^{119} variant capable of metabolizing DDT and conferring resistance in this specie.

DDT has ChemScore of less than -30 but the fact that DDT produced unproductive poses in all the docking solutions with alleles from the resistant strains as well as *FANG* suggests that even if this organochlorine insecticide binds to the pyrethroid, it may not be metabolized. DDT is established from several studies to be metabolized by CYP450s by dehalogenation of trichloromethyl group (Chiu et al., 2008, Amichot et al., 2004) and thus the docking results obtained here predicted DDT docking in either unproductive mode or away from the heme catalytic center for optimal metabolism.

Bendiocarb produced very low docking scores on average half or three-fold less than values obtained with the pyrethroid insecticides. The docking parameters and conformation of bendiocarb in the active sites of *CYP6P9a* and *CYP6P9b* indicated no activity toward this carbamate insecticide.

Docking simulations predicted CYP6P9a and CYP6P9b models from resistant alleles from southern Africa as having high activity towards pyrethroid insecticides. This is consistent with the widespread pyrethroid resistance in *An. funestus* strains where these genes are the most overexpressed. The docking software predicted no activity towards DDT predicting that these genes are not involved directly in DDT resistance observed in East and West African population of *An. funestus*. For DDT resistance in West Africa, it has been established that *CYP6P9a* and *CYP6P9b* are not involved; rather a *GSTe2* variant is responsible for the extreme resistance in *An. funestus* from Benin, West Africa (Riveron et al., 2014b). The software predicted no activity toward bendiocarb as well, suggesting that these P450s are not involved in carbamate resistance observed in West and southern African

population of *An. funestus*. Factors responsible for carbamate resistance in these regions need to be found urgently.

Molecular docking predictions are subject to experimental validation and thus pyrethroid-metabolizing activity predicted by the docking algorithm and inactivity toward DDT and bendiocarb must be validated with laboratory experiments including probes assay to assess binding affinities and metabolism assays to determine catalytic activities toward these insecticides screened.

3. ASSESSMENT OF METABOLIC EFFICIENCY OF ALLELIC VARIANTS USING FLUORESCENT PROBES, METABOLISM ASSAY AND TRANSGENIC EXPRESSION OF *CYP6P9a* and *CYP6P9b* ALLELES

3.1 Background

Modelling and docking analyses predicted that the *CYP6P9a* and *CYP6P9b* alleles from resistant strains of *An. funestus* are capable of metabolizing Type I and Type II pyrethroids with higher efficiency compared with corresponding alleles from susceptible strain. Even between the resistant alleles, variations in metabolic activities were predicted with the southern African alleles especially of *CYP6P9b* anticipated to have highest activity of all the alleles screened. The docking software also predicted that recombinant CYP6P9a and CYP6P9b possess no enzymatic activity toward non-pyrethroid insecticides DDT and bendiocarb. However, docking is *in silico* simulations and not enough evidence in itself and therefore subject to experimental validations. *In vitro* heterologous expression and estimation of P450 activity as established using mammalian cells (COS cells), yeast cells like *S. cerevisiae,* insect cells (Baculovirus *sf9* cells), as well bacterial (*E. coli*) expression systems (Gonzalez and Korzekwa, 1995, Waterman and Johnson, 1991, Pritchard et al., 2006a) have been widely applied to characterise the metabolic activity of candidate P450s. Heterologous expression of P450s and functional characterisation using fluorescent probes assays have been used for functional validation of modelling predictions. For example: (i) modelling analysis, heterologous expression in *E. coli*, probes assay and metabolism assays revealed that *An. gambie* CYP6Z2 can bind pyrethroids permethrin and cypermethrin but cannot metabolize them (McLaughlin et al., 2008), (ii) *in silico* modelling and heterologous expression of *Ae. aegypti* CYP6Z8 (ortholog of *An. gambiae CYP6Z2*) in recombinant yeast cells coupled with fluorescent probes assay, HPLC metabolism assays and MS/MS identification of metabolites have revealed that this P450 is capable of metabolizing primary products of pyrethroid metabolism from carboxylesterases, including 3-phenoxybenzoic alcohol and 3-phenoxybenzaldehyde into 3-phenoxybenzoic acid (Chandor-Proust et al., 2013).

Site-directed mutagenesis (SDM) have evolved into a powerful approach that allows molecular biologists to unveil the protein-structure function relationships. It is an invaluable tool that makes it realisable to modify DNA sequences for desired end (Zheng et al., 2004) with random or target mutations introduction in the protein coding sequence followed by screening the mutant library for functional activity changes. SDM has been used extensively to identify key amino acid residues that are involved in catalysis. For example, (i) Glu^{216}Leu/Gln/Phe mutation of CYP2D6 have been shown to result in 100-fold decrease in affinity in the K_M of bufurarol and dextromethorphan (Paine et al., 2003); (ii) Asp^{293}Ala replacement in human CYP2C9 resulted in 90% decrease in activity and 3-10 times increased K_M for diclofenac, dextromethorphan and tolbutamide (Flanagan et al., 2003); (iii) Val^{92}Ala substitution in *D. pastinacella* CYP6AB3v1 caused quantitative changes making the P450 as efficient as CYP6AB3v2 in metabolizing plants allelochemical imperatorin (Mao et al., 2007).

Several other insect P450s implicated as insecticides metabolisers have been functionally characterised by various approaches, including liquid chromatography (Stevenson et al., 2012, Duangkaew et al., 2011, Mitchell et al., 2012) as well as combination of LC/MS and NMR-spectroscopy (Stevenson et al., 2011). On *Anopheles funestus*, we have already functionally characterized the role of duplicated P450s (*CYP6P9a* and *CYP6P9b* alleles from southern Africa: see Appendix 5 for list of publications derived from this study). Both CYP6P9a and CYP6P9b recombinant proteins metabolize Type I and II pyrethroids (Riveron et al., 2013, Riveron et al., 2014a).

In vivo transgenic expression of candidate genes has also been used in several studies to establish the role of P450s in metabolism of insecticides and resistance. For example, *D. melanogaster CYP6G1* has been implicated as the cause of DDT resistance using transgenic overexpression (Daborn et al., 2007), and transgenic expression of *T. castenaum CYP6BQ9* in *D. melanogaster* established its involvement in deltamethrin resistance (Zhu et al., 2010). Using transgenesis, we have also established that the southern African *CYP6P9a* and *CYP6P9b*, as well as *CYP6M7* confer resistance to Type I and Type II pyrethroids in *An. funestus, in vivo* (Riveron et al., 2013, Riveron et al., 2014a) (Appendix 5).

3.2 Aim and Objectives

The main aim of this section was to establish whether the allelic variation observed in the major pyrethroid resistance genes- the cytochrome P450s *CYP6P9a* and *CYP6P9b*, impacts their metabolic efficacy as predicted by modelling and thus could be the key factor responsible for pyrethroid resistance in field populations of *An. funestus*. The specific aims of this study were to:

1-Assess the metabolic activity of various alleles using fluorescent probes followed by kinetics with diethoxyfluorescein and inhibition assays;

2-Establish the activity of various alleles of both genes with pyrethroids, organochlorine and carbamate insecticides, followed by kinetics analyses with permethrin and deltamethrin;

3- Identify the key amino acid change(s) which confer pyrethroid-metabolizing efficiency in the resistant alleles of these genes using site-directed mutagenesis;

4- Predict *in silico* the mechanism by which such amino changes modify metabolic activity of CYP6P9b.

4- Validate the role of allelic variation of *CYP6P9a* and *CYP6P9b* in pyrethroid resistance by comparing resistant and susceptible alleles with *in vivo* transgenic expression in *D. melanogaster* using the GAL4-UAS system.

3.3 Methods

3.3.1 Cloning and Co-Expression of Recombinant *CYP6P9a* and *CYP6P9b* cDNA with *An. gambiae* Cytochrome P450 Reductase (CPR)

3.3.1.1 Construction of pB13::ompA+2-CYP6P9a and pB13::ompA+2-CYP6P9b Plasmids

Six alleles each from *CYP6P9a* and *CYP6P9b* (were selected for cloning and heterologous expression (Table 3.1).

Table 3.1: Country of origin, *CYP6P9a* and *CYP6P9b* alleles selected for functional characterisation

Country	Allele	Amino Sequence Replacement Mutations
		CYP6P9a
Benin	*BENCYP6P9a*	$Ala^{51}Ser$, $Gln^{52}Leu$, $His^{301}Gln$, $Tyr^{320}Ser$, $Ser^{431}Phe$
Uganda	*UGANCYP6P9a*	$Ala^{51}Ser$, $Gln^{52}Leu$, $His^{301}Gln$, $Tyr^{320}Ser$, $Ser^{431}Phe$
Malawi	*MALCYP6P9a*	$Phe^{63}Leu$, $Gln^{66}Lys$, $His^{301}Gln$, $Tyr^{320}Ser$, $Ser^{431}Phe$
Mozambique	*MOZCYP6P9a*	$Phe^{63}Leu$, $Gln^{66}Lys$, $His^{301}Gln$, $Tyr^{320}Ser$, $Ser^{431}Phe$
Zambia	*ZMBCYP6P9a*	$Phe^{63}Leu$, $Gln^{66}Lys$, $His^{301}Gln$, $Tyr^{320}Ser$, $Ser^{431}Phe$
Angola	*FANGCYP6P9a*	Ala^{51}, Gln^{52}, Phe^{63}, Gln^{66}, His^{301}, Tyr^{320}, Ser^{431}
		CYP6P9b
Benin	*BENCYP6P9b*	$Ser^{32}Asn$, $Ile^{109}Val$, $His^{169}Arg$, $Gln^{171}Pro$, $Glu^{172}Asp$, $Glu^{335}Asp$, $Ala^{401}Pro$
Uganda	*UGANCYP6P9b*	$Ser^{32}Asn$, $Ile^{109}Val$, $His^{169}Arg$, $Gln^{171}Pro$, $Glu^{172}Asp$, $Glu^{335}Asp$, $Ser^{384}Asn$, $Ala^{401}Pro$
Malawi	*MALCYP6P9b*	$Ser^{32}Asn$, $Ile^{109}Val$, $His^{169}Arg$, $Gln^{171}Pro$, $Glu^{172}Asp$, $Glu^{335}Asp$, $Ser^{384}Asn$, $Ala^{401}Pro$
Mozambique	*MOZCYP6P9b*	$Ser^{32}Asn$, $Ile^{109}Val$, $His^{169}Arg$, $Gln^{171}Pro$, $Glu^{172}Asp$, $Glu^{335}Asp$, $Ser^{384}Asn$, $Ala^{401}Pro$
Zambia	*ZMBCYP6P9b*	$Ser^{32}Asn$, $Ile^{109}Val$, $His^{169}Arg$, $Gln^{171}Pro$, $Glu^{172}Asp$, $Glu^{335}Asp$, $Ser^{384}Asn$, $Ala^{401}Pro$
Angola	*FANGCYP6P9b*	Ser^{32}, Ile^{109}, His^{169}, Gln^{171}, Glu^{172}, Glu^{335}, Ser^{384}, Ala^{401}

Full-length, unmodified cDNA of *CYP6P9a* and *CYP6P9b* alleles were expressed as microsomal proteins using *ompA+2* strategy (Pritchard et al., 2006a). cDNA fragment encoding the bacterial outer membrane protein A (*ompA*) leader sequence (21 amino acids) and 2 additional spacer residues (Ala-Pro linker) were introduced as signal peptide *ompA+2* to the NH_2-terminus of the P450 cDNAs in frame with the P450 initiation codon as shown in scheme in Figure 3.1. The signal peptide directs the P450 to the membrane surface (Pritchard et al., 1997) and is thereafter cleaved upon expression in a fashion enhanced by the Ala-Pro spacer residues.

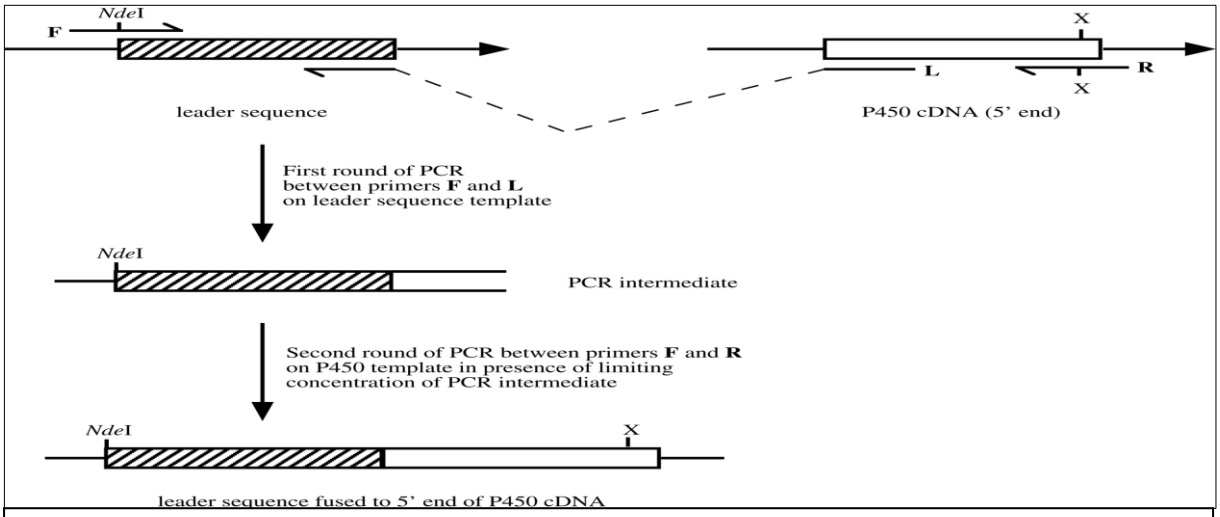

Figure 3.1: General scheme for the PCR-mediated fusion of bacterial leader sequences to P450 cDNAs. Adapted from (Pritchard et al., 1997).

3.3.1.1.1 Construction of ompA+2-CYP6P9a and ompA+2-CYP6P9b cDNA

Initially, a short DNA fragment was synthesized in a fusion PCR using 50ng *E. coli JM109* gDNA as a template with a leader sequence-specific forward primer *ompA+2*F: GGAATTCCATATGAAAAAG ACAGCTATCGCG (*EcoR*I and *Nde*I sites are underlined in green and purple respectively) and a reverse linker primer: *ompA+2CYP6P9a/b*R: CAACACCACGTTAATGAGCTCCATCGGAGCGGCCTGCGCTACGGTAG CGAA which is complementary to the first 24 nucleotides 5' end of *CYP6P9a* and *CYP6P9b* cDNA, underlined in dark red, joined to the last 21 bases linker of the leader sequence. This reverse primer is common to both *CYP6P9a* and *CYP6P9b* that have identical NH_2-terminus. PCR reaction mix is given in Table 3.2 and the High-Fidelity PCR conditions were as follows: 1 cycle at 95°C for 5 min; 35 cycles each of 94°C for 20s, 58°C for 30s, and elongation at 72 °C for 45s; and 1 cycle of final extension at 72°C for 5 min. The PCR product, an intermediate fragment (linker) of less than 100bp (containing the *ompA+2* signal sequence and the first 24 nucleotides was confirmed using gel electrophoresis (Figure 3.2), cleaned with QIAquick® PCR Purification Kit (Qiagen) as explained in section 2.3.2.3(ii) and its quality and quantity assessed with Nanodrop Spectrophotometer (Thermo Fisher).

Table 3.2: PCR reaction mix for *ompA+2* intermediate linker fragment synthesis

Reagent	Final Concentration	Volume (µl)
10x Qiagen Buffer (containing 5mM $MgCl_2$)	1x	5
dNTP mix (25mM)	0.66mM	0.4
*ompA+2*F (10µM)	1µM	1.5
*ompA+2CYP6P9a/b*R (10µM)	1µM	1.5
JM 109 gDNA template	50ng	1.0
dH_2O	-	39.6
HotStar Taq Polymerase	1U/µl	1.0
Total Volume	**-**	50

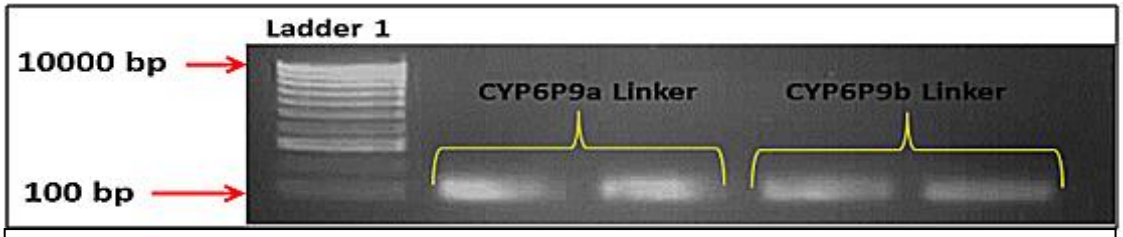

Figure 3.2: ~100 bp intermediate linker product resolved on 1.5% agarose gel stained with Ethidium Bromide.

Next, cDNA minipreps of *CYP6P9a* and *CYP6P9b* alleles prepared in section 2.3.2.3(iii) were used as templates with limiting concentrations of the linker prepared above for second PCR, using the leader sequence-specific forward primer (ompA+2F) and reverse primers:- *ompA+2CYP6P9a*R: TCTAGA GAATTCTCACAATTTTTCCACCTTCAAG and *ompA+2CYP6P9b*R: TCTAGAGAATTCTTACACCTTTTCTACCTTC AAG. These reverse primers designed with *Xba*I and *EcoR*I restriction sites underlined in red and green respectively are complementary to the 3'-terminus of *CYP6P9a* and *CYP6P9b* cDNA. PCR reaction mix is given in Table 3.3 and the High-Fidelity conditions were as follows: 1 cycle at 95°C for 15 mins; 35 cycles each of 94°C for 20s, 50°C for 30s, and elongation at 72 °C for 90s; and 1 cycle of final extension at 72°C for 5 mins. The PCR product, a cDNA containing the *ompA+2* signal peptide joined to the full length cDNA (~1600bp) was confirmed using agarose gel electrophoresis, cleaned with QIAquick® PCR Purification Kit (Qiagen) and its quality and quantity assessed with Nanodrop Spectrophotometer (Thermo Fisher). 5-7ng of these PCR products were ligated into pJET1.2/blunt cloning vector using the CloneJET PCR Cloning Kit (Fermentas) as described in Table 2.2 and transformed into *DH5α* (section 2.3.2.3). Positive colonies screened with pJET1.2 primers listed in Table 2.1 were miniprepped overnight and sequenced using the pJET725 primers for presence of *ompA+2* signal peptide sequence and restriction sites.

Table 3.3: PCR reaction mix for fusion of *ompA+2* leader sequence to CYP6P9a/b cDNA

Reagent	Final Concentration	Volume (µl)
10x Qiagen Buffer (containing 15mM $MgCl_2$)	1x	5
dNTP mix (25mM)	0.66mM	0.4
*ompA+2*F (10µM)	1µM	1.5
*ompA+2CYP6P9a*R/ *ompA+2CYP6P9b*R (10µM)	1µM	1.5
Linker fragment	1ng/µl	0.5
dH_2O	-	40.1
HotStar Taq Polymerase	1U/µl	1.0
Total Volume	**-**	50

3.3.1.1.2 Restriction Digestion of pJET1.2::ompA+2-CYP6P9a/CYP6P9b Construct

The pJET1.2::*ompA+2-CYP6P9b* plasmids were double-digested with restriction enzymes *Nde*I and *Xba*I (Table 3.4) from Fermentas and purified by gel-extraction using the QIAquick® Gel Extraction Kit (QIAgen). Efforts to digest pJET1.2::*ompA+2CYP6P9a* plasmids were unsuccessful and as such the cleaned PCR products from section 3.3.1.1.1 were double digested directly and used for the next step.

Table 3.4: Double digestion of *ompA+2CYP6P9a* and pJET1.2::*ompA+2CYP6P9b* products

Reagent	Final Concentration	Volume (µl)
10x Fast Digest Green Buffer	1x	5
Fast Digest *Nde*I	-	2
Fast Digest *Xba*I	-	2
Plasmid/PCR product	0.1-0.5µg	10-20
dH_2O	As required	20-30
Total Volume	**-**	50

Digestion condition: 37°C for 2 hours and 65°C for 15 mins

3.3.1.1.3 Ligation of Restriction Digests into pCWOri+ Plasmid and Cloning into DH5α

The *ompA+2*-CYP6P9a PCR product and *ompA+2CYP6P9b* plasmid digests were ligated overnight into pCWOri+ expression plasmid already linearized with *Nde*I and *Xba*I restriction enzymes (Table 3.5). pCWOri+ is one of the most convenient expression vector with two *tac* promoter cassettes upstream of *Nde*I ($CA^{\downarrow}TATG$) restriction site coincident with initiation codon ATG (Barnes et al., 1991) as well as a gene encoding *Lac* repressor molecule which prevents transcription from *tac* promoters before addition of inducing agents. A map in Figure 3.3, prepared using the NEB Cutter v2.0 (Vincze et al., 2003) shows the strategy for the construction of the expression plasmid: pB13::*ompACYP6P9b*.

Table 3.5: Ligation of *ompA+2CYP6P9a* and pJET1.2::*ompA+2CYP6P9b* products

Reagent	Final Concentration	Volume (µl)
Restriction Digest	20-50ng	10-25
pCWOri+ Digest	5-10ng	2-4
10x T_4 DNA Ligase Buffer	1x	1
dH_2O	-	As required
T_4 DNA Ligase	1U/µl	1
Total Volume		50

Ligation condition: 16°C for 16 hours

4µl of the ligation product was used to transform high efficiency *DH5α* using the protocol outlined in section 2.3.2.3. Positive colonies were screened with forward (seqpCWF) and reverse (seqpCWR) primers (Table 3.6) designed within the pCWOri+ sequence approximately 100 nucleotides upstream of the *Nde*I restriction site and downstream of the *Xba*I restriction site respectively. A band of around 1800bp comprising the insert gene (1527bp), the *ompA+2* leader sequence as well as the ~200 nucleotides from pCWOri+ flanking the insert confirm the presence of the candidate genes in the expression vector. These colonies were miniprepped overnight and sequenced using the *ompA+2*F and *ompA+2CYP6P9a*/*b*R primers as well as the seqpCWF and seqpCWR primers to confirm the presence of *ompA+2* signal peptide sequence and restriction sites.

Table 3.6: Primers for sequencing of *ompA+2*-CYP6P9a/b in pCWOri+ and CPR in pACYC-184

Primer	Forward Sequence	Reverse Sequence	Product Size (bp)
seqpCW	ATCCCCCTGTTGACAATTAATCATC	ACCTATAAAAATAGGCGTATCACGA	~1800
SeqCPR	CTACTCGATCCATATGACGACGGTGAACAC	TACGGATCCTACAGCACATCCTCGCCCGTGCTC	~600

3.3.1.2 Construction of pACYC-184:: Cytochrome P450 Reductase Plasmid

pACYC-184 (New England Biolabs) containing the ancillary protein *An. gambiae* cytochrome P450 reductase (*Ag*CPR) as well as the His-tagged *An. gambiae* cytochrome b_5 (*Ag*b_5) used on the course of this study were kindly provided by Dr. M.J.I. Paine at LSTM. The P450 reductase expression cassette was prepared as described previously (Pritchard et al., 1998, Pritchard et al., 2006a) with P450 reductase cDNA modified by fusing it with *pelB* leader sequence in a strategy similar to that of the *ompA+2* for P450s but using the plasmid pET-20b as a template for the initial linker PCR. The pACYC-184 expression vector encodes gene for chloramphenicol resistance. More details of the engineering method of this plasmid could be found in (Pritchard et al., 2006a).

3.3.1.3 Construction of pB13 ::(His)$_4$-Cytochrome b_5 and Purification of b_5

Agb$_5$ cDNA isolated by Nikou and colleagues (Nikou et al., 2003) was tagged with histidine residues in its NH_2-terminus and engineered into pB13 plasmid already linearized with *Nde*I and *Hind*III restriction sites. Expression of b_5 protein was done using A183 *E. coli* cells, harvested after 24-30 hours post-induction with 0.5mM δ-ALA and 1mM IPTG to the final concentration. The protein was prepared using the technique outlined by Holmans and colleagues (Holmans et al., 1994) in which the solubilized hemoprotein was purified by nickel affinity chromatography. Concentration of membranous b_5 was measured by determining spectral activity (Omura and Takesue, 1970, Omura and Sato, 1964) as difference between reduced and oxidized b_5 (OD_{423} vs OD_{490}) using the extinction coefficient of 185$mM^{-1}cm^{-1}$. Total protein was determined using Bradford assay. The enzyme was frozen in aliquot in -80^{o}C until required.

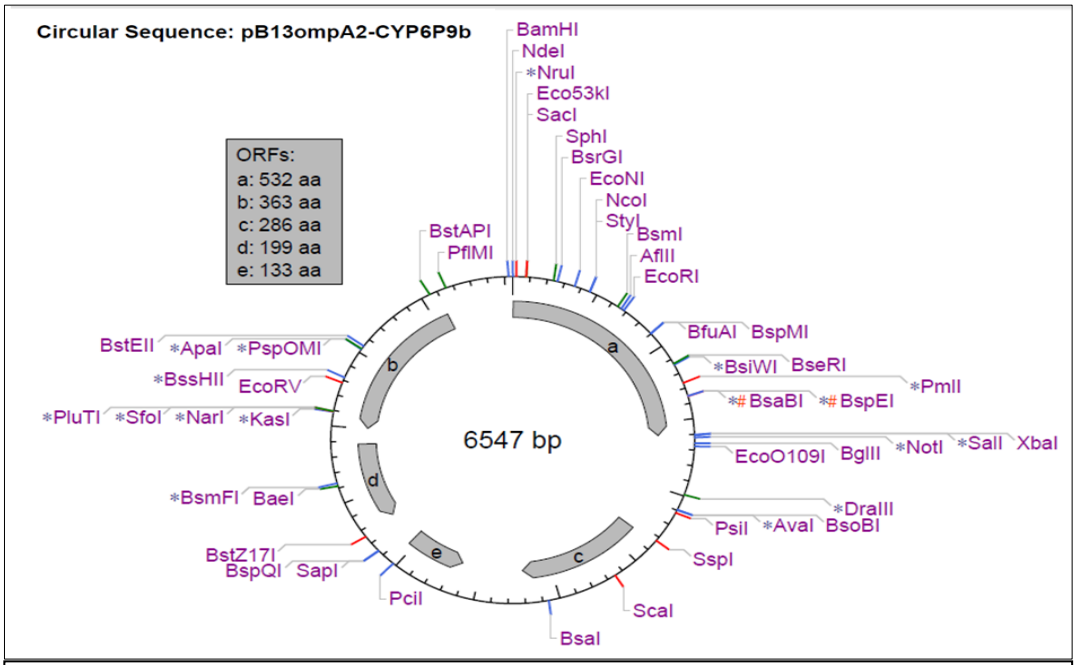

Figure 3.3: Map of pB13::*ompA+2*CYP6P9b showing expression plasmid construct in circular form. a: 21 amino acids of signal peptide plus alanine proline spacer residues, and 509 amino acids encoded by *CYP6P9b* cDNA. b: LacI repressor (NCBI: WB_0002485631); c: β-lactamase (NCBI: WP_000027057.1); d: LacZ-alpha (GenBank: ACA63830.1); e: Ori+. Prepared using the NEB Cutter v2.0 (http://tools.neb.com/NEBcutter2/index.php).

3.3.1.4 Co-transformation of pB13:: ompA+2CYPP9a and pB13::ompA+2CYP6P9b with pACYC-184-An. gambiae CPR

High Efficiency *E. coli JM109* cells (Promega) were co-transformed with plasmid pB13 containing *An. funestus CYP6P9a*/*CYP6P9b* and pACYC-184 bearing *Ag*CPR in a ratio of 2:1. *Ag*CPR was used due to the unavailability of *An. funestus* CPR cloned into pACYC vector; and because *Ag*CPR (96% identical to *An. funestus* CPR) had been used as a surrogate redox partner with other P450s of even lower similarity like *Ae. aegypti* (87% identical) successfully (Stevenson et al., 2012). Co-transformation strategy has been described in (McLaughlin et al., 2008). 100µl of *JM 109* cells was introduced into 15ml tube chilled on ice. 4µl of pB13 plasmid bearing candidate P450 and 2µl of pACYC plasmid bearing CPR were introduced into the tubes. After 30 mins incubation on ice, cells were heat shocked for 90 seconds at 42^{o}C and then chilled on ice for 2 mins. 950µl of S.O.C medium was added and tubes incubated at 37^{o}C with shaking at 200rpm for 2 hours. 100µl of the co-transformed cells were spread onto LB plates with 100mg/ml ampicillin and 34mg/ml chloramphenicol and allowed to grow at 37^{o}C for 16 hours.

Individual colonies were suspended in 20µl distilled water the next day and screened using KAPA PCR (section 2.3.2.3(iii)) using the primers for pCWori+ (seqpCWF and seqPCWR) to confirm presence of candidate P450s and primers seqCPRF and seqCPRR (Table 3.6) for CPR. The seqCPR primers are internal primers designed inside the P450 reductase itself and produced a band of around 600bp on 1.5% agarose gel stained with ethidium bromide.

3.3.1.5 Heterologous co-expression of pB13:: ompA+2-An. funestus CYPP9a and pB13:: ompA+2-An. funestus CYP6P9b with pACYC-184-An. gambiae CPR in E. Coli JM109

For co-expression of *CYP6P9a*/*-b* and CPR, 4µl of co-transformed colony suspended in distilled water was introduced into a 15ml tube containing 3ml LB medium, 3µl of 100mg/ml ampicillin and 5.1µl of 20mg/ml chloramphenicol. Culture was allowed to grow for 12-14 hours at 37^{o}C with shaking

at 200 rpm. The next day 1-2ml of this culture was used to inoculate 200ml of pre-warmed (37^{o}C) TB medium containing 200µl ampicillin and 340µl chloramphenicol. This culture was allowed to grow for 3-4 hours at 37^{o}C and 200 rpm orbital shaking until the optical density at 600nm reached 0.6-0.7. The log-phased cells was then transferred to 21^{o}C (22^{o}C optimal for *CYP6P9a*) and 150 rpm orbital shaking (155 rpm optimal for *CYP6P9a* alleles) and allowed to cool for 30 minutes. Induction was carried out by adding 1mM IPTG and 0.5mM δ-ALA to the final concentrations. Cultures were monitored for P450 activity at 6 hours interval starting from 18 hours. Once P450 activity was detected cultures were then transferred into 250ml tubes chilled on ice and centrifuged at 2800 rpm and 4^{o}C for 20 minutes. Detail of this protocol could be found in (McLaughlin et al., 2008, Pritchard et al., 2006a, Stevenson et al., 2012) and specifically the procedure for co-expression, harvesting of cells, spheroplast preparation and isolation of membranes are given in Appendix 3.1.

3.3.1.6 Determination of concentration of An. funestus **CYP6P9a/CYP6P9b** *proteins and An. gambiae cytochrome P450 reductase activity*

3.3.1.6.1 Measurement of Total Protein, P450 and CPR Activities

Protein content of the membranes was measured colorimetrically with Bio-Rad Protein Assay Kit (Life Science Research) using the Bradford method (Bradford, 1976) with bovine serum albumin standard.

The P450 concentration was quantified through spectral activity as described (Omura and Sato, 1964) by measuring the size of the peak (absorbance) at 450nm and using the absorbance at 490nm as a reference and an extinction coefficient (e_{cyt450} = 0.091µM^{-1}cm^{-1}) for P450s. 50µl of membrane was diluted in 1.5ml of P450 spectrum buffer (80% of 0.1M potassium phosphate buffer, pH 7.5, with 20% v/v glycerol). Few grains of sodium dithionate was added and the mix swirled gently and then divided (750µL each) into two optical cuvettes labelled E (experimental) and B (blank). After running a baseline between 500-400nm, carbon monoxide was bubbled into E for 60s. The extinction coefficient, dilution factor and the Fe^{2+}-CO (E) and Fe^{2+} (B) difference spectra were used to calculate the P450 activity.

CPR activity in the prepared membranes was measured by cytochrome *c* reduction assay (Strobel and Dignam, 1978). Details of the protocol for this assay could be found elsewhere (Pritchard et al., 2006a). Reductase activity was measured spectrophotometrically based on extinction coefficient of reduced cytochrome *c* (21.4 $mM^{-1}cm^{-1}$) as nmol of cytochrome *c* reduced/min/mg protein.

3.3.2 Comparative Assessment of the Activity of Various Alleles of *CYP6P9a* and *CYP6P9b* Using Fluorescent Probes

Four membranes each from CYP6P9a (BENCYP6P9a, UGANCYP6P9a, FANGCYP6P9a and MALCYP6P9a) and CYP6P9b (BENCYP6P9b, UGANCYP6P9b, FANGCYP6P9b and MOZCYP6P9b) were used in a fluorescent probes assay to compare their O-dealkylating catalytic efficiency towards four fluorogenic probes (7-ethoxyresorufin: 7-ER, 7-ethoxy-4-trifluoromethylcoumarin:EFC, 7-methoxy-4-trifluoromethylcoumarin: MFC and diethoxyfluorescein: DEF). ER is an O-alkyl derivative of resorufin which undergoes O-deethylation (Burke et al., 1985) with a large Stoke shift which is quantified fluorometrically (λ_{exc} = 544nm, λ_{emi} = 590nm); EFC and MFC are ethoxy- and methoxy- derivatives of coumarin respectively, which undergo deethylation and demethylation to yield fluorescent 7-hydroxytrifluoromethyl-coumarin (7-HFC) detected at wavelength range λ_{exc} =410nm and λ_{emi} = 535nm respectively. DEF undergoes deethylation into ethoxyfluorescein and fluorescein (White et al., 1987) with excitation and emission wavelength ranges of 485nm and 530nm, respectively. I conducted the probe assay experiments in Cypex BioDundee, Scotland (http://www.cypex.co.uk/intro.htm).

3.3.2.1 Screening of Probes

2mM stock of probe substrates in dimethylsulfoxide (DMSO) was prepared and kept at 2-8^{o}C. Fresh NADPH regeneration system was prepared using 50mM potassium phosphate buffer (KPi at pH 7.4) for each experiment. Initially, 1µM of the probe substrates (ER, EFC, MFC and DEF) were screened for activity with 45pmol of membranes of CYP6P9a and CYP6P9b (Table 3.7) following the protocols previously established (Stevenson et al., 2012, McLaughlin et al., 2008). For each of the four probes

screened, in a total volume of 250µ/well (in an opaque, white 96-well plate) containing 45pmol P450 membrane buffered with 50mM potassium phosphate buffer (KPi at pH 7.4 with 5mM $MgCl_2$), 1µM probe substrate was added. These reactions were carried out in triplicate and one negative control to which 25µl KPi buffer was added instead of the NADPH regeneration buffer to allow for determination of enzymatic activity due only to dealkylation mediated by the P450 activity. The plate was inserted into the fluorescence spectrophotometer Infinite® M200 (TECAN) already set to 37°C. After incubation for 5 mins, 25µl of regeneration buffer was added to the experimental wells and product(s) fluorescence monitored for 11 cycles with shaking and reading 2 seconds apart. The regeneration system contains 1mM glucose-6-phosphate (G6P), 0.25mM $MgCl_2$, 0.1mM NADP and 1U/ml glucose-6-phosphate dehydrogenase (G6PDH). Rate of fluorescent product formation was determined as relative fluorescence per minute by linear regression of measurement between 2- and 8 mins after start of the reaction. Results were analysed with Magellan™ v6.2 Wizard. The excitation and emission wavelength for the probes used on the course of this research are given in Appendix 3.3.

Table 3.7: Reaction mix for fluorescence probes assay

Component	Stock Concentration	Final Reaction Concentration	Volume (µl)
KPi Buffer (containing 5mM $MgCl_2$)	50mM	50mM	Varies
P450 protein	Varies (nmol/ml)	45pmol	Varies
Probe substrate	2mM	1µM	0.125
Incubation at 37°C for 5 minutes			
10X Regeneration system	10x	1X	25µl
Total Volume			250

3.3.2.2 Linearity Measurements

For all membranes highest activities were obtaind with diethoxyfluorescein (DEF). DEF was therefore selected for kinetics analysis and inhibition assays to establish respectively the possible differences in the steady state kinetic parameters from different alleles and to carry out inhibition assays. In order to establish the amount of membranes that produce optimal activity with 1µM DEF substrate protein linearity was conducted with two membranes each from CYP6P9a (BENCYP6P9a and

MALCYP6P9a) and CYP6P9b (MOZCYP6P9b and UGANCYP6P9b). Time-dependent measurement of activity against 1µM DEF was carried out with variable amounts of membranes, prepared by serial dilution (90pml, 30pmol, 10pmol, 3.33pmol, 1.11pmol and 0.37pmol) prior to addition of the substrate. The final solvent concentration was less than 3% of the total volume of the incubation mixture. Plates were read in fluorometer for 30 mins at 30 seconds interval following addition of NADPH-regenerating solution.

3.3.2.3 Kinetic Analysis of Various **CYP6P9a/CYP6P9b** *proteins with Diethoxyfluorescein*

Kinetic analysis was conducted using all alleles utilised for initial screening of probes. This was to establish if there were any differences in the turnover of these alleles with DEF and to establish the Michaelis constant (K_M values) which could indicate differences in the affinity of the different alleles toward DEF substrate. 0-2µM concentrations of DEF (0µM, 0.0009µM, 0.0027µM, 0.0082µM, 0.0247µM, 0.0741µM, 0.2222µM, 0.6666µM and 2.0µM) were assayed with 10pmol membranes of CYP6P9a and 3.33pmol of CYP6P9b proteins in a total volume of 250µl/well. The protocol was as outlined in the initial screening for activity (above), only that the substrate concentration varies and incubation was done under conditions shown to be linear with respect to time and enzyme concentration. Steady-state kinetic parameters were obtained by measuring the rate of reaction under linear conditions for 10 mins while varying the substrate concentration from 0 to 2µM. K_M and V_{max} were established from the plot of substrate concentrations against the initial velocities through a non-linear regression by fitting the data to the Michaelis-Menten equation using GraphPad Prism 6.03 (GraphPad Software Inc., La Jolla, CA, USA). Catalytic constants (K_M and V_{max}) were determined from the steady-state parameters efficiencies calculated as the ratio of K_{cat} to K_M.

3.3.2.4 Inhibition Assay

Inhibition assay is important as it can establish whether a potential subsrate (e.g. insecticide) binds to the candidate enzyme and the degree of binding. It gives information on the affinity but not

metabolic activity of candidate enzyme toward substrate of interest. Fluorometric inhibition assay was conducted with DEF as the probe substrate, a panel of insecticides (test compounds) as inhibitors, and miconazole as positive control inhibitor. Miconazole is a potent polyene azole antifugal agent. It contains imidazole group which binds to the iron of heme P450 C14α-lanesterol demethylase) preventing the demethylation of lanosterol into demethyl-lanosterol intermediate of the HMG-CoA pathway (Lupetti et al., 2002). The ten test insecticides used include pyrethroids: permethrin, bifenthrin, deltamethrin, lambdacyhalothrin, cypermethrin and etofenprox; organochlorine: DDT; carbamates: bendiocarb and propoxur; organophosphate: chlorpyrifos.

The assay was carried out as described in previous studies (Kajbaf et al., 2011, Bambal and Bloomer, 2006) and as described for *An. gambiae* CYP6Z2 with benzyloxyresorufin and pyrethroids, permethrin and cypermethrin, as well as other conventional substrates (McLaughlin et al., 2008). Two 96 well plates: opaque-walled (inhibitors plate) and black (assay plate) were set.

Premix 1: Into well A1 of the inhibitors plate, 200µl of 50mM KPi (with 5mM $MgCl_2$) was added; 200µl of 50mM KPi with $MgCl_2$ containing 2.5mM miconazole prepared in DMSO and dH_2O was added to well A2; into well A3:A12, 200µl each of 50mM KPi containing 2.5mM test inhibitor substrates were individually added. 150µl of 50:50 (v/v) dH_2O:DMSO was added to column B1:H1 for blank, B2:H2 for miconazole and B3:H3 through to B12:H12 for the test insecticides. Next, 50µl mix from rows A1:A12 (spikes) was serially diluted down to row H1:H12 using multichannel pipette with mixing at each row (step). Finally 50µl of mix was removed from rows H1:H12 and discarded. 5µl of this premix 1 were aliquot in correct order onto the black assay plate.

Premix 2: 220µl of 50mM KPi buffer pH 7.4 (with 5mM $MgCl_2$), containing 0.1-0.3µM final concentration of probe substrate (K_M values) and 10pmol membrane (CYP6P9a) or 3.33pmol (CYP6P9b) were aliquoted into the assay plate already containing 5µl (25µM) of miconazole well B2:H2 and 25µM test insecticides serially diluted into eight-fold concentrations (25µM, 8.33µM, 2.77µM, 0.92µM, 0.308µM, 0.102µM, 0.034µM and 0.011µM) B3:H3 to B12:H12.

After incubation for 5 mins at 37^{o}C, reaction was started by addition of 25µl of regeneration system to all wells. The regeneration buffer contains 7.8mg glucose-6-phosphate (G6P), 0.25mM $MgCl_2$, 1.7mg NADP, 6U/ml glucose-6-phosphate dehydrogenase and 2% w/v $NaHCO_3$. Fluorescence was monitored for 21 cycles at interval of 1 min with shaking at every step. Results were analysed using Magellan v6.2 and inhibition at each concentration of inhibitor insecticide was calculated as residual control activity observed from the probe.

3.3.3 Comparative Assessment of Metabolic Activity of *CYP6P9a*/*CYP6P9b* Alleles on Different Insecticide Classes with Reverse-Phase High-Performance Liquid Chromatography (RP-HPLC) Metabolism Assay

The same membranes from CYP6P9a and CYP6P9b used for fluorescent probes assay were used for metabolism assay with panel of insecticides, including representative pyrethroids (permethrin, bifenthrin, deltamethrin, λ-cyhalothrin, etofenprox), organochlorine (DDT) and carbamates (bendiocarb and propoxur). Protocols used followed the procedure as described in previous studies (Muller et al., 2008, Stevenson et al., 2011) for metabolism assays of pyrethroids with *An. gambiae* CYP6P3 and CYP6M2 recombinant proteins, respectively.

3.3.3.1 Substrate Depletion Assay

Initially, 2mM stock concentration of all insecticides were prepared in HPLC-grade methanol and kept in -20^{o}C prior to use. Substrates working solution was prepared by diluting stock to 0.8mM with methanol to reduce precipitation of insecticide. The reaction mix for this protocol including the membrane expressing P450 and CPR, b_5, NADPH-regeneration system as well as the buffer used are tabulated below (Table 3.8). 0.2M Tris-HCl and NADPH-regeneration components (1mM glucose-6-phosphate, 0.25mM $MgCl_2$, 0.1mM $NADP^+$ and 1U/ml glucose-6-phosphate dehydrogenase) were added to the bottom of 1.5ml tube chilled on ice.

Table 3.8: Reaction mix for HPLC metabolic assay

Component	Stock Concentration	Final Reaction Concentration	Volume (µl)
Tris-HCL pH 7.4	0.2M	0.2M	Varies
Membrane (CYP450 + CPR)	Varies (nmol/ml)	45pmol	Varies
Cytochrome b_5	Varies (nmol/ml)	~180-500pmol	~10-20
NADPH +/- (containing 0.25mM $MgCl_2$)	10X	1x	50
Incubation at 30°C and 1200 rpm for 5 mins			
Substrate (Working)	0.8M	20µM	5.0
Total Volume			200

DDT analysis: with or without 1mM sodium cholate as previously described (Mitchell et al., 2012).

Membrane expressing P450 and CPR, and the b_5 proteins were added to the side of the tube and pre-incubated for 5 mins at 30°C, with shaking at 1200 rpm to activate the membrane. 20µM of test insecticide was then added into the final volume of 0.2ml (less than 2.5% v/v methanol in final volume of reaction mix) and reaction started by vortexing at 1200 rpm and 30°C for 1 hour. Reactions were quenched with 0.1ml ice-cold methanol and incubated for 5 more mins at 1200 rpm and 30°C, to dissolve all residual insecticide. Tubes were then centrifuged at 16400 rpm and 4°C for 12 mins and 150µl of supernatant transferred into HPLC vials for analysis. All reactions were carried out in triplicates with experimental samples (+NADPH) and negative control (-NADPH) not containing NADP. 100µl of sample was loaded into an isocratic mobile phase of Agilent 1260 Infinity with a flow rate of 1ml/min and peaks separated with a 250mm C18 column (Acclaim ™ 120, Dionex) at 23°C. Details of the mobile phase composition, column temperatures, and wavelength of detection and retention time of insecticides used in this study are given in the Table 3.9.

Enzyme activity was calculated as the percentage depletion (the difference in the amount of insecticide(s) remaining in the +NADPH tubes compared with the –NADPH) and a paired t-test was used for statistical analysis.

Table 3.9: Conditions used for Reverse-Phase HPLC Analysis

Insecticides	Mobile Phase (v/v)	Column Temperature (°C)	UV-Vis Wavelength (nm)	Retention Time (min)
Permethrin	MeOH:H_2O (90:10)	23	226	*cis* ~12, *trans* ~ 14
Bifenthrin	MeOH:H_2O (90:10)	23	226	~16
Deltamethrin	MeOH:H_2O (90:10)	23	226	*cis* ~9, *trans* ~11
λ-cyhalothrin	MeOH:H_2O (90:10)	23	226	~8
Etofenprox	MeOH:H_2O (90:10)	23	226	~17.5
DDT	MeOH:H_2O (90:10)	23	232	~11
Bendiocarb	ACN:H_2O (65:35)	40	205	*cis* ~13, *trans* ~15
Propoxur	ACN:H_2O (60:40)	40	270	~6

MeOH = Methanol and ACN = Acetonitrile

3.3.3.2 Steady-State Kinetic Parameters Analysis

Establishment of kinetic parameters for CYP6P9a and CYP6P9b protein variants will provide important information on turnover (the speed with which the different alleles metabolise and clear pyrethroid insecticides) and K_M (the affinity of the different alleles toward different insecticides). This will help establish differences in the catalytic efficiencies of the different alleles from resistant strain and identify whether the alleles from resistant strains differ in their pyrethroid-metabolising activity compared to alleles from susceptible strain. Enzyme response to variation in substrate concentration was determined using the pyrethroids permethrin and deltamethrin. Steady-state kinetic parameters were obtained by measuring the rate of reaction under linear conditions for 10 minutes while varying the substrate concentration from 2.5 to 20µM (2.5, 5.0, 7.5, 10, 12.5, 15, 17.5 and 20µM). Reactions were performed in triplicates with +NADPH (experimental tubes) in parallel with –NADPH (negative control). K_M and V_{max} were established from the plot of substrate concentrations against the initial velocities and fitting of the data to the Michaelis-Menten equation using the non-linear regression as implemented in the GraphPad Prism 6.03. Catalytic constants and efficiencies were automatically predicted from the steady-state parameters by the software.

3.3.4 Detection of Key Amino Acid Changes Conferring Pyrethroid Resistance Using Site-Directed Mutagenesis

Modelling and docking analyses of the allele variants of *CYP6P9a* and *CYP6P9b* as well as fluorescent and metabolism assays established profound differences in the metabolic profiles of the resistant alleles compared with the susceptible ones. It becomes apparent that amino acid differences may be the driving force behind such differences. As such finding out which amino acid(s) is/are responsibe for these difference is of paramount importance. Such information will shed light on the mechanism of resistance at molecular level and make it possible to design appropriate diagnostic tool that can allow detection of the mutation(s) in the field. For example, a PCR diagnostic tool for the single mutation Leu^{119}Phe in *GSTe2* gene in highly DDT-resistant strain of *An. funestus* from Benin allows for a fast detection and tracking of such type of resistance across Africa (Riveron et al., 2014b).

3.3.4.1 Selection of Candidate Amino Acids

A hypothesis-driven approach was used to select candidate amino acids that may impact on catalytic activity of the resistant alleles. Characterisation of amino acid sequences of *CYP6P9a* and *CYP6P9b*, as well modelling and docking analyses of alleles with pyrethroid insecticides (Chapter Two) helped in the choice of candidate mutations to investigate. For both *CYP6P9a* and CYP6P9b alleles, list of amino acids selected for mutagenesis, their polymorphic positions, as well as the potential contribution of the substitution are summarised in Table 3.10, below. Details of the potential impact of these mutations have been discussed in details in Chapter Two.

Candidate amino acids were substituted individually with amino acid variant present in the allele from susceptible individual (*FANGCYP6P9a* and *FANGCYP6P9b,* respectively). The mutant proteins were then expressed and used alongside wild type proteins to screen fluorescent probes for activity, as well as metabolism assay with permethrin and deltamethrin to assess the impact of each mutation.

Table 3.10: Nucleotide polymorphism and amino acid substitutions between resistant alleles of *CYP6P9a* and *CYP6P9b* and FANG: the amino acid substitutions selected for mutagenesis

Amino acid substitution	Mutation	Countries	Location and potential Impact
		CYP6P9a	
Phe^{63}Leu	189: T->G	Malawi, Mozambique, Zambia	Within the highly variable αA region, possible membrane targeting increasing stability
Gln^{66}Lys	196: C->A	Malawi, Mozambique, Zambia	Within the highly variable αA region, possible membrane targeting increasing stability
His^{301}Gln	903: A->C	Uganda, Malawi, Mozambique, Zambia	Two residues upstream the substrate recognition site 4 (SRS4)
Tyr^{320}Ser	959: A->C	Benin, Uganda, Malawi, Mozambique, Zambia	Middle of the αI helix and within SRS4; one residue downstream the oxygen binding pocket in *CYP6P9a*
Ser^{431}Phe	1292: T->C	Benin, Uganda, Malawi, Mozambique, Zambia	Within the loop joining the meander with the cysteine pocket; the loop is purported to house the reductase interaction site 2 (RIS-2)
		CYP6P9b	
Ile^{109}Val	325: A->G	Benin, Uganda, Malawi, Mozambique, Zambia	Within the SRS1 and the B'C loop purported to be involved in substrate access and channelling
Glu^{335}Asp	1005: A->C	Benin, Uganda, Malawi, Mozambique, Zambia	In the –COOH terminus of the αI helix, possible impact as RIS-1 component mediating interaction with CPR
Ser^{384}Asn	1151: G->A	Uganda, Malawi, Mozambique, Zambia	In the β1_4 (αK') and within the highly conserved SRS5, with possible impact on substrate recognition
Ala^{401}Pro	12001: G->C	Benin, Uganda, Malawi, Mozambique, Zambia	Within the β2_2 domain; pyrrolidine ring can restrict conformational space and 3D folding

3.3.4.2 Primer Design

Mutagenic sense and antisense oligonucleotide primers were designed to incorporate the desired mismatch into the template DNA in a double-stranded DNA-plasmid constructs. Primer pair incorporates at least 10 oligonucleotide residues upstream and downstream of the target nucleotide to mutate. With the exception of primer pair for *MALCYP6P9a* Leu^{63}Phe_Lys^{66}Gln double mutant, all primers contain no more than 30 nucleotides so as to narrow the T_m to less than 70^{o}C to avoid primer dimer formation (Zheng et al., 2004) becoming more favourable than primer-template annealing. Care was also taken to avoid GC content of more than 50% though unavoidable in some of the primers. Though primers were designed using an automated web tool Primer*X* (http://www.bioinformatics.org/primerx/), *CYP6P9a* mutants PCR amplifications did not work over several attempts. List of all primers used are given in Table 3.11 with mutagenised positions in red.

Table 3.11: List of mutagenic primer pairs with respective T_m

Primer	Sequence	T_m (°C)
MALCYP6P9a_L63F_K66Q_F	CTGGAATTTTACAAACAATTCAAGCAGCGCCGTG	69.09
MALCYP6P9a_L63F_K66Q_R	CTTGAATTGTTTGTAAAATTCCAGATGGATGTCGG	65.33
MALCYP6P9a_Q301H_F	GAATGACACACCGAGAACTTGCGG	64.38
MALCYP6P9a_Q301H_R	GTTCTCGGTGTGTCATTCCTACTTC	61.36
MALCYP6P9a_S320Y_F	GACATCATACACGACGCAAAGCTTC	62.88
MALCYP6P9a_S320Y_R	GCGTCGTGTATGATGTCTCGAAACC	64.09
MALCYP6P9a_F431S_F	GATCGCTCCTCACCGGAGGAAGTGAAG	68.15
MALCYP6P9a_F431_R	CTTCACTTCCTCCGGTGAGGAGCGATCC	69.66
MOZCYP6P9b_V109I_F	GATCGCGGTATTTTCACTAATGCAAG	61.26
MOZCYP6P9b_D335E_F	GAACCCTGAAATCCAGGAGCGCCTTAG	67.06
MOZCYP6P9b_D335E_R	CCTGGATTTCAGGGTTCTTTGCCAGC	66.28
MOZCYP6P9b_N384S_F	GAATCGTTGAGTCGTGTGCCGTC	64.29
MOZCYP6P9b_N384S_R	CACGACTCAACGATTCTACCGGG	63.09
MOZCYP6P9b_P401A_F	CACGTGATTGCCAAACGAACGTTAG	63.47
MOZCYP6P9b_P401A_R	CGTTTGGCAATCACGTGTTTCG	61.71

3.3.4.3 Construction of Mutant ompA+2-CYP6P9a and ompA+2-CYP6P9b Plasmids

3.3.4.3.1 Primer Extension PCR

Efforts to introduce mutations using the plasmidic expression vector pB13::*ompA+2CYP6P9a*/ pB13::*ompA+2CYP6P9b* were not fruitful due possibly to the larger size of pCWOri+ (5030bp) over the pJET1.2 (2974bp). Full length pJET1.2::*ompA+2CYP6Pb* mutants were successfully amplified via primer extension PCR (Zheng et al., 2004) using as a template pJET1.2 miniprep from section 2.3.2.3(ii). This one-step approach involved linear amplification of whole plasmid with the mutagenic primers as described by Rabhi and colleagues (Li and Wilkinson, 1997) followed by self-ligation at the transformation step. Primers annealed back-to-back on the opposite strands of the target template and through primer extension amplified the whole plasmid without need for introduction of restriction sites. Details of the reaction mix are given in Table 3.12 and the strategy of primer extension technique depicted in Figure 3.4.

The reaction mix contains 5X Buffer HF with 7.5mM $MgCl_2$, dNTP mixes, forward and reverse mutagenic primers, 1-4ng/µl plasmidic DNA template, 0.5-1U of High-Fidelity Phusion Hot Start II DNA Polymerase (Thermo SCIENTIFIC, MA, USA) and sterile water. The reaction was started by preheating the mixture to 98°C for 10 mins; followed by 35 cycles of 94°C for 30 seconds, annealing (at 65°C) for 30 seconds and extension at 72°C for 2.5 mins. This is followed with final extension at 72°C for 10 mins and 4°C hold. 3µl of the PCR product was then electrophoresed on 1.5% (w/v) with visualisation using ethidium bromide. Mutagenic amplification from plasmid pB13::*ompA+2CYP6P9a* failed even with QuickChange™ Site-Directed Mutagenesis Kit (Stratagene). Even though mutagenic PCR worked with pJET1.2::*ompA+2-CYP6P9a* plasmid, the cloned product refused to get digested from the pJET1.2, and as such could not be ligated into the expression vector pCWori+. Consequently, efforts were then concentrated on cloning, expression and characterisation of CYP6P9b mutant proteins.

Table 3.12: PCR reaction mix for mutant pJET1.2-*ompA+2*-CYP6P9b Amplification

Reagent	Final Concentration	Volume (µl)
5x Buffer HF (containing 7.5mM $MgCl_2$)	1x	10
dNTP mix (10mM)	80µM	0.4
Mutagenic Primer_F (10µM)	0.3µM	1.5
Mutagenic Primer_R (10µM)	0.3µM	1.5
Plasmidic DNA Template	2-4ng	0.5-1.0
dH_2O	-	35.1-34.6
HotStart Taq Polymerase II	0.04/µl	1.0
Total Volume	**-**	50

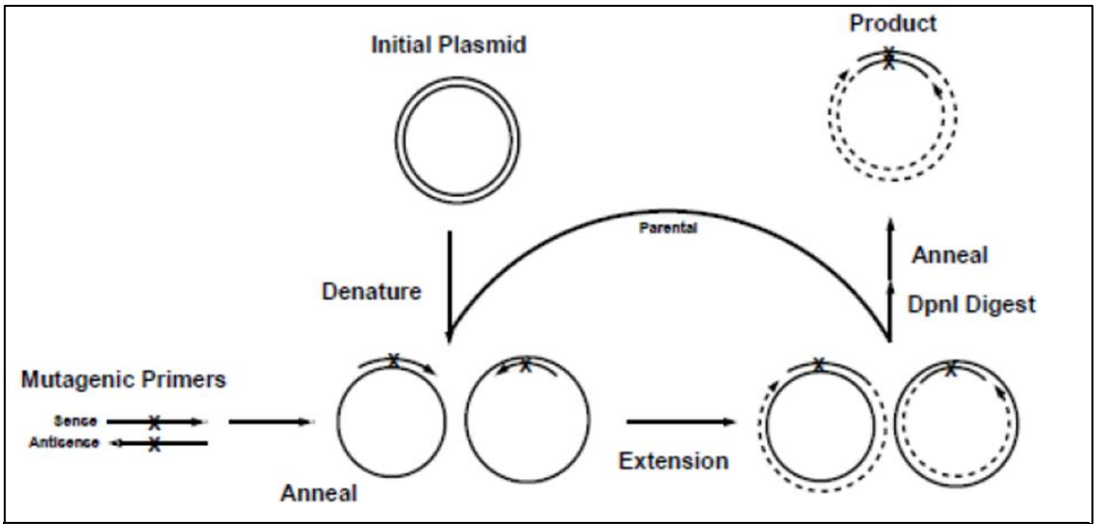

Figure 3.4: Schematic diagram of the primer extension PCR. Adapted from (Zheng et al., 2004, Reikofski and Tao, 1992).

3.3.4.4 Restriction Digestion of the Parental DNA Template

The parental plasmidic template is *Dam*$^{+}$-methylated from transformation into *DH5α*. This makes it possible to cleave the unwanted template by restriction enzyme *Dpn*I (Thermo SCIENTIFIC, MA, USA) as described in (Zheng et al., 2004). 2µl of 1X FastDigest Buffer and 1µl of *Dpn*I was added to the PCR-amplification product and incubated for one hour at 37^{o}C. The restriction enzyme cut the parental template at position 5'…G m6 $^{\downarrow}$ATC…3' which is absent in the desired mutant PCR product since its newly synthesized and not passed through *E. coli DH5α* cloning.

3.3.4.5 Construction of Plasmidic Expression Vector pB13::ompA+2CYP6P9b

4µl of the digest was transformed into *DH5α*, positive colonies mini-prepped and sequenced on both strands with pJET725 primers to confirm presence of mutations. The PCR product was then digested with *Nde*I and *Xba*I (see Table 3.4), gel extracted with QIAquick Gel Extraction Kit (QIAGEN) and then ligated into pCWOri+ already linearized with the same restriction enzymes (Table 3.5).

3.3.4.6 Transformation and Co-transformation of Expression Vector with An. gambiae CPR

The ligation product was then transformed into *DH5α* as described in section 3.3, positive colonies mini-prepped and sequenced on both strands with seqPCW primers to confirm the presence of the ompA leader and target mutations again. The miniprep was then co-transformed with *Ag*CPR using the protocol outlined in section 3.3 into *JM109* cells.

3.3.4.7 Heterologous Co-Expression pB13::ompA+2-CYP6P9b mutant with An. gambiae CPR

Expression and preparation of mutant membranes (Val^{109}Ile, Asp^{335}Glu, Asn^{384}Ser and Pro^{401}Ala), with the wild type MOZCYP6P9b membrane protein was conducted as previously described previously. Membrane concentrations were determined from difference in Fe^{2+}-CO vs Fe^{2+} spectra.

3.3.4.8 Fluorescent Probes Assay

3.3.4.8.1 Screening for Activity, Linearity and Kinetics

10pmol of mutant CYP6P9b protein successfully expressed were screened with 1µM of 7-ER, resorufin-benzylether: RBE, resorufin methyl ether: RME and resorufin-pentylether: RPE); two cuomarin-based probes (7-EFC and MFC) and diethoxyfluorescein (DEF). The initial test of O-dealkylating activity and protein linearity was as described in sections 3.3.2.1 and 3.3.2.2 respectively.

Protein linearity was carried out as described previously and steady-state kinetic parameters established with 0-2µM DEF and 3.33pmol or 6.66pmol mutant membranes depending on activities obtained from test of linearity. This was carried out as described in section 3.3.2.3.

3.3.4.9 Metabolism Assay

3.3.4.9.1 Substrate Depletion Assays and Kinetics

To determine whether the amino acid substitutions lead to lose of activity or modify kinetic parameters, metabolism assay was conducted with the mutant membranes with permethrin and deltamethrin. Substrate depletion was carried out as previously described (section 3.3.3.1).

Steady-state kinetic parameters were established varying the amount of pyrethroid substrates from 1-16µM, in a total volume of 200µl incubated for 15 mins for all mutants excepting the $Asn^{384}Ser$ mutant, which was assayed with 30 mins incubation following its unusually low activity. The protocol used for the experiment and interpretation of the results were as described in section 3.3.3.3.

3.3.4.10 In silico Analysis of Key Amino Acid Residues

To establish spatial positioning and role of key amino acid changes with respect to pyrethroid activity, MOZCYP6P9b and FANGCYP6P9b models docked with pyrethroids were overlayed and analysed using the PyMOL and MMV. Position of residues Asp^{335} and Asn^{384} in MOZCYP6P9b were compared with the corresponding variants Glu^{335} and Ser^{384} from FANGCYP6P9b.

3.3.5 Comparative Assessment of Ability of Allele Variants of *CYP6P9a* and *CYP6P9b* to Confer Pyrethroid Resistance in *D. melanogaster* Using GAL4-UAS System

Predictions of a drug's *in vivo* clearance is usually made based on kinetic parameters obtained from *in vitro* estimated intrinsic clearance (Tracy, 2003). However, *in vitro-in vivo* extrapolation is an assumption with some shortcomings, for *in vitro* experiments discount the influence of other metabolizing enzymes and factors within the biological system. Other proteins may be involved in binding and/or metabolism of a substrate and as such *in vitro* results may not reflect the holistic pharmacokinetics taking place. *In vitro* kinetic analyses have revealed differences in kinetic profiles between the membrane proteins from resistant and susceptible alleles of *CYP6P9a* and *CYP6P9b*. But, to further confirm the involvement of the resistant alleles of these genes, a comparative analysis was conducted by introducing and expressing these genes in *D. melanogaster* using GAL4-UAS system. The transgenic flies over-expressing the genes were then screened for pyrethroid resistance. GAL4-UAS system is a veritable Swiss army knife (Duffy, 2002) which allows ectopic and targeted expression of gene of interest *in vivo* in a temporal and/or spatial fashion (Elliott and Brand, 2008, Duffy, 2002). The technology is increasingly used to validate insecticide resistance genes as described in the background to this chapter (Daborn et al., 2007, Zhu et al., 2010, Riveron et al., 2013, Riveron et al., 2014a). GAL4-UAS system is a bipartite system in which the expression of gene of interest (responder) is controlled by the presence of the UAS element, a 5 tandemly arrayed and optimized GAL4 binding sites (Duffy, 2002). Transcription of the responder requires presence of GAL4, thus the absence of GAL4 in the responder lines maintains them in a transcriptionally silent state; to activate transcription, the responder lines are mated to flies expressing GAL4 in a particular pattern termed the driver (Duffy, 2002). The progeny then expresses the responder (target gene) in a configuration that reflects the GAL4 pattern of the respective driver (Figure 3.5). The success of this technique is because GAL4 equivalent is absent in most species, and as such the candidate gene is only expressed in the progeny of the crosses between drivers and responder lines, when GAL4 and UAS transgenes are brought together in the same genome (Lynd and Lycett, 2012).

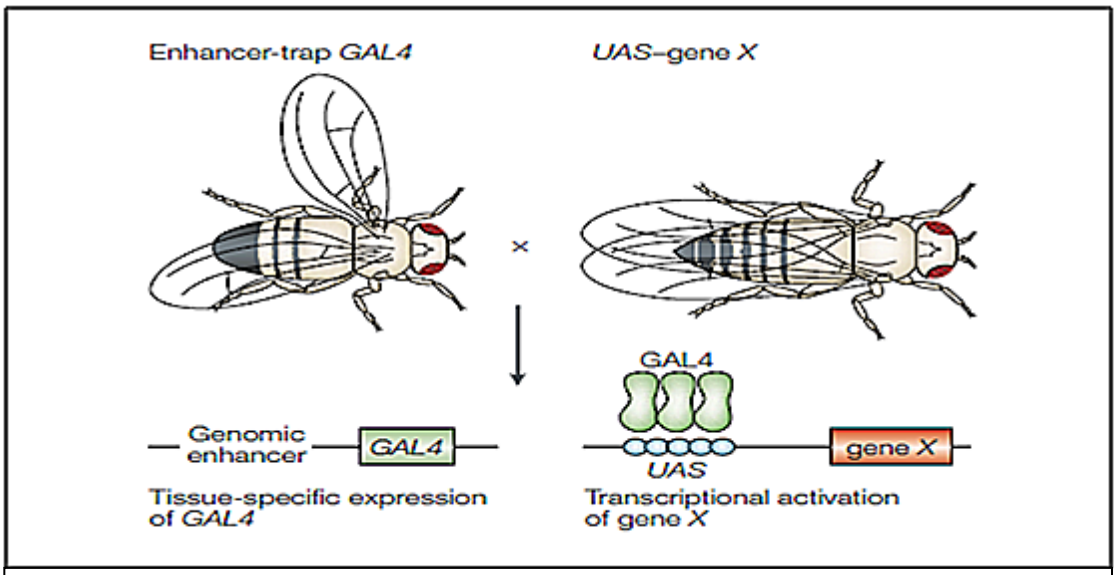

Figure 3.5: The *GAL4-UAS* System for directed gene expression. Adapted from (St Johnston, 2002)

3.3.5.1 Cloning and Construction of pUASattB::CYP6P9a and pUASattB::CYP6P9b Plasmids

Forward and reverse primers were designed for *CYP6P9a* and *CYP6P9b* with *Bgl*II and *Xba*I restriction sites respectively to allow cloning into pUAST vector. Full length cDNA encoding *CYP6P9a* (*MALCYP6P9a* and *FANGCYP6P9a*) and *CYP6P9b* (*MOZCYP6P9b* and *FANGCYP6P9b*) were amplified using HotStarTaq Polymerase (QIAGEN) and 0.5-1µg miniprep templates prepared in section 2.3.2.3. Protocol for amplification (Table 3.13) involves initial denaturation at 95^{o}C for 15 mins followed by 35 cycles each of 94^{o}C for 30 seconds; 57^{o}C for 30 seconds and 72^{o}C for 90 seconds. This is followed with final extension for 5 mins at 72^{o}C and holding at 4^{o}C. The primers for the amplification of these genes as well as primers for qPCR validation are given in Table 3.14.

Table 3.13: PCR reaction mix for amplification of CYP6P9a/CYP6P9b cDNA for transgenic analysis

Reagent	Final Concentration	Volume (µl)
10x Qiagen Buffer (containing 15mM $MgCl_2$)	1x	1.5
dNTP mix (25mM)	0.8mM	0.2
CYP6P9a/*CYP6P9b*_pUAS_*Bgl*II_F (10µM)	0.22µM	0.325
CYP6P9a/*CYP6P9b*_pUAS_*Xba*I_R (10µM)	0.22µM	0.325
Miniprep Template	0.5-1µg	0.5-1.0
dH_2O	variable	variable
HotStarTaq Polymerase	1U	0.2
Total Volume		15

PCR product was cleaned and cloned into pJET1.2 blunt, transformed into *DH5α*, as described previously (section 2.3.2.3) and screened with the pJET1.2 primers. Positive colonies were miniprepped overnight and sequenced on both strands to confirm presence of genes. The minipreps were then double-digested with *Bgl*II and *Xba*I restriction enzymes using the protocol as described in Table 3.4. Restriction digests were then gel extracted and ligated into pUASattB vector already linearised with same restriction enzymes, overnight and at 16°C as described (Table 3.5). 4µl of ligation product, a construct of target genes in pUAS vector were transformed into *DH5α* and screened for positive colonies using the KAPPA PCR.

Table 3.14: Primers used for cloning into pUASattB vector and plasmid sequencing

Primer	Sequences
CYP6P9a_pUAS_*Bgl*II_F	AGATCTATGGAGCTCATTAACGTGGTG
CYP6P9a_pUAS_*Xba*I_R	TCTAGATCACAATTTTTCCACCTTCAAGTAA
CYP6P9b_pUAS_*Bgl*II_F	AGATCTATGGAGCTCATTAACGTGGTGTT
CYP6P9b_pUAS_*Xba*I_R	TCTAGACTACAAAAACCCCTTCCGCT
CYP6P9a_qPCR_F	CAGCGCGTACACCAGATTGTGTAA
CYP6P9a-qPCR_R	TCA CAA TTT TTC CAC CTT CAA GTA ATT ACC CGC
*C*YP6P9b_qPCR_F	CAGCGCGTACACCAGATTGTGTAA
CYP6P9b_qPCR_R	TTA CAC CTT TTC TAC CTT CAA GTA ATT ACC CGC
RPL11_F	CGATCCCTCCATCGGTATCT
RPL11_R	AACCACTTCATGGCATCCTC

*Bgl*II restriction site is in green and underlined and *Xba*I is in red and underlined.

Medium scale plasmid preparation (Midiprep) was carried out using HiSpeed Plasmid Midi Kit (QIAGEN) according to manufacturer's protocol. 5ml TB medium starter culture containing 5µl of 100mg/ml ampicillin, 5µl colony in dH_2O was allowed to grow at 37°C and 300 rpm for 6 hours. 4ml of the starter was transferred into a 1L flask with 150ml pre-warmed TB medium and 150µl of ampicillin and allowed to grow at 37°C and 220 rpm for 14-16 hours. Bacterial culture was then harvested and divided into three 50ml tubes chilled on ice and centrifuged for 10 mins at 4°C and 5000 rpm. Pellets were miniprepped and sequenced to confirm presence of the genes. Midiprep was sent to Genetic Services, MA, USA (http://www.geneticservices.com/) for injection into flies. Using PhiC31 system clones were transformed into germ line of a *D. melanogaster* strain carrying the attP40 docking site on

chromosome 2[“y1w67c23; P attP40”, “1; 2”]. Four transgenic lines, UAS-MALCYP6P9a, UAS-FANGCYP6P9a, UAS-MOZCYP6P9b and UAS-FANGCYP6P9b were constructed successfully.

3.3.5.2 Crossing and Preparation of Flies

GAL4 lines were purchased from Bloomington Stock Centre (http://flystocks.bio.indiana.edu/). Ubiquitous expression of candidate genes in the transgenes in adult F_1 progeny (the experimental group) was achieved after crossing homozygote males (UAS line with gene of interest) with virgin females from the driver strain Actin5C-GAL4 ["y [1] w[*]; P(Act5C-GAL4-w)E1/CyO","1;2"]. For control group, flies with the same background as the experimental group but devoid of the UAS and the candidate genes were crossed with the driver Actin5C-GAL4 lines to generate null-Actin5C-GAL4 lines without insertion. All flies were maintained at 25^{o}C in plastic vials with food.

3.3.5.3 Drosophila Insecticides Contact Assay

Insecticide papers (2% permethrin and 0.15% deltamethrin-impregnated) filter papers were prepared in acetone and Dow Corning 556 Silicone Fluid (BDH/Merk, Germany) and kept at 4^{o}C prior to bioassay. These papers were rolled and introduced into 45cc plastic vials. The vials were then plugged with cotton wool soaked in 5% sucrose. 20-25 (2-4 days old post-eclosion females) were selected for the bioassays and introduced into the vials. Mortality plus knockdown was scored after 1 hr, 2hrs, 3hrs, 6hrs, 12hrs and 24hrs post-exposure to the discriminating doses of the insecticides. For each assay, at least six replicates were performed and t-test was used to carry out statistical analysis of mortality plus knockdown obtained between experimental groups and control.

3.3.5.4 qRT-PCR validation of Overexpression

In order to confirm relative expression of the candidate genes in the experimental flies and absence of expression in the control groups qRT-PCR was carried out as described previously (Riveron et al., 2014a, Riveron et al., 2013). RNA was extracted from three pools of 5 F_1 experimental and control flies separately and cDNA synthesized as described in section 2.3.2. qPCR for both *CYP6P9a*

and *CYP6P9b* was conducted using the qPCR primers given in Table 3.14, with normalization using the housekeeping gene *RPL11*. A serial dilution of cDNA was used to establish standard curves for each gene in order to validate PCR efficiencies of the target and endogenous control(s) and assess quantitative differences between samples. qPCR ampilification was carried using MX 3005 real-time PCR system (Agilent Technologies) with Brilliant III Ultra-Fast SYBR® Green qPCR Master Mix. 10ng of cDNA was utilised as a template in a 3-steps thermocycling involving denaturation at 95^{o}C for 3 mins, followed by 40 cycles each of 10 seconds at 95^{o}C and 10 seconds at 60^{o}C; this is then followed with 1 min at 95^{o}C, 30 seconds at 55^{o}C and 30 seconds 95^{o}C. The relative expression and fold-change of each target gene from the resistant and experimental and control samples was calculated using the comparative C_T Method ($2^{-\Delta\Delta C}{}_T$) as described (Schmittgen and Livak, 2008).

3.4 Results

3.4.1 Pattern of Co-expression of *ompA+2CYP6P9a*/*ompA+2CYP6P9b* Alleles with *CPR*

Recombinant CYP6P9b proteins were successfully expressed as we did previously (Riveron et al., 2013) with optimal expression at 48-56 hours post-induction. For CYP6P9a, I obtained optimal expression at 36-40 hours with modifications of growth conditions and concentrations of δ-ALA and IPTG as I described in this paper (Riveron et al., 2014a) (Appendix 5). The two P450s differ in their expression patterns in that CYP6P9a show consistently higher expression than CYP6P9b (Figure 3.6). On average for CYP6P9a lowest expression was observed from ZMBCYP6P9a (4.35nmol/ml±0.12, n =2) and highest with FANGCYP6P9a (16.28nmol/ml±3.53, n = 3); while for CYP6P9b, lowest expression was obtained from ZMBCYP6P9b (7.05nmol/ml±0.25, n= 2) and highest with UGANCYP6P9b (12.02nmol/ml ± 9.29)(Figure 3.7).

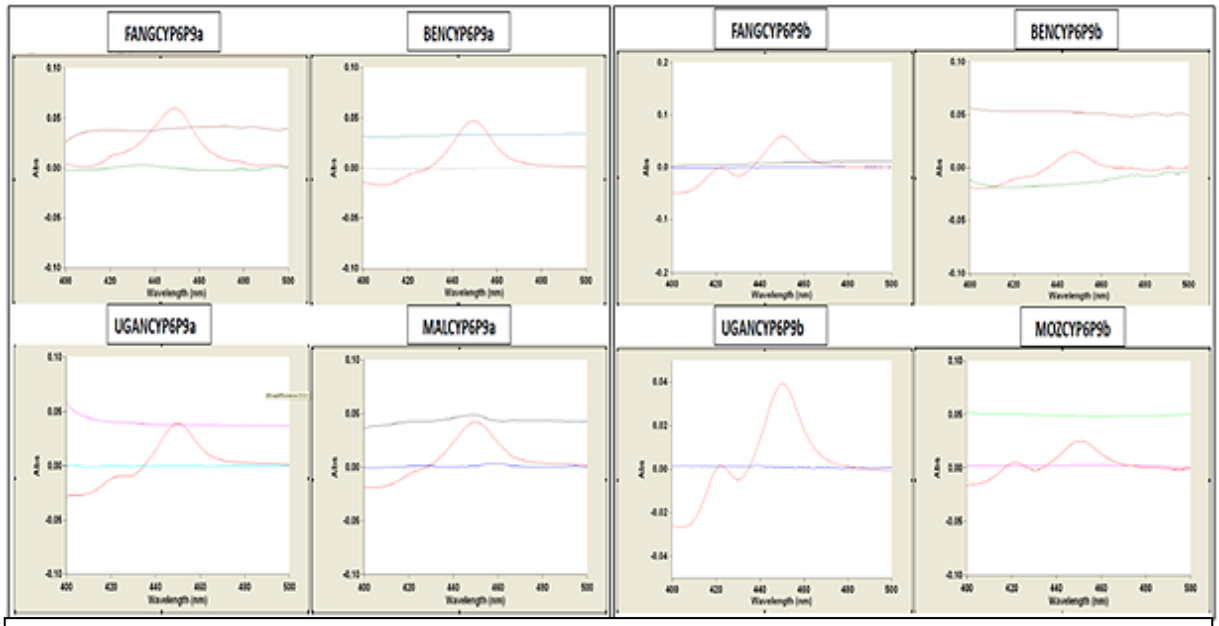

Figure 3.6: Fe^{2+}-CO vs Fe^{2+} difference spectrum obtained from some of *An. funestus* CYP6P9a and CYP6P9b recombinant proteins. Soret peak at 450nm shown in red spectra.

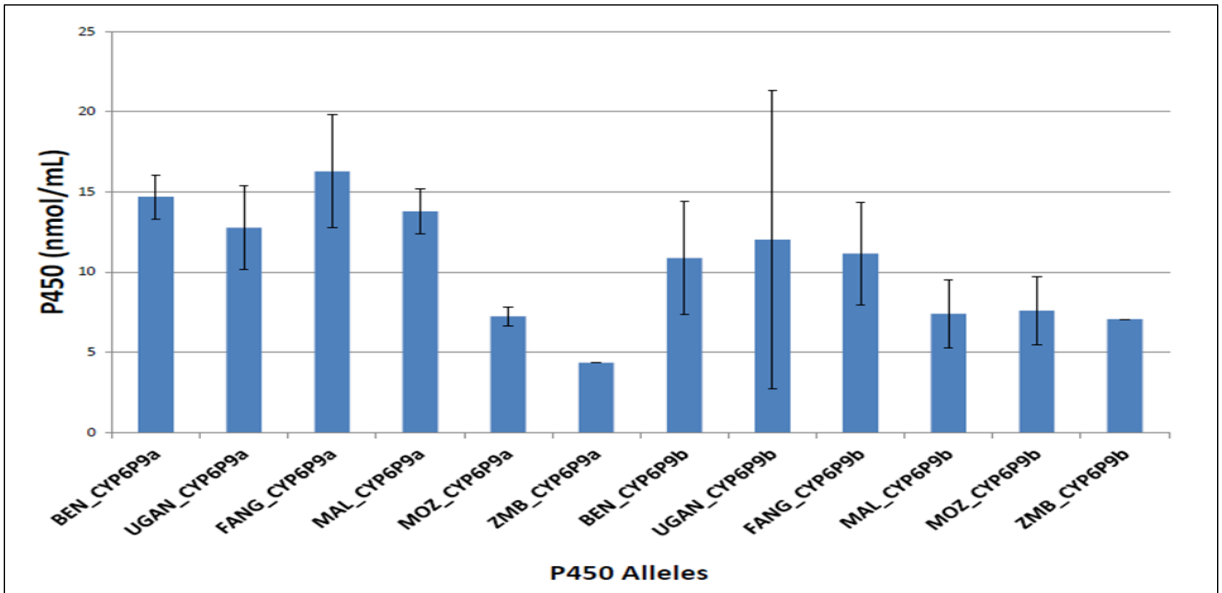

Figure 3.7: Amount of P450 expressed by CYP6P9a and CYP6P9b recombinant proteins. Error bars are variations in the amount of membrane independently expressed from same allele at different times. n (number of replicates = 3 for all alleles except ZMBCYP6P9a and ZMBCYP6P9b in which n = 2)

Membranes contain comparable amount of CPR with BENCYP6P9a on average exhibiting the lowest reductase activity (119.6nmol cytochrome *c* reduced/min/mg protein±20.01) and MOZCYP6P9b having the highest activity (205.29nmol cytochrome *c* reduced/min/mg protein±19.19) (Figure 3.8B).

No statistically significant differences were obtained when reductase content of the membranes from resistant alleles were compared to those from susceptible individuals ($p>0.05$). The total protein content of all membranes were also within same range (Appendix 3.2) with few differences. For CYP6P9a lowest protein content was obtained from UGANCYP6P9a (15.79mg/ml±1.58) and highest with MALCYP6P9a (19.49mg/ml±1.74). CYP6P9b produced slightly higher protein content with the lowest observed from FANGCYP6P9b (24.54mg/ml±1.95) and highest obtained from BENCYP6P9b (27.72mg/ml±3.23). Membrane content was calculated as the ratio of P450 yield (amount expressed) to the total protein content. On average CYP6P9a show higher membrane content than CYP6P9b (Figure 3.8A). Protein concentration was not quantified for ZMBCYP6P9a and ZMBCYP6P9b alleles and as such membrane content and CPR activity were not determined for these alleles. This is because MALCYP6P9a and MOZCYP6P9b alleles were already pre-selected for analysis as representative alleles from southern Africa and were to be used in subsequent experiments.

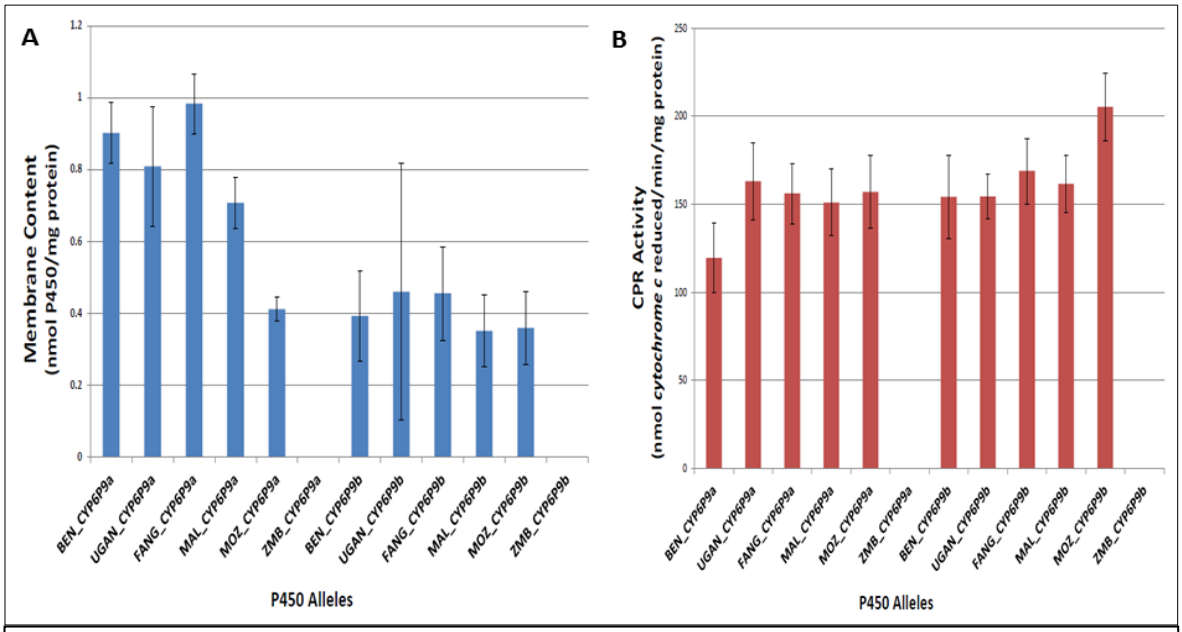

Figure 3.8: Membrane content (A) and CPR activity (B) of CYP6P9a and CYP6P9b proteins. Error bars represent (A) variation in the amount of membrane and/or total protein; (B) variations in the CPR activities determined independently from membranes expressed from the same allele. Number of replicates, n = 3.

3.4.2 Comparative Analysis of Metabolic Activity of Various Alleles of *CYP6P9a* and *CYP6P9b* Using Fluorescent Probes

3.4.2.1 Probe Substrates Metabolism

Four probe substrates: ER, EFC, MFC and DEF were screened with membranes from variants of CYP6P9a (BENCYP6P9a, UGANCYP6P9a, MALCYP6P9a and the susceptible FANGCYP6P9a) and CYP6P9b (BENCYP6P9b, UGANCYP6P9b, MOZCYP6P9b and the susceptible FANGCYP6P9b).

CYP6P9a: Lowest fluorescent activities were observed with 7-ER and MFC, while higher activities were obtained with 7-EFC and especially DEF. However, in all cases FANGCYP6P9a has lowest activity for all test probes. For example, with DEF, FANG has the lowest activity (0.13RFU/min/pmol± 0.01), followed by UGANCYP6P9a and MALCYP6P9a with 0.50RFU/min/pmol±0.02 and 0.76 RFU/min/pmol±0.11, respectively (Figure 3.9). BENCYP6P9a exhibited the highest activity towards DEF with an average activity of 0.92RFU/min/pmol±0.16. This initial test of dealkylation clearly reveals the resistant alleles as having several fold higher activity than the allele from FANG. However, lower activities toward all probes were obtained with CYP6P9a alleles compared with CYP6P9b though MALCYP6P9a has a very high activity towards 7-ER, compared with the rest of the proteins screened.

CYP6P9b: The same pattern of activity was observed with CYP6P9b proteins with lowest activity obtained from 7-ER and MFC, and highest with 7-EFC and DEF. However, lowest activity with DEF was obtained from FANGCYP6P9b (0.49RFU/min/pmol±0.001), followed by West African (BENCYP6P9b) and southern African (MOZCYP6P9b) proteins with activities of 4.36RFU/min/pmol±1.2 and 5.61RFU/min/pmol±0.8 respectively (Figure 3.9). East African (UGANCYP6P9b) exhibited the highest activity with DEF with turnover of 7.93RFU/min/pmol±1.33. Thus, the activities obtained from recombinant proteins from resistant alleles range from 11-fold higher for BENCYP6P9b to 16-fold higher for UGANCYP6P9b compared with the susceptible FANGCYP6P9b protein.

Both FANGCYP6P9a and FANGCYP6P9b proteins exhibited lowest activity toward all the probes tested reflecting their low efficiency of O-dealkylation compared with proteins from resistant strains (especially CYP6P9b) which exhibited high turnover (O-dealkylation) for ER, EFC, MFC and DEF. Higher activities were obtained from CYP6P9b, on average 4 to 8-folds than obtained with CYP6P9a reflecting the possible higher enzymatic activity of *CYP6P9b* gene over *CYP6P9a*.

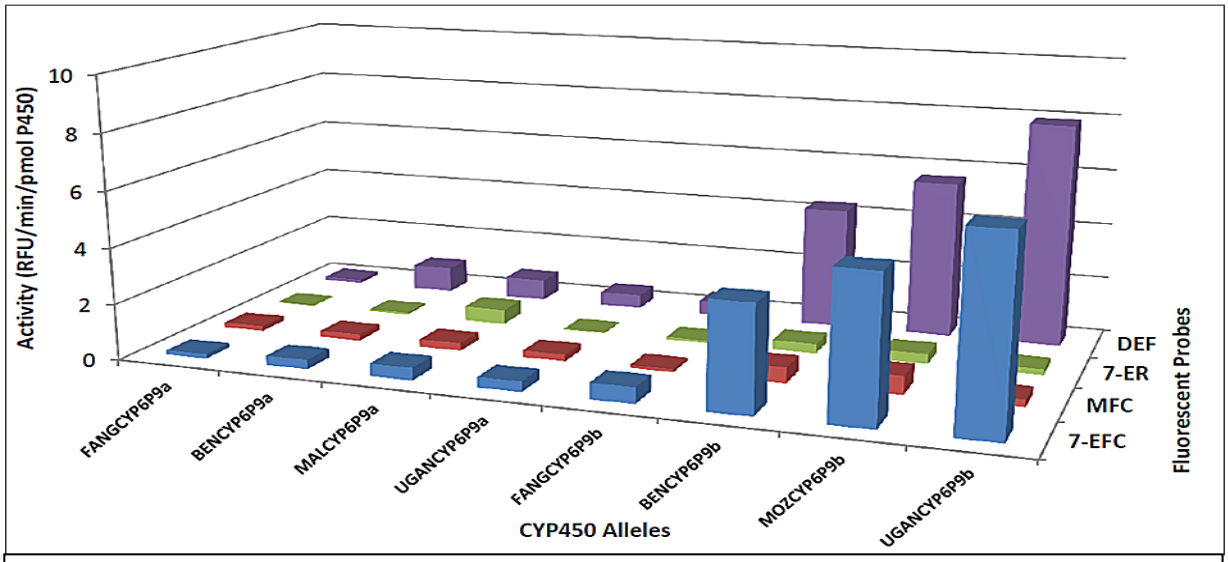

Figure 3.9: Metabolism of probe substrates by variants of recombinant CYP6P9a and CYP69b. The solid bars indicate average of significant turnovers of three experimental replicates (n =3) compared to negative controls (NADPH-). FG = FANG, BN =Benin, UG = Uganda, MAL = Malawi, and MOZ = Mozambique.

3.4.2.2 Test for Linearity and Enzymes Kinetics

In order to establish optimal conditions for linear activity with respect to time and enzyme concentrations, 1µM diethoxyfluorescein (DEF) was incubated with varying amount of CYP6P9a and CYP6P9b membranes proteins (Appendix 3.4). Increase in activity was measured up to 30 minutes. Higher activities were obtained from CYP6P9b compared with CYP6P9a proteins.

Figure 3.10 depicts the plot initial velocities of O-deethylation of DEF by the P450 proteins screened. Reactions followed Michaelis-Menten fashion with proteins expressed from resistant strains having higher activities compared with those from the susceptible strain, FANG.

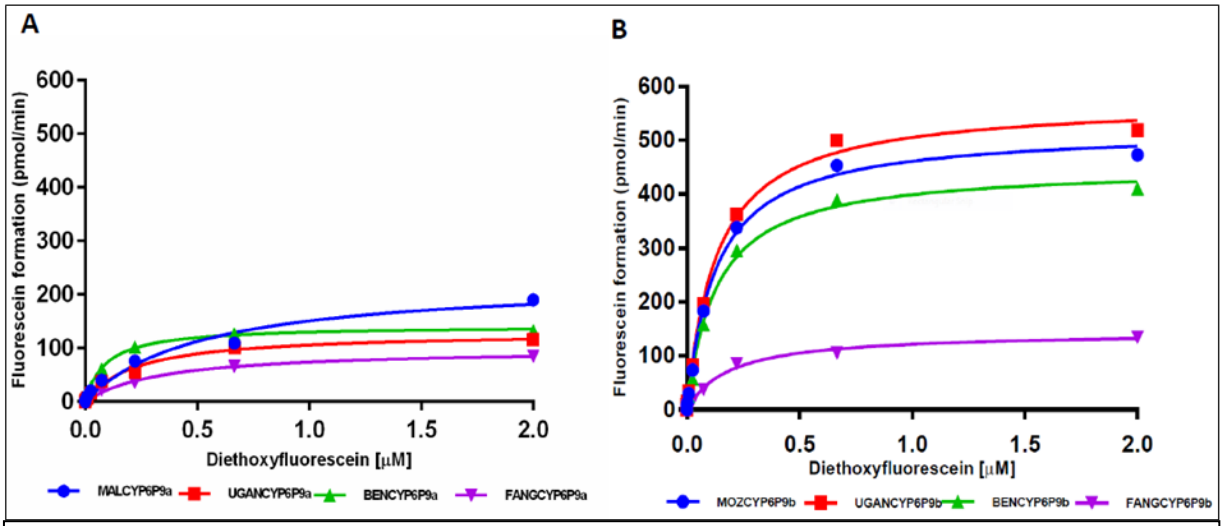

Figure 3.10: Michaelis-Menten plots for (A) CYP6P9a and (B) CYP6P9b recombinant proteins metabolism of diethoxyfluorescein.

***CYP6P9a* Alleles:** Membranes expressed from resistant alleles (BENCYP6P9a, UGANCYP6P9a and MALCYP6P9a) showed higher maximal catalytic activity (K_{cat}) and affinity (lower K_M) with DEF compared with that from FANG (FANGCYP6P9a) (Table 3.15 and Figure 3.11). These K_M values are statistically significant ($p<0.05$) compared with K_M from FANGCYP6P9a, with the lowest K_M value obtained from BENCYP6P9a (0.091µM±0.006) and highest K_M produced by FANGCYP6P9a (0.34µM±0.035). The catalytic activity (K_{cat}) for BENCYP6P9a and MALCYP6P9a were also statistically significantly different from that of FANGCYP6P9a, with values from MALCYP6P9a being more than two-fold the K_{cat} from FANGCYP6P9a. Therefore, UGANCYP6P9a protein was calculated as more than two-fold as catalytically efficient than FANGCYP6P9a while BENCYP6P9a and MALCYP6P9a were more than six-fold more efficient than FANGCYP6P9a. These differences in catalytic efficiencies were established as statistically significant using ANOVA Tukey's multiple comparison test ($p<0.05$)

Table 3.15: Kinetic constants for CYP6P9a- and CYP6P9b proteins-mediated DEF metabolism

Recombinant Proteins	Membrane (pmol)	K_M (µM)	K_{cat} (min^{-1})	K_{cat}/K_M (min^{-1} $µM^{-1}$)
BENCYP6P9a	10	0.091±0.006[a]	14.16±0.23[c]	155.60±10.56*
UGANCYP6P9a	10	0.226±0.035[a]	12.98±0.61	57.43±9.29*
FANGCYP6P9a	10	0.34±0.035	9.52±0.33	27.99±3.04
MALCYP6P9a	10	0.14±0.013[a]	22.84±2.21[c]	163.1±22.24*
BENCYP6P9b	3.33	0.13±0.01[b]	135.43±3.12[d]	1049.84±84.92[$]
UGANCYP6P9b	3.33	0.13±0.01[b]	171.86±3.76[d]	1301.96±102.66[$]
FANGCYP6P9b	3.33	0.24±0.02	14.93±0.500	62.20±5.58
MOZCYP6P9b	3.33	0.12±0.01[b]	156.27±3.306[d]	1220.85±98.81[$]

Values are mean ±S.D. of three replicates
Apparent K_{cat} was calculated as pmol fluorescein produced/min/pmol P450; Catalytic efficiency was calculated as K_{cat}/K_M
[a,b] Significantly different K_M values compared with FANGCYP6P9a and FANGCYP6P9b respectively.
[c,d] Significantly different *Kcat* values compared with FANGCYP6P9a and FANGCYP6P9b respectively.
*,[$] Significant differences between K_{cat}/K_M values respectivelycompared with FANCYP6P9a and FANGCYP6P9b

***CYP6P9b* Alleles:** The same pattern of O-deethylation of DEF was also evident from alleles of *CYP6P9b* in which the K_{cat} of BENCYP6P9b, UGANCYP6P9b and MOZCYP6P9b with DEF were on average ten-fold higher than obtained with FANGCYP6P9b protein ($p<0.05$) (Table 3.15 and Figure 3.11). The affinities of the resistant CYP6P9b proteins towards DEF were also within the same ranges and on average twice the affinities (half the K_M values, $p<0.05$) obtained from FANGCYP6P9b. Thus, the catalytic efficiency of BENCYP6P9b with DEF was established as sixteen-fold higher than that of FANGCYP6P9b ($p<0.05$) and values from UGANCYP6P9b and MOZCYP6P9b were approximately twenty-fold higher ($p<0.05$) than those obtained from FANGCYP6P9b.

These results supported initial testing of O-dealkylation that CYP6P9b proteins from resistant alleles are more enzymatically efficient than the corresponding enzymes from susceptible strain. Equally also, in agreement with the initial testing of O-dealkylation, the turnover with CYP6P9b proteins from resistant strains were more than ten-fold higher than values obtained with CYP6P9a, demonstrating the central role of *CYP6P9b* as more efficient P450 in comparison with *CYP6P9a*.

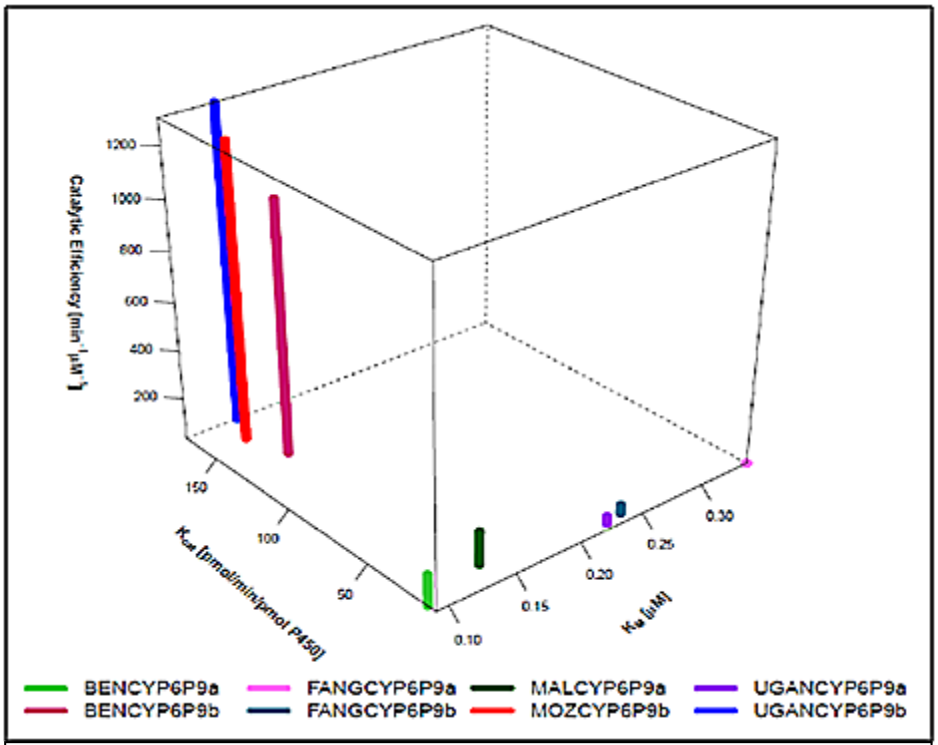

Figure 3.11: 4D plot of the kinetic constants and catalytic efficiencies of recombinant CYP6P9a and CYP6P9b dealkyaltion of DEF.

3.4.2.3 Inhibition Assays

In order to investigate the enzymatic affinity of various recombinant proteins of CYP6P9a and CYP6P9b towards different classes of insecticides: pyrethroids, carbamates (bendiocarb and propoxur), DDT and chlorpyrifos were used in an inhibition assay with diethoxyfluorescein (DEF). The mean values of IC_{50} for the test inhibitors for the fluorogenic probe DEF used in this study is shown in Figure 3.12. Lowest IC_{50} was obtained with the positive control inhibitor miconazole, a potent reversible inhibitor shown from several studies to have very low IC_{50} against several recombinant, human CYP450s including CYP3A4, CYP1A2, CYP2D6, CYP2E1 and CYP2B6 (Yan et al., 2002, Niwa et al., 2005, Zhang et al., 2002). Type II pyrethroids deltamethrin, λ-cyhalothrin and α-cypermethrin showed the most potent inhibitory activity against CYP6P9a/CYP6P9b-mediated deethylation of DEF, with IC_{50} of less than 0.5µM of which the lowest IC_{50} was produced by MOZCYP6P9b. This trend of low IC_{50} was followed by Type I pyrethroids, the pseudo-pyrethroid etofenprox and the organophosphate,

chlorpyrifos. MALCYP6P9a exhibited the lowest IC_{50} with bifenthrin and MOZCYP6P9b lowest with permethrin and etofenprox. The IC_{50} for chlorpyrifos was found to be lower than values obtained from Type I pyrethroids. It's possible that this organophosphate binds more tightly to these P450s than the Type I pyrethroids. With DDT, IC_{50} values were on average 10µM for all proteins except UGANCYP6P9b (IC_{50} >25µM) suggestive of low affinity of these P450s to DDT, even though the low potency of DDT maybe caused by its low partitioning in water when compared with pyrethroids (Laskowski, 2002). IC_{50} values greater than 25µM of the test insecticides were obtained with bendiocarb and propoxur indicating that the carbamate insecticides are weak binders to the recombinant P450s CYP6P9a and CYP6P9b. This low affinity toward these P450s is in line with the docking prediction for bendiocarb which produced the lowest score.

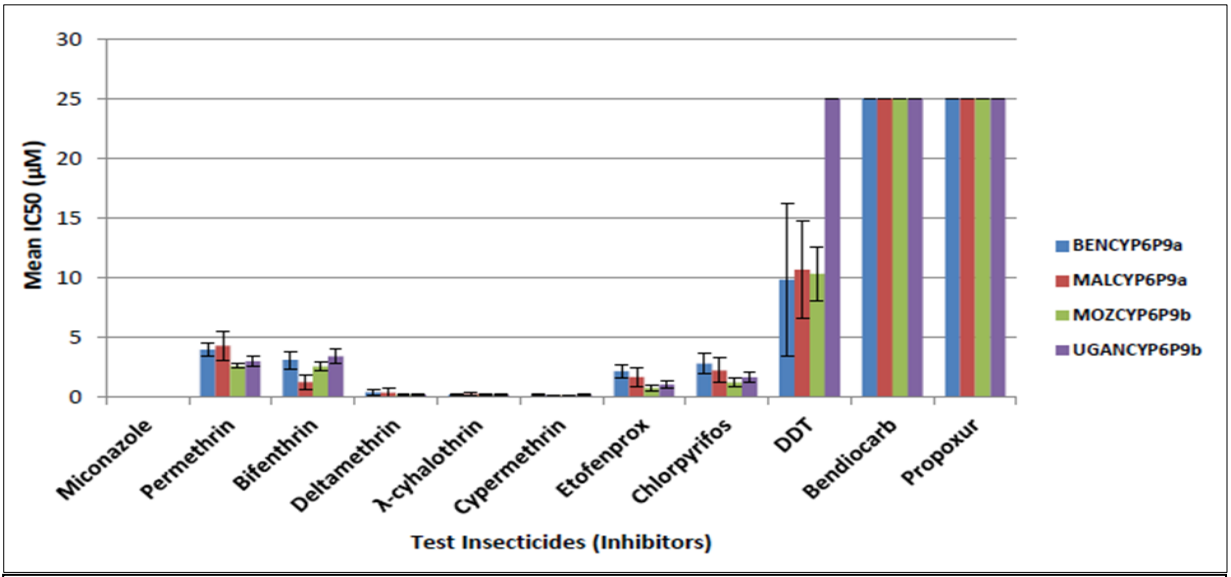

Figure 3.12: Mean IC_{50} of the test insecticide inhibitors against CYP6P9a and CYP6P9b dealkylation of DEF. Data represent mean IC_{50} at eight concentrations of each insecticide ±S.D. Error bars variation in the values of the IC_{50} between different concentrations.

All the pyrethroids insecticides tested and chlorpyrifos showed reversible inhibitory trend towards CYP6P9a and CYP6P9b-mediated dealkylation of DEF; the IC_{50} increased though not sharply with increase in incubation time. In theory, IC_{50} value of a reversible inhibitor does not change significantly with incubation time if the inhibitor strictly follows simple Michaelis-Menten kinetics (Yan

et al., 2002). As such non-Michaelis-Menten kinetics for pyrethroids cannot be ruled out with the alleles tested. However, IC_{50} with the positive control inhibitor miconazole was found to be non-time dependent. It remained consistent with little variation throughout the incubation time (regression coefficient, r^2 = 0.18). The summary of IC_{50} for all the insecticides tested as well as miconazole are given in Appendix 3.5 and Figure 3.13 depicts the plot of the effect of incubation time on IC_{50} of the test insecticides and miconazole for MOZCYP6P9b, with the highest activity towards DEF and highest affinity toward permethrin and deltamethrin from this assay. A good correlation was observed between increase in IC_{50} with time in the case of the following insecticides: cypermethrin (r^2 = 0.94), deltamethrin (r^2 = 0.98), lambda-cyhalothrin (r^2 = 0.96), etofenprox (r^2 = 0.98), chlorpyrifos (r^2 = 0.98), permethrin (r^2 = 0.7) and bifenthrin (r^2 = 0.8). Bendiocarb and propoxur both have a perfect fit with r^2 = 1, because these insecticides exhibited a very low affinity towards CYP6P9a and CYP6P9b. DDT exhibited poor correlation with r^2 of 0.24 indicative of possible low affinity which decreased with time.

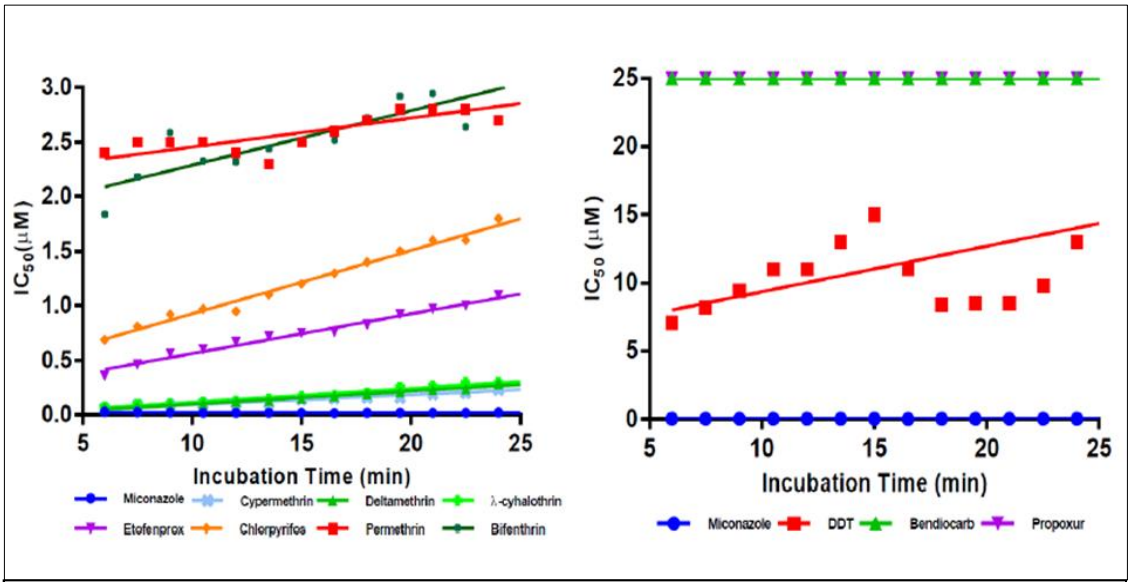

Figure 3.13: Effect of increase in incubation time on IC_{50} of test insecticide inhibitors on MOZCYP6P9b dealkylation of diethoxyfluorescein.

To determine the robustness of docking software, ChemScore values obtained with the model of MOZCYP6P9 with insecticide ligands were compared with the IC_{50}s from the same insecticides. A good correlation (Figure 3.14) was observed between IC_{50} and Chemscores in the case of the following

insecticides: permethrin (r^2 = 0.55), deltamethrin (r^2 = 0.85) and etofenprox (r^2 = 0.93). No correlation was observed from bendiocarb (r^2 = 1), while DDT produced a very poor correlation (r^2 = 0.06).

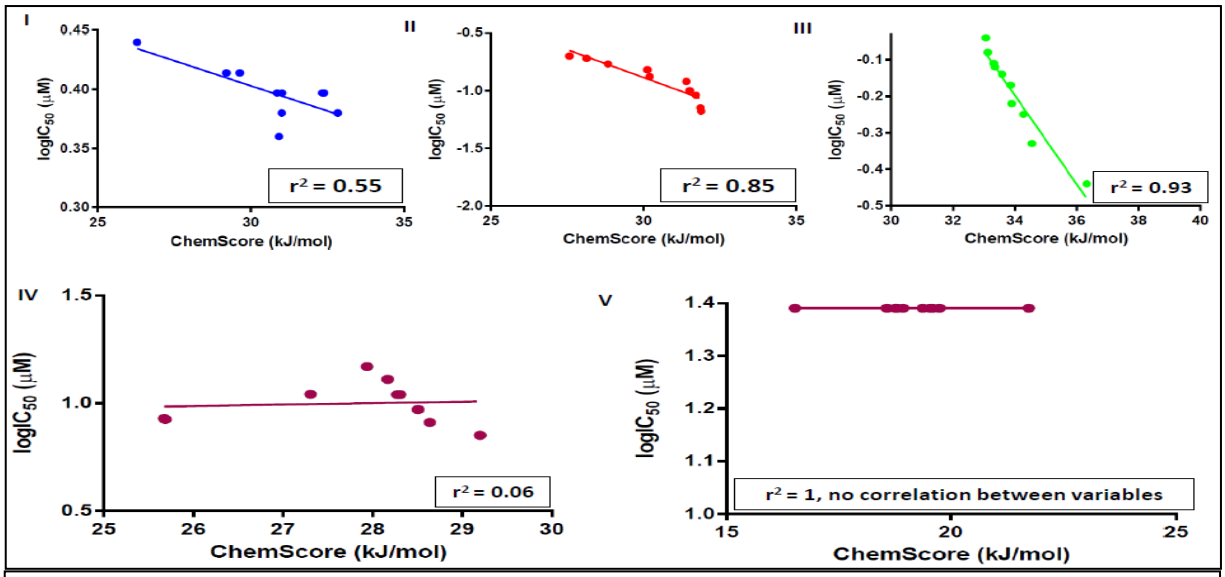

Figure 3.14: Correlation between IC_{50} of test insecticide inhibitors on MOZCYP6P9b bmetabolism of DEF and the ChemScore values from docking with GOLD. IC_{50} values vs Chemscore for MOZCYP6P9b with (I) permethrin, (II) deltamethrin, (III) etofenprox, (IV) DDT, and (V) bendiocarb.

3.4.3 Comparative Assessment of Metabolic Activity of Various Alleles of *CYP6P9a* and *CYP6P9b* on Different Insecticide Classes Using Metabolism Assay

3.4.3.1 Metabolism of Insecticides

To assess the metabolic profiles of the different CYP6P9a and CYP6P9b proteins with different classes of insecticides (Types I and II pyrethroids, etofenprox, bendiocarb, propoxur, DDT and malathion), metabolism assay was conducted using HPLC. Both CYP6P9a and CYP6P9b metabolizes Type I and Type II pyrethroids, with statistically significant depletion (+NADPH vs –NADPH) obtained from all proteins from resistant alleles compared with corresponding proteins from FANG. No significant activities were obtained against DDT, bendiocarb, propoxur and malathion), consistent with the molecular docking predictions as well as probes substrates analysis, in which no activities were respectively predicted and/or obtained against bendiocarb, propoxur and DDT.

***CYP6P9a* Alleles:**

Recombinant proteins expressed from alleles of resistant strains produced higher activities against pyrethroid insecticides compared with FANGCYP6P9a. These differences were statistically significant ($p<0.05$) for all pyrethroid insecticides. Highest activities were obtained from MALCYP6P9a which deplete 65.38%±1.5, 60.48%±2.65, 68.38%±1.83, 75.41%±1.72 and 46.04%±1.26 each of permethrin, bifenthrin, deltamethrin, λ-cyhalothrin and etofenprox, respectively (Table 3.16 and Figure 3.15A). In contrast, FANGCYP6P9a with lowest activities deplete only 29.0%±1.42, 16.6%±5.41, 18.11%±2.5, 15.46%±4.43 and 7.28%±1.53 each of permethrin, bifenthrin, deltamethrin, λ-cyhalothrin and etofenprox, respectively. This clearly indicated that the protein from the susceptible allele, FANG is a poor metaboliser of pyrethroid insecticides compared with those from the resistant alleles.

Table 3.16: Percentage depletion of pyrethroid insecticides by recombinant CYP6P9a and CYP6P9b

Recombinant Proteins	Permethrin	Bifenthrin	Deltamethrin	λ-cyhalothrin	Etofenprox
FANGCYP6P9a	29.0±1.42	16.6±5.41	18.11±2.15	15.46±4.43	7.28±1.53
UGANCYP6P9a	60.71±0.92*	50.31±3.8*	57.9±2.74*	47.74±1.5*	42.55±1.03*
BENCYP6P9a	66.42±2.23*	51.02±0.75*	59.54±5.11*	52.45±1.74*	41.22±1.54*
MALCYP6P9a	65.38±1.5*	60.48±2.65**	68.38±1.83**	75.41±1.72*	46.04±1.26*
FANGCYP6P9b	13.7±4.23	22.38±5.08	6.2±1.5	15.49±3.13	16.88±3.06
UGANCYP6P9b	88.58±3.48**	88.8±1.61**	62.53±4.04**	78.76±1.31**	57.91±1.55*
BENCYP6P9b	89.63±0.63**	89.19±1.01**	62.03±1.14**	49.35±4.41*	37.15±4.15*
MOZCYP6P9b	91.6±2.5**	81.6±0.25**	81.69±2.27**	86.51±1.14**	71.59±1.42**

Values are mean ± S.D. of three replicates compared with negative control (-NADPH);
* and **Significantly different from FANGCYP6P9a or FANGCYP6Pb at $p<0.05$ or $p<0.01$ respectively.

***CYP6P9b* Alleles:**

Recombinant proteins from CYP6P9b of resistant strains metabolizes pyrethroid insecticides with higher activities several fold more than the protein from susceptibe allele, FANGCYP6P9b (Table 3.16 and Figure 3.15B). These differences were statistically significant with the southern African allele MOZCYP6P9b having highest activity: 91.6%±2.5, 81.6%±0.25, 81.69%±2.27, 86.51%±1.14, 71.59%±1.42 depletion, respectively for permethrin, bifenthrin, deltamethrin, λ-cyahalothrin and etofenprox, compared with FANGCYP6P9b which depleted only 13.7±4.23, 22.38%±5.08, 6.2%±1.5,

15.49%±3.13 and 16.88%±3.03 of these insecticides. The differences between the resistant and susceptible alleles possibly explained the reason why FANG strain is susceptible to pyrethroids.

As observed with CYP6P9a, recombinant protein from the southern African allele of CYP6P9b (*MOZCYP6P9b*) has the highest activity consistent with the highest pyrethroid resistance reported in this region. However, as in fluorescent probes assay, CYP6P9b proteins exhibited higher activities against pyrethroids compared with CYP6P9a, confirming that *CYP6P9b* is more efficient metaboliser than *CYP6P9a*. *MOZCYP6P9b* has the highest activity of all the alleles screened with pyrethroids is not surprising for MOZCYP6P9b protein was predicted to have the highest activity of all alleles, and has been established as having high activity with probe substrates and portrayed the tightest binding to Type I and Type II pyrethroids from inhibition assay.

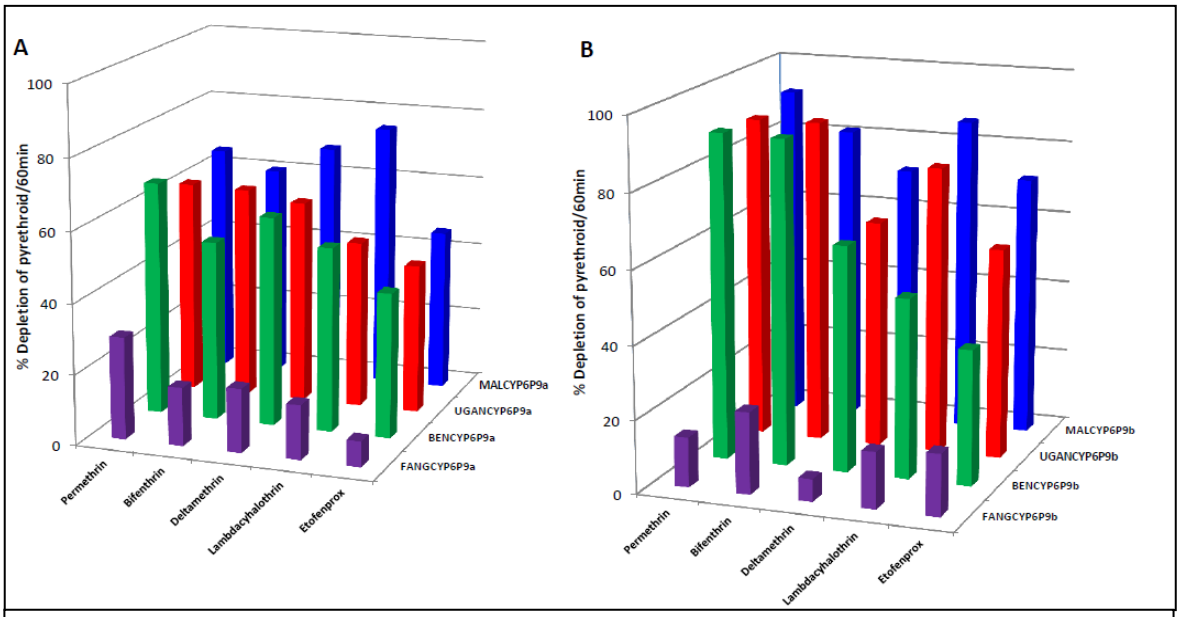

Figure 3.15: Percentage depletion of 20µM pyrethroids by recombinant CYP6P9a (A) and CYP6P9b (B). Results are average of three replicates (n = 3) compared with negative control (-NADPH).

3.4.3.2 Kinetics Analysis with Permethrin and Deltamethrin

Kinetics analysis was carried out with recombinant protein variants of four alleles each of CYP6P9a and MOZCYP6P9b, in order to establish the catalytic constant (K_{cat}) and Michaelis constant

(K_M) for permethrin and deltamethrin. The K_{cat} provides information on the speed with which different protein variants metabolise (clear) insecticide toxicant *in vitro,* while the K_M will highlight the affinity of each allele toward the insecticides tested. These parameters can help in assessing any differences in metabolic efficiencies between the alleles from resistant strains and those from FANG. Steady-state kinetic parameters for CYP6P9a and CYP6P9b with permethrin and deltamethrin are given in Table 3.17. Reactions followed Michaelis-Menten pattern (Figure 3.16) with K_M values within ranges (1-50µM) described for binding and metabolism of pyrethroids by insect cDNA-expressed P450s (Stevenson et al., 2012, Stevenson et al., 2011) and lower than K_M values obtained from *An. minimus'* CYP6P7 and CYP6AA3 with pyrethroids (Duangkaew et al., 2011). K_{cat} values obtained were also within the broad ranges recorded in the literature (1-20min^{-1}) for the activities of insect P450s with pyrethroids (Stevenson et al., 2012) but higher than established for some cDNA-expressed P450s, including *An. gambiae* CYP6M2, *Ae. aegypti CYP9J* families, as well as *An. gambiae* CYP6P3 with permethrin (Stevenson et al., 2011, Stevenson et al., 2012, Muller et al., 2008).

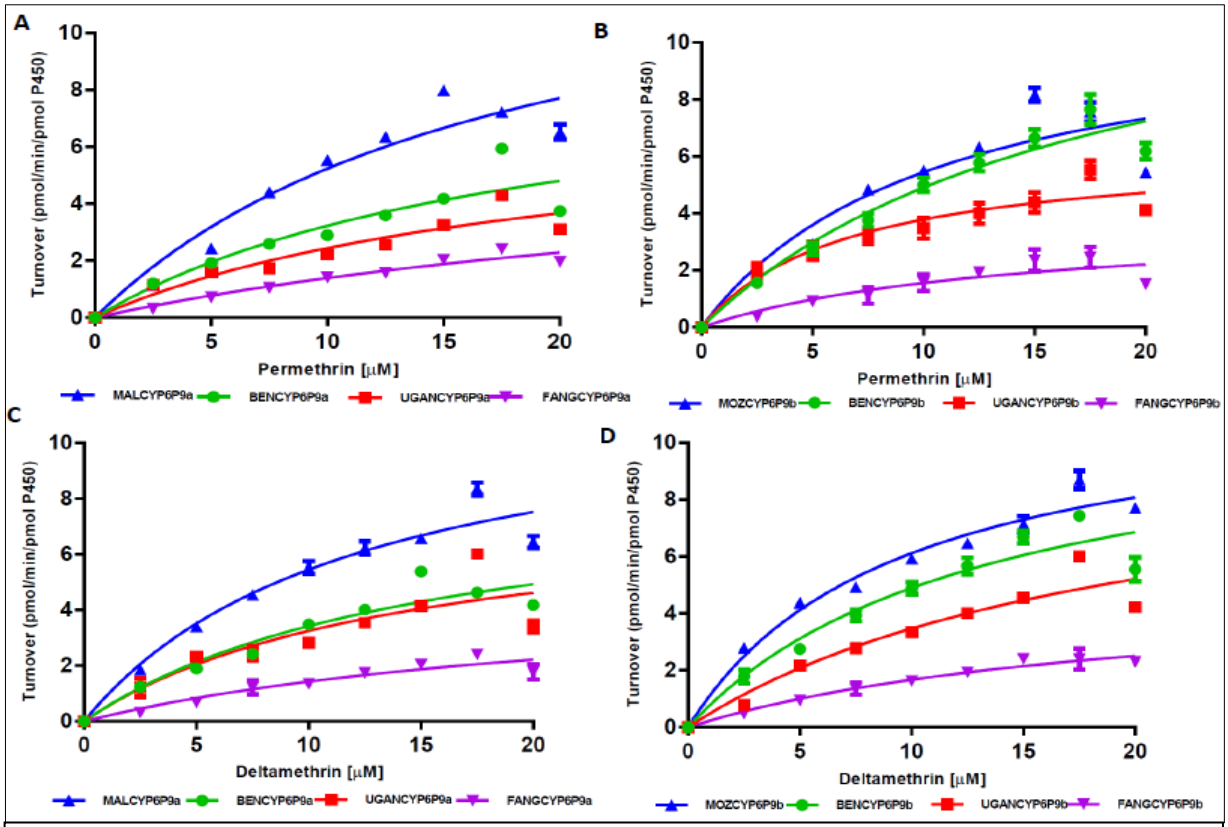

Figure 3.16: Michaelis-Menten plot of permethrin (A) and (B) and deltamethrin (C) and (D) metabolism by recombinant CYP6P9a and CYP6P9a. Each point is a mean±S.E.M. of three replicates.

***CYP6P9a* Alleles:**

Kinetic parameters obtaind revealed that CYP6P9a proteins from the resistant alleles possess higher K_{cat} and higher affinity (low K_M) compared with proteins expressed from the susceptible FANG. The K_{cat} of UGANCYP6P9a and MALCYP6P9a with permethrin are two- and three-fold higher than values obtained from FANGCYP6P9a, respectively (Table 3.17), and that of BENCYP6P9a and MALCYP6P9a with deltamethrin are as well two- and three-fold higher compared with the K_{cat} obtained from FANGCYP6P9a. These differences were statistically significant ($p<0.05$) for BENCYP6P9a and MALCYP6P9a compared with FANGCYP6P9a. In terms of K_M, for permethrin, statistically significant differences were also obtained with FANGCYP6P9a on average having half the affinity (K_M values two-fold higher) compared with the CYP6P9a from resistant alleles. This translated into statistically significant differences (ANOVA Tukey's test of significant at $p<0.05$) in terms of efficiency with BENCYP6P9a and UGANCYP6P9a having catalytic efficiencies for permethrin (three-fold higher) than FANGCYP6P9a while MALCYP6P9a exhibited catalytic efficiency for permethrin six-fold higher than FANGCYP6P9a. While FANGCYP6P9a exhibited higher affinity for deltamethrin than permethrin, the CYP6P9a from resistant alleles showed comparable K_M for both permethrin and deltamethrin. As a result of these differences the catalytic efficiencies of BENCYP6P9a and UGANCYP6P9a for deltamethrin were on average three-fold the values from FANGCYP6P9a while the K_{cat} for deltamethrin from MALCYP6P9a was four-fold higher than values from FANGCYP6P9a (Figure 3.17).

***CYP6P9b* Alleles:**

For permethrin *CYP6P9b* alleles from resistant individuals produced higher K_{cat} values compared with *FANGCYP6P9b*; these statistically significant differences ranged from twice the K_{cat} of *FANGCYP6P9b* as obtained from *UGANCYP6P9b*, to three-fold higher K_{cat} as observed from *MOZCYP6P9b*, to four-fold higher K_{cat} as obtained from *BENCYP6P9b* (Table 3.17).

Table 3.17: Kinetic Constants for Recombinant CYP6P9a- and CYP6P9b Permethrin and Deltamethrin Metabolism

Recombinant Proteins	K_{cat} (min^{-1})	K_M (µM)	K_{cat}/K_M (min^{-1} $µM^{-1}$)
		Permethrin	
BENCYP6P9a	9.37±3.32[a]	19.02±3.13[c]	0.49±0.19*
UGANCYP6P9a	7.35±1.02	20.11±3.91[c]	0.37±0.08*
FANGCYP6P9a	4.95±1.92	36.25±15.22	0.14±0.07
MALCYP6P9a	15.41±6.30[a]	18.77±11.76[c]	0.82±0.06*
BENCYP6P9b	15.91±5.45[b]	21.94±7.97	0.73±0.36[$]
UGANCYP6P9b	8.61±3.40[b]	21.22±10.32	0.41±0.3[$]
FANGCYP6P9b	4.5±1.35	20.47±8.31	0.21±0.11[$]
MOZCYP6P9b	12.38±4.5[b]	12.68±2.68[d]	0.97±0.41[$]
		Deltamethrin	
BENCYP6P9a	8.78±2.62[a]	15.67±4.64[c]	0.56±0.23*
UGANCYP6P9a	7.96±3.62	14.48±3.58[c]	0.54±0.28*
FANGCYP6P9a	4.87±2.06[a]	24.03±3.12	0.20±0.08
MALCYP6P9a	14.65±4.12[a]	18.26±6.97	0.80±0.38*
BENCYP6P9b	13.63±5.40[b]	15.98±5.63	0.85±0.45[$]
UGANCYP6P9b	10.44±4.00[b]	12.97±4.96[d]	0.80±0.35[$]
FANGCYP6P9b	4.92±0.82	19.5±5.53	0.25±0.08
MOZCYP6P9b	12.09±1.44[b]	9.9±1.65[d]	1.22±0.25[$]
BENCYP6P9a	8.78±2.62[a]	15.67±4.64[c]	0.56±0.23*

Values are mean ±S.D. of three replicates

Apparent K_{cat} was calculated as pmol/min/pmol P450; Catalytic efficiency was calculated as K_{cat}/K_M

[a,b] Significantly different K_{cat} values compared with FANGCYP6P9*a* and FANGCYP6P9b respectively, p<0.05.

[c,d] Significantly different K_M values compared with FANGCYP6P9a and FANGCYP6P9b respectively, p<0.05.

*,[$] Significant differences between K_{cat}/K_M values, respectively compared with FANCYP6P9a and FANGCYP6P9b, p<0.05.

Same pattern was obtained with deltamethrin, with UGANCYP6P9b having two-fold K_{cat} compared with FANGCYP6P9b, while BENCYP6P9b and MOZCYP6P9b exhibited K_{cat} values on average three-fold that of FANGCYP6P9b. No major difference in terms of K_M for permethrin and deltamethrin were observed between recombinant proteins from susceptible and resistant alleles of CYP6P9b, with the exception of UGANCYP6P9b with deltamethrin, and the southern African MOZCYP6P9b which consistently exhibited lowest, reproducible K_M both for permethrin and deltamethrin). These low K_M values from MOZCYP6P9b protein showed that the *MOZCYP6P9b* allele occupies a central position in terms of pyrethroid metabolism and the high affinity it exhibited, which is consistent with the molecular docking simulations in which the MOZCYP6P9b portrayed multiple, productive binding conformations, as well as fluorescent probes assay from which recombinant MOZCYP6P9b portrayed a

very high activity with the probe substrate diethoxyfluorescein, as well as tightest binding with pyrethroids, especially the Type II class, as obtained from inhibition assay.

For permethrin, UGANCYP6P9b, BENCYP6P9b and MOZCYP6P9b were calculated as having two-fold, three-fold and five-hold higher catalytic efficiencies respectively compared with FANGCYP6P9b (Figure 3.17). With deltamethrin, BENCYP6P9b and UGANCYP6P9b possess catalytic efficiencies more than three-fold higher than FANGCYP6P9b, while MOZCYP6P9b with the highest catalytic efficiency of 1.22 $min^{-1}\mu M^{-1}$±0.25 is five times more efficient in deltamethrin metabolism than the recombinant FANGCYP6P9b from the susceptible allele.

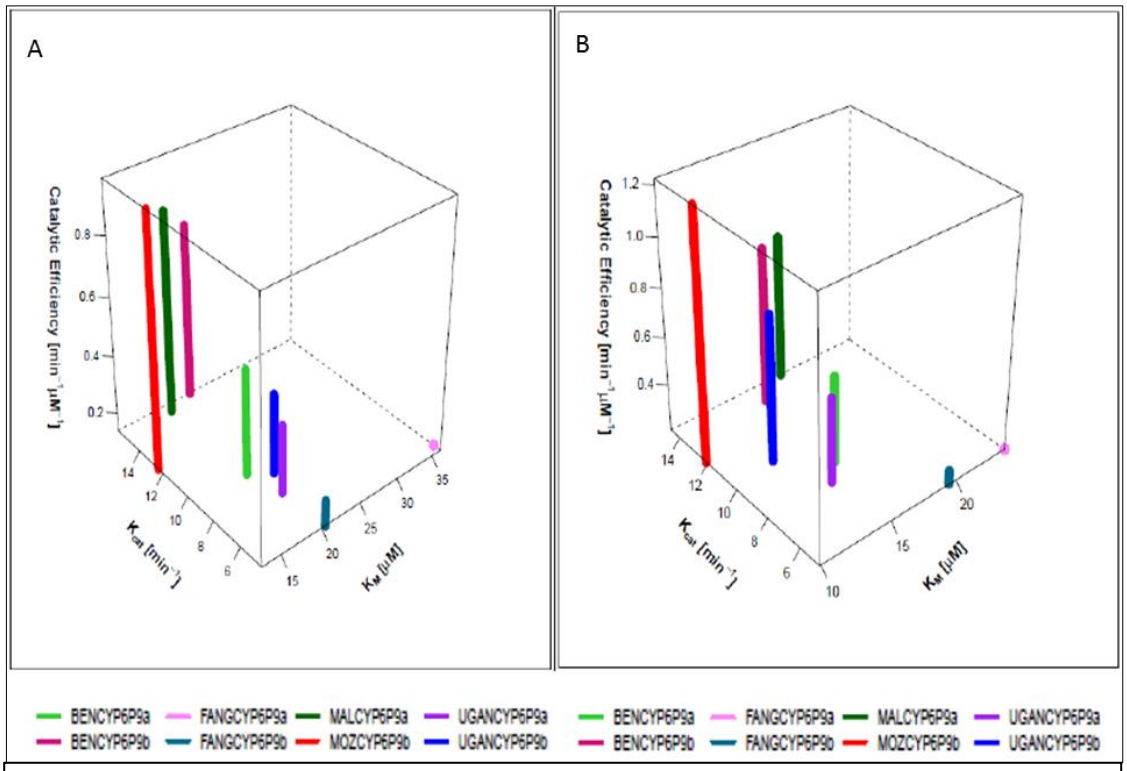

Figure 3.17: 4D plot of the kinetic constants and catalytic efficiencies of recombinant proteins of CYP6P9a and CYP6P9b with (A) permethrin and (B) deltamethrin. x-axis is the K_{cat} (min^{-1}); y-axis is the K_M (µM); catalytic efficiency is calculated as x/y (min^{-1} μM^{-1}).

In agreement with the results from fluorescent probes assays and initial testing of depletion of pyrethroids, recombinant CYP6P9b exhibited higher activities compared with their corresponding CYP6P9a, reflecting the central position of *CYP6P9b* in pyrethroid metabolism and resistance, especially *MOZCYP6P9b* with highest intrinsic clearance (CL_{int}) for both permethrin and deltamethrin.

3.4.4 Detection of Key Amino Acid Changes Conferring Pyrethroid Resistance

To assess the potential role of key amino acids in metabolism of pyrethroids, amino acid variants from *MOZCYP6P9b* were mutagenized into residues present in *FANGCYP6P9b*. Proteins were expressed and used in probe susbtrates and metabolism assays with pyrethroids, to establish the impact of the replaced amino acids on catalysis. Efforts to amplify mutant sequences from *CYP6P9a* were not successful on several attempts and several approaches. As resistant *CYP6P9b* alleles possess higher potential mutations compared with *FANGCYP6P9b*, seems to be undergoing more directional selection than *CYP6P9a* alleles, has portrayed higher activities with probes substrates and pyrethroids insecticides, it was decided to proceed with the mutagenesis using the resistant allele, *MOZCYP6P9b*.

3.4.4.1 Sequence Characterisation of CYP6P9b of Mutant Libraries

The mutant libraries were screened with pJET1.2 primers, sequenced on both strands and manually analysed using the BioEdit to confirm presence of desired nucleotides substitutions. The sequencing results confirmed presence of the desired mutations and absence of any unwanted substitutions in the mutated DNA sequence of *CYP6P9b*.

3.4.4.2 Pattern of Expression of Mutant CYP6P9b Membranes

Recombinant proteins of the mutant membranes of *MOZCYP6P9b* along with the wild type were expressed successfully at 21^{o}C and 150 rpm using *JM109* cells as described previously. The only exception was the Val^{109}Ile mutant that was successfully expressed rather using *E. coli DH5α* by lowering the orbital shaking speed to 120 rpm after induction of the log-phased cells with 0.5mM each of δ-ALA and IPTG to the final concentration in 200ml culture. With the exception of Pro^{401}Ala mutant all the mutants have lower expression (<3.0 nmol/ml) compared with the wild type MOZCYP6P9b (Table 3.18). Specifically, the Val^{109}Ile mutant produced functional P450 with concentrations of less than 1.0nmol/ml in all the three successful attempts. Pro^{401}Ala mutant consistently produced higher functional protein than all the other mutants as well as the wild type MOZCYP6P9b. Time to optimal

expression for all the mutants is around 40-48 hours with the exception of Pro^{401}Ala mutant which expresses optimally before 30 hours after induction and the Val^{109}Ile mutant which as a result of low concentration of IPTG and/or different *E. coli* system (*DH5α* cells) expressed more slowly with optimal expression between 60 to 72 hours.

Table 3.18: Pattern of expression of *MOZCYP6P9b* mutants

Recombinant Proteins	Time to optimal expression (hr)	n	Yield (nmol/ml)
Val^{109}Ile-MOZCYP6P9b	60-72	3	0.85±0.28
Asp^{335}Glu-MOZCYP6P9b	40-48	3	2.97±0.47
Asn^{384}Ser-MOZCYP6P9b	40-48	4	2.77±0.41
Pro^{401}Ala-MOZCYP6P9b	24-30	3	5.31±1.81
MOZCYP6P9b (Wild Type)	36-40	4	4.89±0.46

Yield of P450 presented as means ± S.D. of concentrations of membranes independently expressed.
n = number of times membrane is expressed.

3.4.4.3 Comparative Assessment of Role of Amino Acids Replacement on Metabolic Activities Using Fluorescent Probes Assays

Seven fluorogenic probe substrates were tested for O-dealkylating activity with the mutant CYP6P9b membranes alongside the wild type MOZCYP6P9b. More probes were screened with the mutants because of availability and for replacement of key amino acid residues is known to change both qualitative and quantitave activities of some P450s (Szklarz and Halpert, 1997). Highest activity was observed with DEF and lowest with the resorufin and coumarin-based substrates (Figure 3.18). However, significant reduction in activity towards DEF was observed in all the mutants compared with MOZCYP6P9b. This reduction in activity is most profoundly significant ($p<0.001$) with Asp^{335}Glu mutant as well as the Asn^{384}Ser mutant ($p<0.05$) compared with MOZCYP6P9b. Val^{109}Ile acquired some quantitative activity towards RME, values which are statistically significant compared with Pro^{401}Ala and MOZCYP6P9b, while the other mutants exhibited no activity at all towards RME. The Asp^{335}Glu mutant exhibited lowest activity towards all probes tested with no detectable of even low activity toward all the resorufin-based probes. The mutants and the wild type allele exhibited some activity

toward 7-EFC and MFC as described previously, but with sharp decline in activity within seconds of initial burst of activity which makes it unwise to use these probes for kinetic analysis.

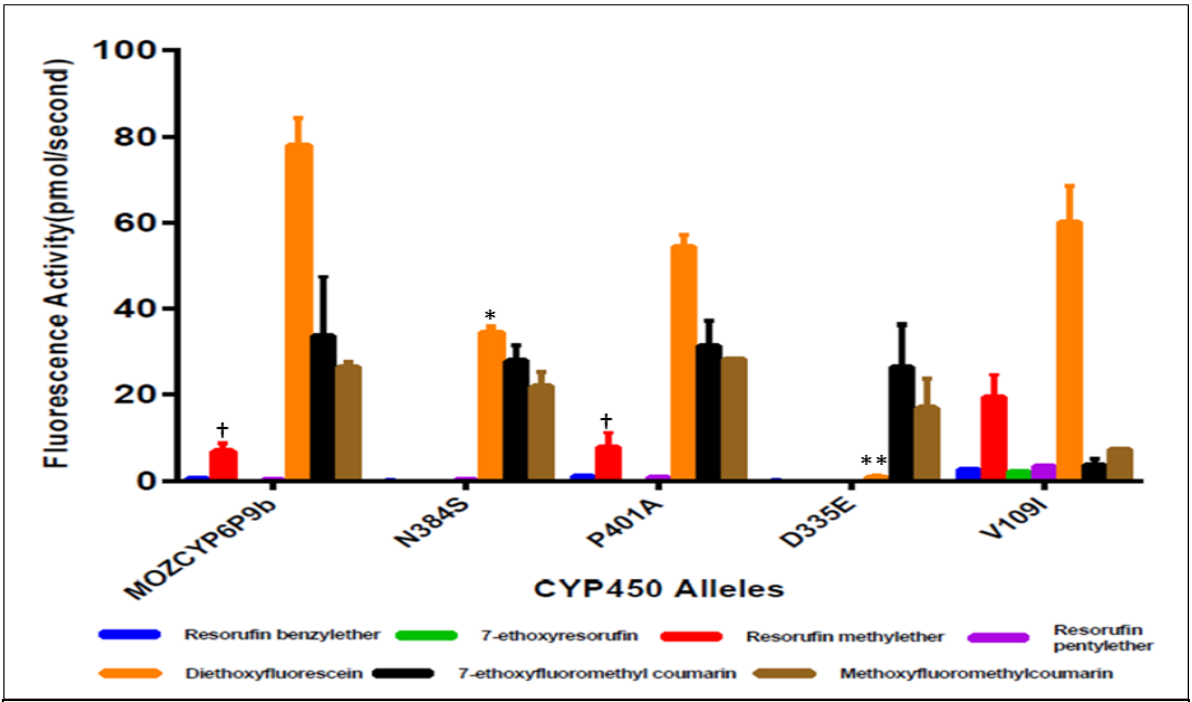

Figure 3.18: Metabolism of probe substrates by mutant CYP6P9b membranes. The solid bars indicate average of activity in three experimental replicates compared to negative control (NADPH-). * and **statistically significant at $p<0.05$ and $p<0.01$ compared with MOZCYP6P9b; †statistically significant compared with Val^{109}Ile mutant.

Kinetic analysis was carried out with DEF which produced highest and more consistent activities from the initial test of dealkylation. For all mutants and MOZCYP6P9b proteins fluorescein formation follows Michaelis-Menten pattern (Figure 3.19) but kinetic parameters of MOZCYP6P9b-mediated O-dealkylation of DEF differed greatly from that of the mutant proteins. In terms of turnover, the K_{cat} produced by MOZCYP6P9b is 19-fold, 14-fold and five-fold higher than obtained with Asn^{384}Ser, Val^{109}Ile and Asp^{335}Glu mutants, respectively (Figure 3.20 and Appendix 3.6A) reflecting a quantitative decrease in the catalytic activity of these mutants. No major difference was observed between the wild type *MOZCYP6P9b* and the Pro^{401}Ala mutant in terms of K_{cat}.

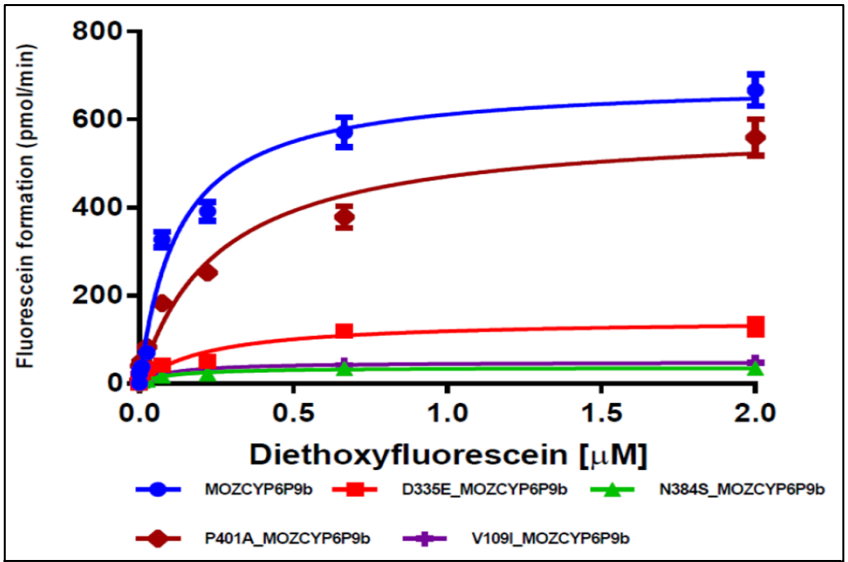

Figure 3.19: Michaelis-Menten plots of mutant CYP6P9b proteins dealkylation of DEF.

While no major shift in K_M was observed between the wild type MOZCYP6P9b and the mutants Val^{109}Ile and Asn^{384}Ser, the affinity for DEF is halved (K_M values doubled) with Asp^{335}Glu and Pro^{401}Ala replacements suggesting that modification in this position reduces affinity to DEF. This is in opposition to the observation made from in *CYP1A2* Glu^{318}Asp substitution, shown to increase the K_{cat} of O-dealkylation of 7-ethoxycoumarin 13-fold without affecting the K_M. Hiroya and colleagues (Hiroya et al., 1994) reported that conservative replacement of glutamate to aspartate resulted in the large increase in the K_{cat} without any apparent change in K_M, because the aspartate carboxyl group is better positioned for oxygen activation than the glutamate carboxyl moiety. Neutralization of Glu^{216} and Asp^{301} have also been shown to result in both qualitative and quantitative changes in catalysis by human CYP2D6 protein (Paine et al., 2003) with the negatively charged group of Asp and Glu playing a role in electrostatic attraction, enhancing binding of basic substrates.

The catalytic efficiency of the wild type MOZCYP6P9b is established as more than two-fold, eight-fold, ten-fold and fifteen-fold greater than values from Pro^{401}Ala, Asp^{335}Glu, Val^{109}Ile and Asn^{384}Ser mutants, respectively, suggesting that each of this amino acid change impact the metabolic efficiency

of CYP6P9b. However, the Asn[384]Ser mutant has the lowest catalytic efficiency among all the mutant proteins tested.

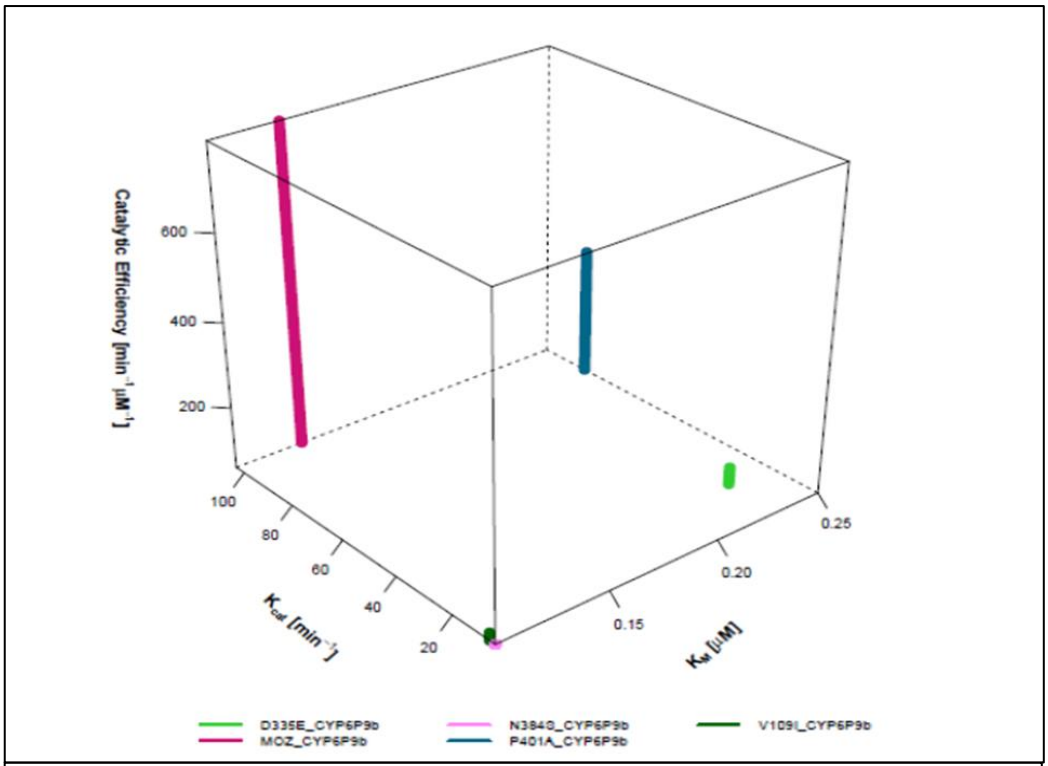

Figure 3.20: 4D plot of the kinetic constants and catalytic efficiencies from dealkylation of diethoxyfluorescein by mutant recombinant proteins CYP6P9b.

3.4.4.4 Comparative Assessment of Role of Amino Acids Replacement on Metabolic Activities of Mutant Proteins Using Pyrethroids Metabolism Assays

Significant differences in the metabolic profiles of the mutant membranes compared with the wild type MOZCYP6P9b were discovered using metabolism assay with permethrin and deltamethrin. Initial depletion assay repeated three times consistently established that the mutants Asp[335]Glu and Asn[384]Ser, as well as Val[109]Ile have low activity against pyrethroid insecticides especially deltamethrin.

Deltamethrin: With the exception of Pro[401]Ala mutant, profound quantitative decrease in the activity towards deltamethrin was observed in all the mutants (Figure 3.21A). Asp[335]Glu mutant has the lowest activity with only 4.15%±1.41 depletion on one hour of incubation; a loss of 96% activity

which is statistically significant ($p<0.01$) compared with the wild type MOZCYP6P9b with depletion of 92.04%±0.34. Asn^{384}Ser and Val^{109}Ile mutants with depletions of 18.15%±0.42 and 17.88%±1.00 respectvely, have lost on average 80% of activity compared with MOZCYP6P9b ($p<0.01$). This loss of activity clearly reflects that these three amino acid variants (Asp^{335}, Asn^{384} and Val^{109}) in MOZCYP6P9b are critical for catalysis. Of course, analysis of substrate access channel in Chapter Two have identified Val^{109} residue as a *pw2a* tunnel lining residue important for pyrethroids affinity. Its not surprising that replacement of this amino acid into isoleucine variant of FANG resulted in a drastic loss of activity. Lowest activities were observed with Asp^{335}Glu mutant with only one-fourth activity compared with Asn^{384}Ser and Val^{109}Ile mutants. Only 12% loss of activity was observed when depletion of Pro^{401}Ala mutant (81.25%±0.17) was compared with MOZCYP6P9b, indicating that replacement of prolyl residue with aliphatic side chain did not modify the activity of the enzyme significantly towards deltamethrin. This is not surprising as of all the four mutations, Pro^{401}Ala replacement is the least expected to have the most significant impact from sequence characterisation and mapping of mutations to critical domains of the P450. The percentage depletion from this mutant was also found to be statistically significant compared with the other mutants (Asp^{335}Glu, Asn^{384}Ser and Val^{109}Ile).

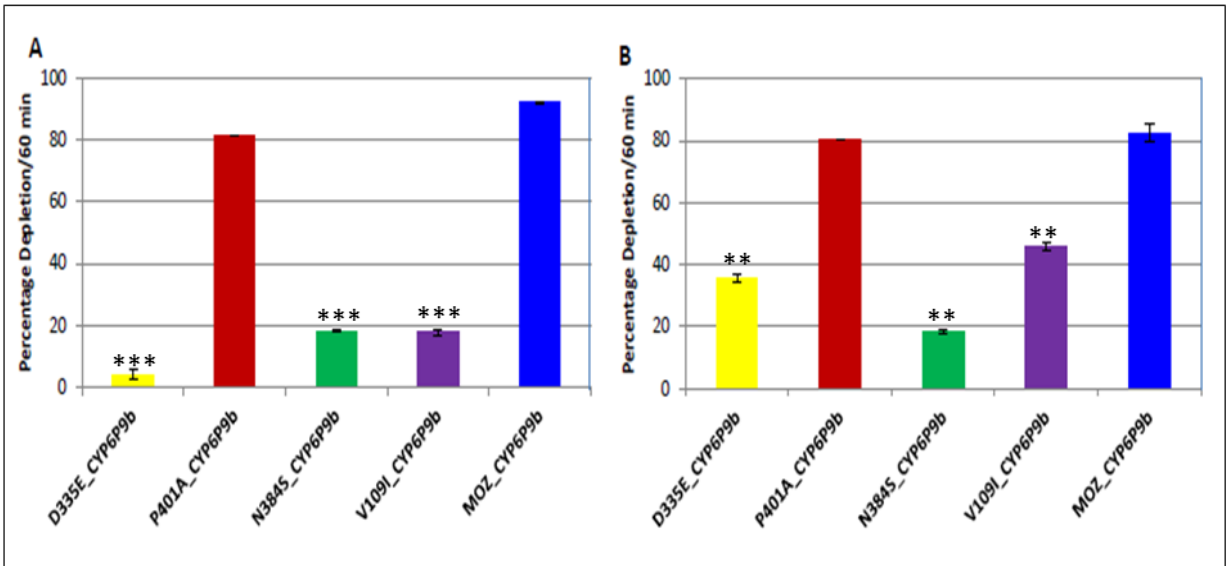

Figure 3.21: Percentage depletion of 20µM deltamethrin (A) and permethrin (B) by CYP6P9b mutants. Results are an average of three replicates (n = 3) compared with negative control.
** and *** Significantly different at $p<0.05$ and $p<0.01$ compared with MOZCYP6P9b and Pro^{401}Ala mutant.

Permethrin: Surprisingly, the mutants Val^{109}Ile exhibited higher activity with depletions for permethrin doubled the values from deltamethrin, while Asn^{384}Ser mutant exhibited comparable depletion for both permethrin and deltamethrin and Asp^{335}Glu activity for permethrin was nine-fold higher than obtained with deltamethrin. However, these depletions were statisitically significantly lower ($p<0.05$) compared with the values from wild type MOZCYP6P9b and the mutant Pro^{401}Ala, which show comparable depletions (Figure 3.21B and Appendix 3.6B). Compared with MOZCYP6P9b (depletion of 82.59±3.15 for permethrin), Asp^{335}Glu, Asn^{384}Ser and Val^{109}Ile mutants with percentage depletion of 35.65%±1.55, 18.33%±0.64 and 46.02%±1.43 respectively, have lost 57%, 78% and 43% of their enzymatic activities. This clearly established that the three mutations resulted in a drastic loss of activity and the amino acids knocked down are critical for affinity and/or activity towards permethrin. Unlike the case of deltamethrin, Pro^{401}Ala replacement was found not to modify activity towards permethrin.

From the inhibition assays MOZCYP6P9b was established to have highest affinity towards Type II pyrethroids especially deltamethrin and its assumed that the profound loss of activity observed in the mutants reflects the loss of affinity due to the change of the critical amino acid residues into the variants present in FANG.

To establish kinetic constants for all the mutants alongside the reference MOZCYP6P9b, kinetic analysis was conducted with permethrin. The decision to use permethrin was because experiments with deltamethrin and Asp^{335}Glu, Val^{109}Ile and Asn^{384}Ser produced no reasonable activity for calculation of K_M and K_{cat}. Reactions follow typical Michaelis-Menten pattern with differences observed between the mutants and wild type enzyme (Figure 3.22A and Appendix 3.6C). Remarkable, statistically significant differences were observed when the K_{cat} of the four mutants were compared with the values obtained from the wild type MOZCYP6P9b. Lowest K_{cat} was obtaind with the Asn^{384}Ser ($0.98min^{-1}$ ±0.12) compared with MOZCYP6P9b in line with the lowest activity towards permethrin in this mutant as obtained from the initial depletion assay. The K_{cat} of MOZCYP6P9b with permethrin was

two-fold that of Pro^{401}Ala mutant and, on average six-fold, eight-fold and nine-fold the K_{cat} from Val^{109}Ile, Asp^{335}Glu and Asn^{384}Ser mutants respectively. Significant increase ($p<0.05$) in K_M for permethrin were observed when Pro^{401}Ala, Asn^{384}Ser and Val^{109}Ile mutants were compared with the wild type MOZCYP6P9b. This established that the wild type amino acid variants in MOZCYP6P9b are important for affinity towards permethrin. Surprisingly, Asp^{335}Glu mutant exhibited lowest K_M (highest affinity) with values half those obtained from the wild type MOZCYP6P9b. This demonstrates that whatever was the catalytic attribute conferred by Asp^{335} in MOZCYP6P9b has no effect on affinity towards permethrin, but rather via another mechanism which could quantitatively modify the K_{cat}.

The differences of the mutant alleles' kinetic constants reflected in their catalytic efficiencies compared with MOZCYP6P9b which was established to be three-fold, four-fold, thirteen-fold and nineteen-fold more catalytically efficient towards permethrin, than the mutants Pro^{401}Ala, Asp^{335}Glu, Val^{109}Ile and Asn^{384}Ser, respectively (Figure 3.22B).

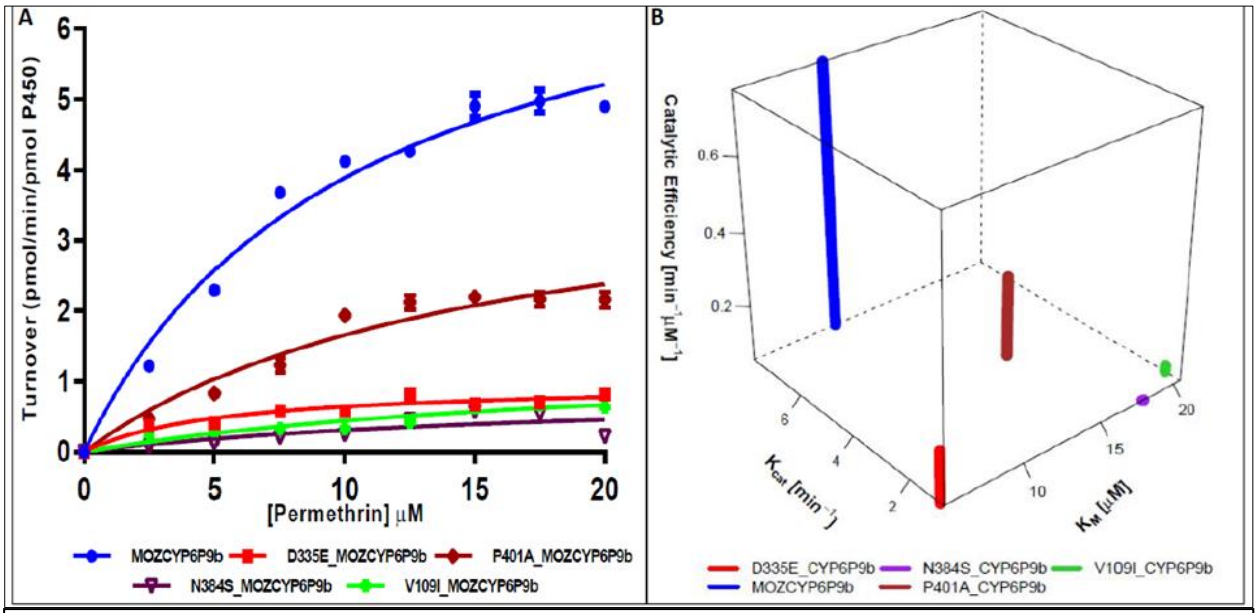

Figure 3.22: (A) Michaelis-Menten plot of mutant CYP6P9b proteins metabolism of permethrin (B) 4D plot of kinetic constants and catalytic efficiency of CYP6P9b mutants with for permethrin.

3.4.4.5 Comparative Assessment of Spatial Positioning of Criticial Amino Acid Residues in **MOZCYP6P9b *and* FANGCYP6P9b *Models***

Overlay of MOZCYP6P9b and FANGCYP6P9b revealed striking differences in the overall 3D folding and backbone of the proteins though models were generated from identical template (Figure 3.23). Ser^{384} in FANGCYP6P9b is located within the *β-1_4* placing the guanidinium group of Arg^{385} away (within 9.6Å from 4' spot of deltamethrin), while the peptide bond between Asn^{384} and Arg^{385} in MOZCYP6Pb (~120^{o}) positioned Asn^{384} and Arg^{385} within the loop joining *β-1_4* with *β-2_1*. The amido group of Asn^{384} is thus situated within 6.6Å distance from guanidinium group of Arg^{385} which in turn is within 6.9Å of the 4' spot of the phenoxybenzyl group of deltamethrin oriented towards the heme.

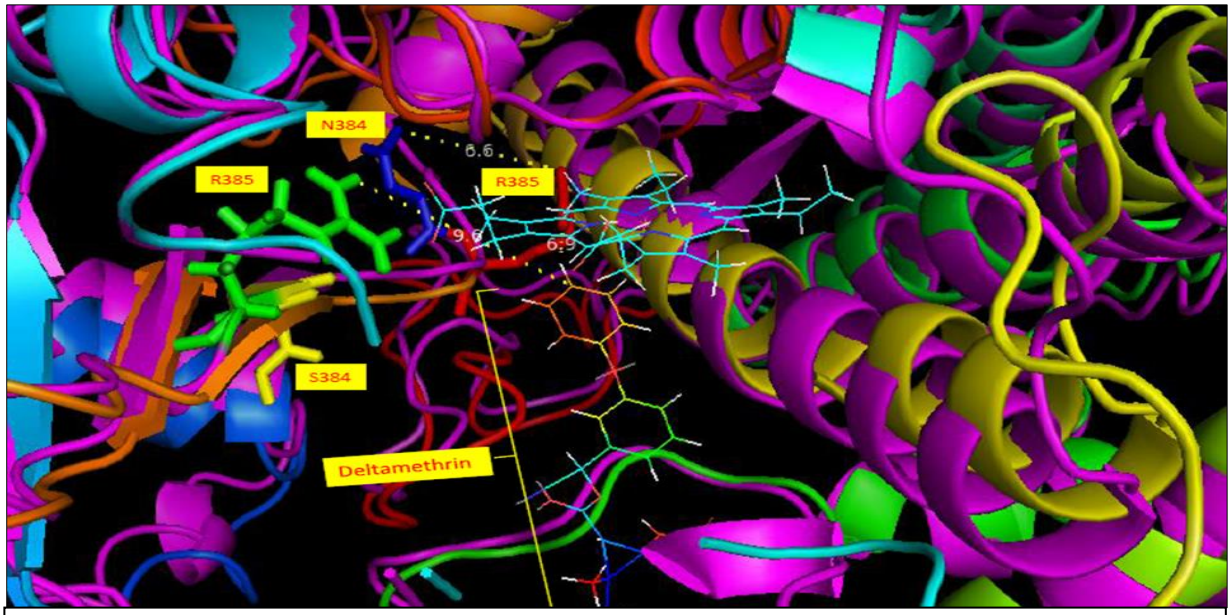

Figure 3.23: Overlay of MOZCYP6P9b model (helices A-L in spectrum and cartoon format) and FANGCYP6P9b (helices A-L in purple cartoon) with deltamethrin (spectrum lines) docked in productive conformation. Ser^{384}: yellow stick; FANGCYP6P9*b*_Arg^{385}: green stick; Asn^{384} : blue stick; MOZCYP6P9b_Arg^{385}: red stick; heme atoms: cyan lines.

These subtle difference may account for the reason why Arg^{385} is a *pw2a* tunnel lining residue in MOZCYP6P9b and involved in substrate accessing the heme catalytic centre, while the corresponding residue is absent in *pw2a* from FANGCYP6P9b. The Asn^{384}-Arg^{385} peptide bond positioned guanidinium moiety of Arg^{385} within 5.0Å distance of Ser^{324} (Figure 3.24). Its assumed that

catalysis may be effected in MOZCYP6P9b through hydrogen bonding network involving polar residues arrayed round the binding site, including Asn^{384} and Arg^{385} (SRS5), Arg^{452} and Cys^{454} (heme-binding region), Asn^{502}, Asp^{217} (of SRS2), Ser^{320} (O_2-binding pocket), Ser^{324} as well as Gln^{323} (αI).

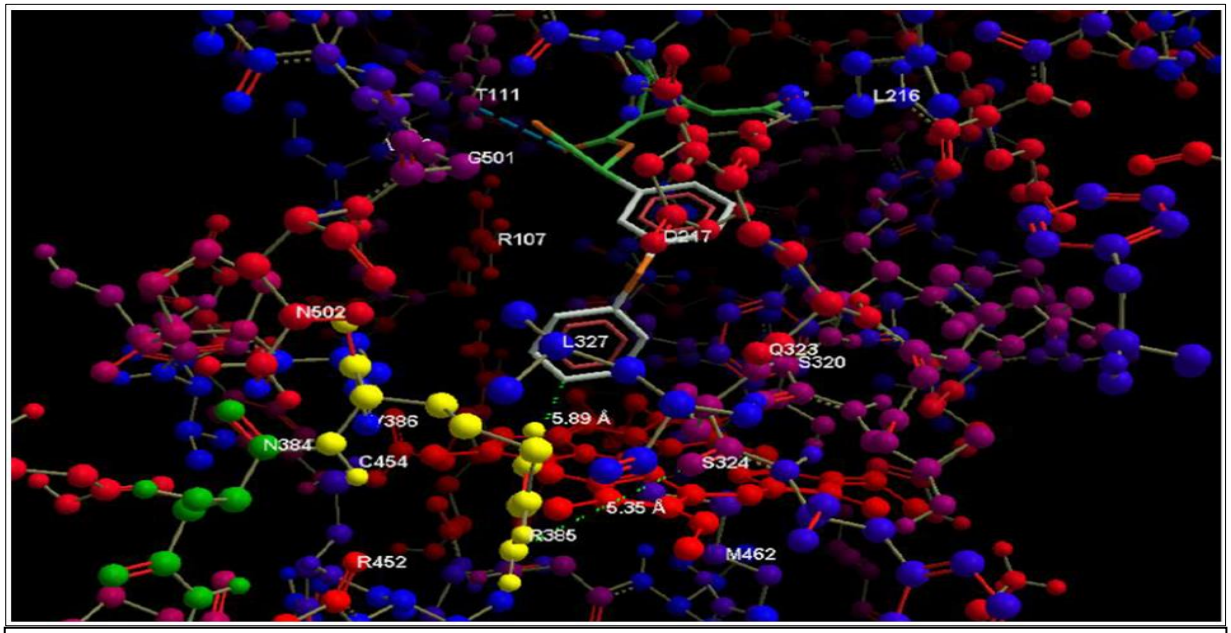

Figure 3.24: Active site residues of MOZCYP6P9b docked with deltamethrin. Asn^{384} is in green, Arg^{385} in yellow, distance between its guanidium group to Ser^{324} and 4' spot of deltamethrin annotated.

In contrast, in the productive pose of deltamethrin in FANGCYP6P9b, residues Ser^{384} and Arg^{385} located within the *β-1_4* are not within 9.0Å of deltamethrin or heme (Figure 3.25).

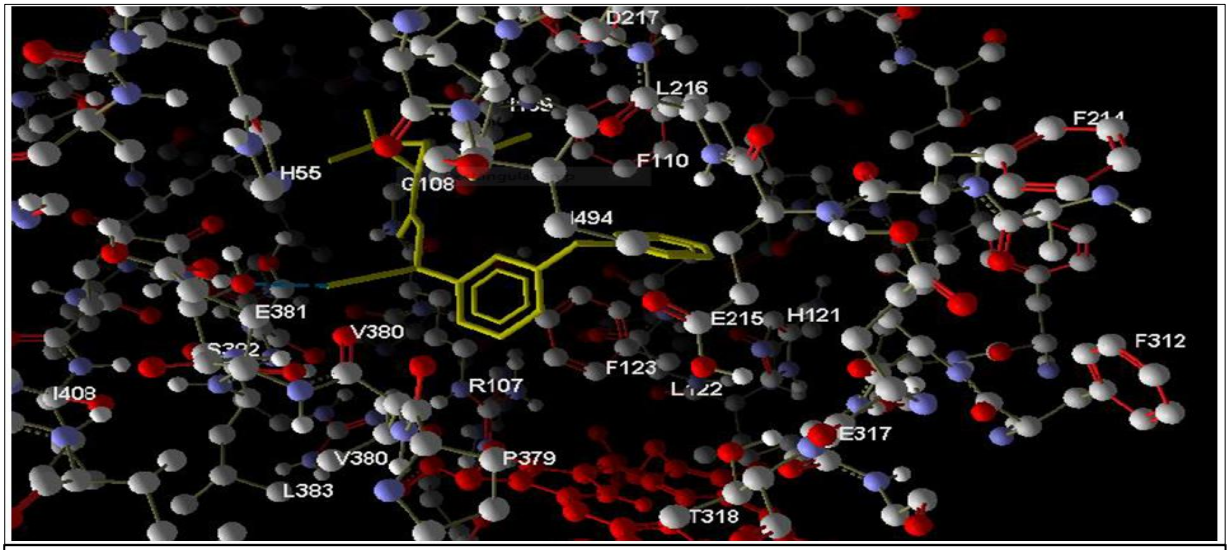

Figure 3.25: Active site residues of FANGCYP6P9b docked with deltamethrin, showing residues within 9.0Å.

The same pattern of differences in the backbone folding of CYP6P9b models affected the positionin of residue 335. In this respect Glu^{335} residue in the FANGCYP6P9b is located in the *N*-terminus of αJ helix and within a distance of 30.7Å from the heme (Figure 3.26), while the smaller Asp^{335} in MOZCYP6P9b is positioned in the *C*-terminus of helix I and within 20.3Å from heme. Glu^{335} in FANGCYP6P9b mapped to the putative reductase interaction site 1 (RIS-1) (Sirim et al., 2010) and its assumed that the presence of this residue in the αJ helix may result in ionic repulsion with the corresponding negatively charged residues at the FMN face of CPR reducing optimal interaction with the redox partner and by that the overall catalysis.

Each of the residues in MOZCYP6P9b implicated as critical are assumed to contribute towards catalysis either through channeling and/or affinity (Val^{109} and Asn^{384}), hydrogen bonding network (Asn^{384} through proper positioning of Arg^{385}) or interaction of the proximal residues with CPR (absence of Asp^{335} in the MOZCYP6P9b RIS-1, which optimizes interation with the FMN binding domain of CPR).

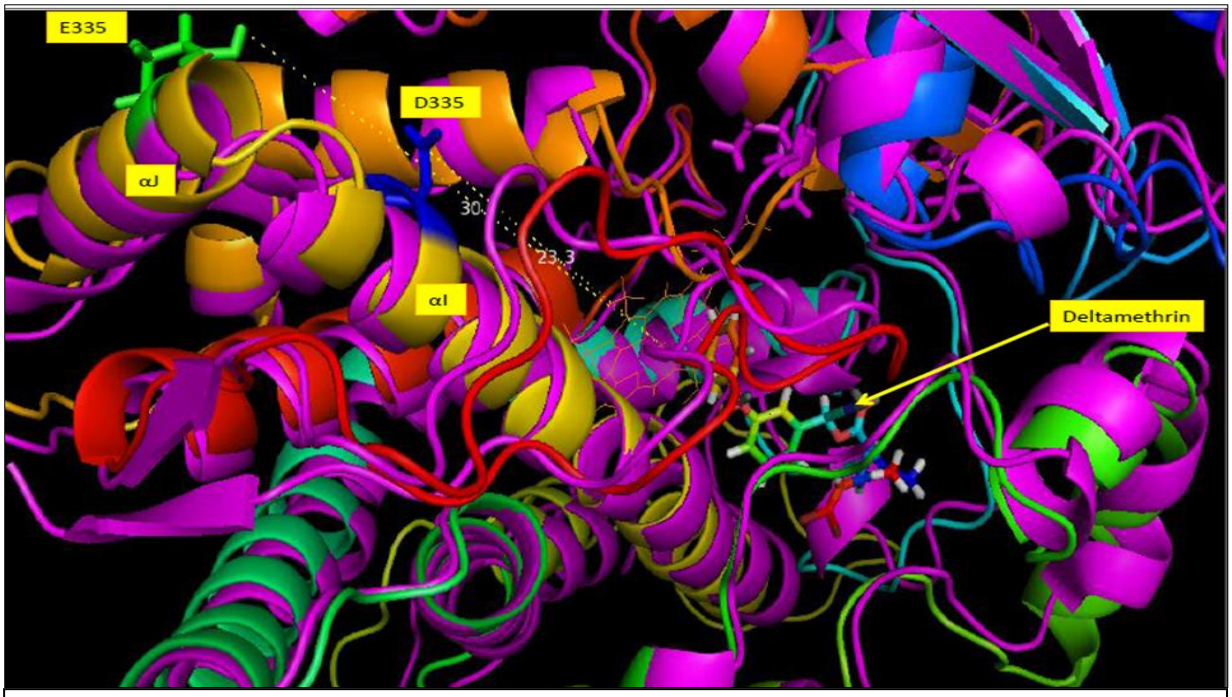

Figure 3.26: Overlay of MOZCYP6P9b models (helices A-L in spectrum and cartoon format) and FANGCYP6P9b (helices A-L in purple cartoon) with deltamethrin (spectrum stick) docked in productive conformation. Asp^{335}: blue stick; Glu^{335}: green stick; heme atoms: magenta lines.

3.4.5 Comparative Assessment of Ability of *CYP6P9a* and *CYP6P9b* Alleles to Confer Pyrethroid Resistance in *D. melanogaster* Using GAL4-UAS System

3.4.5.1 Insecticides Contact Bioassay

To find out whether the allelic variation observed between the resistant and susceptible alleles of *CYP6P9a* and *CYP6P9b* alone was sufficient to confer pyrethroid resistance *in vivo*, transgenic *D. melanogaster* overexpressing these genes from resistant and susceptible populations were constructed separately, using the GAL4-UAS System. Bioassays with permethrin and deltamethrin revealed that the flies overexpressing *CYP6P9a* and *CYP6P9b* from resistant individuals were significantly more resistant to both pyrethroids, resulting in a reduced mortality and knockdown compared with the flies overexpressing same genes from susceptible strain, (FANG) and control flies.

Permethrin: With permethrin, lower mortality was observed in flies expressing *CYP6P9b* than those expressing *CYP6P9a* (Figure 3.27A and B). However, transgenic Actin5C-UAS-*MALCYP6P9a* flies showed statistically significant ($p<0.05$), lower mortalities (less than 10%, 30% and 45% in the first 2hrs, 3hrs and 6hrs, respectively) from permethrin exposure, compared with Actin5C-UAS-*FANGCYP6P9a* (30%, 60% and 70% mortalities respectively, at the same time). The same pattern was observed with *CYP6P9b* with flies overexpressing the gene from resistant strain (Actin5C-UAS-*MOZCYP6P9b*) showing significantly lower mortalities compared with the flies overexpressing gene from susceptible strain (Actin5C-UAS-*FANGCYP6P9b*) in the following exposure times: 12hrs (30% vs 55%, $p<0.05$), 24hrs (30% vs 60%, $p <0.01$). This demonstrated that *MALCYP6P9a* and *MOZCYP6P9b* alleles from resistant strains can confer higher resistance to permethrin compared with corresponding genes from susceptible, FANG (*FANGCYP6P9a* and *FANGCYP6P9b*) and the control flies. Nevertheless, the mortalities from *MALCYP6P9a* flies in the first 12 hours reached 70% compared with only less than 30% mortality from *MOZCYP6P9b* flies. *MOZCYP6P9b* conferring higher tolerance to permethrin is in keeping with the higher *in vitro* activities of recombinant CYP6P9b with pyrethroid insecticides compared with results from CYP6P9a protein variants.

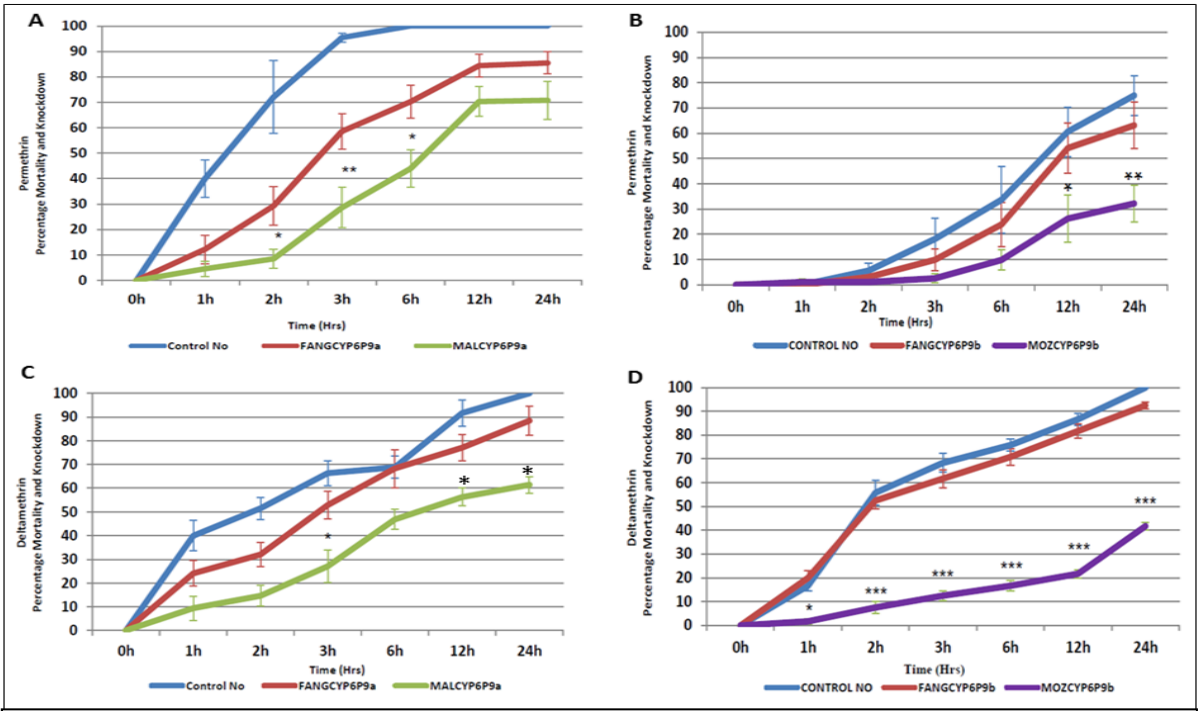

Figure 3.27: Bioassay results with transgenic strains of (A) Actin5C-UAS-*CYP6P9a* flies with permethrin; (B) Actin5C-UAS-*CYP6P9b* flies with permethrin; (C) Actin5C-UAS-*CYP6P9a* flies with deltamethrin, and (D) Actin5C-UAS-*CYP6P9b* flies with deltamethrin. Results are mean ±S.E.M. significantly different: * p<0.05, ** p<0.01 and *** p<0.001

Deltamethrin: The Actin5C-UAS-*MALCYP6P9a* flies showed lower mortalities with deltamethrin compared to Actin5C-UAS-*FANGCYP6P9a* (Figure 3.27C); however these mortalities were only statistically significant at 3 different hours of exposure: 3 hours (28% vs 53%, p<0.05); 12 hours (55% vs 78%, p<0.05) and 24 hours (62% vs 88%, p<0.05). Highest tolerance to deltamethrin was obtained with flies overexpressing Actin5C-UAS-*MOZCYP6P9b*, compared with the flies expressing susceptible alleles of *CYP6P9a* and *CYP6P9b*, as well as those expressing the resistant allele *MALCYP6P9a*. The Actin5C-UAS-*MOZCYP6P9b* flies exhibited lowest mortality, of less than 21% up to 12 hours after exposure to discriminating dose of deltamethrin (Figure 3.27D). Specifically compared with flies overexpressing gene from susceptible strain (Actin5C-UAS-*FANG-CYP6P9b*), significant differences were obtained at every hour of exposure: 1 hour (1.5% vs 20%, p <0.05), 2 hours (7.5% vs 53%, p <0.001), 3 hours (12.5% vs 62%, p <0.001), 6 hours (16% vs 70%, p <0.001), 12 hours (21% vs 81%, p <0.001) and 24 hours (41% vs 93%, p <0.001).

These results strengthened the pattern obtained from *in vitro* metabolism assay and kinetics in which highest K_{cat} and efficiencies were obtained with deltamethrin compared with permethrin and especially with *MOZCYP6P9b* allele. Also, from the site-directed mutagenesis analysis it was observed that mutants have higher activities toward permethrin than deltamethrin; a result which is consistent with lower mortalities obtained with permethrin (62% at 24 hours) from the *FANGCYP6P9b* flies compared with the higher mortalities obtained with deltamethrin (93% at 24 hours). In conclusion, overexpression of *MALCYP6P9a* and *MOZCYP6P9b* from resistant populations of *An. funestus* confer spermethrin and deltamethrin resistance to naive transgenic flies, with the latter conferring higher tolerance to these insecticies, reflecting once more its central position in pyrethroids resistance.

3.4.5.2 qPCR Confirmation of Expression of CYP6P9a and CYP6P9b Transgenes in *Flies*

To validate the overexpression of the candidate genes (*CYP6P9a* and *CYP6P9b*) in the experimental flies, qPCR was carried out using the flies expressing both resistant alleles (Actin5C-UAS-*MALCYP6P9a* and Actin5C-UAS-*MOZCYP6P9b*) and susceptible alleles (Actin5C-UAS-*CYP6P9a* and Actin5C-UAS-*CYP6P9b*), as well the control flies (Actin5C-UAS-*null* flies).

Both *CYP6P9a* and *CYP6P9b* were found to be expressed only in the transgenic F_1 progenies from the crosses with Actin5C, used for the contact bioassays, and not expressed in the control flies (Figure 3.28A and B). The *CYP6P9a* mRNA were found to be overexpressed with a fold change of 22% and 24% respectively, in the flies overexpressing the gene from Malawi (Actin5C-UAS-*MALCYP6P9a*) and gene from FANG (Actin5C-UAS-*FANGCYP6P9a*). *CYP6P9b* was also found to be overexpressed in the transgenic flies but in contrast, the fold change of the gene from flies expressing susceptible gene (Actin5C-UAS-*FANGCYP6P9b*) was four times higher compared with the flies expressing the resistance gene (Actin5C-UAS-*MOZCYP6P9b*).

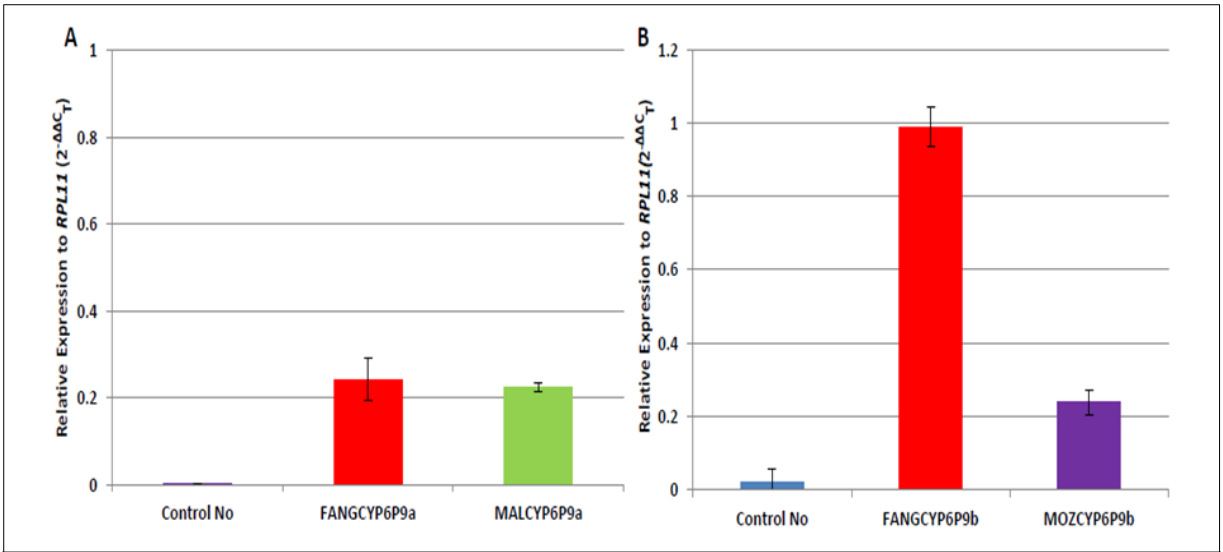

Figure 3.28: Quantitative PCR Results: Fold change of *CYP6P9a* (A) and *CYP6P9b* (B) mRNA from transgenic flies relative to house-keeping gene *RPL11.*

3.5 Discussion and Conclusions

The membrane contents and reductase activity obtained with both recombinant CYP6P9a and CYP6P9b were comparable to those reported from several studies, including respectively the amounts reported from *An. gambiae* CYP6M2 (0.5-1.0nmol/mg and 100-200nmol cytochrome *c* reduced/min/mg) (Stevenson et al., 2011), CYP6Z2 (0.9-1.5nmol/mg and 100-120 nmol cytochrome *c* reduced/min/mg (McLaughlin et al., 2008), as well as *Ae. aegypti* CYP9J sub-family (0.3-1.56nmol/mg protein and 32-157 nmol cytochrome *c* reduced/min/mg)(Stevenson et al., 2012). Measurement of reductase activity is important for differences in its content may possibly influence its interaction with the P450 and enhance/diminish catalysis and thus making it difficult to compare different metabolic activities in case of significant difference between membrane preparations. However, the ratio of CPR to P450 in endoplasmic reticulum was estimated to be 1:20 (Kenaan et al., 2011), and thus even small amount of the reductase may be sufficient to drive the P450-mediated catalysis. Both membrane contents of P450 and reductase contents were within the same ranges for both recombinant CYP6P9a and CYP6P9b from resistant and susceptible strains. In fact FANGCYP6P9a exhibited the highest P450

content of all the CYP6P9a proteins and thus its safe to assume that whatever differences observed in terms of P450 activities between the resistant and susceptible proteins does not stem from variation in P450 contents and/or reductase activities.

Recombinant CYP6P9a and CYP6P9b from resistant strains are capable of dealkylating fluorogenic probes particularly DEF with consistently high efficiency. The proteins from resistant alleles exhibited very low K_M (high affinity) towards DEF compared with corresponding ones from susceptible FANG. The K_M values obtained with CYP6P9a and CYP6P9b from resistant alleles were comparable to the K_M established for *An. gambiae* CYP6Z2- and *Ae. aegypti* CYP6Z8-mediated de-benzylation of benzyloxyresorufin (K_M ~0.13μM)(McLaughlin et al., 2008, Chandor-Proust et al., 2013) while the K_M from FANGCYP6P9a and FANGCYP6P9b are three-fold and two-fold higher than these values, respectively. The dealkylation of DEF proceeds with high turnover, greater than established for some probes with insect P450s; e.g. *An. gambiae* CYP6Z2 with benzyloxyresorufin (K_{cat} ~1.5 min^{-1}) (McLaughlin et al., 2008) and *Ae. aegypti* CYP6Z8 with benzyoxyresorufin and ethoxyresorufin (0.097min^{-1} and 1.19min^{-1}), respectively. This resulted in higher catalytic efficiency obtained from the resistant CYP6P9a and CYP6P9b compared with FANGCYP6P9a and FANGCYP6P9b, and above the values from the studies cited above. The CYP6P9a and CYP6P9b from resistant strains are in essence more efficient as probe substrate metabolisers compared with the corresponding proteins from susceptible alleles. For example, MOZCYP6P9b with catalytic efficiency of 1220.85 $min^{-1}\mu M^{-1}$ is roughly 20-fold more efficient than FANGCYP6P9b. Allelic variation seems to be impacting on enzymatic activity towards fluorescent probes, modifying kinetic constants and efficiency of O-dealkylation of the probe substrates.

Pyrethroids, especially of Type II class, pseudo-pyrethroid etofenprox, as well as the organophosphate chlorpyrifos diminished the catalytic activity of both CYP6P9a and CYP6P9b with DEF, while DDT, bendiocarb and propoxur were established not to inhibit the O-dealkylation of DEF. Tight-binding inhibitors have been defined as compounds with a ChemScores of < -30 kJ/mol and an

IC_{50} values of <10µM (Kemp et al., 2004). Based on this Type II pyrethroids (cypermethrin, deltamethrin and λ-cyhalothrin can be described as the most potent binders (inhibitors) of CYP6P9a and CYP6P9b of all test insecticides screened. Type I pyrethroids and chlorpyrifos also show very low IC_{50} indicating tight binding. DDT, bendiocarb and propoxur with high IC_{50} displayed very low affinity and were expected not to be metabolised by CYP6P9a and CYP6P9b screened. These findings were confirmed with substrate metabolism assays with pyrethroids, DDT, bendiocarb and propoxur.

Metabolism assay established that the recombinant CYP6P9a and CYP6P9b metabolise permethrin and deltamethrin insecticides with a very high turnover (depletion) compared with the proteins from susceptible alleles, which exhibited low depletion. Highest activities were obtained from southern African alelles consistent with the highest pyrethroid resistance recorded in this region (Riveron et al., 2013, Riveron et al., 2014a). Very low (insignificant) activities were obtained from DDT, bendiocarb, propoxur and malathion metabolism consistent with the results from molecular docking simulations and probe assays. DDT is interesting in this case for it exhibited an IC_{50} on average of less than 10µM for both CYP6P9a and CYP6P9b and its assumed that it could be metabolised but as stated above binding of substrates to the P450 enzyme does not necessarily reflect metabolism.

Kinetic constants (parameters) also differ significantly between recombinant CYP6P9a and CYP6P9b from resistant and the susceptible alleles. The proteins from resistant alleles exhibited high turnover (high K_{cat}) and high affinity (lower K_M) compared with those from susceptible alleles, translating into a very high efficiency of pyrethroid metabolism several fold in the former compared with the latter. The K_M values obtained for both permethrin and deltamethrin from resistant CYP6P9a and CYP6P9b were very close to the K_M values established for *An. gambie* CYP6M2 with permethrin (12.0µM) and higher than with deltamethrin (2.0µM) (Stevenson et al., 2011). The K_{cat} values obtained from the resistant recombinant CYP6P9a and CYP6P9b, for both permethrin and deltamethrin are higher than values established in the study cited above (6.1min^{-1} and 1.1min^{-1}, respectively).

The differences observed in activities resulted in a very high catalytic efficiency in the resistant CYP6P9a and CYP6P9b, especially those from southern Africa compared with FANGCYP6P9a and FANGCYP6P9b, as well as other P450s. For example, MOZCYP6P9b exhibited catalytici efficiency of $0.97min^{-1}\mu M^{-1}$ and $1.22min^{-1}\mu M^{-1}$ respectively, for permethrin and deltamethrin, compared with FANGCYP6P9b ($0.21min^{-1}\mu M^{-1}$ and $0.25min^{-1}\mu M^{-1}$), *An. gambiae* CYP6M2 ($0.5min^{-1}\mu M^{-1}$) (Stevenson et al., 2011) and some CYP9J P450s from *Ae. aegypti* ($<1min^{-1}\mu M^{-1}$) (Stevenson et al., 2012). This established that the resistant CYP6P9a and CYP6P9b (especially those from southern African strains) are efficient metabolisers of pyrethroids (permethrin and deltamethrin) compared with corresponding enzymes from the susceptible strain (FANGCYP6P9a and FANCYP6P9b), and also compared with some insect 450s functionally characterised. If its assumed that the only differences between the resistant and susceptible alleles of these genes is in the coding region its safe to reason that the amino acid variations are responsible for these differences in the metabolic profile; and that the allelic variation alone modify the enzymatic activities, impacting on catalysis, making the alleles from resistant strains more efficient in terms of pyrethroid metabolism and conferring pyrethroid resistance to resistant populations of *An. funestus*.

With allelic variation impacting on pyrethroid metabolism successfully established, the next task was to identify the potential amino acids that are critical to high efficiency pyrethroids metabolism. Site-directed mutagenesis identified three key residues (Val^{109}, Asp^{335} and Asn^{384}) whose replacement in *MOZCYP6P9b* with variants from *FANGCYP6P9b* correlated with significant loss of metabolic efficiency towards permethrin and deltamethrin. The three mutants above exhibited significant, quantitative reduction in activity towards probe substrate DEF compared with recombinant MOZCYP6P9b, with the lowest activity towards all 7 probes screened produced by $Asp^{335}Glu$ mutant, while $Val^{109}Ile$ mutant acquired quantitative enhancement in activity towards RME compared with the rest of the alleles. The maximum catalytic rate of MOZCYP6P9b metabolism of DEF was several-fold higher than the three mutants $Val^{109}Ile$, $Asp^{335}Glu$ and $Asn^{384}Ser$; mutants $Pro^{401}Ala$ and $Asp^{335}Glu$ portaryed a shift in K_M (reduced affinity for DEF). This resulted in higher catalytic efficiency several

folds from the wild type MOZCYP6P9b compared with all the four mutants, Val^{109}Ile, Asp^{335}Glu, Asn^{384}Ser and Pro^{401}Ala, with Asn^{384}Ser having the lowest efficiency. This phenomena established the fact that mutants have lost significant potency for O-dealkylation of probe substrates and the reason is because the amino acids replaced are critical for catalysis toward DEF. This kind of phenomenon was reported before in several studies, including the Glu^{318}Asp substitution in CYP1A2 that has been shown to increase the K_{cat} of O-dealkylation of 7-ethoxycoumarin 13-fold without affecting the K_M. Hiroya and colleagues (Hiroya et al., 1994) reported that conservative replacement of glutamate to aspartate resulted in the large increase in the K_{cat} without any apparent change in K_M, because the aspartate carboxyl group is better positioned for oxygen activation than the glutamate carboxyl moiety. Leu^{209}Ala replacements in CYP2B1 has been established to result in qualitative changes in activity, allowing progesterone to bind in a new orientation (Szklarz et al., 1995). The larger Leu hinders the substrate from assuming productive orientation due to vdW overlaps. This maybe the case in Val^{109}Ile mutant in which the smaller side chain of valine is replaced with the larger isoleucine.

With pyrethroids, same pattern of metabolic profiles were observed. Initial depletion assay revealed that the mutants with the exception of Pro^{401}Ala have lost activities compared with MOZCYP6P9b, with Asp^{335}Glu mutant having lowest activity for deltamethrin while Asn^{384}Ser portrayed lowest activity with permethrin. Kinetic analysis revealed that with the exception of Asp^{335}Glu which exhibited low K_M with permethrin, the mutants have lost significant affinities toward permethrin. Maximal catalytic rate also fell compared with MOZCYP6P9b and as a result of that the wild type protein was several fold more efficient than all the four mutants. This is in line with the probes assays and reflect the importance of the amino acids knocked down in *MOZCYP6P9b.* This kind of lose or gain of function due to single amino acid change has been described in several studies. For example, Val^{92}Ala replacement in CYP6AB3v1 makes this allelic variant capable of metabolising plant allelochemical imperatorin nearly as effective as CYP6AB3v2 furanocoumarins metaboliser (Mao et al., 2007). Neutralization of Glu^{216} and Asp^{301} have also been shown to result in both qualitative and quantitative changes in catalysis by human CYP2D6 (Paine et al., 2003). Replacement of Asp^{293} to Ala^{293}

in human CYP2C9 has been shown to result in decrease in activity by more than 90%, as well as 3-10 fold increase in K_M for tolbutamide, dextromethorphan and diclofenac (Flanagan et al., 2003). Thus, replacement of even a single amino acid can have profound effort on regio-selectivity, specificity, affinity and/or activity towards particular substrate or broad range of substrates.

With the exception of Pro^{401} (amino acid located neither in the active site of *MOZCYP6P9b* nor near the putative RIS), the three residues Val^{109}, Asp^{335} and Asn^{384} could be described as important residues which confer pyrethroid-metabolising efficiency to recombinant CYP6P9b from resistant alleles (strains). Val^{109} is assumed to exert its effect by the virtue of being part of substrate access channel *pw2a* and as such important for accessibility, specificity and/or affinity; Asp^{335} exert its effect by being present in the tip of helix I and thus away from the putative RIS-1, reducing ionic repulsion as the FMN-binding domain of CPR approaches the P450; while Asn^{384} by the virtue of its location within the loop joining *β-1_4* with *β-2_1* placed itself and guanidinium group of Arg^{385} within vdW contact with the heme and other polar charged and neutral side chain with possibility of hydrogen bonding networks, enhancing catalysis several fold. These three amino acids are assumed to be working in concert each one contributing in its way to catalysis, efficient metabolism of pyrethroids, especially deltamethrin, conferring pyrethroids resistance.

Expression of alleles of *CYP6P9a* and *CYP6P9b* from resistance strains in D. melanogaster alone, confers resistance to pyrethroids permethrin and deltamethrin, *in vivo*. Flies overexpressing CYP6P9a and CYP6P9b from susceptible FANG have higher mortalities (values which are statistically significant) for permethrin and deltamethrin compared with transgenes overexpressing MALCYP6P9a and MOZCYP6P9b from the resistant alleles. The experiments with the flies further confirmed the pattern observed from the *in silico* and *in vitro* analysis that *CYP6P9b* is more potent P450 than *CYP6P9a*, able to confer higher tolerance to pyrethroids, *in vivo*. As confirmed from qPCR validation of expression of transgenes, *FANGCYP6P9b* was overexpressed four-fold higher than *MOZCYP6P9b*, but

even that failed to make the susceptible allele match *MOZCYP6P9b* in conferring resistance to transgenic *D. melanogaster*.

Transgenic expression of candidate P450s and bioassays with insecticides have been conducted in several studies. For example, transgenic expression of *T. castenaum CYP6BQ9* responsible for deltamethrin resistance in *D. melanogaster* resulted in tolerance of a diagnostic dose of 10µg deltamethrin with a survival rates of 40% at 25^{o}C compared with control flies (survival rates of less than 10%) (Zhu et al., 2010). Transgenic expression of *CYP6G1* and *CYP12D1* in *D. melanogaster* was also reported to result in an resistance to chemically unrelated insecticides (DDT, nitenpyram and dicyclanil in the case of *CYP6G1*) and DDT and dicyclanil in the case of *CYP12D1* (Daborn et al., 2007). Also, we have used transgenic analysis (Appendix 5) to show that a single mutation Leu^{119}Phe in *GSTe2* gene from *An. funestus* population is responsible for extreme resistance to DDT and cross-resistance to permethrin. Thus, transgenic analysis allow for establishment of cross-resistance genes.

In conclusion, allelic variation is impacting pyrethroid resistance, with the resistant alleles of *CYP6P9a* and especially *CYP6P9b* able to metabolise pyrethroid insecticides with a significantly, very high efficiency compared with the corresponding alleles from susceptible strain, FANG. These pyrethroid-metabolising efficiency is as a result of differences in amino acid sequences between resistant and susceptible alleles. Specifically, in *CYP6P9b* three amino acid Val^{109}, Asp^{335} and Asn^{384} in the resistant alleles accounted for these metabolic differences. Replacement of these residues into variants from susceptible allele (*FANGCYP6P9b*) resulted in profound loss of activity towards pyrethroid insecticides as well as probe substrates. The resistant alleles from *CYP6P9b* all across Africa are undergoing directional selection in their coding regions with these and possibly other beneficial mutations not characterised becoming fixed. These three amino acids could be used to design a diagnostic tool that can allow detection of the resistance alleles in field populations of *An. funestus* across Africa, which will make possible tracking the spread of the resistant alleles and helping the selection of appropriate insecticide intervention tools.

4. FUNCTIONAL CHARACTERISATION OF ADDITIONAL *An. funestus* CYTOCHROME P450s

4.1 Background

The tandemly duplicated *An. funestus CYP6P9a* and *CYP6P9b* have been implicated as the major pyrethroid resistance genes across Africa, but several candidate genes have always appeared also as top up-regulated genes from genome-wide transcriptional analysis. Irving and colleagues reported two genes *CYP6M7* and *CYP6Z1* from resistant *An. funestus* (FUMOZ-R) significantly overexpressed, with a fold change of a 2.4 and 2.82 respectively, compared with same genes from the susceptible strain FANG (Irving et al., 2012). These genes were located within the pyrethroid resistance *rp2* QTL. Genome-wide transcription analysis using microarrays and validation of up-regulation through qRT-PCR revealed that the most commonly overexpressed genes from pyrethroid resistant *An. funestus* from Malawi and Mozambique were *CYP6P9a* and *CYP6P9b*, as well as *CYP6Z1*, *CYP9J11* and *CYP6Z3* (Riveron et al., 2013). However, the Zambian population of *An. funestus* from the northern range of the pyrethroid resistance front were recently found to be multiple resistant to pyrethroids, bendiocarb and DDT (Riveron et al., 2014a). Synergist assays with piperonyl butoxide (PBO) restored susceptibility to permethrin, bendiocarb and to some extent (though moderately) DDT, suggesting possible involvement of P450s in resistance to these insecticides, in the absence of *kdr* mutation in the VGSC (Riveron et al 2014a). The pre-eminent role of P450s even in DDT resistance was further strengthened by the absence in the southern African *An. funestus* population of the *GSTe2* Leu^{119}Phe mutation shown to confer extreme DDT resistance in West/Central Afican *An. funestus* (Riveron et al., 2014b). Transcriptional profiling of the multiple resistant, Zambian *An. funestus* along with Malawi and Mozambique, using new custom Agilent microarray chip with 60, 000 probes (60mer) revealed that the *CYP6M7* was more overexpressed than the duplicated *CYP6P9a* and *CYP6P9b,* indicating that this gene could play a bigger role in pyrethroid resistance in this population. But no evidence exist that it could actually metabolise pyrethroid and if it does it remain to be known how it compares to the

duplicated P450s *CYP6P9a* and *CYP6P9b*. Additionally, beside *CYP6M7* and *CYP6P9a* and *CYP6P9b*, the top 10 up-regulated genes also included other P450 genes, such as *CYP6AA4*, *CYP9J11*, *CYP6Y2*, *CYP6Z1*, *CYP6AG1* and *CYP6P2* (Riveron et al., 2014a). Their ability to confer pyrethroid resistance remain unclear in these populations of *An. funestus*. In addition, the contribution of these various P450s to the multiple resistance observed in these populations has not yet been investigated. It is possible that some of these P450s could be conferring cross-resistance between pyrethroids and carbamates as previously suggested by (Brooke et al., 2001) or even confer DDT resistance. It is crucial to address these questions in order to help design suitable resistance management strategies in the region as suggested by the Global Programme of insecticide Resistance Management (WHO, 2012).

4.2 Aim and Objectives

The aim of this section was to validate the role of other overexpressed cytochrome P450 genes in the resistance to insecticides in southern African populations of *An. funestus*.

More specifically, this chapter aims to:

1-Validate the role of the overexpressed P450s: *CYP6M7*, *CYP6Z1*, *CYP9J11* and *CYP6AA4* in the resistance to pyrethroids, and compare them to the duplicated *CYP6P9a* and *CYP6P9b*;

2-Assess the contribution of these additional P450s to the multiple resistance observed or to possible cross-resistance between pyrethroids and other insecticide classes.

4.3 Methods

4.3.1 Cloning and Heterologous Co-expression of *CYP6M7*, *CYP6Z1*, *CYP9J11* and *CYP6AA4* Proteins with *An. gambiae* Cytochrome P450 Reductase

Cloning and plasmid preparation for these candidate genes follow the *ompA+2* strategies (Pritchard et al., 1997). Plasmids pB13::*ompA+2-CYP6M7*, pB13::*ompA+2-CYP6Z1*, pB13:*ompA+2-CYP9J11* and pB13::*ompA+2-CYP6AA4* were constructed as described for *CYP6P9a* and *CYP6P9b* in

Chapter 3. The primer pairs used for amplification of each gene with the *ompA+2* leader for optimal expression is given in Table 4.1. Plasmid bearing *An. gambiae* P450 reductase (pACYC-184-CPR) was also constructed as described previously. Each P450 construct was individually co-transformed together with CPR into *JM109* cells as described in Chapter 3. *CYP6M7* (Afun007663), *CYP6Z1* (Afun012197), *CYP9J11* (Afun007469) and *CYP6AA4*/*CYP6AA1*(Afun008614) are orthologs of *An. gambiae CYP6M3* (AGAP008213-PA*)*, *CYP6Z1* (AGAP003066-PA), AGAP012296-PA and AGAP002862-PA, respectively. Functional membranes of these P450s were co-expressed with *ompA+2* modifications together with CPR at 21^{o}C and 150 rpm as described previously (Pritchard et al., 1997, Pritchard et al., 2006b) to produce recombinant *CYP6M7* (*rCYP6M7*), *rCYP6Z1*, *rCYP9J11* and *rCYP6AA4*. Optimal expression was obtained 36-40 hours post-induction with 0.5mM δ-ALA and 1mm IPTG for all the genes. P450 activity was measured using the spectral analysis (Omura and Sato, 1964). Total protein content was measured using the Bradford assay (Bradford, 1976) and CPR activity determined using cytochrome *c* reduction assay (Strobel and Dignam, 1978).

Table 4.1: Primers used for amplification of candidate P450s with *ompA+2* modifications

Primer	Sequences
ompA+2F	GGAATTCCATATGAAAAAGACAGCTATCGCG
*ompA+2CYP6M7*_F	CAAAATGTCTAGCGGCTCCATCGGAGCGGCCTGCGCTACGGTAGCGAA
*ompA+2CYP6M7*_R	TCTAGAGAATTCTCATGTGCTCAGCTTTTCCACC
*ompA+2CYP6Z1*_F	CACCGCGATAGCGTAAAGGATCATCGGAGCGGCCTGCGCTACGGTAGCGAA
*ompA+2CYP6Z1*_R	TCTAGAGAATTCTCACACTCTTCTTTCAATCCTC
*ompA+2CYP9J11*_F	AACCATCAAATCGATCTCCATCGGAGCGGCCTGCGCTACGGTAGCGAA
*ompA+2CYP9J11*_R	TCTAGATCTAGATTACATACTAACTTCGTTATCTTTC
*ompA+2CYP6AA4*_F	CACCACGTTGACGTAACCCATCGGAGCGGCCTGCGCTACGGTAGCGAA
*ompA+2CYP6AA4*_R	TCTAGAGAATTCCTACAGCTTAGTGCCATTCAGCCAGAT

Restriction site (s) are underlined; *Eco*RI: green, *Xba*I: red. *Nde*I for common primer ompA+2F: purple.

4.3.2 Preparation of Cytochrome b_5

The ancillary protein b_5 from *An. gambiae* was expressed and prepared as described (Stevenson et al., 2011, Holmans et al., 1994) and quantified through spectral activity (Omura and Takesue, 1970).

4.3.3 Insecticides Metabolism Assays

Pyrethoids permethrin and deltamethrin, carbamates bendiocarb and propoxur, organochlorine DDT and organophosphate malathion were tested with the recombinant protein of *CYP6M7*, *CYP6Z1*, *CYP9J11* and *CYP6AA4* in a metabolism assay reconstituted with b_5.

4.3.3.1 Substrate Depletion Assay and Kinetics Analysis

Substrate depletion assays and kinetics analysis were carried out as described in Chapter 3 with conditions as outlined in Table 3.8, section 3.33. Enzyme activity was calculated as the percentage depletion (the difference in the amount of insecticide(s) remaining in the +NADPH tubes compared with the –NADPH) and a paired t-test was used for statistical analysis.

4.3.3.2 Fluorescent Probes Assay with Recombinant CYP6Z1

Probes assay was conducted only with rCYP6Z1, partly because evidences from metabolism assay with bendiocarb suggests it to be a cross resistance gene, and also for the ortholog of this gene, *An. gambiae CYP6Z1* (83%) identity had been established as DDT dechlorinase (Chiu et al., 2008); as such *An. funestus CYP6Z1* is suspected to metabolise DDT as well, unless otherwise established.

In order determine potential O-dealkylating property CYP6Z1 a battery of test was conducted with seven fluorescent probes (the same probes utilised to assay mutant membranes of CYP6P9b in Chapter 3). Protocol for initial test of dealkyaltion as well as kinetic was as described in Chapter 3. For kinetics, 0 to 2µM DEF, RBE and RME was assayed with 3.33pmol rCYP6Z1 in a total volume of 250µl. Assay was was carried out under conditions shown to be linear with respect to time.

In order to find out if the results from metabolism assays with pyrethroids, bendiocarb and DDT can be consistent with binding parameters of these insecticides (IC_{50}) inhibition assay was conducted with DEF, test inhibitors (permethrin, deltamethrin, etofenprox, bendiocarb, propoxur, DDT, malathion and chlorpyrifos) and miconazole as positive inhibitor. The assay was carried out as described in section 3.3.2 with 0.13µM DEF (K_M with *CYP6Z1*) and 3.33pmol rCYP6Z1 membrane.

4.3.4 *In silico* Analysis of *CYP6Z1*

In order to establish the binding free energy and binding conformations of *CYP6Z1* with pyrethroid insecticides, bendiocarb and DDT, 3D model of this P450 was created using the crystal structure of human CYP3A4 (PDB:1TQN) (as described in Chapter 2) and molecular docking simulation carried out with the GOLD software. The docking parameters and conformations of insecticide ligands were analyzed using PyMOL and MMV and compared with results from established literature and those from dockings with CYP6P9a and CYP6P9b models.

4.4 Results

4.4.1 Pattern of Co-xpression of Recombinant CYP6M7, CYP6Z1, CYP9J11 and CYP6AA4

On average CYP6Z1 consistently expressed at low concentration (0.10±0.05nmol/mg protein) compared with CYP9J11 (0.13±0.007nmol/mg protein), CYP6M7 (0.15±0.0nmol/mg protein) and CYP6AA4 (0.17±0.02nmol/mg protein). For all proteins however, membrane content of P450 were lower than obtained for CYP6P9a (0.42-1.0 nmol/mg) and CYP6P9b (0.35-0.42nmol/mg), respectively. CYP9J11 and CYP6Z1 exhibited higher reductase content (91.29- and 77.68 nmol cytochrome *c* reduced/min/mg protein, respectively), higher than reductase contents obtained from CYP6M7 (44.93 nmol cytochrome *c* reduced/min/mg protein) and CYP6AA4 (31.46 nmol cytochrome *c* reduced/min/ mg protein) recombinant proteins.

4.4.2 Assessment of Insecticide Activities Using Metabolism Assays

4.4.2.1 Pyrethroids

Disappearance of 20µM insecticides substrates was determined after one hour of incubation with the recombinant enzymes, in the presence of reconstituted cytochrome b_5 and NADPH-regeneration buffer. All the recombinant enzymes screened metabolise permethrin and deltamethrin (Figure 4.1).

CYP6M7 is of special importance for we have recently discovered that its highly overexpressed in southern African populations of *An. funestus* (Riveron et al., 2014a). Specifically, from microarray studies, this gene was found to be the most consistenly overexpressed in Zambian population of multiple resistant *An. funestus* with a higher fold change (FC = 37.7) compared with *CYP6P9a* (FC = 12.5) and *CYP6P9b* (FC =25.7). CYP6M7 metabolizes permethrin and deltamethrin with significant depletions of 68.28%±0.16 ($p<0.001$) and 53.60%±3.5 ($p<0.001$), respectively. The depletion obtained for permethrin is slightly higher than values from CYP6P9a-mediated metabolism (60-66% depletion), but lower than obtained from CYP6P9b (89-92%). However, both CYP6P9a and CYP6P9b have slightly higher depletion for deltamethrin (57-68% and 63-82%, respectively) compared with CYP6M7.

The other three genes studied are also of field importance for they are as well overexpressed across southern Africa in the resistant populations of *An. funestus,* compared with susceptible strains (Riveron et al., 2014a, Riveron et al., 2013) with relatively high fold change: C*YP6AA4* (FC = 5.2, 5.3 and 13.2, for Malawi, Zambia and Mozambique, respectively); *CYP6Z1* (FC = 2.8, 2.9 and 3.9 for Zambia, Malawi and Mozambique, respectively) and *CYP9J11* (FC = 4.0, 4.1 and 4.8, respectively for Malawi and Mozambique).

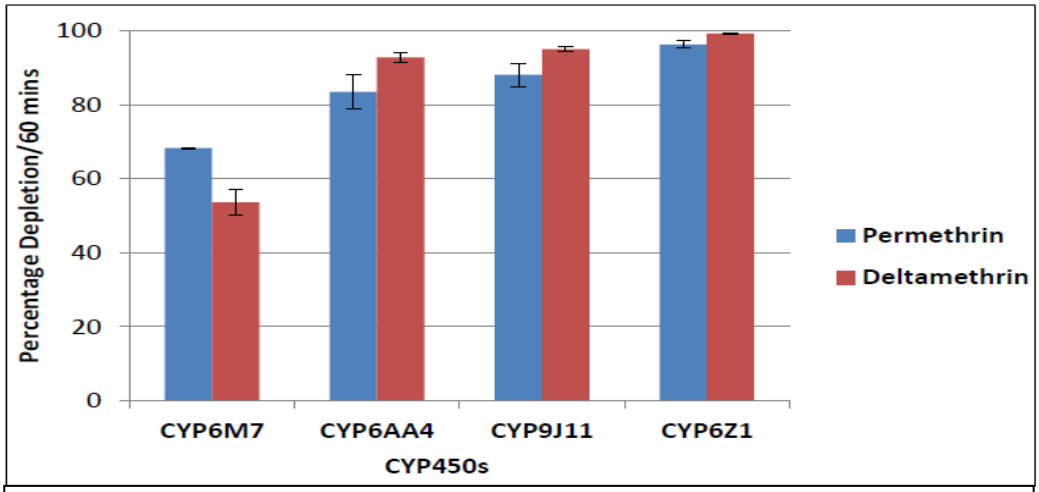

Figure 4.1: Percentage depletion of permethrin and deltamethrin by various recombinant P450s. Results are mean±S.E.M. of 3 replicates. Error bars: variation in the depletion between replicates.

CYP6Z1 depleted 96.28%±1.002 ($p<0.001$) of permethrin and 99.21%±0.11 ($p<0.001$) of deltamethrin after one hour of incubation. **CYP9J11** metabolize permethrin and deltamethrin with significant depletions of 88.05%±3.23 ($p<0.0001$) and 95.05%+0.74 ($p<0.0001$) respectively. This is comparable to the depletion obtained with permethrin (83.48%±4.64, $p<0.0071$ and deltamethrin (92.77%±1.23, $p<0.0001$) from **CYP6AA4**-mediated metabolism. These depletions were higher than obtained with recombinant proteins from CYP6P9a and CYP6P9b.

4.4.2.2 Carbamates and Organophosphate

Carbamates, bendiocarb and propoxur, as well as the organophosphate malathion were screened in order to investigate potential cross-resistance phenomenon. None of the recombinant enzymes screened (CYP6M7, CYP6Z1, CYP6AA64 and CYP9J11) depleted more than 5% of malathion incubated for up to 90 minutes; same results not as obtained from recombinant CYP6P9a and CYP6P9b. This result is consistent with malathion susceptibility across Africa. CYP6Z1 and CYP9J11 significantly depleted bendiocarb (Figure 4.2); particularly, CYP6Z1 depleted more than 50% bendiocarb incubated (54.72%±0.45, $p<0.05$), while CYP9J11 and CYP6AA4 with lower depletion consumed 38.34%±7.01 ($p = 0.05$) and 17.72%±4.84 ($p=0.07$) of this carbamate, respectively. In constrast with results from CYP6M7, CYP6P9a and CYP6P9b (less than 10% depletions), CYP6Z1, CYPJ11 and CYP6AA4-mediated metabolism of bendiocarb proceeded with polar metabolites eluting in the beginning of the HPLC chromatogram (Figure 4.3). Of course, initial reaction of carbamate metabolism has been described to produce very polar products that remain at the origin of the chromatogram (Kuhr, 1970).

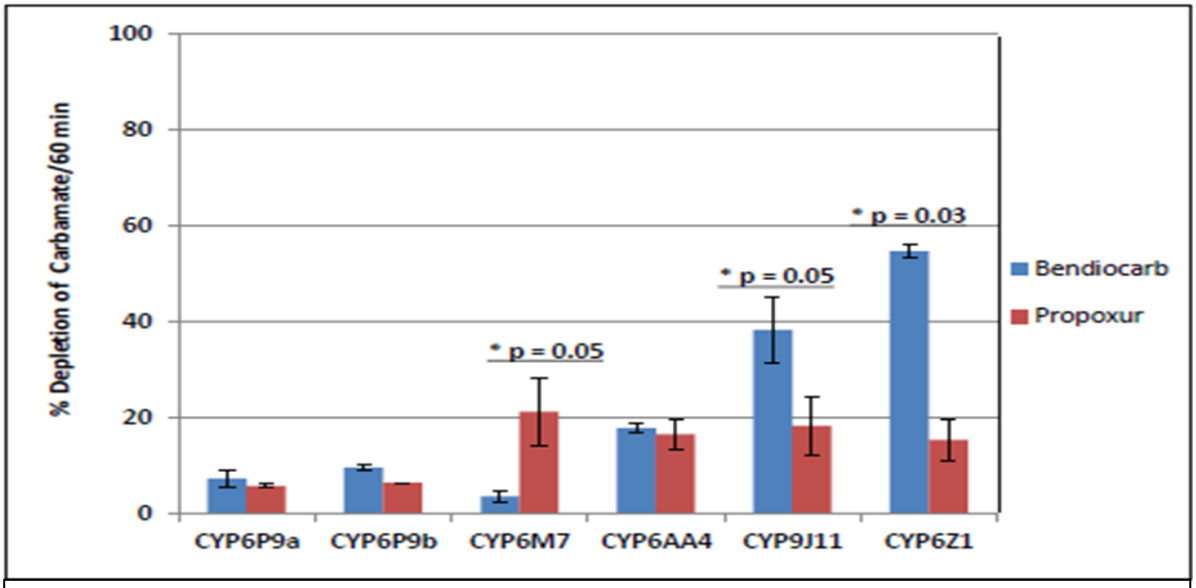

Figure 4.2: Percentage depletion of 20µM carbamate insecticides with *An. funestus* CYP450s. Results are an average of three replicates (n = 3) compared with negative control. *Significantly different from negative control (-NADPH) at p<0.05.

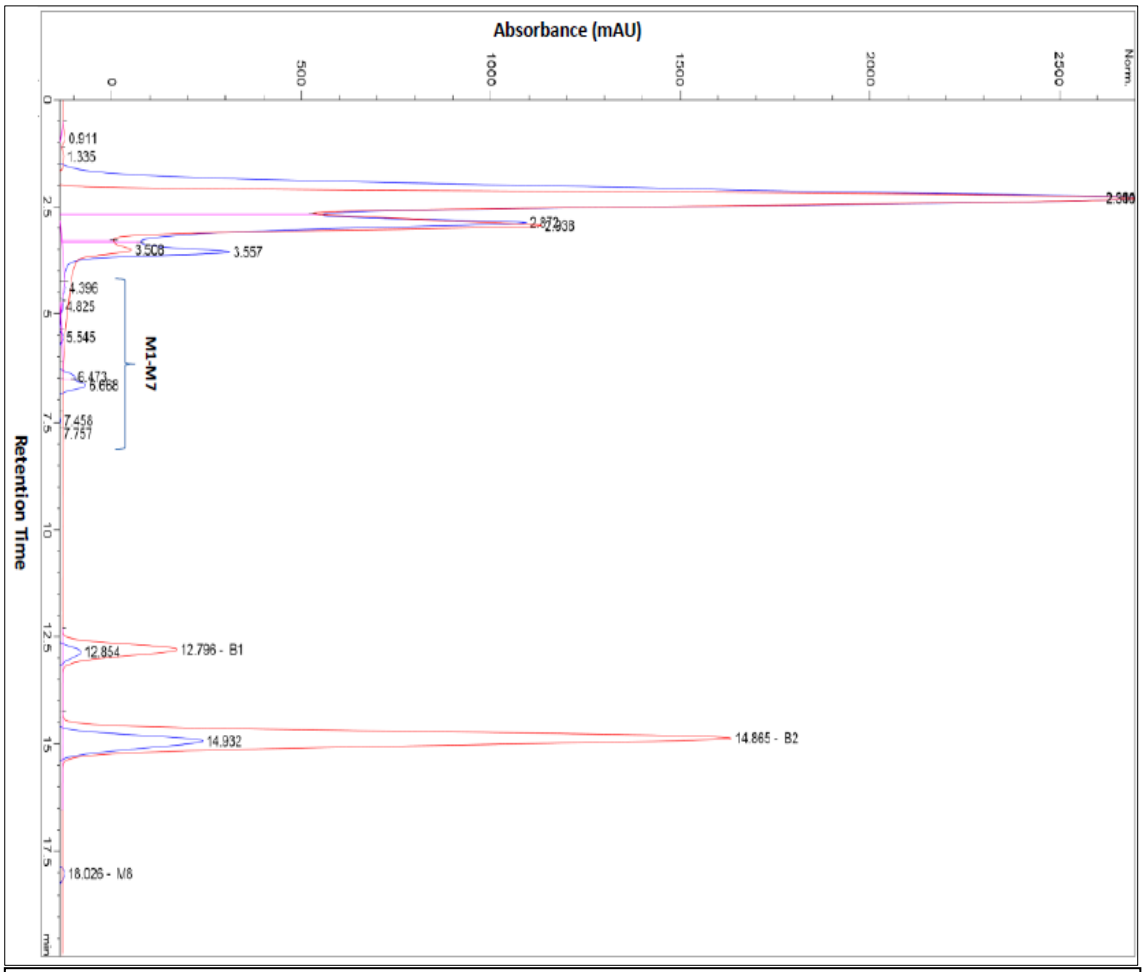

Figure 4.3: Overlay of HPLC chromatogram of the CYP6Z1 metabolism of bendiocarb with –NADPH in red and +NADPH in blue. Bendiocarb peaks are designated B1 and B2 and putative metabolites peaks from +NADP samples designated M1-M7 (4.396-7.75 mins) and M8 (18.026 mins).

These findings implicated *CYP6Z1* as well as *CYP9J11* and *CYP6AA4* as cross-resistance genes that can confer resistance to Type I and Type II pyrethroids as well as bendiocarb.

However, only CYP6M7 showed significant depletion of propoxur (22.22%±7.08, p = 0.05) but with no polar metabolites different from the control (-NADPH). Possibly, recombinant CYP6M7 sequester this carbamate insecticide.

4.4.2.3 DDT

With DDT, metabolism assay was conducted with CYP6Z1, CYP9J11, CYP6AA4, CYP6M7. Only CYP6Z1 was established to be capable of oxidative attack on DDT to produce kelthane with depletion of 46.04% ±2.34 ($p<0.05$). Though CYP6M7 could significantly deplete 37.46%±0.52 of DDT ($p<0.05$) the absence of metabolite peaks make it difficult to ascertain the nature of metabolism. Its assumed that like the case of propoxur, CYP6M7 sequesters DDT. The southern African CYP6P9a and CYP6P9b also depleted 25.79%±2.96 and 26.32%±2.34 of DDT respectively, but with no metabolite peaks. This is somehow consistent with the results from probes inhibition assay in which recombinant CYP6P9a and CYP6P9b portrayed an IC_{50} value of averagely less than 10µM for DDT. Possibly DDT can bind to these P450s but is not metabolised. CYP9J11 and CYP6AA4 depleted only less than 10% of the DDT following 90 minutes incubation.

4.4.2.4 Establishment of Kinetic Constants with Metabolism Assay

4.4.2.4.1 Pyrethroids: Permethrin and Deltamethrin

CYP6M7: CYP6M7 metabolism of permethrin and deltamethrin follows Michaelis-Menten pattern (Figure 4.4) with K_{cat}, K_M and catalytic efficiency respectively of 6.6±0.24min^{-1}, 13.81±7.08µM and 0.45±0.034 $min^{-1}µM^{-1}$ for permethrin and 7.035±0.204min^{-1}, 19.64±10.69µM and 0.36±0.04 $min^{-1}µM^{-1}$ for deltamethrin (Appendix 4.1A). Compared with CYP6P9a and CYP6P9b this enzymes is less efficient, especially with deltamethrin to which it exhibited high K_M. However, it has K_M values for pyrethroids and catalytic efficiencies closer to those described for *An. gambie* CYP6M2 (Stevenson et al., 2011).

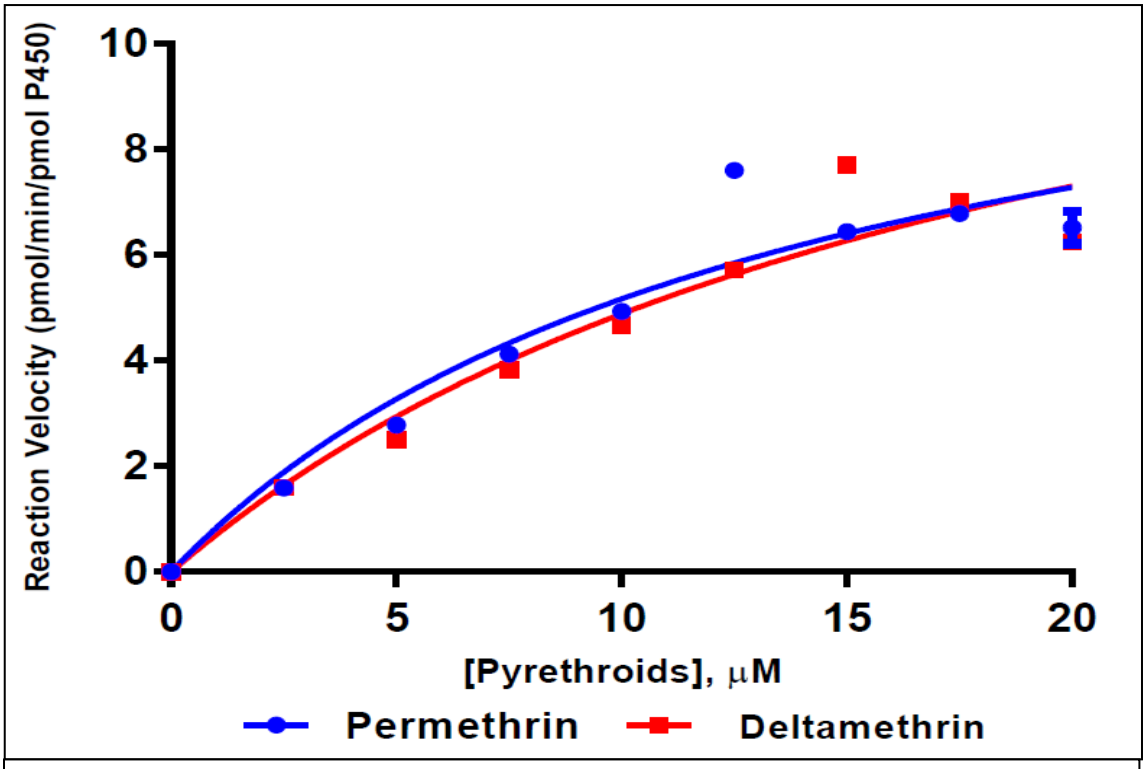

Figure 4.4: Michaelis-Menten plot of CYP6M7 metabolism of permethrin and deltamethrin. Results are average of 3 replicates (n = 3) compared with control (-NADPH).

CYP6Z1: CYP6Z1 metabolism of pyrethroids also followed Michaelis-Menten pattern with a high affinity toward permethrin and deltamethrin (Figure 4.5 and Appendix 4.1A); K_M in magnitude almost three-fold lower than values we established for the *An. funestus* CYP6P9a and CYP6P9b (Riveron et al., 2014a). This sharp difference in terms of K_M possibly reflects a contrasting pattern of mechanism of metabolism in which CYP6P9a, CYP6P9b and CYP6M7 with high catalytic rate portrayed lower affinity for pyrethroids while CYP6Z1 with low turnover bind pyrethroid insecticides more tightly leading to comparable efficiencies. Thus, the catalytic efficiencies of CYP6Z1 towards permethrin and deltamethrin are comparable to values we have established with CYP6P9a and CYP6M7 but lower than values from southern African CYP6P9b (Riveron et al., 2014a).

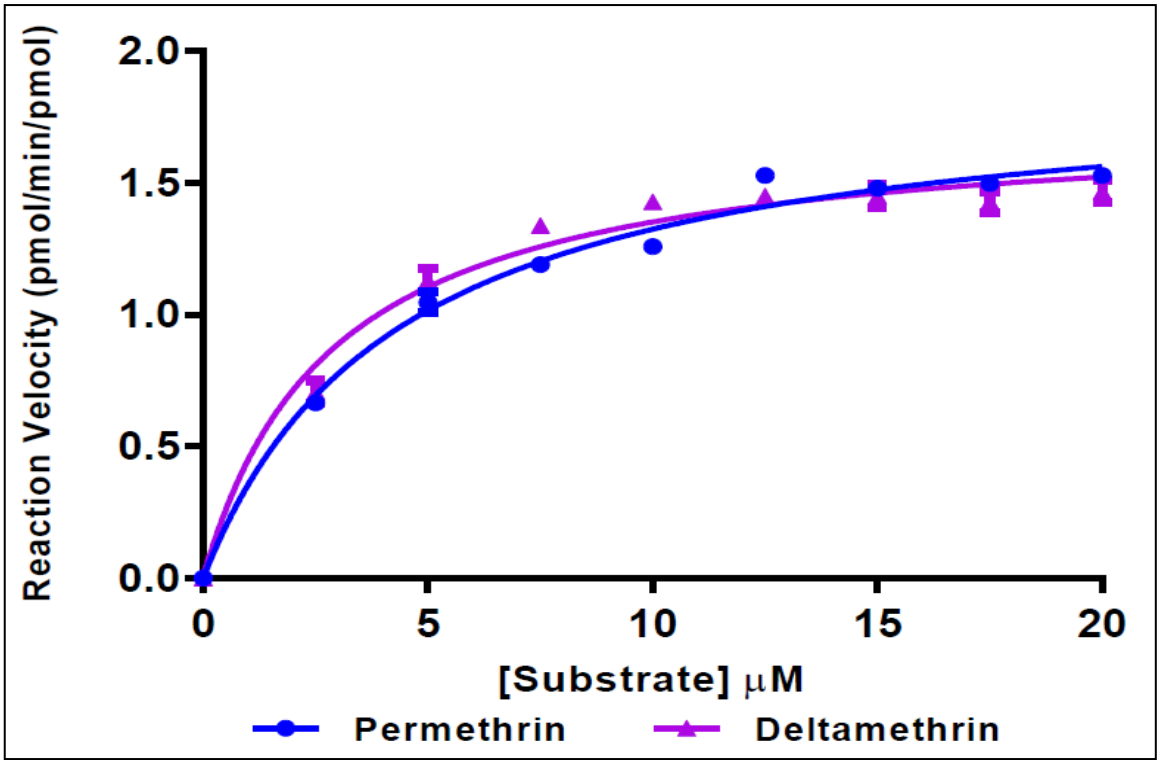

Figure 4.5: Michaelis-Menten plot of CYP6Z1 metabolism of permethrin and deltamethrin.
Results are an average of three replicates (n = 3) compared with negative control (-NADPH).

CYP9J11: The CYP9J11 metabolism of permethrin and deltamethrin follows Michaelis-Menten pattern, but sharp decline in activity was observed with deltamethrin, above 12.5µM concentration (Figure 4.6). This is attributed to substrate or product inhibition especially as evident from the apparen K_M of the enzyme toward deltamethrin. The K_{cat} with permethrin was higher than with deltamethrin, but the high K_M obtained with permethrin makes the enzyme exhibit catalytic efficiency towards deltamethrin almost two-fold the value obtained with permethrin (Figure 4.6 and Appendix 4.1A). CYP9J11 exhibited high K_{cat} and high K_M with permethrin and low K_{cat} and a very low K_M for deltamethrin, leading to catalytic efficiency for deltamethrin approximately two-fold the efficiency with permethrin, but lower than obtained from CYP6P9a and CYP6P9b metabolism.

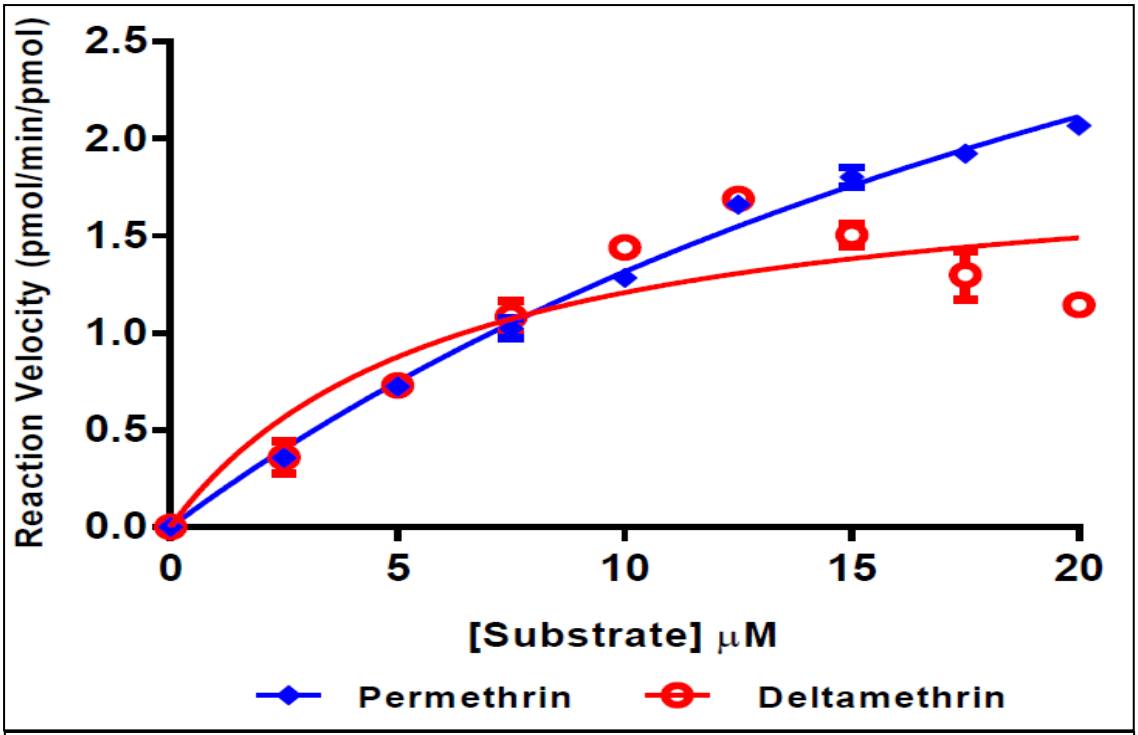

Figure 4.6: Michaelis-Menten plot of CYP9J11 metabolism of permethrin and deltamethrin. Results are average of three replicates (n = 3) compared with control (-NADPH).

CYP6AA4: Pyrethroids metabolism by recombinant P450s followed Michael-Menten pattern Recombinant (details of kinetic profile of this P450 coud be found in Kayla et al., 2015, the title which is given in the list of publications: Appendix 5). CYP6AA4 exhibited high turnover for permethrin (Appendix 4.1A), comparable to ranges obtained with CYP6P9a and CYP6P9b and two-fold higher than the K_{cat} obtained from CYP6M7 and CYP9J11. It showed higher activity towards deltamethrin with a very high K_{cat} double the values obtained with CYP6M7 and eight-fold higher than the K_{cat}s respectively from CYP6Z1 and CYP9J11. The K_M values obtained from CYP6AA4 are comparable to those from CYP9J11 with permethrin and approximately double the values from CYP6M7 with both pyrethroids. Thus, CYP6AA4 exhibited catalytic efficiencies for permethrin and deltamethrin, respectively of 0.36- and 0.52min^{-1} μM^{-1}, values which are comparable to those obtained from CYP6Z1 and CYP6M7 but lower than CYP6P9a and CYP6P9b from resistant alleles.

4.4.2.4.2 Bendiocarb

CYP6Z1 and CYP9J11 were tested with 20µM bendiocarb and both enzymes were discovered to behave in allosteric fashion with this carbamate insecticide, with positive cooperativity (h = 5.82±0.34 for CYP6Z1) and for CYP9J11 (h = 2.29±0.38) (Appendix 4.1B). Allosteric enzymes exhibit positive cooperativity, which refers to the binding of the substrate at one site of the enzyme which affects the affinity of the other sites for the substrates (Atkins, 2004). Presence of multiple substrate binding sites increase affinity for the substrate with a rapid but coordinated increase in velocity until maximal rate is achieved. Allosteric enzymes are modulated by the presence of effectors which can be the substrate itself, a coenzyme or a cofactor. For example, in the case of reconstituted P450 system for metabolism assays, substrate concentrations and presence and concentrations of cytochrome b_5 can change the whole kinetic profile of the reaction leading to varying catalytic output. Degree of cooperativity is measured by the Hill coefficient (h); when h<1 there is a negative cooperativity, when h = 1 there is no cooperativity and when h>1 there is a positive cooperativity.

CYP6Z1 and CYP9J11 portrayed sigmoidal curve with low K_{half} (lower than K_M obtained with pyrethroids) and low maximal catalytic rate (Figure 4.7) (Appendix 4.1B). Dose-response curve was thus modelled using the GraphPad prism with relevant module as described (Copeland, 2004). The catalytic efficiencies for bendiocarb were very low compared with the values obtained with pyrethroid insecticides.

Various P450s that exhibit allosteric phenomenon have already being documented, including the promiscuous CYP3A4 (Wang et al., 2000) and CYP2C9 (Tracy et al., 2002). Functional allostery using distributive catalysis, has been described for some P450s that exhibit atypical kinetics to minimize toxicological effect of substrates (Atkins et al., 2002). Its been described that at low substrate concentrations, the slower substrate turnover afforded by cooperative CYPs compared with Michaelis-Menten enzymes can be a significant toxicological advantage, when toxic thresholds exist. Possibly,

bendiocarb is highly toxic to CYP6Z1 and CYP9J11, though the two P450s can metabolise it, and this is why the enzyme employ distributive catalysis to effect catalysis.

These results revealed that CYP6Z1 and at some extent CYP9J11 confer a cross-resistance between pyrethroids and carbamates, using different mechanisms to effect catalysis.

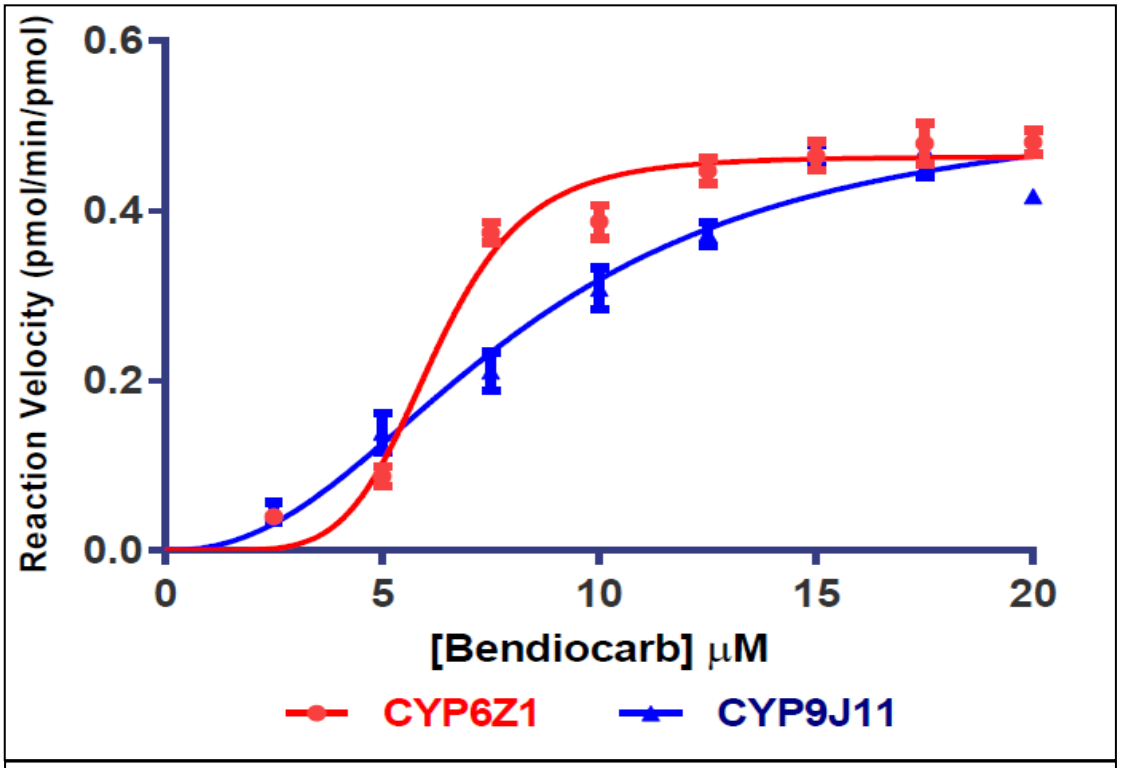

Figure 4.7: Sigmoidal curve of CYP6Z1 and CYP9J11 metabolism of bendiocarb. Results are average of three replicates (n = 3) compared with negative control (-NADPH).

4.4.2.4.3 DDT

In line with the established literature on insects P450s from CYP6 family metabolizing the organochlorine, DDT (Chiu et al., 2008, Mitchell et al., 2012), we tested the P450 candidates with DDT. *An. funestus* CYP6Z1 metabolizes DDT, generating dicofol (kelthane) with a minor peak around 7th minute on HPLC chromatogram. Unlike *An. gambiae* CYP6M2, DDT metabolizer which breaks down DDT into dicofol and DDE (as a minor metabolite) (Mitchell et al., 2012), *An. funestus* CYP6Z1 oxidized DDT into dichlorodiphenyltrichloroethanol (dicofol). The dicofol formation also portrayed atypical

kinetics with cooperativity (h = 2.603±0.67) (Figure 4.8 and Appendix 4.1B). The V_{max} for DDT metabolism is several fold higher than obtained with bendiocarb and thus catalytic efficiency for DDT metabolism was 100-fold higher than with bendiocarb. This result reveals that *CYP6Z1* is possibly involved in the cross-resistance to carbamates and DDT observed in southern Africa populations of *An. funestus* such as those from Zambia, as well as populations from Benin where this gene is overexpressed.

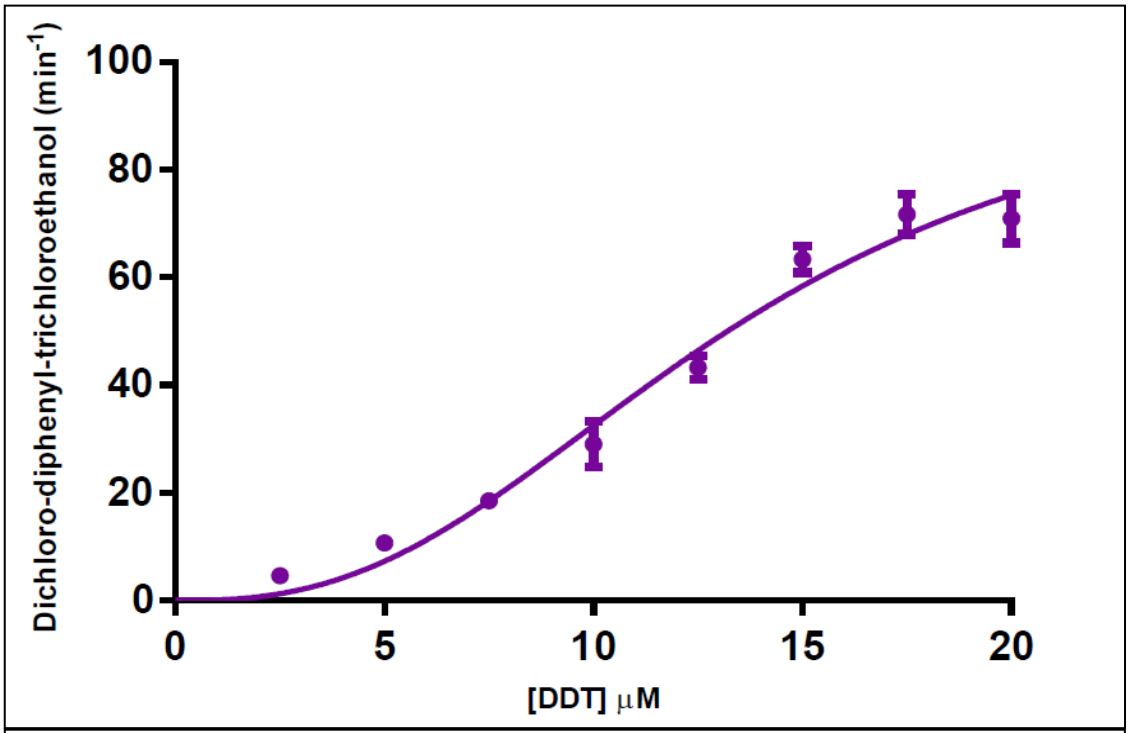

Figure 4.8: Sigmoidal curve of CYP6Z1 metabolism of DDT. Results are average of three independent replicates (n = 3) compared with negative control (-NADPH).

4.4.3 Assessment of O-dealkylating Properties and Insecticides Binding Affinities of Recombinant CYP6Z1 using Fluorescent Probes Assays

In order to establish more information that can implicate *CYP6Z1* as a potential cross-resistance gene, the recombinant CYP6Z1 was used to screen fluorescent probes, establish kinetic profiles and affinity toward pyrethroid, carbamate, organochlorine and organophosphate insecticides using

inhibition assay. It was hoped that the inhibition assay can shed light on affinity of the CYP6Z1 to different insecticide classes, the ones it could metabolise (permethrin and deltamethrin, bendiocarb and DDT) and those it could not metabolise (propoxur, malathion, etc).

4.4.3.1 Screening of Probes and Kinetics with Diethoxyfluorescein

CYP6Z1 showed preferential activity toward diethoxyfluorescein especially and resorufin-based probe RME and RBE, as well (Figure 4.9). Dealkylation of DEF followed Michaelis-Menten pattern (Figure 4.10) with kinetic constants different from values obtained with CYP6P9a and CYP6P9b. The P450 portrayed strong affinity toward DEF with K_M comparable with CYP6P9b, but a maximal catalytic activity three fold higher than obtained with CYP6P9b (Appendix 4.1C). Therefore, the catalytic efficiency of CYP6Z1 toward DEF was almost three-fold higher the values from CYP6P9b. This shows that CYP6Z1 is more efficient O-dealkylating enzyme compared with CYP6P9a and CYP6P9b.

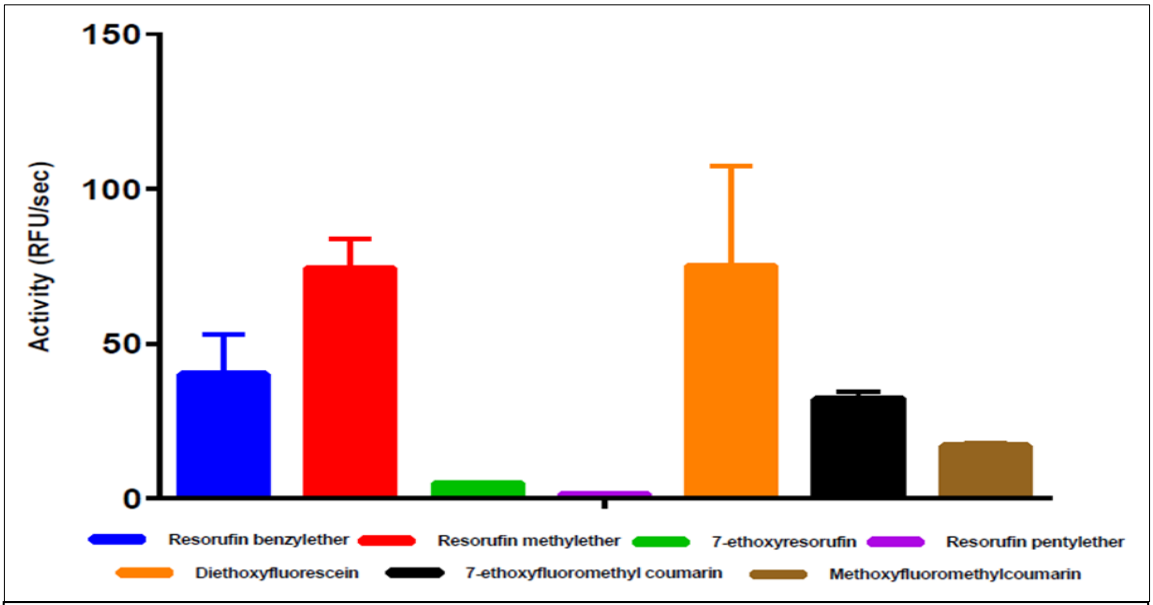

Figure 4.9: Metabolism of probe substrates by CYP6PZ1. The solid bars indicate average of significant activity in three experimental replicates compared to negative controls (-NADPH).

RME and RBE were also used for kinetics analysis. CYP6Z1 exhibited highest maximal catalytic rate with RBE (two-fold higher than values from DEF), but with a very high K_M which resulted in low

catalytic efficiency, six-fold and four-fold lower than the efficiency obtained with DEF and RME, respectively (Appendix 4.1C). The K_M of *An. funestus* CYP6Z1 with RBE is 15-fold higher than the K_M established for RBE with *Ae. aegypti* CYP6Z8 (Chandor-Proust et al., 2013) and *An. gambiae* CYP6Z2 (McLaughlin et al., 2008). However, the K_{cat} of de-benzylation of RBE from the above researchers are way too low compared with the K_{cat} obtained from *An. funestus* CYP6Z1.

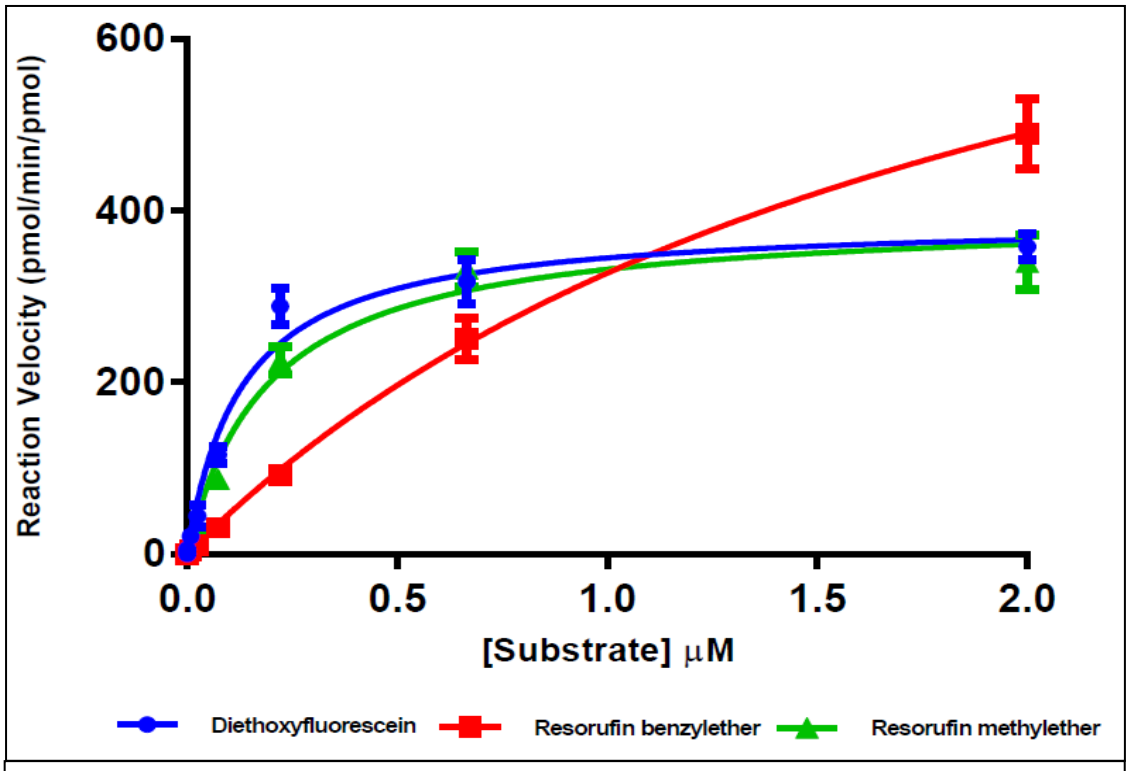

Figure 4.10: Michaelis-Menten plots of CYP6Z1 dealkylation of probe substrates DEF, RBE and RME.

4.4.3.2 Determination of Affinity of CYP6Z1 to Insecticides Using Inhibition Assays

In order to establish the affinity of recombinant CYP6Z1 towards different insecticide classes, inhibition assay was conducted with DEF and a panel of insecticides. The mean values of IC_{50} for the test inhibitors for the fluorogenic probe DEF used in this study is shown in Figure 4.11. Lowest IC_{50}s were obtained with miconazole, a potent P450 inhibitor (Lupetti et al., 2002) used in various inhibition studies (Niwa et al., 2005). CYP6Z1 shows lower affinity for both permethrin (IC_{50} = 6.80μM±0.18) and deltamethrin (IC_{50} = 4.98μM±0.07) compared with CYP6P9a and CYP6P9b respectively, with IC_{50}s

slightly lower with deltamethrin than permethrin. The enzyme shows comparable affinity towards etofenprox and stronger affinity to chlorpyrifos (IC_{50} = 0.7µM±0.01). It exhibited low affinity towards malathion (IC_{50} = 16.9µM±3.9. In contrast with CYP6P9a and CYP6P9b, IC_{50} values of 9.5µM±0.9 and 8.9µM±0.9 respectively, were obtained for bendiocarb and DDT, with CYP6Z1, indicative of binding especially toward bendiocarb to which IC_{50}s for CYP6P9a and CYP6P9b were greater than 25µM. Tight-binding inhibitors have been defined as compounds with a IC_{50} values of <10µM (Kemp et al., 2004) and thus bendiocarb and DDT are considered good binders of CYP6Z1. The IC_{50} values increased drastically with decrease in the concentration of those insecticides that show strong inhibition toward the CYP6Z1-mediated dealkylation of DEF (Figure 4.11B). The high IC_{50} obtained with propoxur is consistent with the inability of CYP6Z1 to metabolise this insecticide as established from substrate depletion assays.

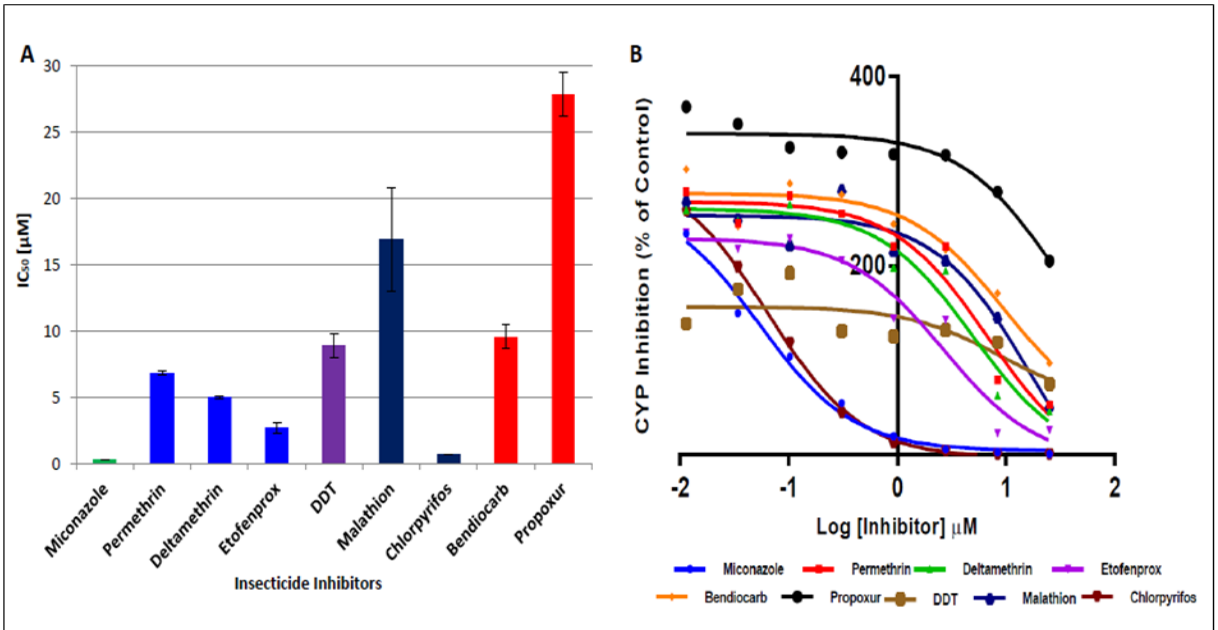

Figure 4.11: (A) Mean IC_{50} of the test insecticide inhibitors against CY6Z1 dealkylation of DEF. Data represent mean IC_{50} at eight concentrations of each insecticide ± S.D. Error bars represent variation in the values of the IC_{50} between different concentrations; (B) Effect of test insecticides on the CYP6Z1-mediated metabolism of DEF. Results are mean ± S.D. of three independent replicates.

4.4.4 Comparative Modelling and Molecular Docking Simulation of CYP6Z1 with Insecticides

In order to shed more light on the possible pattern of binding of insecticides to CYP6Z1 model virtual insecticide structures were docked to its active site. It was hoped that the docking simulation could shed light on what makes the gene able to metabolise non-pyrethroid insecticides, conferring cross-resistance in contrast with *CYP6P9a* and *CYP6P9b* pyrethroid-metabolism specialists. Here docking results with deltamethrin, bendiocarb and DDT were analysed.

The docking parameters of CYP6Z1 with permethrin, deltamethrin, bendiocarb and DDT were summarized in Appendix 4.2. ChemScore values lower than observed with CYP6P9a and CYP6P9b were obtained with permethrin and deltamethrin. In contrast, docking with DDT produced higher ChemScore values and lower free binding energy than obtained with CYP6P9a and CYP6P9b, though no hydrogen bonding contribution was predicted for all 50 solutions. Another exception is the ChemScore values for docking with bendiocarb; these values were consistently higher than those obtained with CYP6P9a and CYP6P9b models.

Within the active site of *CYP6Z1* permethrin docked above the heme plane with 4' spot of the phenoxy group positioned at a distance of 3.6Å. Two of the ten top docking solutions in CYP6Z1 have gem dimethyl group at close proximity to the heme, thus, just like MOZCYP6P9b, multiple metabolites can be generated with permethrin. Deltamethrin also docked with the 4' spotof the phenoxy ring at a distance of 3.54Å. One of the top ten ranked poses has the gem dimethyl group facing the heme, implying possibility of more than one primary metabolite, as well. It has been established that recombinant *An. gambiae* C*YP6M2* preferentially hydrolyses deltamethrin to initial product at 4' position, with trans-methyl hydroxylation being a minor route (Stevenson et al., 2011); thus its interesting that CYP6P9b and CYP6Z1 which metabolise deltamethrin docked with the same conformation multiple conformations.

Within the active site of CYP6Z1 deltamethrin is surrounded within 5.0Å radius by nonpolar aliphatic residues Val[101] (SRS1), Ile[216](SRS2), Lue[295] and Ala[299] (SRS4), Ala[364], Leu[365], Ala[366] and Leu[368] (SRS5), all of which makes the binding site highly hydrophobic (Figure 4.12A). Bulky hydrophobes include Phe[212] (SRS2) and Phe[115] (SRS1), the latter which point toward and could π-stack with the phenoxybenzyl ring of deltamethrin at a distance of 3.8Å (Figure 4.13A). The catalytic importance of this Phe together with other critical residues (Leu[295], Leu[365], Ala[366], Leu[368], Asn[369] and Arg[99]) has been described for *An. gambiae* CYP6Z1 model (Chiu et al., 2008).

The polar neutral residues Asn[208] (SRS2), Thr[303] (SRS4) and Asn[369] (SRS5) could possibly be important residues involved in hydrogen bonding network with Tyr[102] while the positive guanidinium group of Arg[99] could be involved in electrostatic interactions or form a salt-bridge with the propionate moiety of the heme stabilizing the binding cavity. This residue is conserved between CYP6Z1 and CYP6P9b, and occupies the same spacial position. A hydrogen bonding was predicted between the ε-amino group of Lys[48] and the acyl carbon atom of the acid moiety (Figure 4.14A). This hydrogen bond within 2.98Å alone is predicted to contribute -2.5kJ/mole of energy and possibly is networked to. The hydrogen bonding network is predicted to Glu[210] and Ser[211] both residues from the SRS2.

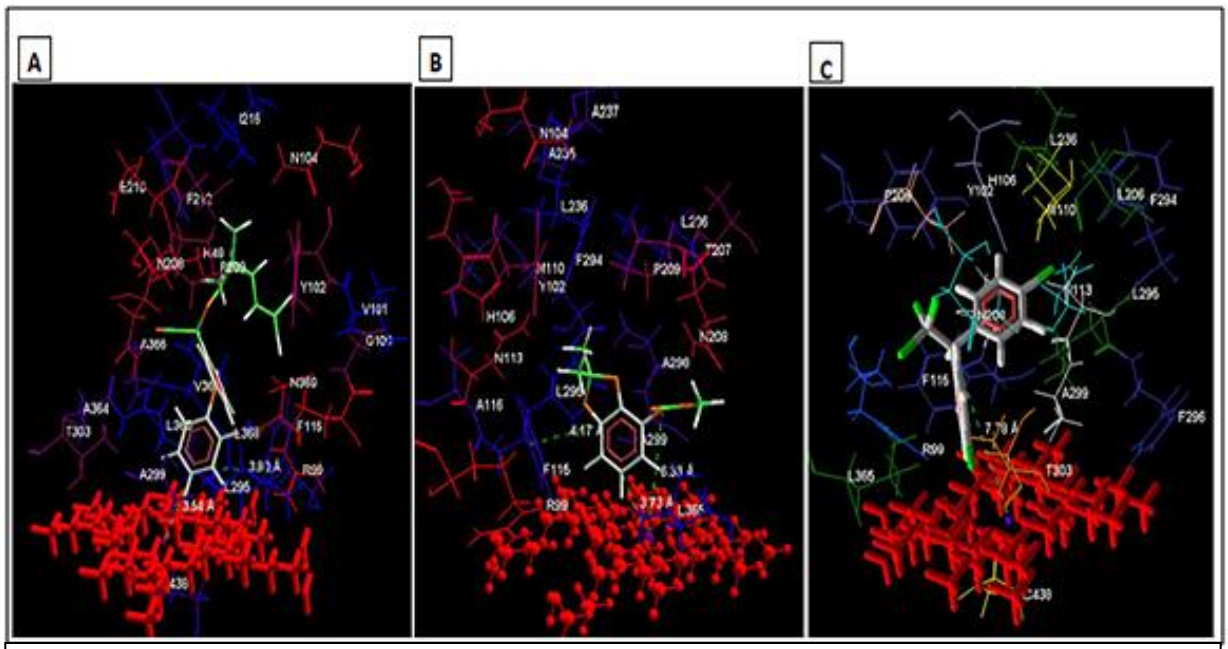

Figure 4.12: Predicted residues within 5.0Å of (A) deltamethrin, (B) bendiocarb and (C) DDT in the active site of CYP6Z1.

Bendiocarb docked into the active site of CYP6Z1 above the heme with the C-4 of the phenyl ring and the carbamate ester located 3.73Å and 6.33Å respectively, from the heme iron (Figure 4.12B). In this posture, ring hydroxylation product (4- or 5-hydroxybendiocarb) are predicted to be the major metabolites, with ester cleavage to generate benzodioxol-4-ol being of minor priority. The dimethyl group are pointed away from the heme catalytic site. Phe^{115} of SRS1 and occupying the same position as Phe^{123} of CYP6P9a and CYP6P9b is located at a distance of 4.17Å from the phenyl ring of bendiocarb, with the possibility of a face-to-face π-stacking. Critical residues within 5.0Å radius of bendiocarb (Figure 4.13B) include: (i) non-polar aliphatic side chains important for hydrophobicity: Met^{110} and Ala^{116} of SRS1, Ala^{235}, Ala^{237}, Leu^{236} all three belonging to SRS3, Leu^{295} and Ala^{298} both from SRS4 as well as Ala^{299} which belongs both to the SRS4 and the O_2-binding pocket, as well of Leu^{365} from the SRS5; (ii) polar residues that could be involved in ionic interaction and/or hydrogen bonding include two residues from SRS1, His^{106} and Tyr^{102}; (iii) polar neutral side chains that could be involved in hydrogen bonding include Asn^{104} and Asn^{113} both from SRS1, Thr^{207} and Asn^{208} both from SRS2.

The residue Arg^{99} of SRS1 which was found to be within close contact with the propionate moiety of heme in docking with pyrethroids also appeared in the same position with the docked pose of bendiocarb. As with docking with deltamethrin we hypothesize that this residue forms a salt-bridge with the propionate moiety of the heme stabilizing the active site and enhancing catalysis.

Two hydrogen bonding were predicted: (i) the alcohol side chains of Thr^{207} to the N-methyl group of the carbamate moiety (2.94Å and -2.5kJ/mol) (ii) the phenyl oxygen of Tyr^{102} (2.89Å and -2.5kJ/mol) (Figure 4.14B). Both this intermolecular hydrogen bonding appeared to have no acceptor group from bendiocarb; possibly they were meant for the *N*-dimethyl group of bendiocarb which was out of reach as the insecticide docked closer to the heme.

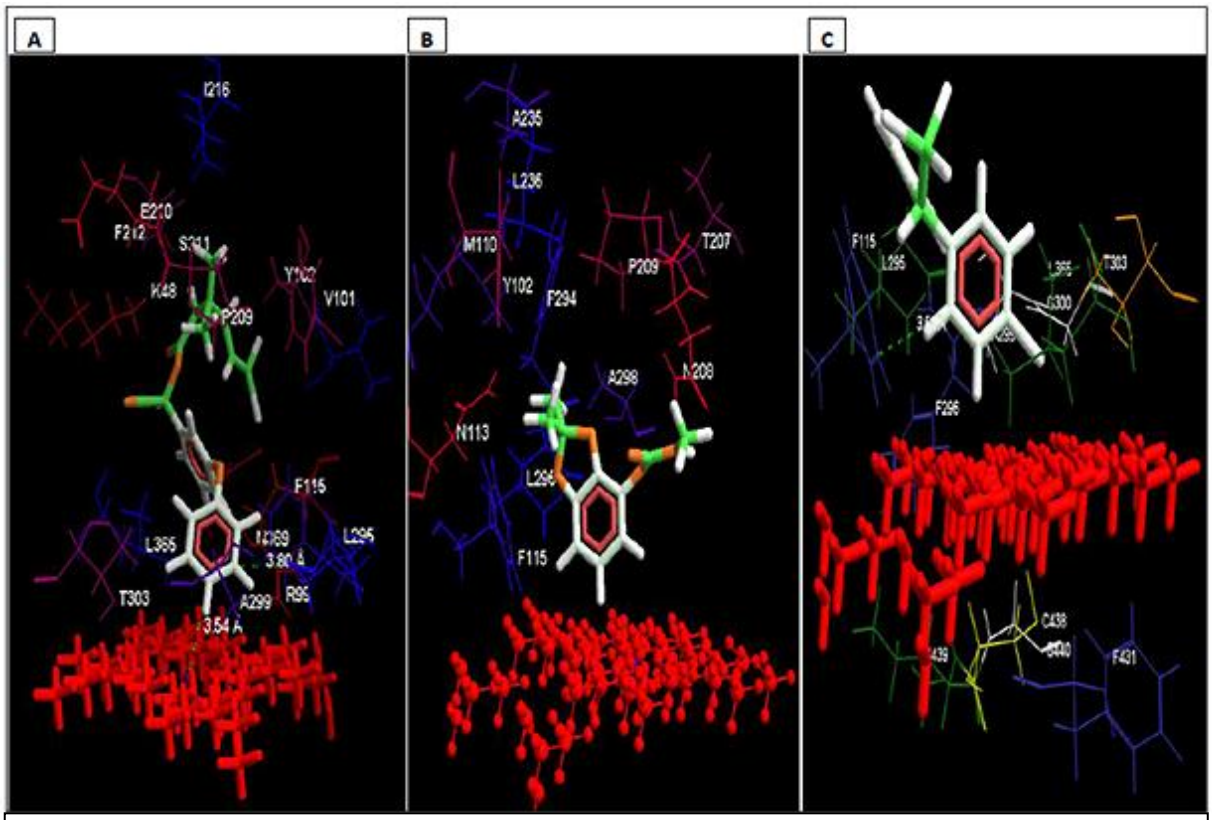

Figure 4.13: Predicted residues in hydrophobic contact with substrates within 5.0Å of (A) deltamethrin, (B) bendiocarb and (C) DDT in the active site of CYP6Z1

All the 50 predicted bound conformation on DDT in the active site of CYP6Z1 were not optimally productive. One of the benzyl rings approached the heme obstructing access to the trichloromethyl group. Though ChemScore values were higher than obtained with deltamethrin, with all the poses with DDT no hydrogen bonding contribution was predicted by GOLD (see Figure 4.14C). Individual residues within 5Å of DDT include the non-polar aliphatic Ala[116] of SRS1, Leu[206] of SRS2, Leu[236] of SRS3, Leu[295] and Ala[299] both of which belong to SRS4, as well as Leu[365] of SRS5 (Figure 4.12C). Other polar residues include Thr[303] of SRS4, Tyr[102] of SRS1, His[106] of SRS1, and two polar, neutral asparagine residues (Asn[208] of SRS2 and Asn[113] of SRS1). The binding site of DDT in CYP6Z1 contains many bulky hydrophobes including Phe[115] of SRS1 which point toward the benzyl group approaching heme at a distance of 3.52Å with possibility of π-stacking leading to stabilization, Phe[294] and Phe[296] both of which belong to SRS4. Arg[99] of SRS1 is also located as usual close to the propionate moiety of the heme with possibility of forming a salt-bridge. Residues predicted to be in hydrophobic contact

with the substrate include Phe[431], Gly[440] and Ile[439] (both of heme-binding domain), Phe[296], Leu[295], Gly[300], Ala[299] (all four from SRS4) Lue[365] as well as Phe[115] (Figure 4.13C). No residue within 5.0Å residue of DDT was predicted to be involved in intermolecular hydrogen bonding with the substrate. Results from docking with DDT just like the case of CYP6P9a and CYP6P9b was not conclusive. It opened more questions than it answered, for none of the first top ten ranked poses seems to be reliably productive.

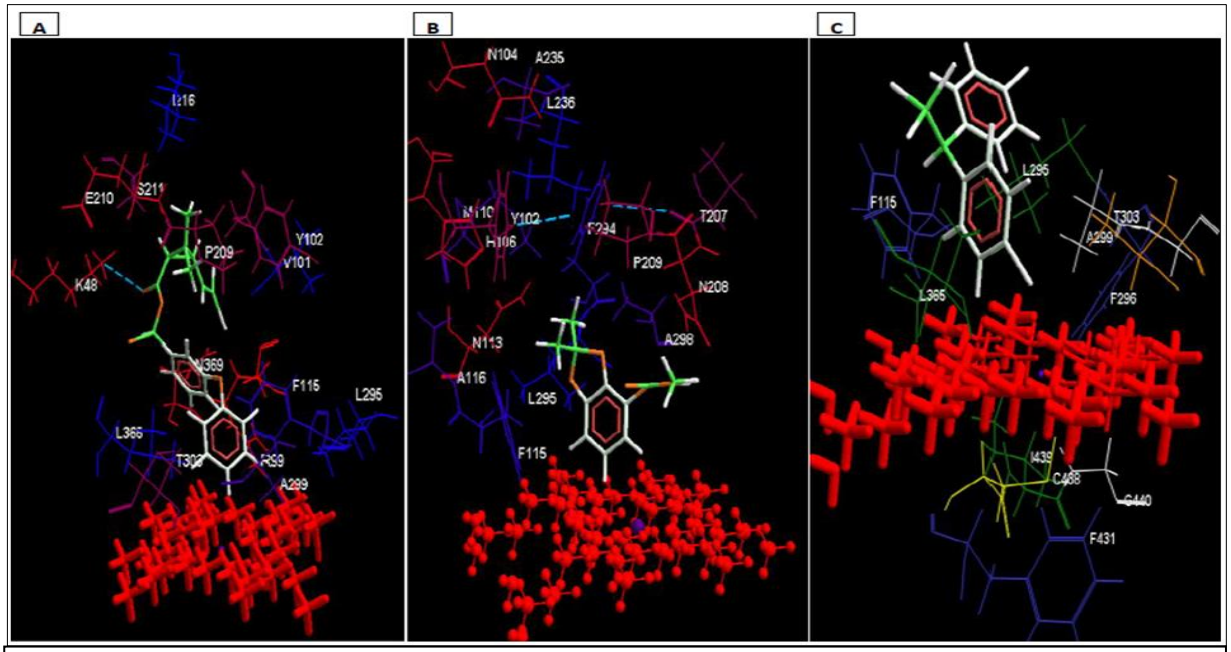

Figure 4.14: Predicted residues within 5.0Å of (A) deltamethrin, (B) bendiocarb and (C) DDT in the active site of *CYP6Z1*. Hydrogen bonds between insecticide atom (s) and amino acids residue (s) are shown as blue dotted lines.

4.5 Discussion and Conclusion

Molecular docking simulations predicted CYP6Z1 to have activities toward pyrethroid insecticides comparable to CYP6P9a and CYP6P9b. The gene was also predicted to have activity against bendiocarb and to some extent DDT. Fluorescent probes and inhibition assays, and pyrethroid metabolism assays have implicated *CYP6Z1* as cross-resistance gene that binds to pyrethroids, bendiocarb and DDT. This is in contrast with *CYP6M7*, *CYP6P9a* and *CYP6P9b,* established to specialize only on pyrethroids metabolism, with no activity towards organochlorine DDT, and carbamate, bendiocarb. I have

established herein that *CYP6Z1* can metabolise pyrethroids, bendiocarb and DDT, but has no significant activity towards propoxur and malathion. The presence of benzodioxol- ring in bendiocarb and simpler phenyl ring in propoxur, or the presence of isopropoxy- group in propoxur and its absence in bendiocarb may account for the incapability of the CYP6Z1 and CYP9J11 to metabolize propoxur. I also discovered another gene *CYP6M7* which was highly overexpressed in multiple resistant populations from Zambia, able to metabolise Type I and Type II pyrethroids with high efficiency. While the gene has no significant activity towards bendiocarb and DDT, based on the data obtained I suspect it to sequester propoxur and possibly DDT. Other pyrethroid metabolisers discovered include *CYP9J11* and *CYP6AA4* both which also exhibited low activity towards bendiocarb.

Its now apparent that in *An. funestus* resistance to pyrethroid is mediated by more than P450s *CYP6P9a* and *CYP6P9b* as previously thought. Pyrethroid resistance is mediated by all these P450s studied: *CYP6P9a, CYP6P9b, CYP6M7, CYP6Z1, CYP9J11* and *CYP6AA4,* and possibly other P450s yet to be characterized. All these genes fall within the originally described three QTLs: *rp1* (2R chromosomal arm for *CYP6P9a*, *CYP6P9b* and *CYP6AA4*), *rp2* (2L in the case of *CYP6M7* and *CYP6Z1*) and *rp3* (3L in the case of *CYP9J11*) (Wondji et al., 2009, Wondji et al., 2007b, Irving et al., 2012) associated with pyrethroid resistance. In addition to the ability to metabolise pyrethroids and confer resistance to *An. funestus* by all of these genes, we found that some of these genes, *CYP6AA4*, *CYP9J11* and especially *CYP6Z1* are cross-resistance genes, meaning that they can metabolise non-pyrethroid insecticides used in public health using subtler kinetic mechanisms. An important property observed with *CYP9J11* and *CYP6Z1* with bendiocarb and also *CYP6Z1* with DDT is that the metabolism of these insecticides proceed allosterically with positive cooperativity, while metabolism of pyrethroids followed canonical Michaelis-Menten fashion. As described earlier, functional allostery using distributive catalysis has been described for some P450s that exhibit atypical kinetics to minimize toxicological effect of substrates (Atkins et al., 2002). These genes possibly utilize this mechanism in the face of challenge from highly toxic insecticides. This makes establishment of the catalysis by the P450s conferring

resistance difficult and parameterization and extrapolation of kinetics from resistance P450s all the more difficult to easily interprete.

Cross-resistance had been described for many resistant insect populations. For example, a multiple resistance *An. gambiae* populations from Tiassale', Coˆte d'Ivoire, West Africa, was recently described (Edi et al., 2014). Two P450s *CYP6P3* and *CYP6M2* were implicated via microarray and transgenic studies as responsible for the pyrethroid resistance and cross-resistance to bendiocarb in these populations from Tiassale', while *CYP6M2* was also fingered as responsible for DDT resistance. In the same study, recombinant CYP6P3 was shown to be able to metabolize bendiocarb *in vitro*. *An. gambiae CYP6M2* however, had already been established as pyrethroid and DDT metaboliser from several studies (Mitchell et al., 2012, Stevenson et al., 2011). In *D. melanogaster,* transgenic expression of two P450s *CYP6G1* and *CYP12D1* conferred cross-resistance to chemically unrelated insecticides (DDT, nitenpyram and dicyclanil in the case of *CYP6G1*) and DDT and dicyclanil in the case of *CYP12D1* (Daborn et al., 2007), clearly confirming that presence of cross-resistance gene can confer resistance to more than one class of insecticide.

The impact of many genes conferring resistance and cross-resistance to multiple resistant populations of *An. funestus* in sub-Saharan African is a source of concern. This phenomenon makes the resistance highly heterogenous and complex, making design of appropriate diagnostic tools operationally challenging. Equally, also the flow of these resistance genes can introduce resistance hitherto unknown into new environments confounding problems; for example, underlying resistance could shift according to region as observed with the highly overexpressed *CYP6M7* from Zambia which can metabolise Type I and Type II pyrethroids and possibly sequester propoxur. There is thus an urgent need to find newer tools to combat insecticide resistance. Also, there is an overwhelming need for newer classes of insecticides that are safe (low mammalian toxicity) but potent enough to control mosquito vectors of malaria, and other diseases effectively. But caution must be exercised because the number of new enzymes classes that can confer cross-resistance is in increase and a new

insecticide may already be doomed before being deployed if resistance genes can already metabolise it. There is a need to also find more of the new chemical entities (synergists) that can be incorporated into the insecticides formulation so that they can block the enzyme systems from breaking down the insecticides in question.

5. DISCUSSION, CONCLUSION AND FUTURE PERSPECTIVES

5.1 Discussion

An. funestus s.s. is a major malaria vector in the African continent, and it is the most widely, geographically distributed amongst all vectors from the *An. funestus* complex. It has high vectorial capacity, an attribute conferred by its highly anthropophilic and endophilic behaviours, and in some localities its ability to transmit malarial parasite (parasite infection rates) exceed those of *An. gambiae*.

Several studies across Africa have documented *An. funestus* becoming increasingly resistant especially to three of the four classes of insecticides used in public health (pyrethroids, carbamates and organochlorines) with resistance patterns being heterogeneous. The pyrethroid resistance in particular is threatening to derail the effectiveness of malaria intervention tools, e.g. ITNs and LLINs. In the absence of *kdr* and *AChE*-type mutations in *An. funestus*, evidences have implicated a handful of monooxygenases (especially from CYP6 family) as mediators of pyrethroid resistance, while GSTs (especially *GSTe2*) have been shown to be responsible for DDT resistance, especially in some regions of Africa (Riveron et al., 2014b). Despite the progress made, there is an overwhelming need to elucidate the actual molecular mechanisms of metabolic resistance because the bulk of the studies so far carried out involves analysis of overexpression of candidate genes, which neither establish the ability of the genes in question to metabolise the insecticide(s) of interest nor does it pinpoint the factors responsible for the resistance. Presence of polymorphism in the main candidate genes established as metabolisers of pyrethroids suggested a role of allelic variation in resistance pattern. Equally also the role of other candidate genes overexpressed in the multiple resistance populations of *An. funestus* still needed to be confirmed, for such information can identify other genes that confer pyrethroid resistance, as well as cross-resistance to different insecticide classes used in public health.

The continued effectiveness of vector control through insecticide-based tools require design and implementation of suitable resistance management strategies, to limit the negative impact of

resistance (WHO, 2012). One prerequisite that can help is the development of appropriate resistance diagnostic tools to facilitate the monitoring of insecticide resistance at an early stage, in order to inform control programs of the best course of action to take, to minimise the impact of the resistance. However, the design of DNA-based diagnostic tools requires a thorough understanding of the molecular basis of pyrethroid resistance especially in major malaria vectors such as *An. funestus* in which resistance is mainly metabolic. To date, efforts to characterise pyrethroid resistance in *An. funestus* have revealed metabolic resistance through elevated expression of cytochrome P450s as the underlying mechanism playing the major role (Wondji et al., 2012, Riveron et al., 2013, Coetzee and Koekemoer, 2013). Despite the numerous reports of implications of P450s in pyrethroid resistance, the detailed molecular mechanisms through which P450s confer pyrethroid resistance in mosquitos remain largely uncharacterised. Overexpression of several P450s is commonly reported in association with resistance, however, it remains unclear what drives the overexpression or whether other mechanisms in addition to overexpression are involved. These other factors may include variation in the coding sequences through substitutions of catalytically important amino acid which could modify the activity of the enzymes or *cis* and/or *trans* mutations that could impact the up-regulation of the candidate P450s linked with resistance. Previous works have reported that allelic variations through amino acid changes in the *CYP6A2* gene variants in *D. melanogaster* impacted DDT metabolism with striking quantitative changes in catalytic activity, and recently, in *An. funestus*, a single point mutation detected in resistant populations was established to alone confer DDT resistance. However, little was known on the impact of allelic variation of P450 genes on pyrethroid resistance. Observation of important polymorphism variation for the two most important pyrethroid resistance genes *CYP6P9a* and *CYP6P9b* (Riveron et al., 2013, Wondji et al., 2009) in *An. funestus* suggested that this mosquito species is an excellent candidate to assess the impact of allelic variation on insecticide resistance.

The goal of this study was to assess whether allelic variation is impacting pyrethroid resistance and if causative mutation(s) could be identified for pyrethroid resistance mediated by P450 genes, which will facilitate the design of DNA-based diagnostic tools to easily detect and track such resistance

in field populations. Additionally, several other candidate P450 genes previously associated with pyrethroid resistance or cross resistance to other insecticides, still needed to be validated to confirm their role in respective resistance in the field.

In this study, molecular basis of monooxygenase-mediated resistance to pyrethroid in *An. funestus* was dissected. Exisence of cross-resistance genes that metabolise bendiocarb and DDT was also established. The major findings of this study include: (i) Allelic variation is a key mechanism conferring pyrethroid resistance in *An. funestus*, (ii) Key amino acid changes in pyrethroid metabolising P450 *CYP6P9b*, from resistant populations are responsible for pyrethroids-metabolising efficiency; this finding could help create DNA-based diagnostic tools that can allow for detection of such mutations in the field, (iii) Pyrethroid resistance is multi-genic in field populations of *An. funestus;* in addition to *CYP6P9a* and *CYP6P9b* (the major pyrethroid resistance genes in *An. funestus*), other genes overexpressed in resistant populations were functionally validated for ability to metabolise pyrethroids and non-pyrethroid insecticides, (iv) Validation of these other genes led to the discovery of P450s that confer cross-resistance to pyrethroids, as well as DDT and bendiocarb in *An. funestus*. These findings are discussed in detail below:

5.1.1 Allelic Variation is a Key Mechanism Conferring Pyrethroid Resistance *in An. funestus*

The fact that the predominant haplotypes of the pyrethroid resistance genes *CYP6P9a* and *CYP6P9b* from resistant mosquito populations across Africa share key amino acid variants in common compared with the haplotypes from FANG suggested that allelic variation in these genes is impacting their ability to metabolise the pyrethroids, and confer resistance. This was also supported by *in silico* simulation of the activities of these P450s towards different classes of insecticides which predicted the allelic variants from the resistant populations to metabolise pyrethroids with high efficiency compared with the susceptible alleles. *In silico* predictions have been applied in several studies to predict the ability of insect P450s to metabolise pyrethroids and other substrates (Stevenson et al., 2011, Chandor-Proust et al., 2013, Schuler and Berenbaum, 2013). Validation of *in silico* predictions

confirmed that allelic variation is conferring pyrethroid-metabolising efficiency in the *CYP6P9a* and *CYP6P9b* alleles from resistant populations of *An. funestus* compared with the corresponding genes from FANG which has lower metabolic activities toward pyrethroid insecticide and probe substrates. The robustness of the *in silico* prediction was also strengthened by the inability of the recombinant proteins of these genes to metabolise non-pyrethroid insecticides, including bendiocarb, propoxur and DDT. These findings were further strengthened through *in vivo* analysis; with presence of alleles from resistant populations (*MALCYP6P9a* and *MOZCYP6P9b*) alone conferring pyrethroid resistance to transgenic *D. melanogaster*. This established that CYP6P9a and CYP6P9b gene products which are overexpressed in resistant populations of *An. funestus* across Africa, compared with FANG are specialist pyrethroid metabolising P450s. The findings of these genes especially *CYP6P9b* undergoing directional selection all across Africa is in line with the previous observations from several studies (Riveron et al., 2013, Wondji et al., 2012). Important polymorphisms in the resistant alleles of *CYP6P9a* and *CYP6P9b* were mapped to catalytic domains (active sites) of these genes with potential impact on activity and substrates specificity. This is an important finding that identifies markers of resistance in *An. funestus* which can allow for tracking of these pyrethroids metabolically-mediated resistance alleles across Africa, with special operational applications towards management of insecticides resistance. It also set a pace for studies of this kind to be carried out on other organisms, e.g. major malaria vectors (*An. gambiae* and *An. arabiensis*), dengue vector *Ae. aegypti,* as well filarial worm vector *Cx. quinquefasciatus*. These insects have been shown to be resistant to a wide variety of insecticides, and like *An. funestus* and the major enzyme systems which confer the resistance to them may possess allelic variants that need to be investigated. Markers of resistance and diagnostic tools can be established in these insect species helping towards implementation of well-informed resistance management strategy. To establish whether allelic variation in pyrethroid/insecticide resistance genes is multi-genic, further studies need to be carried out to find out whether allelic variants exist in the other overexpressed P450s from resistant populations across Africa.

However, the mechanism of pyrethroid resistance in *An. funestus* is complex and non-uniform. For example, allelic variation may not explain all the pyrethroid resistance, for it was not observed in the other major pyrethroid metabolising P450, *CYP6M7* (Riveron et al., 2014a).

Another important frontier to investigate is the role of overexpression compared with allelic variation in *An. funestus*. Which one amongst these two phenomena is more important to insecticide resistance? Overexpression is obviously important for higher turnover of a particular candidate gene, which can make it more abundant to detoxify insecticides, but if and only if the gene product can metabolise the insecticide in question, then activity can be several-fold higher. Coupled with allelic variation through replacement of key residues, the activity can become sharpen via several mechanisms which can modify catalytic activity toward range of substrates, enhancing catalysis.

5.1.2 Key Amino acid Changes Control Pyrethroid Resistance and Could Lead to DNA-based Diagnostic Tools

Site-directed mutagenesis implicated three major amino acid residues in the resistant allele (*MOZCYP6P9b*) which explained high metabolic activity toward pyrethroids, especially the Type II class. These amino acid variants differ in their spatial positioning in the resistant allele compared with the corresponding residues in the allele from the susceptible strain, with different impact on specificity toward pyrethroids. One of these amino acids from resistant allele, a non-polar aliphatic residue (Val^{109}) is a component of *pw2a* tunnel lining residue and involved in substrate-access channelling and enhanced specificity toward pyrethroid insecticides; the second residue, Asp^{335} is positioned away from the putative reductase interacting site 1 at the proximal face of the P450 from resistant strain reducing ionic repulsion with the negatively charged FMN residues involved in electrons transfer; the third residue Asn^{384} located within the loop joining *β-1_4* with *β-2_1* with Asn^{384}-Arg^{385} position both Asn^{384} and Arg^{385} in closer proximity to the pyrethroid insecticide and heme catalytic centre, with the possibility of extensive hydrogen bonding, enhancing catalysis. Knocking down these amino acid variants into residues present in the susceptible strain (Ile^{109}, Glu^{335} and Ser^{384})

resulted in drastic reduction in catalytic activity and affinity towards pyrethroids, especially Type II class, indicating that each of these mutations alone is important for efficient metabolism of pyrethroids. However, it's thought that the presence of these three amino acids in the resistant allele harnessed several mechanisms to optimise catalytic efficiency, through substrate channelling, affinity, enhanced coupling to redox partners and maximal hydrogen bonding interactions.

As this is the first marker of metabolic resistance to pyrethroids involving P450s in the *An. funestus* and/or even other mosquito species, DNA-based diagnostic test was sought to be created for these mutations to allow for tracking them in the field. However, unlike the case of DDT-resistance gene *An. funestus GSTe2* (Leu^{119}Phe substitution) recently described, and the Central and West African *An. funestus Rdl* mutation, *CYP6P9a* and *CYP6P9b* are duplicated genes; these makes it difficult to create a simple diagnostic test like RFLP based on polymorphic site(s).

5.1.3 Pyrethroid Resistance is Multigenic in Field Populations of *An. funestus*

Other candidate genes especially from CYP6 family (*CYP6M7* and *CYP6Z1*) belonging to *rp2* QTL, *rp1* (*CYP6AA4*), *rp3* (*CYP9J11*) and overexpressed in multiple resistant population of *An. funestus* from southern Africa were found to metabolise pyrethroids as well. This clearly established that pyrethroid resistance is more complex than previously thought. The finding of these pyrethroid metabolisers fits the presence of 3 QTLs described previously (Wondji et al., 2009). The impact of multiple genes involved in pyrethroid resistance added another twist to the already complex pattern and makes it difficult to implement resistance management based on straightforward evidences. Examples of these complexities include overexpression as in the case of all the genes from the three QTLs, duplication as in *CYP6P9* and *CYP6P4*, allelic variation as established in *CYP6P9a* and *CYP6P9b* and yet to be investigated in other candidate P450s, and absence of allelic variation explaining resistance as in *CYP6M7*. Nevertheless, P450s from *rp1* QTL occupy a central position in terms of pyrethroid resistance for two reasons: (i) the major resistance genes *CYP6P9a* and *CYP6P9b*, in addition to *CYP6AA4* and other P450s yet to be validated are component of this QTL; (ii) *CYP6P9a* and *CYP6P9b* are the most

consistently overexpressed P450 genes in pyrethroid resistant populations of *An. funestus* across Africa, and (iii) The *rp1* QTL (*CYP6P9a* and *CYP6P9b*) explained 87% of pyrethroid resistance in the FUMOZ lab strain. Thus, decisions on pyrethroid resistance management could be made based on the features of *rp1* QTL genes than attribute of genes from the other two QTLs.

Involvement of multiple P450s in pyrethroid metabolism is not unique to *An. funestus*; it has been described for other mosquito species including *Ae. aegypti* and *An. gambiae* (Stevenson et al., 2012, Edi et al., 2014). For *An. funestus* it remains to be known if these multiple genes are all part of the same pyrethroid resistance network and coordinated via the same mechanism or if they operate independent of one another. Future study notably metabolomics and fingerprinting can help sort this puzzle.

5.1.4 CYP450 Genes Confer Cross Resistance to Bendiocarb and DDT in *An. funestus*

Multiple resistances in *An. funestus* from southern Africa have been documented with CYPs involvement described through synergist assays, biochemical analysis and genome-wide transcription analysis. On the basis of this some of the top upregulated genes were functionally characterised to find out if they can metabolise non-pyrethroid insecticides. It was discovered that *CYP6Z1*, *CYP9J11* and to some extent *CYP6AA4* are bendiocarb metabolisers, while *CYP6Z1* metabolises DDT. These findings are of tremendous importance for it shows that the use of non-pyrethroid insecticides in malaria control as in IRS has great limitations. These P450s especially *CYP6Z1* were found to adapt different mechanism of catalysis for different insecticide substrates in order to achieve optimal detoxification. For example, for bendiocarb and DDT the cross-resistance genes *CYP6Z1* exhibited atypical, allosteric kinetics with distributive catalysis. This kind of allostery has also been described for several CYPs as a strategy to minimize the toxic effect of the toxophore like insecticides. However, the lower up-regulation of these cross-resistance genes (*CYP6Z1*, *CYP9J11* and *CYP6AA4*) and the non-involvement of the top upregulated candidates (*CYP6P9a*, *CYP6P9b* and *CYP6M7*) in metabolism of bendiocarb and DDT indicated that cross resistance is of secondary priority to the pyrethroid

resistance; at least in southern Africa. Cross-resistance P450s have been described for several insect species as well, including *An. gambiae* and *D. melanogaster* (Mitchell et al., 2012, Daborn et al., 2007).

5.2 Conclusion

Drawing from the findings accrued on the course of this study, the following conclusions could be made: (i) the duplicated P450s *CYP6P9a* and *CYP6P9b* are the major pyrethroid resistance genes in *An.* funestus across Africa; (ii) the two genes differ extensively in their active site topology and composition and these differences are responsible for the variation observed in their metabolic profiles; (iii) allelic variation in these genes is impacting their pyrethroid-metabolizing capability, with specific mutations selected and fixed in resistant populations, able to confer high activity towards pyrethroids; (iv) the genes *CYP6P9a* and *CYP6P9b* cannot metabolise representative carbamate (bendiocarb and propoxur), organochlorine (DDT) and organophosphate (malathion) insecticides; the genes are directionally selected specialist enzymes involvedin pyrethroid metabolism. This makes it possible to use non-pyrethroid insecticide as alternative insecticides, for IRS, even when *CYP6P9a* and *CYP6P9b* are overexpressed in *An. funestus*, although other P450s should be taken into consideration; (v) the highly polymorphic *CYP6M7* gene, also a pyrethroid metabolizer, and suspected to sequester propoxur (though evidences are not conclusive) partners with *CYP6P9a* and *CYP6P9b* to confer pyrethroid resistance across southern Africa; (vi) other candidate genes, overexpressed in *An. funestus,* including *CYP6Z1*, *CYP6AA4* and *CYP9J11* metabolises pyrethroid insecticides as well, making the resistance multi-genic; (vii) these second group of genes especially *CYP6Z1* confer cross-resistance to bendiocarb and DDT in the multiple resistant *An. funestus* populations from southern Africa, where other important non-monooxygenase mechanisms like Leu^{119}Phe *GSTe2* mutation is absent; (vii) the finding of cross-resistance genes make pyrethroid resistance phenomena in the major malaria vector, *An. funestus* more complex confounding the problem of resistance management.

5.3 Future Perspectives

The results obtained on the course of this research are in no way exhaustive within the context of monooxygenase-mediated resistance mechanism. Overexpression of the protein of the detoxification gene can be due to changes at transcriptional level, e.g. higher constitutive production of transcripts, due to mutation in promoter sequences, higher inducible expression due to mutations in the *trans*-acting factors or greater responsiveness to transcriptional inducers. This is a frontier that needs to be explored in *An. funestus* detoxification genes, especially in *CYP6P9a* and *CYP6P9b* in order to elucidate what, why and how these genes are switched on and off in relation to the environmental response. Factors responsible for *cis*- or *trans*-regulation of P450s involved in detoxification may also be capable of regulating expression of other P450s that are not necessarily involved in the said resistance (this has been shown to be the case in housefly). Knowing which subsets of P450s are elevated by the same regulatory factors may help to elucidate cross-resistance phenomena.

Herein, we studied mutations at the protein level which can impact on metabolism, e.g. mutations at the catalytic sites that may affect range (qualitative) or rate (quantitative) of substrate metabolism, and mutations in the proximal surface residues that may affect electron transfer from cytochrome P450 reductase and/or cytochrome b_5.

Throughout this research we adopted as surrogates electron transfer partners (cytochrome P450 reductase and cytochrome b_5) from *An. gambiae*. It is possible that the interaction of *An. funestus*-specific electron transfer partners may affect the qualitative and quantitative activity of its CYP450s. Potential mutations in such partners may also possibly alter their coupling with the respective *An. funestus* CYP450s.

The whole picture of the resistance phenomena can only be obtained using metabolomics studies. There is an overwhelming need to find out which subsets of genes are switched on and/or off in response to insecticide exposure, and which intermediates and products are generated from

insecticide metabolisms. These could be achieved using targeted transcriptomics, proteomics and MS/MS. LC/MS could also be utilised to identify the metabolites generated by these P450s, and this could help in piecing together the pyrethroid resistance network.

Modelling simulation has great shortcoming, there is an urgent need to create a crystal structure of the P450s involved in pyrethroids metabolism with the insecticides in its active site. This will greatly facilitate our understanding of the mechanism of action of these P450s, as well as help in design and production of potential synergists that could be used in combination with the insecticide to block the resistance P450s.

Successful site-directed mutagenesis of resistant allele of *CYP6P9a* could potentially reveal the identity of the amino acids responsible for the ability of this gene to metabolize wide range of Type I and Type II pyrethroids. This is important, for the amino acid substitutions that could potentially impact on catalytic activity of *CYP6P9a* mapped to different domains of the P450 compared with those mutations characterised for *CYP6P9b*.

CYP6P9a and *CYP6P9b* are duplicated genes, a phenomenon which makes it challenging to design an easy DNA-based diagnostics, such as PCR-RFLP. More efforts are needed to achieve this goal in order to track *CYP6P9a* and *CYP6P9b* mutations in the field population of *An. funestus* across Africa.

REFERENCE

ABEDI, Z. & BROWN, A. 1961. Peritrophic membrane as vehicle for DDT and DDE excretion in Aedes aegypti larvae. *Annals of the Entomological Society of America,* 54**,** 539-542.

AIZOUN, N., AIKPON, R., PADONOU, G. G., OUSSOU, O., OKE-AGBO, F., GNANGUENON, V., OSSE, R. & AKOGBETO, M. 2013. Mixed-function oxidases and esterases associated with permethrin, deltamethrin and bendiocarb resistance in Anopheles gambiae s.l. in the south-north transect Benin, West Africa. *Parasit Vectors,* 6**,** 223.

ALKER, A. P., KAZADI, W. M., KUTELEMENI, A. K., BLOLAND, P. B., TSHEFU, A. K. & MESHNICK, S. R. 2008. dhfr and dhps genotype and sulfadoxine-pyrimethamine treatment failure in children with falciparum malaria in the Democratic Republic of Congo. *Trop Med Int Health,* 13**,** 1384-91.

ALTALHI, A. D. 2005. Investigation of Mosquito Survival Associated with Bacillus thuringensis israelensis and Aquatic Plant, Lemna minor. *Pakistan Journal of Biological Sciences,* 8**,** 314-317.

ALTSCHUL, S. F., GISH, W., MILLER, W., MYERS, E. W. & LIPMAN, D. J. 1990. Basic local alignment search tool. *J Mol Biol,* 215**,** 403-10.

AMENYA, D. A., NAGURAN, R., LO, T. C., RANSON, H., SPILLINGS, B. L., WOOD, O. R., BROOKE, B. D., COETZEE, M. & KOEKEMOER, L. L. 2008. Over expression of a cytochrome P450 (CYP6P9) in a major African malaria vector, Anopheles Funestus, resistant to pyrethroids. *Insect Mol Biol,* 17**,** 19-25.

AMICHOT, M., TARES, S., BRUN-BARALE, A., ARTHAUD, L., BRIDE, J. M. & BERGE, J. B. 2004. Point mutations associated with insecticide resistance in the Drosophila cytochrome P450 Cyp6a2 enable DDT metabolism. *Eur J Biochem,* 271**,** 1250-7.

ANTO, F., ASOALA, V., ANYORIGIYA, T., ODURO, A., ADJUIK, M., OWUSU-AGYEI, S., DERY, D., BIMI, L. & HODGSON, A. 2009. Insecticide resistance profiles for malaria vectors in the Kassena-Nankana district of Ghana. *Malar J,* 8**,** 81.

ARENSBURGER, P., MEGY, K., WATERHOUSE, R. M., ABRUDAN, J., AMEDEO, P., ANTELO, B., BARTHOLOMAY, L., BIDWELL, S., CALER, E., CAMARA, F., CAMPBELL, C. L., CAMPBELL, K. S., CASOLA, C., CASTRO, M. T., CHANDRAMOULISWARAN, I., CHAPMAN, S. B., CHRISTLEY, S., COSTAS, J., EISENSTADT, E., FESCHOTTE, C., FRASER-LIGGETT, C., GUIGO, R., HAAS, B., HAMMOND, M., HANSSON, B. S., HEMINGWAY, J., HILL, S. R., HOWARTH, C., IGNELL, R., KENNEDY, R. C., KODIRA, C. D., LOBO, N. F., MAO, C., MAYHEW, G., MICHEL, K., MORI, A., LIU, N., NAVEIRA, H., NENE, V., NGUYEN, N., PEARSON, M. D., PRITHAM, E. J., PUIU, D., QI, Y., RANSON, H., RIBEIRO, J. M., ROBERSTON, H. M., SEVERSON, D. W., SHUMWAY, M., STANKE, M., STRAUSBERG, R. L., SUN, C., SUTTON, G., TU, Z. J., TUBIO, J. M., UNGER, M. F., VANLANDINGHAM, D. L., VILELLA, A. J., WHITE, O., WHITE, J. R., WONDJI, C. S., WORTMAN, J., ZDOBNOV, E. M., BIRREN, B., CHRISTENSEN, B. M., COLLINS, F. H., CORNEL, A., DIMOPOULOS, G., HANNICK, L. I., HIGGS, S., LANZARO, G. C., LAWSON, D., LEE, N. H., MUSKAVITCH, M. A., RAIKHEL, A. S. & ATKINSON, P. W. 2010. Sequencing of Culex quinquefasciatus establishes a platform for mosquito comparative genomics. *Science,* 330**,** 86-8.

ARMOUGOM, F., MORETTI, S., POIROT, O., AUDIC, S., DUMAS, P., SCHAELI, B., KEDUAS, V. & NOTREDAME, C. 2006. Expresso: automatic incorporation of structural information in multiple sequence alignments using 3D-Coffee. *Nucleic Acids Res,* 34**,** W604-8.

ASHLEY, E. A., DHORDA, M., FAIRHURST, R. M., AMARATUNGA, C., LIM, P., SUON, S., SRENG, S., ANDERSON, J. M., MAO, S., SAM, B., SOPHA, C., CHUOR, C. M., NGUON, C., SOVANNAROTH, S., PUKRITTAYAKAMEE, S., JITTAMALA, P., CHOTIVANICH, K., CHUTASMIT, K., SUCHATSOONTHORN, C., RUNCHAROEN, R., HIEN, T. T., THUY-NHIEN, N. T., THANH, N. V., PHU, N. H., HTUT, Y., HAN, K. T., AYE, K. H., MOKUOLU, O. A., OLAOSEBIKAN, R. R., FOLARANMI, O. O., MAYXAY, M., KHANTHAVONG, M., HONGVANTHONG, B., NEWTON, P. N., ONYAMBOKO, M. A., FANELLO, C. I., TSHEFU, A. K., MISHRA, N., VALECHA, N., PHYO, A. P.,

NOSTEN, F., YI, P., TRIPURA, R., BORRMANN, S., BASHRAHEIL, M., PESHU, J., FAIZ, M. A., GHOSE, A., HOSSAIN, M. A., SAMAD, R., RAHMAN, M. R., HASAN, M. M., ISLAM, A., MIOTTO, O., AMATO, R., MACINNIS, B., STALKER, J., KWIATKOWSKI, D. P., BOZDECH, Z., JEEYAPANT, A., CHEAH, P. Y., SAKULTHAEW, T., CHALK, J., INTHARABUT, B., SILAMUT, K., LEE, S. J., VIHOKHERN, B., KUNASOL, C., IMWONG, M., TARNING, J., TAYLOR, W. J., YEUNG, S., WOODROW, C. J., FLEGG, J. A., DAS, D., SMITH, J., VENKATESAN, M., PLOWE, C. V., STEPNIEWSKA, K., GUERIN, P. J., DONDORP, A. M., DAY, N. P., WHITE, N. J. & TRACKING RESISTANCE TO ARTEMISININ, C. 2014. Spread of artemisinin resistance in Plasmodium falciparum malaria. *N Engl J Med,* 371**,** 411-23.

ATKINS, W. M. 2004. Implications of the allosteric kinetics of cytochrome P450s. *Drug Discov Today,* 9**,** 478-84.

ATKINS, W. M., LU, W. D. & COOK, D. L. 2002. Is there a toxicological advantage for non-hyperbolic kinetics in cytochrome P450 catalysis? Functional allostery from "distributive catalysis". *J Biol Chem,* 277**,** 33258-66.

AWOLOLA, T., ODUOLA, O., STRODE, C., KOEKEMOER, L., BROOKE, B. & RANSON, H. 2009a. Evidence of multiple pyrethroid resistance mechanisms in the malaria vector Anopheles gambiae sensu stricto from Nigeria. *Transactions of the Royal Society of Tropical Medicine and Hygiene,* 103**,** 1139-1145.

AWOLOLA, T. S., ODUOLA, O. A., STRODE, C., KOEKEMOER, L. L., BROOKE, B. & RANSON, H. 2009b. Evidence of multiple pyrethroid resistance mechanisms in the malaria vector Anopheles gambiae sensu stricto from Nigeria. *Trans R Soc Trop Med Hyg,* 103**,** 1139-45.

BACKES, W. L. & KELLEY, R. W. 2003. Organization of multiple cytochrome P450s with NADPH-cytochrome P450 reductase in membranes. *Pharmacol Ther,* 98**,** 221-33.

BAI, D., LUMMIS, S. C., LEICHT, W., BREER, H. & SATTELLE, D. B. 1991. Actions of imidacloprid and a related nitromethylene on cholinergic receptors of an identified insect motor neurone. *Pesticide science,* 33**,** 197-204.

BAMBAL, R. B. & BLOOMER, J. C. 2006. Screening assay for inhibitors of human cytochrome P-450. Google Patents.

BARNES, H. J., ARLOTTO, M. P. & WATERMAN, M. R. 1991. Expression and enzymatic activity of recombinant cytochrome P450 17 alpha-hydroxylase in Escherichia coli. *Proc Natl Acad Sci U S A,* 88**,** 5597-601.

BAXTER, C. A., MURRAY, C. W., CLARK, D. E., WESTHEAD, D. R. & ELDRIDGE, M. D. 1998. Flexible docking using Tabu search and an empirical estimate of binding affinity. *Proteins,* 33**,** 367-82.

BENVENISTE, I., LESOT, A., HASENFRATZ, M.-P., KOCHS, G. & DURST, F. 1991. Multiple forms of NADPH-cytochrome P450 reductase in higher plants. *Biochemical and biophysical research communications,* 177**,** 105-112.

BERGÉ, J., FEYEREISEN, R. & AMICHOT, M. 1998. Cytochrome P450 monooxygenases and insecticide resistance in insects. *Philosophical Transactions of the Royal Society of London. Series B: Biological Sciences,* 353**,** 1701-1705.

BERMAN, H. M., BATTISTUZ, T., BHAT, T. N., BLUHM, W. F., BOURNE, P. E., BURKHARDT, K., FENG, Z., GILLILAND, G. L., IYPE, L., JAIN, S., FAGAN, P., MARVIN, J., PADILLA, D., RAVICHANDRAN, V., SCHNEIDER, B., THANKI, N., WEISSIG, H., WESTBROOK, J. D. & ZARDECKI, C. 2002. The Protein Data Bank. *Acta Crystallogr D Biol Crystallogr,* 58**,** 899-907.

BHARATE, S. B., PRINS, J. M., GEORGE, K. M. & THOMPSON, C. M. 2010. Thionate versus Oxon: comparison of stability, uptake, and cell toxicity of ((14)CH(3)O)(2)-labeled methyl parathion and methyl paraoxon with SH-SY5Y cells. *J Agric Food Chem,* 58**,** 8460-6.

BIAN, G., JOSHI, D., DONG, Y., LU, P., ZHOU, G., PAN, X., XU, Y., DIMOPOULOS, G. & XI, Z. 2013. Wolbachia invades Anopheles stephensi populations and induces refractoriness to Plasmodium infection. *Science,* 340**,** 748-51.

BLOOMQUIST, J. R. 1996a. Insecticides: chemistries and characteristics. *From Radcliffe's IPM World textbook, University of Minnesota (http://ipmworld. umn. edu/chapters/bloomq. htm. Accessed 08-March-2006)*.
BLOOMQUIST, J. R. 1996b. Ion channels as targets for insecticides. *Annu Rev Entomol,* 41**,** 163-90.
BOETE, C., AGUSTO, F. B. & REEVES, R. G. 2014. Impact of mating behaviour on the success of malaria control through a single inundative release of transgenic mosquitoes. *J Theor Biol,* 347**,** 33-43.
BRADFORD, M. M. 1976. A rapid and sensitive method for the quantitation of microgram quantities of protein utilizing the principle of protein-dye binding. *Anal Biochem,* 72**,** 248-54.
BRAUN, W. & GO, N. 1985. Calculation of protein conformations by proton-proton distance constraints. A new efficient algorithm. *J Mol Biol,* 186**,** 611-26.
BROGDON, W. G. & MCALLISTER, J. C. 1998. Insecticide resistance and vector control. *Emerging infectious diseases,* 4**,** 605.
BROOKE, B. D., KLOKE, G., HUNT, R. H., KOEKEMOER, L. L., TEMU, E. A., TAYLOR, M. E., SMALL, G., HEMINGWAY, J. & COETZEE, M. 2001. Bioassay and biochemical analyses of insecticide resistance in southern African Anopheles funestus (Diptera: Culicidae). *Bull Entomol Res,* 91**,** 265-72.
BROWN, A. W. 1986. Insecticide resistance in mosquitoes: a pragmatic review. *J Am Mosq Control Assoc,* 2**,** 123-40.
BURKE, M. D., THOMPSON, S., ELCOMBE, C. R., HALPERT, J., HAAPARANTA, T. & MAYER, R. T. 1985. Ethoxy-, pentoxy- and benzyloxyphenoxazones and homologues: a series of substrates to distinguish between different induced cytochromes P-450. *Biochem Pharmacol,* 34**,** 3337-45.
BUSVINE, J. 1951. Mechanism of resistance to insecticide in houseflies.
CASIDA, J. E., GAMMON, D. W., GLICKMAN, A. H. & LAWRENCE, L. J. 1983. Mechanisms of selective action of pyrethroid insecticides. *Annu Rev Pharmacol Toxicol,* 23**,** 413-38.
CASIMIRO, S., COLEMAN, M., MOHLOAI, P., HEMINGWAY, J. & SHARP, B. 2006. Insecticide resistance in Anopheles funestus (Diptera: Culicidae) from Mozambique. *J Med Entomol,* 43**,** 267-75.
CASIMIRO, S. L., HEMINGWAY, J., SHARP, B. L. & COLEMAN, M. 2007. Monitoring the operational impact of insecticide usage for malaria control on Anopheles funestus from Mozambique. *Malar J,* 6**,** 142.
CCDC 2011. GOLD User Guide.
CHANDA, E., HEMINGWAY, J., KLEINSCHMIDT, I., REHMAN, A. M., RAMDEEN, V., PHIRI, F. N., COETZER, S., MTHEMBU, D., SHINONDO, C. J., CHIZEMA-KAWESHA, E., KAMULIWO, M., MUKONKA, V., BABOO, K. S. & COLEMAN, M. 2011. Insecticide resistance and the future of malaria control in Zambia. *PLoS One,* 6**,** e24336.
CHANDOR-PROUST, A., BIBBY, J., REGENT-KLOECKNER, M., ROUX, J., GUITTARD-CRILAT, E., POUPARDIN, R., RIAZ, M. A., PAINE, M., DAUPHIN-VILLEMANT, C., REYNAUD, S. & DAVID, J. P. 2013. The central role of mosquito cytochrome P450 CYP6Zs in insecticide detoxification revealed by functional expression and structural modelling. *Biochem J,* 455**,** 75-85.
CHANDRE, F., DARRIET, F., DUCHON, S., FINOT, L., MANGUIN, S., CARNEVALE, P. & GUILLET, P. 2000. Modifications of pyrethroid effects associated with kdr mutation in Anopheles gambiae. *Medical and veterinary entomology,* 14**,** 81-88.
CHARLWOOD, J., SMITH, T., KIHONDA, J., HEIZ, B., BILLINGSLEY, P. & TAKKEN, W. 1995. Density independent feeding success of malaria vectors (Diptera: Culicidae) in Tanzania. *Bulletin of Entomological Research,* 85**,** 29-35.
CHIU, T. L., WEN, Z., RUPASINGHE, S. G. & SCHULER, M. A. 2008. Comparative molecular modeling of Anopheles gambiae CYP6Z1, a mosquito P450 capable of metabolizing DDT. *Proc Natl Acad Sci U S A,* 105**,** 8855-60.
CHRISTIAN, R., STRODE, C., RANSON, H., COETZER, N., COETZEE, M. & KOEKEMOER, L. L. 2011. Microarray analysis of a pyrethroid resistant African malaria vector,< i> Anopheles funestus</i>, from southern Africa. *Pesticide Biochemistry and Physiology,* 99**,** 140-147.

CLARKE, S. E., BOGH, C., BROWN, R. C., PINDER, M., WALRAVEN, G. E. & LINDSAY, S. W. 2001a. Do untreated bednets protect against malaria? *Trans R Soc Trop Med Hyg,* 95**,** 457-62.
CLARKE, S. E., BØGH, C., BROWN, R. C., PINDER, M., WALRAVEN, G. E. & LINDSAY, S. W. 2001b. Do untreated bednets protect against malaria? *Transactions of the royal society of tropical medicine and hygiene,* 95**,** 457-462.
CLAUDIANOS, C., RANSON, H., JOHNSON, R., BISWAS, S., SCHULER, M., BERENBAUM, M., FEYEREISEN, R. & OAKESHOTT, J. 2006. A deficit of detoxification enzymes: pesticide sensitivity and environmental response in the honeybee. *Insect molecular biology,* 15**,** 615-636.
COETZEE, M. & FONTENILLE, D. 2004. Advances in the study of Anopheles funestus, a major vector of malaria in Africa. *Insect Biochem Mol Biol,* 34**,** 599-605.
COETZEE, M., HUNT, R. H., WILKERSON, R., DELLA TORRE, A., COULIBALY, M. B. & BESANSKY, N. J. 2013. Anopheles coluzzii and Anopheles amharicus, new members of the Anopheles gambiae complex. *Zootaxa,* 3619**,** 246-274.
COETZEE, M. & KOEKEMOER, L. L. 2013. Molecular systematics and insecticide resistance in the major African malaria vector Anopheles funestus. *Annu Rev Entomol,* 58**,** 393-412.
COETZEE, M., VAN WYK, P., BOOMAN, M., KOEKEMOER, L. L. & HUNT, R. H. 2006. Insecticide resistance in malaria vector mosquitoes in a gold mining town in Ghana and implications for malaria control. *Bull Soc Pathol Exot,* 99**,** 400-3.
COHEN, M. B., KOENER, J. F. & FEYEREISEN, R. 1994. Structure and chromosomal localization of CYP6A1, a cytochrome P450-encoding gene from the house fly. *Gene,* 146**,** 267-72.
COJOCARU, V., WINN, P. J. & WADE, R. C. 2007. The ins and outs of cytochrome P450s. *Biochim Biophys Acta,* 1770**,** 390-401.
COLOVOS, C. & YEATES, T. O. 1993. Verification of protein structures: patterns of nonbonded atomic interactions. *Protein Sci,* 2**,** 1511-9.
COPELAND, R. A. 2004. *Enzymes: a practical introduction to structure, mechanism, and data analysis*, John Wiley & Sons.
CORBEL, V. & N'GUESSAN, R. 2013. Distribution, mechanisms, impact and management of insecticide resistance in malaria vectors: a pragmatic review.
COX, F. E. 2010. History of the discovery of the malaria parasites and their vectors. *Parasit Vectors,* 3**,** 5.
CROSBY, D. 1971. Minor insecticides of plant origin. *Naturally occurring insecticides***,** 177-239.
CUAMBA, N., MORGAN, J. C., IRVING, H., STEVEN, A. & WONDJI, C. S. 2010. High level of pyrethroid resistance in an Anopheles funestus population of the Chokwe District in Mozambique. *PLoS One,* 5**,** e11010.
CURTIS, C. 1992. Personal protection methods against vectors of disease. *Rev Med Vet Entomol,* 80**,** 543-53.
CURTIS, C. F. 1989. Malaria control through anti-mosquito measures. *J R Soc Med,* 82 Suppl 17**,** 18-21; discussion 21-2.
DABIRE, K. R., BALDET, T., DIABATE, A., DIA, I., COSTANTINI, C., COHUET, A., GUIGUEMDE, T. R. & FONTENILLE, D. 2007. Anopheles funestus (Diptera: Culicidae) in a humid savannah area of western Burkina Faso: bionomics, insecticide resistance status, and role in malaria transmission. *J Med Entomol,* 44**,** 990-7.
DABORN, P. J., LUMB, C., BOEY, A., WONG, W., FFRENCH-CONSTANT, R. H. & BATTERHAM, P. 2007. Evaluating the insecticide resistance potential of eight Drosophila melanogaster cytochrome P450 genes by transgenic over-expression. *Insect Biochem Mol Biol,* 37**,** 512-9.
DADD, R., KERKUT, G. & GILBERT, L. 1985. Comprehensive insect physiology, biochemistry and pharmacology. *Comprehensive insect physiology, biochemistry and pharmacology,* 4.
DAVIDSON, G. 1957. Insecticide resistance in Anopheles sundaicus. *Nature,* 4598**,** 1333-1335.
DAVIES, T. G., FIELD, L. M., USHERWOOD, P. N. & WILLIAMSON, M. S. 2007. DDT, pyrethrins, pyrethroids and insect sodium channels. *IUBMB Life,* 59**,** 151-62.

DAWSON, J. H., HOLM, R. H., TRUDELL, J. R., BARTH, G., LINDER, R. E., BUNNENBERG, E., DJERASSI, C. & TANG, S. C. 1976. Letter: Oxidized cytochrome P-450. Magnetic circular dichroism evidence for thiolate ligation in the substrate-bound form. Implications for the catalytic mechanism. *J Am Chem Soc,* 98**,** 3707-8.

DE MONTELLANO, P. R. O. 2005. *Cytochrome P450: structure, mechanism, and biochemistry*, Springer.

DE RIENZO, F., FANELLI, F., MENZIANI, M. C. & DE BENEDETTI, P. G. 2000. Theoretical investigation of substrate specificity for cytochromes P450 IA2, P450 IID6 and P450 IIIA4. *J Comput Aided Mol Des,* 14**,** 93-116.

DIA, I., GUELBEOGO, M. W. & AYALA, D. 2013. Advances and Perspectives in the Study of the Malaria Mosquito Anopheles funestus. INTECH.

DJOUAKA, R., IRVING, H., TUKUR, Z. & WONDJI, C. S. 2011. Exploring mechanisms of multiple insecticide resistance in a population of the malaria vector *Anopheles funestus* in Benin. *PLoS One,* 6**,** e27760.

DU, W., AWOLOLA, T. S., HOWELL, P., KOEKEMOER, L. L., BROOKE, B. D., BENEDICT, M. Q., COETZEE, M. & ZHENG, L. 2005. Independent mutations in the Rdl locus confer dieldrin resistance to Anopheles gambiae and An. arabiensis. *Insect Mol Biol,* 14**,** 179-83.

DU, Y., NOMURA, Y., LUO, N., LIU, Z., LEE, J. E., KHAMBAY, B. & DONG, K. 2009. Molecular determinants on the insect sodium channel for the specific action of type II pyrethroid insecticides. *Toxicol Appl Pharmacol,* 234**,** 266-72.

DUANGKAEW, P., PETHUAN, S., KAEWPA, D., BOONSUEPSAKUL, S., SARAPUSIT, S. & RONGNOPARUT, P. 2011. Characterization of mosquito CYP6P7 and CYP6AA3: differences in substrate preference and kinetic properties. *Arch Insect Biochem Physiol,* 76**,** 236-48.

DUFFY, J. B. 2002. GAL4 system in Drosophila: a fly geneticist's Swiss army knife. *Genesis,* 34**,** 1-15.

DÜRR, U. H., WASKELL, L. & RAMAMOORTHY, A. 2007. The cytochromes P450 and their reductases—Promising targets for structural studies by advanced solid-state NMR spectroscopy. *Biochimica et Biophysica Acta (BBA)-Biomembranes,* 1768**,** 3235-3259.

EDI, C. V., DJOGBENOU, L., JENKINS, A. M., REGNA, K., MUSKAVITCH, M. A., POUPARDIN, R., JONES, C. M., ESSANDOH, J., KETOH, G. K., PAINE, M. J., KOUDOU, B. G., DONNELLY, M. J., RANSON, H. & WEETMAN, D. 2014. CYP6 P450 enzymes and ACE-1 duplication produce extreme and multiple insecticide resistance in the malaria mosquito Anopheles gambiae. *PLoS Genet,* 10**,** e1004236.

ELDRIDGE, M. D., MURRAY, C. W., AUTON, T. R., PAOLINI, G. V. & MEE, R. P. 1997. Empirical scoring functions: I. The development of a fast empirical scoring function to estimate the binding affinity of ligands in receptor complexes. *J Comput Aided Mol Des,* 11**,** 425-45.

ELLIOTT, D. A. & BRAND, A. H. 2008. The GAL4 system : a versatile system for the expression of genes. *Methods Mol Biol,* 420**,** 79-95.

ELLIOTT, M., FARNHAM, A., JANES, N., NEEDHAM, P., PULMAN, D. & STEVENSON, J. 1973. A photostable pyrethroid.

ESTABROOK, R. W., HILDEBRANDT, A. G., BARON, J., NETTER, K. J. & LEIBMAN, K. 1971. A new spectral intermediate associated with cytochrome P-450 function in liver microsomes. *Biochem Biophys Res Commun,* 42**,** 132-9.

FARNHAM, A. W., MURRAY, A. W., SAWICKI, R. M., DENHOLM, I. & WHITE, J. C. 1987. Characterization of the structure-activity relationship of kdr and two variants of super-kdr to pyrethroids in the housefly (Musca domestica L.). *Pesticide science,* 19**,** 209-220.

FEYEREISEN, R. 2005. Insect cytochrome P450. *Comprehensive molecular insect science,* 4**,** 1-77.

FEYEREISEN, R. 2006. Evolution of insect P450. *Biochemical Society Transactions,* 34**,** 1252-1255.

FEYEREISEN, R. 2011. Arthropod CYPomes illustrate the tempo and mode in P450 evolution. *Biochim Biophys Acta,* 1814**,** 19-28.

FEYEREISEN, R. 2012. Insect CYP genes and P450 enzymes. *Insect molecular biology and biochemistry***,** 236-316.

FEYEREISEN, R., KOENER, J. F., FARNSWORTH, D. E. & NEBERT, D. W. 1989. Isolation and sequence of cDNA encoding a cytochrome P-450 from an insecticide-resistant strain of the house fly, Musca domestica. *Proc Natl Acad Sci U S A,* 86**,** 1465-9.

FILLINGER, U. & LINDSAY, S. W. 2011. Larval source management for malaria control in Africa: myths and reality. *Malar J,* 10**,** 353.

FISER, A., DO, R. K. & SALI, A. 2000. Modeling of loops in protein structures. *Protein Sci,* 9**,** 1753-73.

FISER, A. & SALI, A. 2003. Modeller: generation and refinement of homology-based protein structure models. *Methods Enzymol,* 374**,** 461-91.

FLANAGAN, J. U., MCLAUGHLIN, L. A., PAINE, M. J., SUTCLIFFE, M. J., ROBERTS, G. C. & WOLF, C. R. 2003. Role of conserved Asp293 of cytochrome P450 2C9 in substrate recognition and catalytic activity. *Biochem J,* 370**,** 921-6.

FONTENILLE, D., LEPERS, J. P., CAMPBELL, G. H., COLUZZI, M., RAKOTOARIVONY, I. & COULANGES, P. 1990. Malaria transmission and vector biology in Manarintsoa, high plateaux of Madagascar. *Am J Trop Med Hyg,* 43**,** 107-15.

FOOTE, S., KYLE, D., MARTIN, R., ODUOLA, A., FORSYTH, K., KEMP, D. & COWMAN, A. 1990. Several alleles of the multidrug-resistance gene are closely linked to chloroquine resistance in Plasmodium falciparum.

FOURNIER, D. 2005. Mutations of acetylcholinesterase which confer insecticide resistance in insect populations. *Chem Biol Interact,* 157-158**,** 257-61.

FRADIN, M. S. & DAY, J. F. 2002. Comparative efficacy of insect repellents against mosquito bites. *N Engl J Med,* 347**,** 13-8.

FUKUTO, T. R. 1990. Mechanism of action of organophosphorus and carbamate insecticides. *Environ Health Perspect,* 87**,** 245-54.

GAMAGE-MENDIS, A. C., CARTER, R., MENDIS, C., DE ZOYSA, A. P., HERATH, P. R. & MENDIS, K. N. 1991. Clustering of malaria infections within an endemic population: risk of malaria associated with the type of housing construction. *Am J Trop Med Hyg,* 45**,** 77-85.

GAN, L., VON MOLTKE, L. L., TREPANIER, L. A., HARMATZ, J. S., GREENBLATT, D. J. & COURT, M. H. 2009. Role of NADPH-cytochrome P450 reductase and cytochrome-b5/NADH-b5 reductase in variability of CYP3A activity in human liver microsomes. *Drug Metab Dispos,* 37**,** 90-6.

GANDHI, R., VARAK, E. & GOLDBERG, M. L. 1992. Molecular analysis of a cytochrome P450 gene of family 4 on the Drosophila X chromosome. *DNA Cell Biol,* 11**,** 397-404.

GILBERT, L. I. & GILL, S. S. 2010. *Insect control: biological and synthetic agents*, Academic Press.

GILLES, M. & DE MEILLON, B. 1968. The Anophelinae of Africa South of Sahara (Ethiopian Zoogeographical Region). *Publication of the South African Institute for Medical Research,* 54**,** 127-150.

GILLIES, M., COETZEE, M. 1987. *A supplement to anophelinae of Africa south of Sahara (Afro-tropical region).* .

GOHLKE, H., HENDLICH, M. & KLEBE, G. 2000. Knowledge-based scoring function to predict protein-ligand interactions. *J Mol Biol,* 295**,** 337-56.

GOLD, B. & BRUNK, G. 1983. Metabolism of 1, 1, 1-trichloro-2, 2-bis (p-chlorophenyl) ethane (DDT), 1, 1-dichloro-2, 2-bis (p-chlorophenyl) ethane, and 1-chloro-2, 2-bis (p-chlorophenyl) ethene in the hamster. *Cancer research,* 43**,** 2644-2647.

GONZALEZ, F. J. & KORZEKWA, K. R. 1995. Cytochromes P450 expression systems. *Annual review of pharmacology and toxicology,* 35**,** 369-390.

GOODSELL, D. S., MORRIS, G. M. & OLSON, A. J. 1996. Automated docking of flexible ligands: applications of AutoDock. *J Mol Recognit,* 9**,** 1-5.

GOTOH, O. 1992. Substrate recognition sites in cytochrome P450 family 2 (CYP2) proteins inferred from comparative analyses of amino acid and coding nucleotide sequences. *J Biol Chem,* 267**,** 83-90.

GREENWOOD, B. M. & TARGETT, G. A. 2011. Malaria vaccines and the new malaria agenda. *Clin Microbiol Infect,* 17**,** 1600-7.

GREGORY, R., DARBY, A. C., IRVING, H., COULIBALY, M. B., HUGHES, M., KOEKEMOER, L. L., COETZEE, M., RANSON, H., HEMINGWAY, J., HALL, N. & WONDJI, C. S. 2011. A de novo expression profiling of Anopheles funestus, malaria vector in Africa, using 454 pyrosequencing. *PLoS One,* 6**,** e17418.

GUENGERICH, F. P. 2005. Reduction of cytochrome b5 by NADPH-cytochrome P450 reductase. *Arch Biochem Biophys,* 440**,** 204-11.

GUERRA, C. A., GIKANDI, P. W., TATEM, A. J., NOOR, A. M., SMITH, D. L., HAY, S. I. & SNOW, R. W. 2008. The limits and intensity of Plasmodium falciparum transmission: implications for malaria control and elimination worldwide. *PLoS Med,* 5**,** e38.

GUPTA, R. C. 2011. *Toxicology of organophosphate & carbamate compounds*, Academic Press.

GUPTA, R. C. 2014. *Biomarkers in Toxicology*, Academic Press.

GUZOV, V. M., HOUSTON, H. L., MURATALIEV, M. B., WALKER, F. A. & FEYEREISEN, R. 1996. Molecular cloning, overexpression in Escherichia coli, structural and functional characterization of house fly cytochrome b5. *J Biol Chem,* 271**,** 26637-45.

HALL, T. A. BioEdit: a user-friendly biological sequence alignment editor and analysis program for Windows 95/98/NT. Nucleic acids symposium series, 1999. 95-98.

HARBACH, R. E. 2004. The classification of genus Anopheles (Diptera: Culicidae): a working hypothesis of phylogenetic relationships. *Bull Entomol Res,* 94**,** 537-53.

HARGREAVES, K., HUNT, R. H., BROOKE, B. D., MTHEMBU, J., WEETO, M. M., AWOLOLA, T. S. & COETZEE, M. 2003. Anopheles arabiensis and An. quadriannulatus resistance to DDT in South Africa. *Med Vet Entomol,* 17**,** 417-22.

HARGREAVES, K., KOEKEMOER, L. L., BROOKE, B. D., HUNT, R. H., MTHEMBU, J. & COETZEE, M. 2000. Anopheles funestus resistant to pyrethroid insecticides in South Africa. *Med Vet Entomol,* 14**,** 181-9.

HASEMANN, C. A., KURUMBAIL, R. G., BODDUPALLI, S. S., PETERSON, J. A. & DEISENHOFER, J. 1995. Structure and function of cytochromes P450: a comparative analysis of three crystal structures. *Structure,* 3**,** 41-62.

HAWKINS, D. R., KIRKPATRICK, D., EWEN, B., MIDGLEY, I., BIGGS, S.R.,WHITBY, B.R., 1985. The biokinetics and metabolism of 14C-

ethofenprox in the rat. Japan.

HELINSKI, M. E., PARKER, A. G. & KNOLS, B. G. 2006. Radiation-induced sterility for pupal and adult stages of the malaria mosquito Anopheles arabiensis. *Malar J,* 5**,** 41.

HELINSKI, M. E., PARKER, A. G. & KNOLS, B. G. 2009. Radiation biology of mosquitoes. *Malar J,* 8 Suppl 2**,** S6.

HEMINGWAY, J. 1983. The genetics of malathion resistance in Anopheles stephensi from Pakistan. *Trans R Soc Trop Med Hyg,* 77**,** 106-8.

HEMINGWAY, J. 2014. The role of vector control in stopping the transmission of malaria: threats and opportunities. *Philos Trans R Soc Lond B Biol Sci,* 369**,** 20130431.

HEMINGWAY, J., HAWKES, N. J., MCCARROLL, L. & RANSON, H. 2004. The molecular basis of insecticide resistance in mosquitoes. *Insect Biochem Mol Biol,* 34**,** 653-65.

HEMINGWAY, J. & RANSON, H. 2000. Insecticide resistance in insect vectors of human disease. *Annu Rev Entomol,* 45**,** 371-91.

HERATH, P. R., MILES, S. J. & DAVIDSON, G. 1981. Fenitrothion (OMS 43) resistance in the taxon Anopheles culicifacies Giles. *J Trop Med Hyg,* 84**,** 87-8.

HIROYA, K., MURAKAMI, Y., SHIMIZU, T., HATANO, M. & ORTIZ DE MONTELLANO, P. R. 1994. Differential roles of Glu318 and Thr319 in cytochrome P450 1A2 catalysis supported by NADPH-cytochrome P450 reductase and tert-butyl hydroperoxide. *Arch Biochem Biophys,* 310**,** 397-401.

HLAVICA, P. 1984. On the function of cytochrome b5 in the cytochrome P-450-dependent oxygenase system. *Arch Biochem Biophys,* 228**,** 600-8.

HLAVICA, P. & LEWIS, D. F. 2001. Allosteric phenomena in cytochrome P450-catalyzed monooxygenations. *Eur J Biochem,* 268**,** 4817-32.
HODGSON, E. 1983. The significance of cytochrome P-450 in insects. *Insect Biochemistry,* 13**,** 237-246.
HOFFMANN, A., MONTGOMERY, B., POPOVICI, J., ITURBE-ORMAETXE, I., JOHNSON, P., MUZZI, F., GREENFIELD, M., DURKAN, M., LEONG, Y. S. & DONG, Y. 2011. Successful establishment of Wolbachia in Aedes populations to suppress dengue transmission. *Nature,* 476**,** 454-457.
HOLMANS, P. L., SHET, M. S., MARTIN-WIXTROM, C. A., FISHER, C. W. & ESTABROOK, R. W. 1994. The high-level expression in Escherichia coli of the membrane-bound form of human and rat cytochrome b5 and studies on their mechanism of function. *Arch Biochem Biophys,* 312**,** 554-65.
HOVEMANN, B. T., SEHLMEYER, F. & MALZ, J. 1997. Drosophila melanogaster NADPH-cytochrome P450 oxidoreductase: pronounced expression in antennae may be related to odorant clearance. *Gene,* 189**,** 213-9.
HSIN, C. & COATS, J. 1987. Bendiocarb metabolism in adults and larvae of the southern corn rootworm, Diabrotica undecimpunctata howardi. *Journal of Pesticide Science,* 12**,** 405-413.
HUNT, R., EDWARDES, M. & COETZEE, M. 2010. Pyrethroid resistance in southern African Anopheles funestus extends to Likoma Island in Lake Malawi. *Parasit Vectors,* 3**,** 122.
HUNT, R. H., BROOKE, B. D., PILLAY, C., KOEKEMOER, L. L. & COETZEE, M. 2005. Laboratory selection for and characteristics of pyrethroid resistance in the malaria vector Anopheles funestus. *Med Vet Entomol,* 19**,** 271-5.
HUNT, R. H., FUSEINI, G., KNOWLES, S., STILES-OCRAN, J., VERSTER, R., KAISER, M. L., CHOI, K. S., KOEKEMOER, L. L. & COETZEE, M. 2011. Insecticide resistance in malaria vector mosquitoes at four localities in Ghana, West Africa. *Parasit Vectors,* 4**,** 107.
IM, S. C. & WASKELL, L. 2011. The interaction of microsomal cytochrome P450 2B4 with its redox partners, cytochrome P450 reductase and cytochrome b(5). *Arch Biochem Biophys,* 507**,** 144-53.
IMAI, Y. & SATO, R. 1977. The roles of cytochrome b5 in a reconstituted N-demethylase system containing cytochrome P-450. *Biochem Biophys Res Commun,* 75**,** 420-6.
IMBAHALE, S. S., MWERESA, C. K., TAKKEN, W. & MUKABANA, W. R. 2011. Development of environmental tools for anopheline larval control. *Parasit Vectors,* 4**,** 130.
IRVING, H., RIVERON, J. M., IBRAHIM, S. S., LOBO, N. F. & WONDJI, C. S. 2012. Positional cloning of rp2 QTL associates the P450 genes CYP6Z1, CYP6Z3 and CYP6M7 with pyrethroid resistance in the malaria vector Anopheles funestus. *Heredity (Edinb),* 109**,** 383-92.
IRWIN, J. J. & SHOICHET, B. K. 2005. ZINC--a free database of commercially available compounds for virtual screening. *J Chem Inf Model,* 45**,** 177-82.
JEFFERIES, P. R., TOIA, R. F., BRANNIGAN, B., PESSAH, I. & CASIDA, J. E. 1992. Ryania insecticide: analysis and biological activity of 10 natural ryanoids. *Journal of agricultural and food chemistry,* 40**,** 142-146.
JONES, G., WILLETT, P., GLEN, R. C., LEACH, A. R. & TAYLOR, R. 1997. Development and validation of a genetic algorithm for flexible docking. *J Mol Biol,* 267**,** 727-48.
JOUSSEN, N., HECKEL, D. G., HAAS, M., SCHUPHAN, I. & SCHMIDT, B. 2008. Metabolism of imidacloprid and DDT by P450 CYP6G1 expressed in cell cultures of Nicotiana tabacum suggests detoxification of these insecticides in Cyp6g1-overexpressing strains of Drosophila melanogaster, leading to resistance. *Pest Manag Sci,* 64**,** 65-73.
KAJBAF, M., LONGHI, R., MONTANARI, D., VINCO, F., RIGO, M., FONTANA, S. & READ, K. D. 2011. A comparative study of the CYP450 inhibition potential of marketed drugs using two fluorescence based assay platforms routinely used in the pharmaceutical industry. *Drug Metab Lett,* 5**,** 30-9.
KARUNAMOORTHI, K. 2014. Malaria vaccine: a future hope to curtail the global malaria burden. *Int J Prev Med,* 5**,** 529-38.

KARUNAMOORTHI, K. & SABESAN, S. 2009. Field trials on the efficacy of DEET-impregnated anklets, wristbands, shoulder, and pocket strips against mosquito vectors of disease. *Parasitol Res,* 105**,** 641-5.

KARUNARATNE, S. P., HEMINGWAY, J., JAYAWARDENA, K. G., DASSANAYAKA, V. & VAUGHAN, A. 1995. Kinetic and molecular differences in the amplified and non-amplified esterases from insecticide-resistant and susceptible Culex quinquefasciatus mosquitoes. *Journal of Biological Chemistry,* 270**,** 31124-31128.

KASAI, S., WEERASHINGHE, I. S. & SHONO, T. 1998. P450 monooxygenases are an important mechanism of permethrin resistance in Culex quinquefasciatus Say larvae. *Archives of insect biochemistry and physiology,* 37**,** 47-56.

KAWADA, H., DIDA, G. O., OHASHI, K., KOMAGATA, O., KASAI, S., TOMITA, T., SONYE, G., MAEKAWA, Y., MWATELE, C., NJENGA, S. M., MWANDAWIRO, C., MINAKAWA, N. & TAKAGI, M. 2011. Multimodal pyrethroid resistance in malaria vectors, Anopheles gambiae s.s., Anopheles arabiensis, and Anopheles funestus s.s. in western Kenya. *PLoS One,* 6**,** e22574.

KEMP, C. A., FLANAGAN, J. U., VAN ELDIK, A. J., MARECHAL, J. D., WOLF, C. R., ROBERTS, G. C., PAINE, M. J. & SUTCLIFFE, M. J. 2004. Validation of model of cytochrome P450 2D6: an in silico tool for predicting metabolism and inhibition. *J Med Chem,* 47**,** 5340-6.

KENAAN, C., ZHANG, H., SHEA, E. V. & HOLLENBERG, P. F. 2011. Uncovering the role of hydrophobic residues in cytochrome P450-cytochrome P450 reductase interactions. *Biochemistry,* 50**,** 3957-67.

KILLEEN, G. F., SMITH, T. A., FERGUSON, H. M., MSHINDA, H., ABDULLA, S., LENGELER, C. & KACHUR, S. P. 2007. Preventing childhood malaria in Africa by protecting adults from mosquitoes with insecticide-treated nets. *PLoS Med,* 4**,** e229.

KITAMURA, S., SHIMIZU, Y., SHIRAGA, Y., YOSHIDA, M., SUGIHARA, K. & OHTA, S. 2002. Reductive metabolism of p,p'-DDT and o,p'-DDT by rat liver cytochrome P450. *Drug Metab Dispos,* 30**,** 113-8.

KNIPLING, E. F. 1959. Sterile-male method of population control. *Science,* 130**,** 902-4.

KOEKEMOER, L., KAMAU, L., HUNT, R. & COETZEE, M. 2002. A cocktail polymerase chain reaction assay to identify members of the Anopheles funestus (Diptera: Culicidae) group. *The American journal of tropical medicine and hygiene,* 66**,** 804-811.

KOENER, J. F., CARINO, F. A. & FEYEREISEN, R. 1993. The cDNA and deduced protein sequence of house fly NADPH-cytochrome P450 reductase. *Insect Biochem Mol Biol,* 23**,** 439-47.

KRIEGER, R. 2010. *Hayes' handbook of pesticide toxicology*, Academic press.

KUHR, R. J. 1970. Metabolism of carbamate insecticide chemicals in plants and insects. *Journal of Agricultural and Food Chemistry,* 18**,** 1023-1030.

KULA, M. E., ALLAY, E. R. & ROZEK, C. E. 1995. Evolutionary divergence of the cytochrome b5 gene of Drosophila. *J Mol Evol,* 41**,** 430-9.

LAI, F. A. & MEISSNER, G. 1989. The muscle ryanodine receptor and its intrinsic Ca2+ channel activity. *Journal of bioenergetics and biomembranes,* 21**,** 227-246.

LASKOWSKI, D. A. 2002. Physical and chemical properties of pyrethroids. *Rev Environ Contam Toxicol,* 174**,** 49-170.

LENGELER, C. 2000. Insecticide-treated bednets and curtains for preventing malaria. *Cochrane Database Syst Rev***,** CD000363.

LERTKIATMONGKOL, P., JENWITHEESUK, E. & RONGNOPARUT, P. 2011. Homology modeling of mosquito cytochrome P450 enzymes involved in pyrethroid metabolism: insights into differences in substrate selectivity. *BMC Res Notes,* 4**,** 321.

LESK, A. M. & CHOTHIA, C. 1980. How different amino acid sequences determine similar protein structures: the structure and evolutionary dynamics of the globins. *J Mol Biol,* 136**,** 225-70.

LI, S. & WILKINSON, M. 1997. Site-directed mutagenesis: a two-step method using PCR and DpnI. *Biotechniques,* 23**,** 588-590.

LI, Y., FARNSWORTH, C. A., COPPIN, C. W., TEESE, M. G., LIU, J. W., SCOTT, C., ZHANG, X., RUSSELL, R. J. & OAKESHOTT, J. G. 2013. Organophosphate and pyrethroid hydrolase activities of mutant Esterases from the cotton bollworm Helicoverpa armigera. *PLoS One,* 8**,** e77685.

LIBRADO, P. & ROZAS, J. 2009. DnaSP v5: a software for comprehensive analysis of DNA polymorphism data. *Bioinformatics,* 25**,** 1451-2.

LINES, J. 1996. Review: mosquito nets and insecticides for net treatment: a discussion of existing and potential distribution systems in Africa. *Trop Med Int Health,* 1**,** 616-32.

LIU, N. & SCOTT, J. G. 1998. Increased transcription of CYP6D1 causes cytochrome P450-mediated insecticide resistance in house fly. *Insect Biochem Mol Biol,* 28**,** 531-5.

LIU, N. & YUE, X. 2000. Insecticide resistance and cross-resistance in the house fly (Diptera: Muscidae). *Journal of economic entomology,* 93**,** 1269-1275.

LUPETTI, A., DANESI, R., CAMPA, M., DEL TACCA, M. & KELLY, S. 2002. Molecular basis of resistance to azole antifungals. *Trends Mol Med,* 8**,** 76-81.

LWETOIJERA, D. W., KIWARE, S. S., MAGENI, Z. D., DONGUS, S., HARRIS, C., DEVINE, G. J. & MAJAMBERE, S. 2013. A need for better housing to further reduce indoor malaria transmission in areas with high bed net coverage. *Parasit Vectors,* 6**,** 57.

LYND, A. & LYCETT, G. J. 2012. Development of the bi-partite Gal4-UAS system in the African malaria mosquito, Anopheles gambiae. *PLoS One,* 7**,** e31552.

MACARTHUR, M. W. & THORNTON, J. M. 1991. Influence of proline residues on protein conformation. *J Mol Biol,* 218**,** 397-412.

MACKERELL, A. D., BASHFORD, D., BELLOTT, M., DUNBRACK, R. L., EVANSECK, J. D., FIELD, M. J., FISCHER, S., GAO, J., GUO, H., HA, S., JOSEPH-MCCARTHY, D., KUCHNIR, L., KUCZERA, K., LAU, F. T., MATTOS, C., MICHNICK, S., NGO, T., NGUYEN, D. T., PRODHOM, B., REIHER, W. E., ROUX, B., SCHLENKRICH, M., SMITH, J. C., STOTE, R., STRAUB, J., WATANABE, M., WIORKIEWICZ-KUCZERA, J., YIN, D. & KARPLUS, M. 1998. All-atom empirical potential for molecular modeling and dynamics studies of proteins. *J Phys Chem B,* 102**,** 3586-616.

MAO, W., RUPASINGHE, S. G., ZANGERL, A. R., BERENBAUM, M. R. & SCHULER, M. A. 2007. Allelic variation in the Depressaria pastinacella CYP6AB3 protein enhances metabolism of plant allelochemicals by altering a proximal surface residue and potential interactions with cytochrome P450 reductase. *J Biol Chem,* 282**,** 10544-52.

MARECHAL, J. D., YU, J., BROWN, S., KAPELIOUKH, I., RANKIN, E. M., WOLF, C. R., ROBERTS, G. C., PAINE, M. J. & SUTCLIFFE, M. J. 2006. In silico and in vitro screening for inhibition of cytochrome P450 CYP3A4 by comedications commonly used by patients with cancer. *Drug Metab Dispos,* 34**,** 534-8.

MARTINEZ-TORRES, D., CHANDRE, F., WILLIAMSON, M. S., DARRIET, F., BERGE, J. B., DEVONSHIRE, A. L., GUILLET, P., PASTEUR, N. & PAURON, D. 1998. Molecular characterization of pyrethroid knockdown resistance (kdr) in the major malaria vector *Anopheles gambiae s.s. Insect Mol Biol,* 7**,** 179-84.

MATAMBO, T. S., PAINE, M. J., COETZEE, M. & KOEKEMOER, L. L. 2010. Sequence characterization of cytochrome P450 CYP6P9 in pyrethroid resistant and susceptible Anopheles funestus (Diptera: Culicidae). *Genet Mol Res,* 9**,** 554-64.

MATIAS, J. R. & ADRIAS, A. Q. 2010. The use of annual killifish in the biocontrol of the aquatic stages of mosquitoes in temporary bodies of fresh water; a potential new tool in vector control. *Parasit Vectors,* 3**,** 46.

MATSUDA, K., BUCKINGHAM, S. D., KLEIER, D., RAUH, J. J., GRAUSO, M. & SATTELLE, D. B. 2001. Neonicotinoids: insecticides acting on insect nicotinic acetylcholine receptors. *Trends Pharmacol Sci,* 22**,** 573-80.

MATSUMURA, F. 1985. *Toxicology of insecticides*, Plenum Press New York.

MCCANN, R. S., OCHOMO, E., BAYOH, M. N., VULULE, J. M., HAMEL, M. J., GIMNIG, J. E., HAWLEY, W. A. & WALKER, E. D. 2014. Reemergence of Anopheles funestus as a vector of Plasmodium

falciparum in western Kenya after long-term implementation of insecticide-treated bed nets. *Am J Trop Med Hyg,* 90**,** 597-604.
MCLAUGHLIN, L. A., NIAZI, U., BIBBY, J., DAVID, J. P., VONTAS, J., HEMINGWAY, J., RANSON, H., SUTCLIFFE, M. J. & PAINE, M. J. 2008. Characterization of inhibitors and substrates of Anopheles gambiae CYP6Z2. *Insect Mol Biol,* 17**,** 125-35.
MELLANBY, K. 1992. *The DDT story*, British Crop Protection Council.
METCALF, R. L. 1971. Structure-activity relationships for insecticidal carbamates. *Bull World Health Organ,* 44**,** 43-78.
MITCHELL, S. N., STEVENSON, B. J., MULLER, P., WILDING, C. S., EGYIR-YAWSON, A., FIELD, S. G., HEMINGWAY, J., PAINE, M. J., RANSON, H. & DONNELLY, M. J. 2012. Identification and validation of a gene causing cross-resistance between insecticide classes in Anopheles gambiae from Ghana. *Proc Natl Acad Sci U S A,* 109**,** 6147-52.
MITOMA, J. & ITO, A. 1992. The carboxy-terminal 10 amino acid residues of cytochrome b5 are necessary for its targeting to the endoplasmic reticulum. *EMBO J,* 11**,** 4197-203.
MOIROUX, N., GOMEZ, M. B., PENNETIER, C., ELANGA, E., DJENONTIN, A., CHANDRE, F., DJEGBE, I., GUIS, H. & CORBEL, V. 2012. Changes in Anopheles funestus biting behavior following universal coverage of long-lasting insecticidal nets in Benin. *J Infect Dis,* 206**,** 1622-9.
MORGAN, J. C., IRVING, H., OKEDI, L. M., STEVEN, A. & WONDJI, C. S. 2010. Pyrethroid resistance in an *Anopheles funestus* population from Uganda. *PLoS One,* 5**,** e11872.
MOUCHET, J. & CARNEVALE, P. 1998. Entomological biodiversity of malaria in the world. *Res Rev Parasitol,* 58**,** 189-195.
MOURYA, D. T., HEMINGWAY, J. & LEAKE, C. J. 1993. Changes in enzyme titres with age in four geographical strains of Aedes aegypti and their association with insecticide resistance. *Med Vet Entomol,* 7**,** 11-6.
MULAMBA, C., IRVING, H., RIVERON, J. M., MUKWAYA, L. G., BIRUNGI, J. & WONDJI, C. S. 2014a. Contrasting Plasmodium infection rates and insecticide susceptibility profiles between the sympatric sibling species Anopheles parensis and Anopheles funestus s.s: a potential challenge for malaria vector control in Uganda. *Parasit Vectors,* 7**,** 71.
MULAMBA, C., RIVERON, J. M., IBRAHIM, S. S., IRVING, H., BARNES, K. G., MUKWAYA, L. G., BIRUNGI, J. & WONDJI, C. S. 2014b. Widespread Pyrethroid and DDT Resistance in the Major Malaria Vector Anopheles funestus in East Africa Is Driven by Metabolic Resistance Mechanisms. *PLoS One,* 9**,** e110058.
MULLER, P., WARR, E., STEVENSON, B. J., PIGNATELLI, P. M., MORGAN, J. C., STEVEN, A., YAWSON, A. E., MITCHELL, S. N., RANSON, H., HEMINGWAY, J., PAINE, M. J. & DONNELLY, M. J. 2008. Field-caught permethrin-resistant Anopheles gambiae overexpress CYP6P3, a P450 that metabolises pyrethroids. *PLoS Genet,* 4**,** e1000286.
MUNRO, A. W., GIRVAN, H. M., MASON, A. E., DUNFORD, A. J. & MCLEAN, K. J. 2013. What makes a P450 tick? *Trends Biochem Sci,* 38**,** 140-50.
MURATALIEV, M. B., FEYEREISEN, R. & WALKER, F. A. 2004. Electron transfer by diflavin reductases. *Biochim Biophys Acta,* 1698**,** 1-26.
MWANGOKA, G., OGUTU, B., MSAMBICHAKA, B., MZEE, T., SALIM, N., KAFURUKI, S., MPINA, M., SHEKALAGHE, S., TANNER, M. & ABDULLA, S. 2013. Experience and challenges from clinical trials with malaria vaccines in Africa. *Malar J,* 12**,** 86.
NELSON, D. L., LEHNINGER, A. L. & COX, M. M. 2012. *Lehninger principles of biochemistry*, Macmillan.
NELSON, D. R., KOYMANS, L., KAMATAKI, T., STEGEMAN, J. J., FEYEREISEN, R., WAXMAN, D. J., WATERMAN, M. R., GOTOH, O., COON, M. J. & ESTABROOK, R. W. 1996. P450 superfamily: update on new sequences, gene mapping, accession numbers and nomenclature. *Pharmacogenetics and Genomics,* 6**,** 1-42.
NIKOU, D., RANSON, H. & HEMINGWAY, J. 2003. An adult-specific CYP6 P450 gene is overexpressed in a pyrethroid-resistant strain of the malaria vector, Anopheles gambiae. *Gene,* 318**,** 91-102.

NIWA, T., INOUE-YAMAMOTO, S., SHIRAGA, T. & TAKAGI, A. 2005. Effect of antifungal drugs on cytochrome P450 (CYP) 1A2, CYP2D6, and CYP2E1 activities in human liver microsomes. *Biol Pharm Bull,* 28**,** 1813-6.

NKYA, T. E., AKHOUAYRI, I., KISINZA, W. & DAVID, J.-P. 2013. Impact of environment on mosquito response to pyrethroid insecticides: facts, evidences and prospects. *Insect biochemistry and molecular biology,* 43**,** 407-416.

NOTREDAME, C., HIGGINS, D. G. & HERINGA, J. 2000. T-Coffee: A novel method for fast and accurate multiple sequence alignment. *J Mol Biol,* 302**,** 205-17.

O'REILLY, A. O., KHAMBAY, B. P., WILLIAMSON, M. S., FIELD, L. M., WALLACE, B. A. & DAVIES, T. G. 2006. Modelling insecticide-binding sites in the voltage-gated sodium channel. *Biochem J,* 396**,** 255-63.

OKOYE, P. N., BROOKE, B. D., KOEKEMOER, L. L., HUNT, R. H. & COETZEE, M. 2008. Characterisation of DDT, pyrethroid and carbamate resistance in Anopheles funestus from Obuasi, Ghana. *Trans R Soc Trop Med Hyg,* 102**,** 591-8.

OLIVA, C. F., VREYSEN, M. J., DUPE, S., LEES, R. S., GILLES, J. R., GOUAGNA, L. C. & CHHEM, R. 2014. Current status and future challenges for controlling malaria with the sterile insect technique: technical and social perspectives. *Acta Trop,* 132 Suppl**,** S130-9.

OMURA, T. & SATO, R. 1964. The Carbon Monoxide-Binding Pigment of Liver Microsomes. I. Evidence for Its Hemoprotein Nature. *J Biol Chem,* 239**,** 2370-8.

OMURA, T. & TAKESUE, S. 1970. A new method for simultaneous purification of cytochrome b5 and NADPH-cytochrome c reductase from rat liver microsomes. *J Biochem,* 67**,** 249-57.

PACKARD, R. M. 2014. The origins of antimalarial-drug resistance. *N Engl J Med,* 371**,** 397-9.

PAINE, M. J., MCLAUGHLIN, L. A., FLANAGAN, J. U., KEMP, C. A., SUTCLIFFE, M. J., ROBERTS, G. C. & WOLF, C. R. 2003. Residues glutamate 216 and aspartate 301 are key determinants of substrate specificity and product regioselectivity in cytochrome P450 2D6. *J Biol Chem,* 278**,** 4021-7.

PAINE, M. J., SCRUTTON, N. S., MUNRO, A. W., GUTIERREZ, A., ROBERTS, G. C. & WOLF, C. R. 2005. Electron transfer partners of cytochrome P450. *Cytochrome P450.* Springer.

PAP, L., KELEMEN, M., TÓTH, A., SZÉKELY, I. & BERTÓK, B. 1996. The synthetic pyrethroid isomers II. Biological activity. *Journal of Environmental Science & Health Part B,* 31**,** 527-543.

PATES, H. & CURTIS, C. 2005. Mosquito behavior and vector control. *Annu. Rev. Entomol.,* 50**,** 53-70.

PETREK, M., OTYEPKA, M., BANAS, P., KOSINOVA, P., KOCA, J. & DAMBORSKY, J. 2006. CAVER: a new tool to explore routes from protein clefts, pockets and cavities. *BMC Bioinformatics,* 7**,** 316.

PIERRI, C. L., PARISI, G. & PORCELLI, V. 2010. Computational approaches for protein function prediction: a combined strategy from multiple sequence alignment to molecular docking-based virtual screening. *Biochim Biophys Acta,* 1804**,** 1695-712.

PLAPP, F. W. 1976. Biochemical genetics of insecticide resistance. *Annual review of entomology,* 21**,** 179-197.

PLUESS, B., TANSER, F. C., LENGELER, C. & SHARP, B. L. 2010. Indoor residual spraying for preventing malaria. *Cochrane Database Syst Rev***,** CD006657.

POULOS, T. L., FINZEL, B. C., GUNSALUS, I. C., WAGNER, G. C. & KRAUT, J. 1985. The 2.6-A crystal structure of Pseudomonas putida cytochrome P-450. *J Biol Chem,* 260**,** 16122-30.

PRATO, M., KHADJAVI, A., MANDILI, G., GIRIBALDI, G. & MINERO, V. G. 2012. *Insecticides as strategic weapons for malaria vector control*, INTECH Open Access Publisher.

PRITCHARD, M. P., GLANCEY, M. J., BLAKE, J. A., GILHAM, D. E., BURCHELL, B., WOLF, C. R. & FRIEDBERG, T. 1998. Functional co-expression of CYP2D6 and human NADPH-cytochrome P450 reductase in Escherichia coli. *Pharmacogenetics,* 8**,** 33-42.

PRITCHARD, M. P., MCLAUGHLIN, L. & FRIEDBERG, T. 2006a. Establishment of functional human cytochrome P450 monooxygenase systems in Escherichia coli. *Methods Mol Biol,* 320**,** 19-29.

PRITCHARD, M. P., MCLAUGHLIN, L. & FRIEDBERG, T. 2006b. Establishment of functional human cytochrome P450 monooxygenase systems in Escherichia coli. *Cytochrome P450 Protocols.* Springer.

PRITCHARD, M. P., OSSETIAN, R., LI, D. N., HENDERSON, C. J., BURCHELL, B., WOLF, C. R. & FRIEDBERG, T. 1997. A general strategy for the expression of recombinant human cytochrome P450s in Escherichia coli using bacterial signal peptides: expression of CYP3A4, CYP2A6, and CYP2E1. *Arch Biochem Biophys,* 345**,** 342-54.

RAAG, R., MARTINIS, S. A., SLIGAR, S. G. & POULOS, T. L. 1991. Crystal structure of the cytochrome P-450CAM active site mutant Thr252Ala. *Biochemistry,* 30**,** 11420-9.

RANSON, H., JENSEN, B., VULULE, J. M., WANG, X., HEMINGWAY, J. & COLLINS, F. H. 2000. Identification of a point mutation in the voltage-gated sodium channel gene of Kenyan *Anopheles gambiae* associated with resistance to DDT and pyrethroids. *Insect Mol Biol,* 9**,** 491-7.

RANSON, H., N'GUESSAN, R., LINES, J., MOIROUX, N., NKUNI, Z. & CORBEL, V. 2011. Pyrethroid resistance in African anopheline mosquitoes: what are the implications for malaria control? *Trends in parasitology,* 27**,** 91-98.

REIKOFSKI, J. & TAO, B. Y. 1992. Polymerase chain reaction (PCR) techniques for site-directed mutagenesis. *Biotechnology advances,* 10**,** 535-547.

RIVERON, J. M., IBRAHIM, S. S., CHANDA, E., MZILAHOWA, T., CUAMBA, N., IRVING, H., BARNES, K. G., NDULA, M. & WONDJI, C. S. 2014a. The highly polymorphic CYP6M7 cytochrome P450 gene partners with the directionally selected CYP6P9a and CYP6P9b genes to expand the pyrethroid resistance front in the malaria vector Anopheles funestus in Africa. *BMC Genomics,* 15**,** 817.

RIVERON, J. M., IRVING, H., NDULA, M., BARNES, K. G., IBRAHIM, S. S., PAINE, M. J. & WONDJI, C. S. 2013. Directionally selected cytochrome P450 alleles are driving the spread of pyrethroid resistance in the major malaria vector Anopheles funestus. *Proc Natl Acad Sci U S A,* 110**,** 252-7.

RIVERON, J. M., YUNTA, C., IBRAHIM, S. S., DJOUAKA, R., IRVING, H., MENZE, B. D., ISMAIL, H. M., HEMINGWAY, J., RANSON, H., ALBERT, A. & WONDJI, C. S. 2014b. A single mutation in the GSTe2 gene allows tracking of metabolically based insecticide resistance in a major malaria vector. *Genome Biol,* 15**,** R27.

ROBERTS, D. R., CHAREONVIRIYAPHAP, T., HARLAN, H. H. & HSHIEH, P. 1997. Methods of testing and analyzing excito-repellency responses of malaria vectors to insecticides. *J Am Mosq Control Assoc,* 13**,** 13-7.

ROBERTS, T. R. & HUTSON, D. H. 1999. *Metabolic pathways of agrochemicals: insecticides and fungicides*, Royal Society of Chemistry.

ROWE, G. E., MARGARITIS, A. & WEI, N. 2003. Specific Oxygen Uptake Rate Variations during Batch Fermentation of Bacillus thuringiensis Subspecies kurstaki HD-1. *Biotechnology progress,* 19**,** 1439-1443.

RTS, S. C. T. P., AGNANDJI, S. T., LELL, B., FERNANDES, J. F., ABOSSOLO, B. P., METHOGO, B. G., KABWENDE, A. L., ADEGNIKA, A. A., MORDMULLER, B., ISSIFOU, S., KREMSNER, P. G., SACARLAL, J., AIDE, P., LANASPA, M., APONTE, J. J., MACHEVO, S., ACACIO, S., BULO, H., SIGAUQUE, B., MACETE, E., ALONSO, P., ABDULLA, S., SALIM, N., MINJA, R., MPINA, M., AHMED, S., ALI, A. M., MTORO, A. T., HAMAD, A. S., MUTANI, P., TANNER, M., TINTO, H., D'ALESSANDRO, U., SORGHO, H., VALEA, I., BIHOUN, B., GUIRAUD, I., KABORE, B., SOMBIE, O., GUIGUEMDE, R. T., OUEDRAOGO, J. B., HAMEL, M. J., KARIUKI, S., ONEKO, M., ODERO, C., OTIENO, K., AWINO, N., MCMORROW, M., MUTURI-KIOI, V., LASERSON, K. F., SLUTSKER, L., OTIENO, W., OTIENO, L., OTSYULA, N., GONDI, S., OTIENO, A., OWIRA, V., OGUK, E., ODONGO, G., WOODS, J. B., OGUTU, B., NJUGUNA, P., CHILENGI, R., AKOO, P., KERUBO, C., MAINGI, C., LANG, T., OLOTU, A., BEJON, P., MARSH, K., MWAMBINGU, G., OWUSU-AGYEI, S., ASANTE, K. P., OSEI-KWAKYE, K., BOAHEN, O., DOSOO, D., ASANTE, I., ADJEI, G., KWARA, E., CHANDRAMOHAN, D., GREENWOOD, B., LUSINGU, J., GESASE, S., MALABEJA, A., ABDUL, O.,

MAHENDE, C., LIHELUKA, E., MALLE, L., LEMNGE, M., THEANDER, T. G., DRAKELEY, C., ANSONG, D., AGBENYEGA, T., ADJEI, S., BOATENG, H. O., RETTIG, T., BAWA, J., SYLVERKEN, J., SAMBIAN, D., SARFO, A., et al. 2012. A phase 3 trial of RTS,S/AS01 malaria vaccine in African infants. *N Engl J Med,* 367**,** 2284-95.

RUSSELL, R. J., SCOTT, C., JACKSON, C. J., PANDEY, R., PANDEY, G., TAYLOR, M. C., COPPIN, C. W., LIU, J. W. & OAKESHOTT, J. G. 2011a. The evolution of new enzyme function: lessons from xenobiotic metabolizing bacteria versus insecticide-resistant insects. *Evol Appl,* 4**,** 225-48.

RUSSELL, T. L., GOVELLA, N. J., AZIZI, S., DRAKELEY, C. J., KACHUR, S. P. & KILLEEN, G. F. 2011b. Increased proportions of outdoor feeding among residual malaria vector populations following increased use of insecticide-treated nets in rural Tanzania. *Malar J,* 10**,** 80.

RUZO, L. O., COHEN, E. & CAPUA, S. 1988. Comparative metabolism of the pyrethroids bifenthrin and deltamethrin in the bulb mite Rhizoglyphus robini. *Journal of Agricultural and Food Chemistry,* 36**,** 1040-1043.

SADASIVAIAH, S., TOZAN, Y. & BREMAN, J. G. 2007. Dichlorodiphenyltrichloroethane (DDT) for indoor residual spraying in Africa: how can it be used for malaria control? *Am J Trop Med Hyg,* 77**,** 249-63.

SALI, A. & BLUNDELL, T. L. 1993. Comparative protein modelling by satisfaction of spatial restraints. *J Mol Biol,* 234**,** 779-815.

SANAHUJA, G., BANAKAR, R., TWYMAN, R. M., CAPELL, T. & CHRISTOU, P. 2011. Bacillus thuringiensis: a century of research, development and commercial applications. *Plant Biotechnol J,* 9**,** 283-300.

SANBORN, R. C. & WILLIAMS, C. M. 1950. The cytochrome system in the cecropia silkworm, with special reference to the properties of a new component. *J Gen Physiol,* 33**,** 579-88.

SCHACTER, B. A., NELSON, E. B., MARVER, H. S. & MASTERS, B. S. 1972. Immunochemical evidence for an association of heme oxygenase with the microsomal electron transport system. *J Biol Chem,* 247**,** 3601-7.

SCHENKMAN, J. B. & JANSSON, I. 2003. The many roles of cytochrome b5. *Pharmacol Ther,* 97**,** 139-52.

SCHLAGENHAUF, P. 2010. Cochrane Review highlights the need for more targeted research on the tolerability of malaria chemoprophylaxis in travellers. *Evid Based Med,* 15**,** 25-6.

SCHLEIER III, J. J. & PETERSON, R. K. 2011. Pyrethrins and pyrethroid insecticides. Royal Society of Chemistry: London, UK.

SCHLITZER, M. 2008. Antimalarial drugs - what is in use and what is in the pipeline. *Arch Pharm (Weinheim),* 341**,** 149-63.

SCHMITTGEN, T. D. & LIVAK, K. J. 2008. Analyzing real-time PCR data by the comparative C(T) method. *Nat Protoc,* 3**,** 1101-8.

SCHULER, M. A. & BERENBAUM, M. R. 2013. Structure and function of cytochrome P450S in insect adaptation to natural and synthetic toxins: insights gained from molecular modeling. *J Chem Ecol,* 39**,** 1232-45.

SCOTT, J. G. 1999. Cytochromes P450 and insecticide resistance. *Insect Biochem Mol Biol,* 29**,** 757-77.

SCOTT, J. G. 2008. Insect cytochrome P450s: thinking beyond detoxification. *Recent advances in insect physiology, toxicology and molecular biology,* 1**,** 17-124.

SCOTT, J. G., LIU, N. & WEN, Z. 1998a. Insect cytochromes P450: diversity, insecticide resistance and tolerance to plant toxins. *Comparative Biochemistry and Physiology Part C: Pharmacology, Toxicology and Endocrinology,* 121**,** 147-155.

SCOTT, J. G., LIU, N. & WEN, Z. 1998b. Insect cytochromes P450: diversity, insecticide resistance and tolerance to plant toxins. *Comp Biochem Physiol C Pharmacol Toxicol Endocrinol,* 121**,** 147-55.

SERAZIN, A. C., DANA, A. N., HILLENMEYER, M. E., LOBO, N. F., COULIBALY, M. B., WILLARD, M. B., HARKER, B. W., SHARAKHOV, I. V., COLLINS, F. H., RIBEIRO, J. M. & BESANSKY, N. J. 2009. Comparative analysis of the global transcriptome of Anopheles funestus from Mali, West Africa. *PLoS One,* 4**,** e7976.

SHAIK, S., KUMAR, D., DE VISSER, S. P., ALTUN, A. & THIEL, W. 2005. Theoretical perspective on the structure and mechanism of cytochrome P450 enzymes. *Chem Rev,* 105**,** 2279-328.
SHERRATT, P. J. & HAYES, J. D. 2001. Glutathione S-transferases. *Enzyme systems that metabolise drugs and other xenobiotics***,** 319.
SHIFF, C. 2002. Integrated approach to malaria control. *Clin Microbiol Rev,* 15**,** 278-93.
SHONO, T., OHSAWA, K. & CASIDA, J. E. 1979. Metabolism of trans- and cis-permethrin, trans- and cis-cypermethrin, and decamethrin by microsomal enzymes. *J Agric Food Chem,* 27**,** 316-25.
SHONO, T., UNAI, T. & CASIDA, J. E. 1978. Metabolism of permethrin isomers in American cockroach adults, house fly adults, and cabbage looper larvae. *Pesticide Biochemistry and Physiology,* 9**,** 96-106.
SINGH, D. K. 2012. *Pesticide Chemistry and Toxicology*, Bentham Science Publishers.
SINKA, M. E., BANGS, M. J., MANGUIN, S., COETZEE, M., MBOGO, C. M., HEMINGWAY, J., PATIL, A. P., TEMPERLEY, W. H., GETHING, P. W., KABARIA, C. W., OKARA, R. M., VAN BOECKEL, T., GODFRAY, H. C., HARBACH, R. E. & HAY, S. I. 2010. The dominant Anopheles vectors of human malaria in Africa, Europe and the Middle East: occurrence data, distribution maps and bionomic precis. *Parasit Vectors,* 3**,** 117.
SIPPL, M. J. 1993. Recognition of errors in three-dimensional structures of proteins. *Proteins,* 17**,** 355-62.
SIRIM, D., WIDMANN, M., WAGNER, F. & PLEISS, J. 2010. Prediction and analysis of the modular structure of cytochrome P450 monooxygenases. *BMC Struct Biol,* 10**,** 34.
SMITH, A. G. 2012. DDT and other chlorinated insecticides. *Mammalian Toxicology of Insecticides***,** 37.
SODERLUND, D. M., CLARK, J. M., SHEETS, L. P., MULLIN, L. S., PICCIRILLO, V. J., SARGENT, D., STEVENS, J. T. & WEINER, M. L. 2002. Mechanisms of pyrethroid neurotoxicity: implications for cumulative risk assessment. *Toxicology,* 171**,** 3-59.
SODERLUND, D. M. & KNIPPLE, D. C. 2003. The molecular biology of knockdown resistance to pyrethroid insecticides. *Insect Biochem Mol Biol,* 33**,** 563-77.
SRIDHAR, J., LIU, J., FOROOZESH, M. & STEVENS, C. L. 2012. Insights on cytochrome P450 enzymes and inhibitors obtained through QSAR studies. *Molecules,* 17**,** 9283-305.
ST JOHNSTON, D. 2002. The art and design of genetic screens: Drosophila melanogaster. *Nat Rev Genet,* 3**,** 176-88.
STEVENSON, B. J., BIBBY, J., PIGNATELLI, P., MUANGNOICHAROEN, S., O'NEILL, P. M., LIAN, L. Y., MULLER, P., NIKOU, D., STEVEN, A., HEMINGWAY, J., SUTCLIFFE, M. J. & PAINE, M. J. 2011. Cytochrome P450 6M2 from the malaria vector Anopheles gambiae metabolizes pyrethroids: Sequential metabolism of deltamethrin revealed. *Insect Biochem Mol Biol,* 41**,** 492-502.
STEVENSON, B. J., PIGNATELLI, P., NIKOU, D. & PAINE, M. J. 2012. Pinpointing P450s associated with pyrethroid metabolism in the dengue vector, Aedes aegypti: developing new tools to combat insecticide resistance. *PLoS Negl Trop Dis,* 6**,** e1595.
STRITTMATTER, C. F. & BALL, E. G. 1952. A hemochromogen component of liver microsomes. *Proceedings of the National Academy of Sciences of the United States of America,* 38**,** 19.
STRITTMATTER, C. F. & BALL, E. G. 1954. The intracellular distribution of cytochrome components and of oxidative enzyme activity in rat liver. *Journal of Cellular and Comparative Physiology,* 43**,** 57-78.
STROBEL, H. W. & DIGNAM, J. D. 1978. Purification and properties of NADPH-cytochrome P-450 reductase. *Methods Enzymol,* 52**,** 89-96.
SZKLARZ, G. D. & HALPERT, J. R. 1997. Use of homology modeling in conjunction with site-directed mutagenesis for analysis of structure-function relationships of mammalian cytochromes P450. *Life Sci,* 61**,** 2507-20.
SZKLARZ, G. D., HE, Y. A. & HALPERT, J. R. 1995. Site-directed mutagenesis as a tool for molecular modeling of cytochrome P450 2B1. *Biochemistry,* 34**,** 14312-22.
SZKLARZ, G. D. & PAULSEN, M. D. 2002. Molecular modeling of cytochrome P450 1A1: enzyme-substrate interactions and substrate binding affinities. *J Biomol Struct Dyn,* 20**,** 155-62.

TAMURA, K., STECHER, G., PETERSON, D., FILIPSKI, A. & KUMAR, S. 2013. MEGA6: Molecular Evolutionary Genetics Analysis version 6.0. *Mol Biol Evol,* 30**,** 2725-9.
TARGETT, G. A., MOORTHY, V. S. & BROWN, G. V. 2013. Malaria vaccine research and development: the role of the WHO MALVAC committee. *Malar J,* 12**,** 362.
TIJET, N., HELVIG, C. & FEYEREISEN, R. 2001. The cytochrome P450 gene superfamily in< i> Drosophila melanogaster</i>: Annotation, intron-exon organization and phylogeny. *Gene,* 262**,** 189-198.
TRACY, T. S. 2003. Atypical enzyme kinetics: their effect on in vitro-in vivo pharmacokinetic predictions and drug interactions. *Curr Drug Metab,* 4**,** 341-6.
TRACY, T. S., HUTZLER, J. M., HAINING, R. L., RETTIE, A. E., HUMMEL, M. A. & DICKMANN, L. J. 2002. Polymorphic variants (CYP2C9*3 and CYP2C9*5) and the F114L active site mutation of CYP2C9: effect on atypical kinetic metabolism profiles. *Drug Metab Dispos,* 30**,** 385-90.
URBAN, P., MIGNOTTE, C., KAZMAIER, M., DELORME, F. & POMPON, D. 1997. Cloning, yeast expression, and characterization of the coupling of two distantly related Arabidopsis thalianaNADPH-cytochrome P450 reductases with P450 CYP73A5. *Journal of Biological Chemistry,* 272**,** 19176-19186.
VERDONK, M. L., COLE, J. C., HARTSHORN, M. J., MURRAY, C. W. & TAYLOR, R. D. 2003. Improved protein-ligand docking using GOLD. *Proteins,* 52**,** 609-23.
VERGERES, G. & WASKELL, L. 1995. Cytochrome b5, its functions, structure and membrane topology. *Biochimie,* 77**,** 604-620.
VERMILION, J. L., BALLOU, D. P., MASSEY, V. & COON, M. J. 1981. Separate roles for FMN and FAD in catalysis by liver microsomal NADPH-cytochrome P-450 reductase. *J Biol Chem,* 256**,** 266-77.
VIDAKOVIC, M., SLIGAR, S. G., LI, H. & POULOS, T. L. 1998. Understanding the role of the essential Asp251 in cytochrome p450cam using site-directed mutagenesis, crystallography, and kinetic solvent isotope effect. *Biochemistry,* 37**,** 9211-9.
VINCZE, T., POSFAI, J. & ROBERTS, R. J. 2003. NEBcutter: A program to cleave DNA with restriction enzymes. *Nucleic Acids Res,* 31**,** 3688-91.
VONTAS, J., DAVID, J. P., NIKOU, D., HEMINGWAY, J., CHRISTOPHIDES, G. K., LOUIS, C. & RANSON, H. 2007. Transcriptional analysis of insecticide resistance in Anopheles stephensi using cross-species microarray hybridization. *Insect Mol Biol,* 16**,** 315-24.
VONTAS, J. G., SMALL, G. J. & HEMINGWAY, J. 2001. Glutathione S-transferases as antioxidant defence agents confer pyrethroid resistance in Nilaparvata lugens. *Biochem J,* 357**,** 65-72.
VULULE, J., BEACH, R., ATIELI, F., ROBERTS, J., MOUNT, D. & MWANGI, R. 1994. Reduced susceptibility of Anopheles gambiae to permethrin associated with the use of permethrin-impregnated bednets and curtains in Kenya. *Medical and veterinary entomology,* 8**,** 71-75.
VULULE, J. M., BEACH, R. F., ATIELI, F. K., MCALLISTER, J. C., BROGDON, W. G., ROBERTS, J. M., MWANGI, R. W. & HAWLEY, W. A. 1999. Elevated oxidase and esterase levels associated with permethrin tolerance in Anopheles gambiae from Kenyan villages using permethrin-impregnated nets. *Med Vet Entomol,* 13**,** 239-44.
WADE, R. C., WINN, P. J., SCHLICHTING, I. & SUDARKO 2004. A survey of active site access channels in cytochromes P450. *J Inorg Biochem,* 98**,** 1175-82.
WANG, B., WESTERHOFF, L. M. & MERZ, K. M., JR. 2007. A critical assessment of the performance of protein-ligand scoring functions based on NMR chemical shift perturbations. *J Med Chem,* 50**,** 5128-34.
WANG, M., ROBERTS, D. L., PASCHKE, R., SHEA, T. M., MASTERS, B. S. & KIM, J. J. 1997. Three-dimensional structure of NADPH-cytochrome P450 reductase: prototype for FMN- and FAD-containing enzymes. *Proc Natl Acad Sci U S A,* 94**,** 8411-6.
WANG, R., LU, Y. & WANG, S. 2003. Comparative evaluation of 11 scoring functions for molecular docking. *J Med Chem,* 46**,** 2287-303.
WANG, R. W., NEWTON, D. J., LIU, N., ATKINS, W. M. & LU, A. Y. 2000. Human cytochrome P-450 3A4: in vitro drug-drug interaction patterns are substrate-dependent. *Drug Metab Dispos,* 28**,** 360-6.

WARE, G. W. & WHITACRE, D. M. 2004. An introduction to insecticides. *The Pesticide Book. Meister Pub. Willoughby, Ohio.[Links]*.
WARREN, G. L., ANDREWS, C. W., CAPELLI, A. M., CLARKE, B., LALONDE, J., LAMBERT, M. H., LINDVALL, M., NEVINS, N., SEMUS, S. F., SENGER, S., TEDESCO, G., WALL, I. D., WOOLVEN, J. M., PEISHOFF, C. E. & HEAD, M. S. 2006. A critical assessment of docking programs and scoring functions. *J Med Chem,* 49**,** 5912-31.
WATERHOUSE, A. L., HOLDEN, I. & CASIDA, J. E. 1984. 9, 21-Didehydroryanodine: a new principal toxic constituent of the botanical insecticide Ryania. *J. Chem. Soc., Chem. Commun.***,** 1265-1266.
WATERMAN, M. R. & JOHNSON, E. F. 1991. *Cytochrome*, Elsevier.
WEILL, M., LUTFALLA, G., MOGENSEN, K., CHANDRE, F., BERTHOMIEU, A., BERTICAT, C., PASTEUR, N., PHILIPS, A., FORT, P. & RAYMOND, M. 2003. Comparative genomics: Insecticide resistance in mosquito vectors. *Nature,* 423**,** 136-7.
WEILL, M., MALCOLM, C., CHANDRE, F., MOGENSEN, K., BERTHOMIEU, A., MARQUINE, M. & RAYMOND, M. 2004. The unique mutation in ace-1 giving high insecticide resistance is easily detectable in mosquito vectors. *Insect Mol Biol,* 13**,** 1-7.
WEN, Z., RUPASINGHE, S., NIU, G., BERENBAUM, M. R. & SCHULER, M. A. 2006. CYP6B1 and CYP6B3 of the black swallowtail (Papilio polyxenes): adaptive evolution through subfunctionalization. *Mol Biol Evol,* 23**,** 2434-43.
WERCK-REICHHART, D. & FEYEREISEN, R. 2000. Cytochromes P450: a success story. *Genome Biol,* 1**,** 3003.1-3003.9.
WHITE, G. 1985. Anopheles bwambae sp. n., a malaria vector in the Semliki Valley, Uganda, and its relationships with other sibling species of the An. gambiae complex (Diptera: Culicidae). *Systematic Entomology,* 10**,** 501-522.
WHITE, I. N., GREEN, M. L. & LEGG, R. F. 1987. Fluorescence-activated sorting of rat hepatocytes based on their mixed function oxidase activities towards diethoxyfluorescein. *Biochem J,* 247**,** 23-8.
WHITE, N. J. 2014. Malaria: a molecular marker of artemisinin resistance. *Lancet,* 383**,** 1439-40.
WHO 2012. Global Plan for Insecticide Resistance Management (GPIRM). Geneva, Switzerland: World Health Organization.
WHO 2013a. Report of the sixteenth WHOPES working group meeting: WHO/HQ, Geneva, 22-30 July 2013: review of Pirimiphos-methyl 300 CS, Chlorfenapyr 240 SC, Deltamethrin 62.5 SC-PE, Duranet LN, Netprotect LN, Yahe LN, Spinosad 83.3 Monolayer DT, Spinosad 25 Extended release GR. Geneva, Switzerland: World Health Organization.
WHO 2013b. World Malaria Report. *WHO Global Malaria Programme.* Geneva, Switzerland.
WILDING, C. S., WEETMAN, D., STEEN, K. & DONNELLY, M. J. 2009. High, clustered, nucleotide diversity in the genome of Anopheles gambiae revealed through pooled-template sequencing: implications for high-throughput genotyping protocols. *BMC Genomics,* 10**,** 320.
WILKES, T. J., MATOLA, Y. G. & CHARLWOOD, J. D. 1996. Anopheles rivulorum, a vector of human malaria in Africa. *Med Vet Entomol,* 10**,** 108-10.
WILLIAMS, C. H., JR. & KAMIN, H. 1962. Microsomal triphosphopyridine nucleotide-cytochrome c reductase of liver. *J Biol Chem,* 237**,** 587-95.
WILLIAMS, P. A., COSME, J., SRIDHAR, V., JOHNSON, E. F. & MCREE, D. E. 2000. Mammalian microsomal cytochrome P450 monooxygenase: structural adaptations for membrane binding and functional diversity. *Molecular cell,* 5**,** 121-131.
WONDJI, C. S., COLEMAN, M., KLEINSCHMIDT, I., MZILAHOWA, T., IRVING, H., NDULA, M., REHMAN, A., MORGAN, J., BARNES, K. G. & HEMINGWAY, J. 2012. Impact of pyrethroid resistance on operational malaria control in Malawi. *Proc Natl Acad Sci U S A,* 109**,** 19063-70.
WONDJI, C. S., DABIRE, R. K., TUKUR, Z., IRVING, H., DJOUAKA, R. & MORGAN, J. C. 2011. Identification and distribution of a GABA receptor mutation conferring dieldrin resistance in the malaria vector Anopheles funestus in Africa. *Insect Biochem Mol Biol,* 41**,** 484-91.

WONDJI, C. S., HEMINGWAY, J. & RANSON, H. 2007a. Identification and analysis of single nucleotide polymorphisms (SNPs) in the mosquito Anopheles funestus, malaria vector. *BMC genomics,* 8**,** 5.

WONDJI, C. S., HUNT, R. H., PIGNATELLI, P., STEEN, K., COETZEE, M., BESANSKY, N., LOBO, N., COLLINS, F. H., HEMINGWAY, J. & RANSON, H. 2005. An integrated genetic and physical map for the malaria vector Anopheles funestus. *Genetics,* 171**,** 1779-87.

WONDJI, C. S., IRVING, H., MORGAN, J., LOBO, N. F., COLLINS, F. H., HUNT, R. H., COETZEE, M., HEMINGWAY, J. & RANSON, H. 2009. Two duplicated P450 genes are associated with pyrethroid resistance in Anopheles funestus, a major malaria vector. *Genome Res,* 19**,** 452-9.

WONDJI, C. S., MORGAN, J., COETZEE, M., HUNT, R. H., STEEN, K., BLACK, W. C. T., HEMINGWAY, J. & RANSON, H. 2007b. Mapping a quantitative trait locus (QTL) conferring pyrethroid resistance in the African malaria vector Anopheles funestus. *BMC Genomics,* 8**,** 34.

WOOD, O., HANRAHAN, S., COETZEE, M., KOEKEMOER, L. & BROOKE, B. 2010. Cuticle thickening associated with pyrethroid resistance in the major malaria vector Anopheles funestus. *Parasit Vectors,* 3**,** 67.

WORLD HEALTH ORGANIZATION 2007. Insecticide-treated mosquito nets: . *WHO Position Statement.* Geneva, Switzerland.

XU, Q., LIU, H., ZHANG, L. & LIU, N. 2005. Resistance in the mosquito, Culex quinquefasciatus, and possible mechanisms for resistance. *Pest management science,* 61**,** 1096-1102.

YAMAZAKI, H., JOHNSON, W. W., UENG, Y. F., SHIMADA, T. & GUENGERICH, F. P. 1996. Lack of electron transfer from cytochrome b5 in stimulation of catalytic activities of cytochrome P450 3A4. Characterization of a reconstituted cytochrome P450 3A4/NADPH-cytochrome P450 reductase system and studies with apo-cytochrome b5. *J Biol Chem,* 271**,** 27438-44.

YAMAZAKI, H., UENG, Y. F., SHIMADA, T. & GUENGERICH, F. P. 1995. Roles of divalent metal ions in oxidations catalyzed by recombinant cytochrome P450 3A4 and replacement of NADPH--cytochrome P450 reductase with other flavoproteins, ferredoxin, and oxygen surrogates. *Biochemistry,* 34**,** 8380-9.

YAN, Z., RAFFERTY, B., CALDWELL, G. W. & MASUCCI, J. A. 2002. Rapidly distinguishing reversible and irreversible CYP450 inhibitors by using fluorometric kinetic analyses. *Eur J Drug Metab Pharmacokinet,* 27**,** 281-7.

YANO, J. K., WESTER, M. R., SCHOCH, G. A., GRIFFIN, K. J., STOUT, C. D. & JOHNSON, E. F. 2004. The structure of human microsomal cytochrome P450 3A4 determined by X-ray crystallography to 2.05-A resolution. *J Biol Chem,* 279**,** 38091-4.

YOSHIOKA, S., TOSHA, T., TAKAHASHI, S., ISHIMORI, K., HORI, H. & MORISHIMA, I. 2002. Roles of the proximal hydrogen bonding network in cytochrome P450cam-catalyzed oxygenation. *J Am Chem Soc,* 124**,** 14571-9.

ZHANG, W., RAMAMOORTHY, Y., KILICARSLAN, T., NOLTE, H., TYNDALE, R. F. & SELLERS, E. M. 2002. Inhibition of cytochromes P450 by antifungal imidazole derivatives. *Drug Metab Dispos,* 30**,** 314-8.

ZHENG, L., BAUMANN, U. & REYMOND, J. L. 2004. An efficient one-step site-directed and site-saturation mutagenesis protocol. *Nucleic Acids Res,* 32**,** e115.

ZHOU, Y. & JOHNSON, M. E. 1999. Comparative molecular modeling analysis of-5-amidinoindole and benzamidine binding to thrombin and trypsin: specific H-bond formation contributes to high 5-amidinoindole potency and selectivity for thrombin and factor Xa. *J Mol Recognit,* 12**,** 235-41.

ZHU, F., PARTHASARATHY, R., BAI, H., WOITHE, K., KAUSSMANN, M., NAUEN, R., HARRISON, D. A. & PALLI, S. R. 2010. A brain-specific cytochrome P450 responsible for the majority of deltamethrin resistance in the QTC279 strain of Tribolium castaneum. *Proc Natl Acad Sci U S A,* 107**,** 8557-62.

APPENDIX 2.1

A: Maximum likelihood tree of *An. funestus CYP6P9a* and *CYP6P9b*; B: Python scripts used for model building.

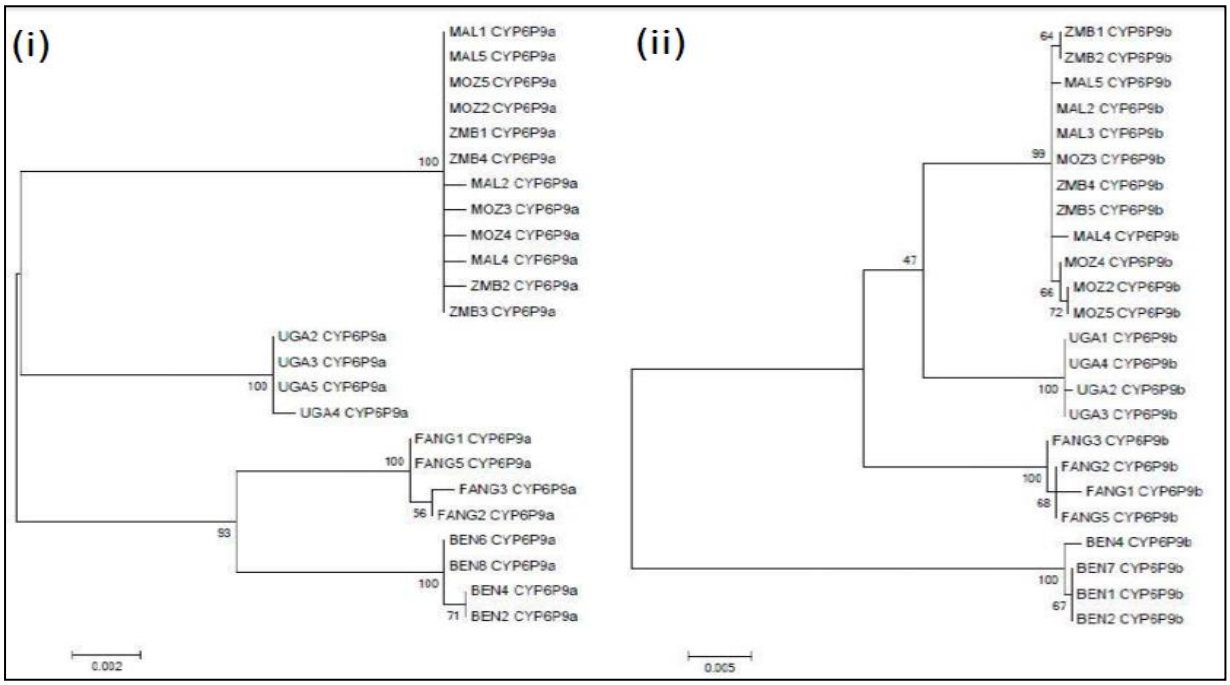

A: Maximum likelihood tree of *An. funestus CYP6P9a* (i) and *CYP6P9b* (ii) cDNA across Africa showing clades relationship. A number is given to each haplotype preceded by BEN, MAL, MOZ, UGA or FANG if it is unique to BENIN, MALAWI, MOZAMBIQUE, UGANDA or FANG strains, respectively.

(B) Python script used to build models using the MODELLER 9v2.0

```
from modeller import *    # Load the automodel class
from modeller.automodel import *
log.verbose()    # request verbose output
env = environ()  # create a new MODELLER environment to build this model in
env.io.atom_files_directory = '/directory/folder/subfolder'
env.io.hetatm = True
a = automodel(env,
        alnfile  = '/directory/folder/subfolder/alignment.ali',
        knowns   = ( '1TQN' ), # codes of the templates
        sequence = 'SEQUENCE NAME'
       )          # code of the target
a.starting_model= 1             # index of the first model
a.ending_model  = 50            # index of the last model
a.make()                    # do the actual homology modelling
```

APPENDIX 2.2

Errat profiles of CYP6P9a and CYP6P9b models and CYP3A4 (PDB:1TQN)

Serial Number	Model Name	Overall Quality Factor (%)
1	BENCYP6P9a.pdb	55.876
2	FANGCYP6P9a.pdb	52.731
3	MALCYP6P9a.pdb	51.527
4	MOZCYP6P9a.pdb	51.527
5	ZMBCYP6P9a.pdb	55.441
6	UGANCYP6P9a.pdb	52.749
7	BENCYP6P9b.pdb	55.072
8	FANGCYP6P9b.pdb	59.175
9	MALCYP6P9b.pdb	55.230
10	MOZCYP6P9b.pdb	55.464
11	ZMBCYP6P9b.pdb	53.992
12	UGANCYP6P9b.pdb	62.134
13	CYP3A4 (1TQN.pdb)	93.696

APPENDIX 2. 3

Transmembrane domain prediction for CYP6P9a using DAS

(a) Potential transmembrane segments of CYP6P9a protein sequence

Start	Stop	Length	~	Cutoff
6	20	15	~	2.2
6	21	16	~	1.7
80	89	10	~	1.7
84	86	3	~	2.2
186	187	2	~	1.7
217	228	12	~	1.7
219	226	8	~	2.2
307	315	9	~	1.7
309	313	5	~	2.2
466	471	6	~	1.7
495	498	4	~	1.7

The 2.2 strict cut off is informative score in terms of matching segment while the loose score of 1.7 gives the actual location of the transmembrane segment.

(b) DAS plot of transmembrane domains of CYP6P9a protein sequence

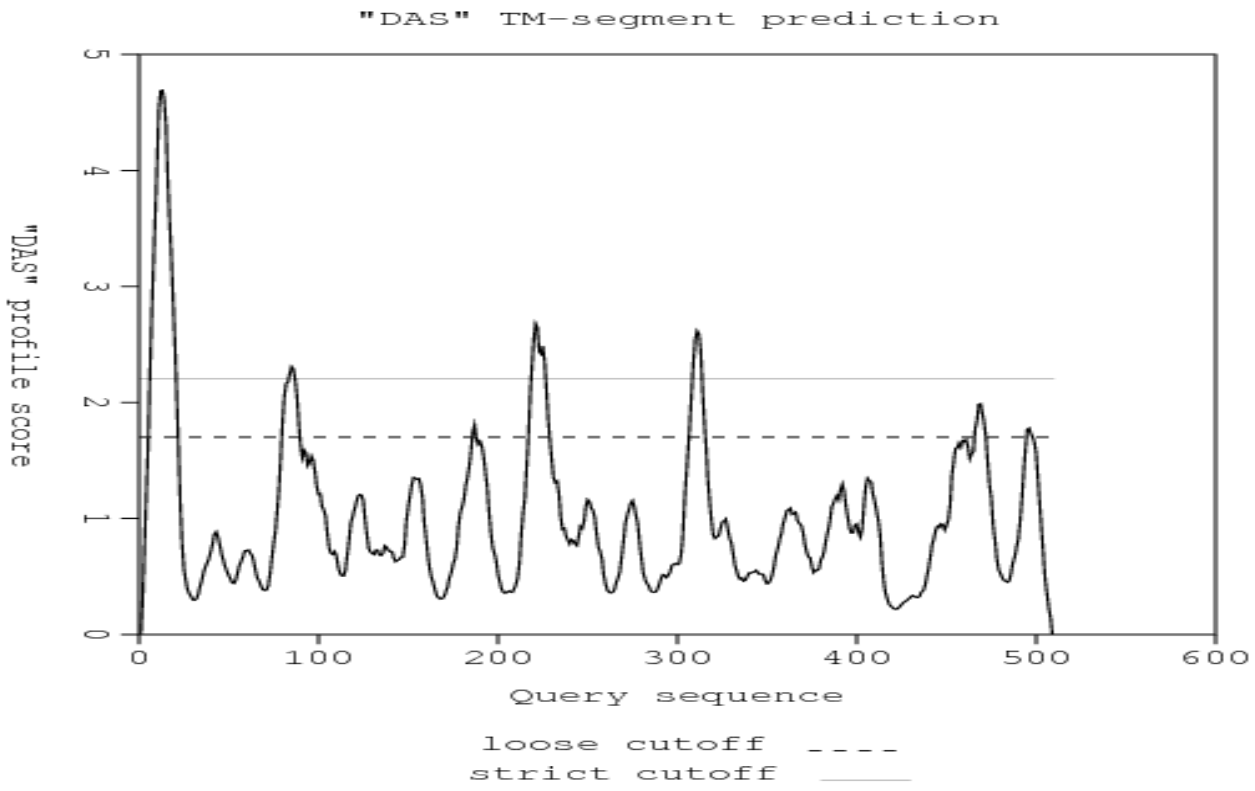

APPENDIX 2.4

Transmembrane domain prediction for CYP6P9b using DAS

(a) Potential transmembrane segments of CYP6P9b protein sequence

Start	Stop	Length	~	Cutoff
6	21	16	~	1.7
7	20	14	~	2.2
79	89	11	~	1.7
81	86	6	~	2.2
186	187	2	~	1.7
218	228	11	~	1.7
219	225	7	~	2.2
305	315	11	~	1.7
308	314	7	~	2.2
466	471	6	~	1.7

The 2.2 strict cut off is informative score in terms of matching segment while the loose score of 1.7 gives the actual location of the transmembrane segment.

(b) DAS plot of transmembrane domains of CYP6P9b protein sequence

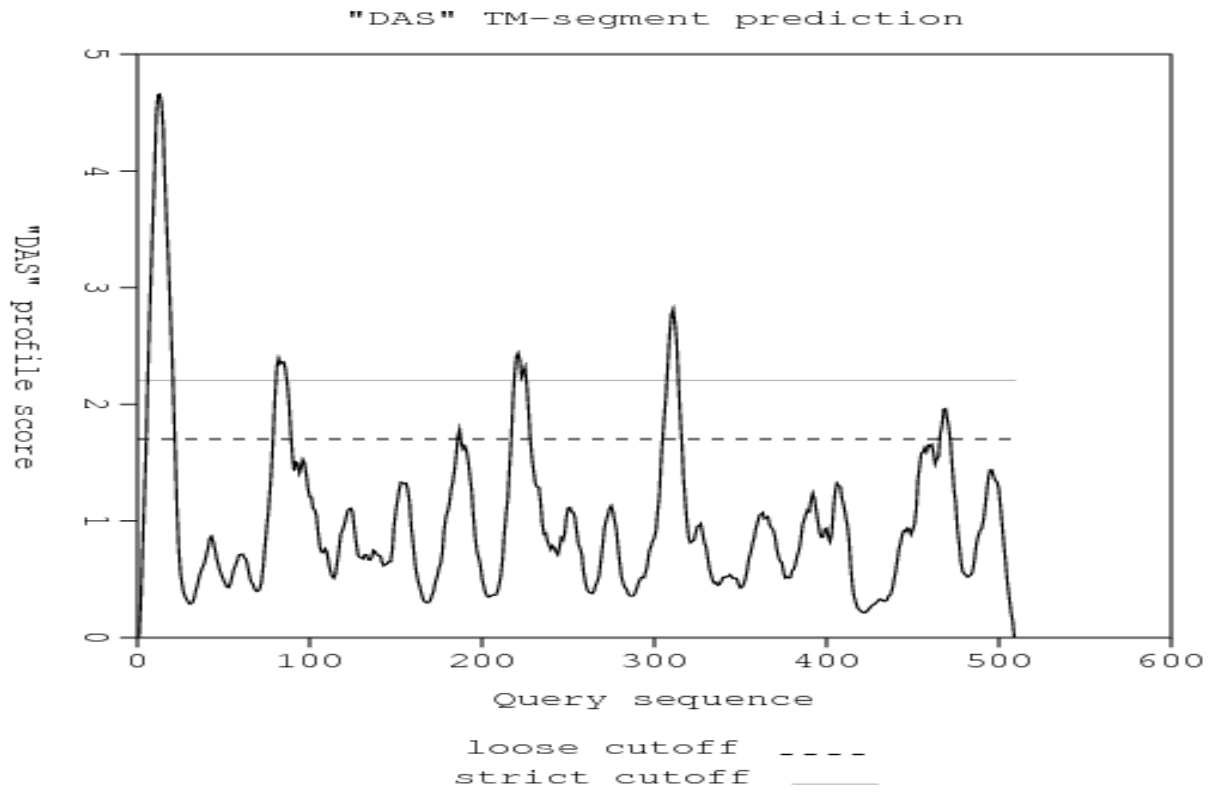

APPENDIX 2.5

Binding modes of etofenprox in 1.0 CYP6P9a and 2.0 CYP6P9b models.

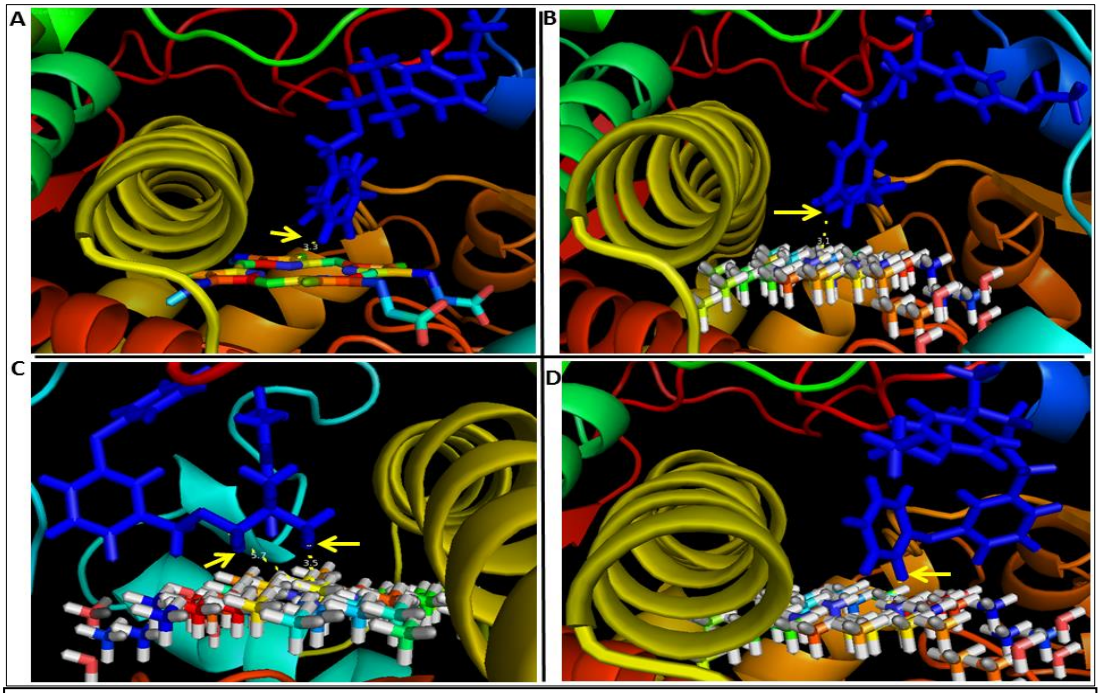

1.0 Binding modes of etofenprox in (A) BENIN, (B) UGANDA, (C) FANG and (D) MALAWI CYP6P9a models. Etofenprox is in stick format and blue colour. Heme atoms are in stick and spectrum. Possible sites of metabolism are indicated with yellow arrows.

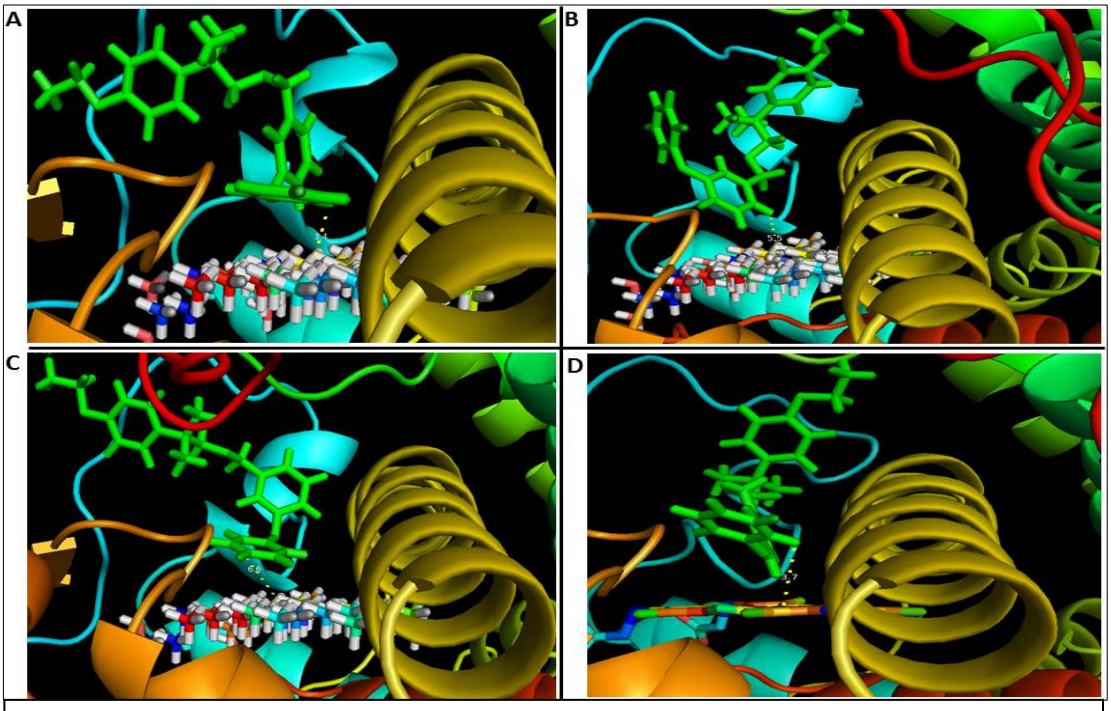

2.0 Binding modes of etofenprox in (A) BENIN, (B) UGANDA, (C) FANG and (D) MOZAMBIQUE CYP6P9b models. Etofenprox is in stick format and green. Heme atoms are in stick format and spectrum.

APPENDIX 2.6

Binding modes of DDT in 1.0 CYP6P9a and 2.0 CYP6P9b models.

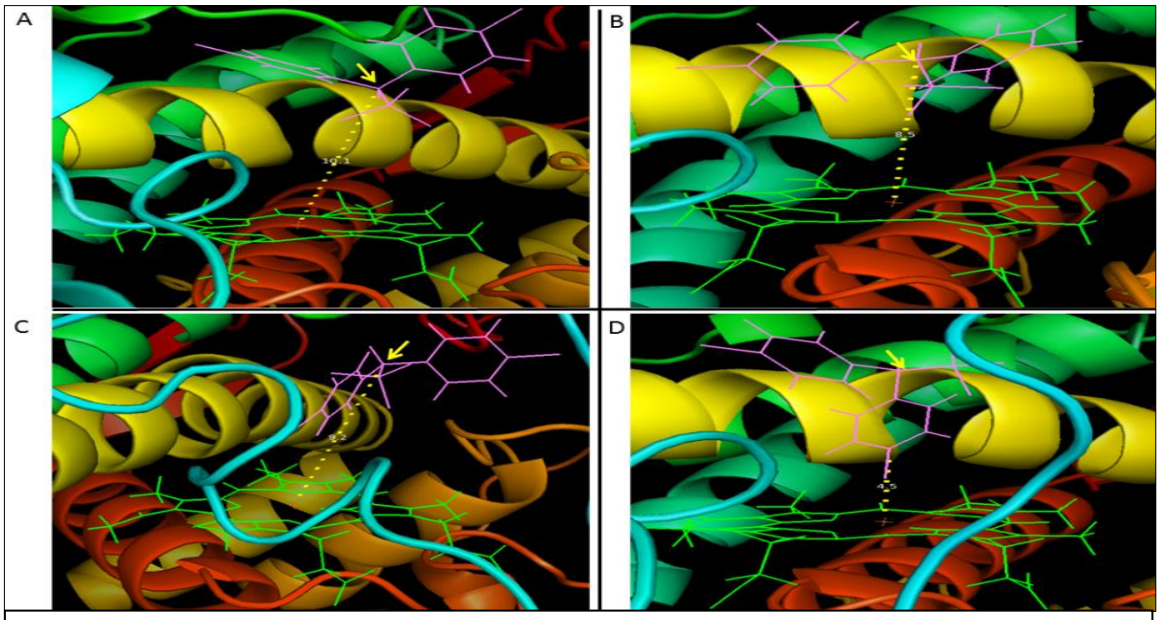

1.0 Binding modes of DDT in (A) BENIN, (B) UGANDA, (C) FANG and (D) MALAWI CYP6P9a models. DDT is in line format and purple. Heme atoms are in green. C-2 is indicated with yellow arrow.

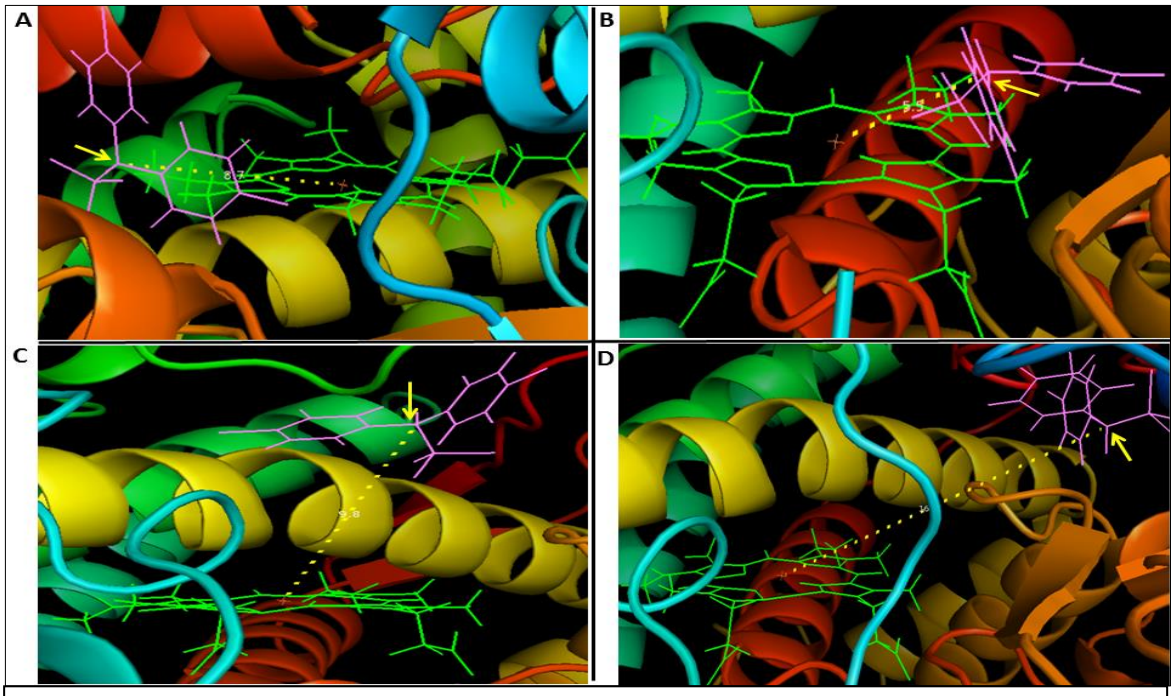

2.0 Binding modes of DDT in (A) BENIN, (B) UGANDA, (C) FANG and (D) MOZAMBIQUE CYP6P9b models. DDT is in line format and violet. Heme atoms are in green. C-2 is indicated with yellow arrow.

APPENDIX 2.7

Binding modes of bendiocarb in 1.0 CYP6P9a and 2.0 CYP6P9b models.

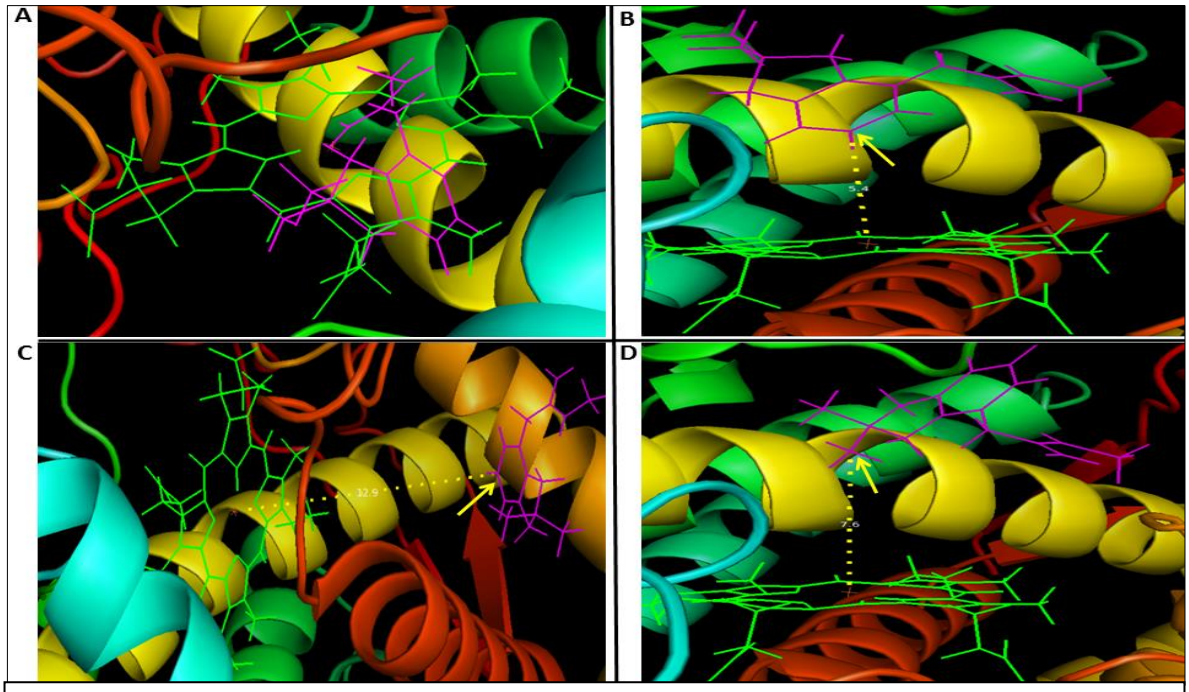

1.0 Binding modes of bendiocarb in (A) BENIN, (B) UGANDA, (C) FANG and (D) MALAWI CYP6P9a models. Bendiocarb is in line format and purple. Heme atoms are in green. Probable sites of metabolism are indicated with yellow arrow.

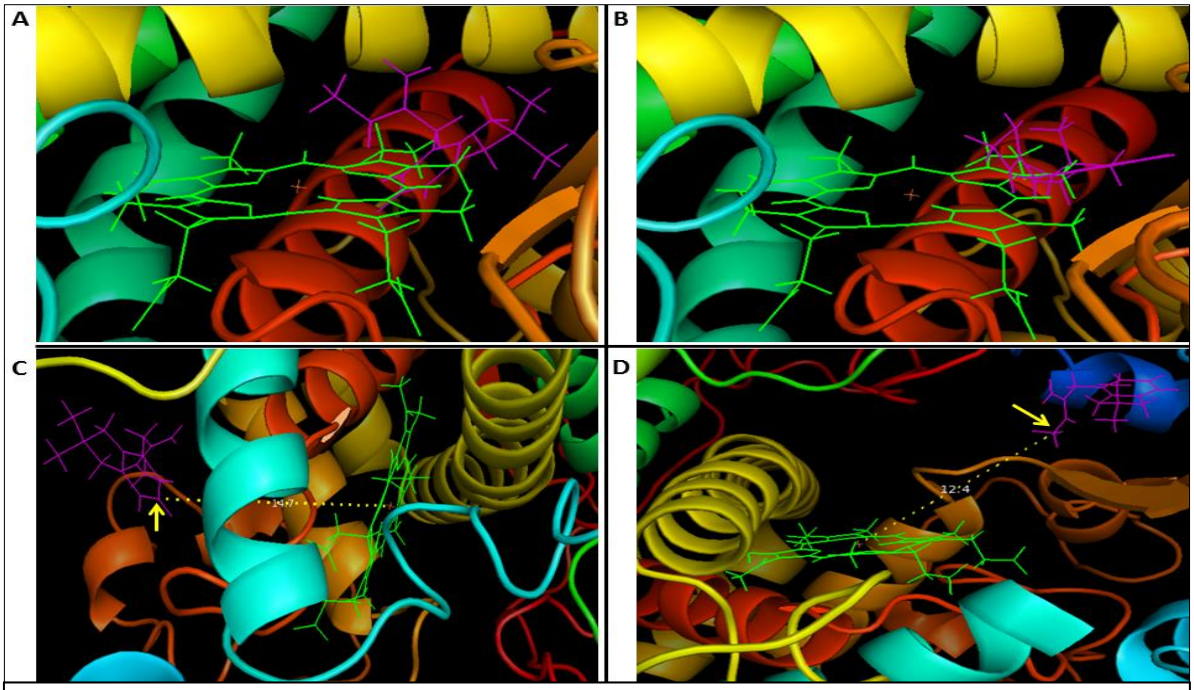

2.0 Binding modes of bendiocarb in (A) BENIN, (B) UGANDA, (C) FANG and (D) MOZAMBIQUE CYP6P9b models. Bendiocarb is in line format and purple. Heme atoms are in green. Probable sites of metabolism are indicated with yellow arrow.

APPENDIX 2.8

Haplotype Diversity and Nucleotide Variations of *CYP6P9a* cDNA Sequences Across Africa.

```
                                                                       111111111111111111
                 Hap     11111111111112222333344444445555556777778888899999999000111111233344445
                         01225556788890279147801156780457785123581234600025678349236899923936672
                         87091350167961834555464778422023924132359646136919088047244247264245930
MAL1_CYP6P9a      1      TCAGGCAACACGACTGACCTCAGACATATTAAGTGGACAACTTTCAAAGCCTTACTTATATCTCTGATAGA
MAL5_CYP6P9a      1      .......................................................................
MOZ2_CYP6P9a      1      .......................................................................
MOZ5_CYP6P9a      1      .......................................................................
ZMB1_CYP6P9a      1      .......................................................................
ZMB3_CYP6P9a      1      .......................................................................
ZMB4_CYP6P9a      1      .......................................................................
MOZ1_CYP6P9a      2      .......G...........................................................C..G
MAL2_CYP6P9a      3      ..G....................................................................
MAL6_CYP6P9a      4      .......................................G........................C......
MAL4_CYP6P9a      5      ...........................G...........................................
MOZ4_CYP6P9a      6      ....................................................................G..
ZMB2_CYP6P9a      7      .......................................................C...............
ZMB5_CYP6P9a      7      .......................................................C...............
MOZ3_CYP6P9a      8      .....................G.................................................
FANG4_CYP6P9a     9      CT.......GTT....................A.A.C.G..........A.CC..................
UGAN1_CYP6P9a     10     .T.TTTT.GGTTCTCCC..G.....G..C.CTACAAC.G........G..........G.CG.......A.
UGAN2_CYP6P9a     10     .T.TTTT.GGTTCTCCC..G.....G..C.CTACAAC.G........G..........G.CG.......A.
UGAN3_CYP6P9a     10     .T.TTTT.GGTTCTCCC..G.....G..C.CTACAAC.G........G..........G.CG.......A.
UGAN5_CYP6P9a     10     .T.TTTT.GGTTCTCCC..G.....G..C.CTACAAC.G........G..........G.CG.......A.
UGAN4_CYP6P9a     11     .T.TTTT.GGTTCTCCC..G.....G..C.CTACAAC.G.A......G..........G.CG.......A.
BEN5_CYP6P9a      12     ....TTT.GGTTC...CT............CTAC.A..G..C........T.....ACG.CG...AG....
FANG2_CYP6P9a     13     CT.......GTTCT....TG....TG....CTACA.CTG...CCTCG.AA.CC.T...GCCGC........
FANG5_CYP6P9a     14     CT.......GTTCT....TG....TG....CTACA.CTG...CCTCG.A..CC.T...GCCGC........
FANG1_CYP6P9a     14     CT.......GTTCT....TG....TG....CTACA.CTG...CCTCG.A..CC.T...GCCGC........
FANG6_CYP6P9a     14     CT.......GTTCT....TG....TG....CTACA.CTG...CCTCG.A..CC.T...GCCGC........
FANG3_CYP6P9a     15     CT.......GTTCT....TG....TG....CTACA.CTG...CCTCG.AA.CC.T...GCCG.........
BEN8_CYP6P9a      16     ....TTT..GTTCT.....GT.CGTGC..CC..CA.CTG...CCTCG.A...C.....GCCG.T.......
BEN6_CYP6P9a      16     ....TTT..GTTCT.....GT.CGTGC..CC..CA.CTG...CCTCG.A...C.....GCCG.T.......
BEN2_CYP6P9a      17     ....TTT..GTTCT.....GT.CGTGC..CC..CA.CTG...CCTCG.A...CG....GCCG.T.......
BEN4_CYP6P9a      17     ....TTT..GTTCT.....GT.CGTGC..CC..CA.CTG...CCTCG.A...CG....GCCG.T.......
```

Schematic representation of *CYP6P9a* haplotypes for the coding region among resistant and susceptible mosquitoes. FANG is highlighted in red. Polymorphic positions are indicated by numbers above the nucleotides and the haplotypes identity reflected with a number in front of the country it belongs. MAL = MALAWI, MOZ = MOZAMBIQUE, ZMB = ZAMBIA, UGAN = UGANDA, BEN = BENIN.

APPENDIX 2.9

Haplotype Diversity and Nucleotide Variations of *CYP6P9b* cDNA Sequences Across Africa.

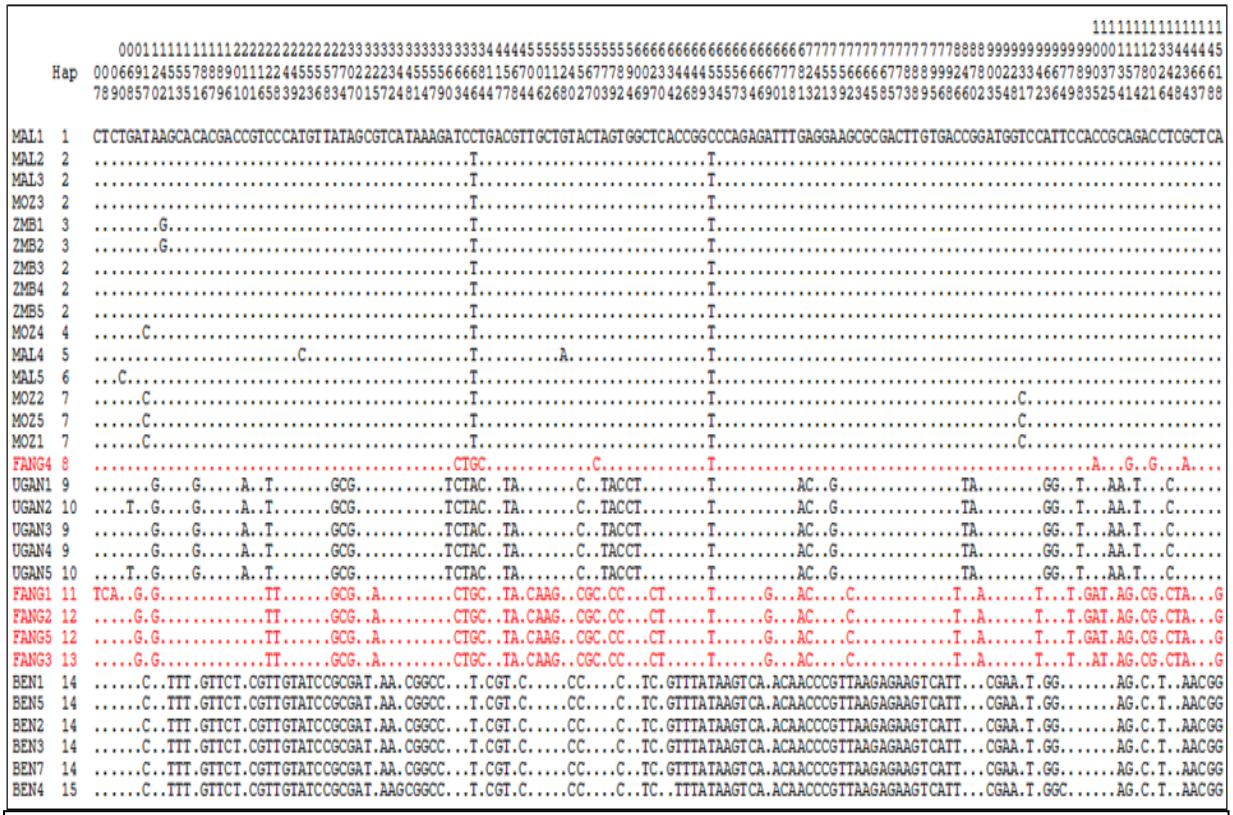

Schematic representation of *CYP6P9b* haplotypes for the coding region among resistant and susceptible mosquitoes. FANG is highlighted in red. Polymorphic positions are indicated by numbers above the nucleotides and the haplotypes identity with a number in front of the country it belongs.

APPENDIX 3.1

Preparation of CYP450 Expressing Bacterial Membranes

MATERIALS

- 50 mgl/ml ampicillin in water (filter-sterilized and stored in aliquots at -20ºC).
- 34 mg/ml chloramphenicol in ethanol (if expressing P450 reductase as well: co-transformation).
- *2 X Tris-Sucrose –EDTA (TSE) buffer*: 0.1M Tris-acetate at pH 7.6 with 0.5M sucrose and 0.5mM EDTA-filter-sterilize and store at 4ºC. 1X TSE is equivalent quantity of 2X TSE + equivalent quantity of distilled water.
- *Spheroplast Resuspension (SR) buffer*: 0.1M potassium phosphate at pH 7.6, 6mM magnesium acetate and 20% (v/v) glycerol-filter-sterilized. Add dithiothreitol immediately before use for a final concentration of 0.1mM using a 100mM filter-sterilized stock solution stored in aliquots at -20ºC.

CULTURES FOR P450 EXPRESSION

1. Transform *JM109* cells with the plasmid that express the P450 and the plasmid which express the P450 reductase. You need to have fresh LB+AMP+Chloramphenicol plates.
2. Pick a single colony from the transformation and inoculate 3ml of LB with antibiotics (50µg/ml ampicillin and 34µg/ml chloramphenicol).
3. Incubate this culture overnight (16 hours) at 37ºC with 150-200 rpm shaking.
4. Use 2 ml of the overnight culture to inoculate 200ml of Terrific Broth in a 1L flask. The media should be pre-warmed to 37ºC, to avoid shocking cells, and include antibiotics as for the overnight culture.
5. Incubate the culture at 37ºC with 200 rpm shaking.
6. Monitor the absorption at of the culture at 595-600 nm (plate reader) and when this value has reached about 0.7-0.8, after ~4 hours, transfer the culture to a 21 or 25ºC incubator and continue with 150 rpm shaking.
7. After 30 min at 21/25ºC (allowing for the culture to cool) add IPTG for a final concentration of 1mM and ALA for 0.5mM (16,759 mg ALA and 47,66 mg IPTG).
8. Continue incubating at 25ºC until the culture is ready for harvesting.

Note: several variables can be optimised for P450 expression: incubation time, incubation temperature, induction time (adding IPTG/ALA), and IPTG or ALA concentration. Cultures should be monitored daily for P450/P420 production using CO difference spectra. Some P450 require only 1 day at 25ºC whereas others need 3-4 days.

SPHEROPLAST PREPARATION

1. Pour the 200 ml bacterial culture into a 250 ml centrifuge bottle. Chill the bottles on ice for at least 10 minutes while checking and preparing the centrifuge and rotor. Centrifuge the cultures at 2800 x g for 20 minutes at 4ºC.
2. Discard the supernatant and retain the pellet
3. Re-suspend the cell pellets in 20 ml of 1x TSE with a 25ml transfer pipette while keeping the bottles on ice (use automatic machine for the pipetting).
4. Add 10 ml dH_20 and mix and mix again (on ice)
5. Prepare a solution of 20mg/mL lysozyme in dH_20 and store on ice. Add 250µl of this lysozyme solution to give 0.25 mg/mL lysozyme in 20 ml of cell suspension.
6. Pipette the mix into 50ml Nalgene centrifuge tube (already chilled on ice)
7. Keep the centrifuge bottles in a polystyrene container with ice, and place the container on a rocking platform to allow gentle mixing for 60 minutes while the cell walls are degraded to allow spheroplast to form.
8. Load the 50mL bottles into the JA 25.50 rotor (Beckman) and centrifuge at 2800xg for 25 minutes at 4ºC. Discard supernatant and retain pellet.
9. Add 8mL of spheroplast re-suspension buffer and 8µl of 0.1M DTT.
10. Proceed to the next step or store the spheroplast in -80 ºC

FROM SPHEROPLASTS TO MEMBRANES

1. Remove the spheroplast from -80ºC and thaw it on ice. Add the following items to 8 mL of spheroplasts:
    a. 40 µl of 0.2 M PMSF (dissolved in ethanol and usually stored in the freezer)
    b. 0.8 µl of 10 mg/mL aprotinin (make aliquots and keep in freezer and use each aliquot only once.
    c. 0.8 µl of 10 mg/mL leupeptin (usually stored in the freezer)
2. Sonicate the suspension three times for 30 seconds with the sonicator (30 seconds on and 30 seconds off/intervals) at about 70% power (this may need optimising) and tip should be kept submerged in the suspension to avoid frothing. Keep the sample on ice between the bursts of

sonication. The sample will initially become viscous during sonication as DNA is released, but this viscosity should drop as the DNA is sheared by the sonication.

3. Dry and balance the weight of the tubes with dH20.
4. Load the 50 ml Nalgene tube with the sonicated sample into the JA 25.50 rotor (Beckman Avanti TM JM 25) along with a balance tube (+/-0.01g). Centrifuge at 30,000 x g for 20 minutes at 4ºC.
5. Transfer the supernatant to a 26.3 ml ultracentrifuge bottles (transparent) on ice. Theses bottles must not be centrifuged when less than half full, can only be used up to 50000 rpm when over half full, and can only be centrifuged at their maximum rate, 60000 rpm, when full. Therefore, add 8 ml of ice-cold water to the 8 ml sample and make sure the bottles are not full to the neck. Prepare a balanced tube (+/-0.005 g) with ice-cold water.
6. Dry and load the balanced ultracentrifuge bottles in the 70Ti rotor and centrifuge at 49600 rpm (180000 x g), for 1 hour at 4ºC.
7. Remove the tubes and discard the supernatant using a transfer pipette. The membranes should appear as a translucent red-brown pellet. Transfer the majority of this pellet to a 1mL Dounce homogeniser on ice using a glass Pasteur pipette to lightly scrape the pellet. Avoid blocking up the pipette with the membrane pellet by using the side of the tip to scrape and transfer bits of the pellet into the Dounce homogeniser. Once most of the pellet has been transferred, add 0.5 ml of ice-cold 1 X TSE buffer and 0.5ml of water and use the same Pasteur pipette to re-suspend the remaining pellet and transfer this to the Dounce homogeniser. Load the liquid from the bottom of the homogeniser to avoid bubbles. Alternatively, 250uL of both 1X TSE and 250uL of ddH20 should be used and then later the same amounts to wash the homogeniser and transfer the contents into the Eppendorf.
8. Aliquot the homogenised membrane into small plastic tubes (100-200µl) and store at -80ºC.

APPENDIX 3.2

CYP450s concentration, total protein and CPR activity of recombinant CYP6P9a and CYP6P9b

Recombinant Proteins	n	P450 Yield	Std Dev	CPR Activity	Std Dev	Total Protein	Std Dev
BENCYP6P9a	**2**	14.70	1.36	119.6	20.01	16.30	1.56
UGANCYP6P9a	**2**	12.77	2.62	163.1	21.98	15.79	1.58
FANGCYP6P9a	**2**	16.28	3.54	156.1	17.03	16.56	0.93
MALCYP6P9a	**2**	13.79	1.41	151.0	18.88	19.49	1.74
MOZCYP6P9a	**3**	7.24	0.59	157.0	20.65	17.62	0.70
ZMBCYP6P9a	**1**	4.35	0.00	N.D.	N.D.	N.D.	N.D.
BENCYP6P9b	**2**	10.88	3.50	154.2	23.71	27.72	3.23
UGANCYP6P9b	**2**	12.02	11.29	154.3	12.74	26.14	1.89
FANGCYP6P9b	**2**	11.16	3.20	168.9	18.60	24.54	1.95
MALCYP6P9b	**2**	7.40	2.13	161.5	16.48	21.08	1.69
MOZCYP6P9b	**4**	7.59	2.13	205.3	19.19	21.17	3.17
ZMBCYP6P9b	**1**	7.05	0	N.D.	N.D.	N.D.	N.D.

n: Number of independent membranes expressed; P450 Yield: nmol/ml; CPR Activity: nmol of cytochrome c reduced/minutes/mg protein; Total protein: mg/ml.

APPENDIX 3.3

Excitation and Emission wavelength of fluorescent probe substrates

S/No	Probe Substrate	Excitation Wavelength (nm)	Emission Wavelength (nm)
1	7-ethoxyresorufin (ER)	544	590
2	Benzyloxyresorufin (BR)	544	590
3	Methoxyresorufin (MR)	544	590
4	Pentoxyresorufin (PR)	544	590
5	7-ethoxy-4-trifloromethyl-coumarin (EFC)	410	535
6	7-methoxy-4-trifloromethyl-coumarin (MFC)	410	535
7	Diethoxyfluorescein (DEF)	485	530

APPENDIX 3.4

Time-course for CYP6P9a and CYP6P9b dealkylation of diethoxyfluorescein

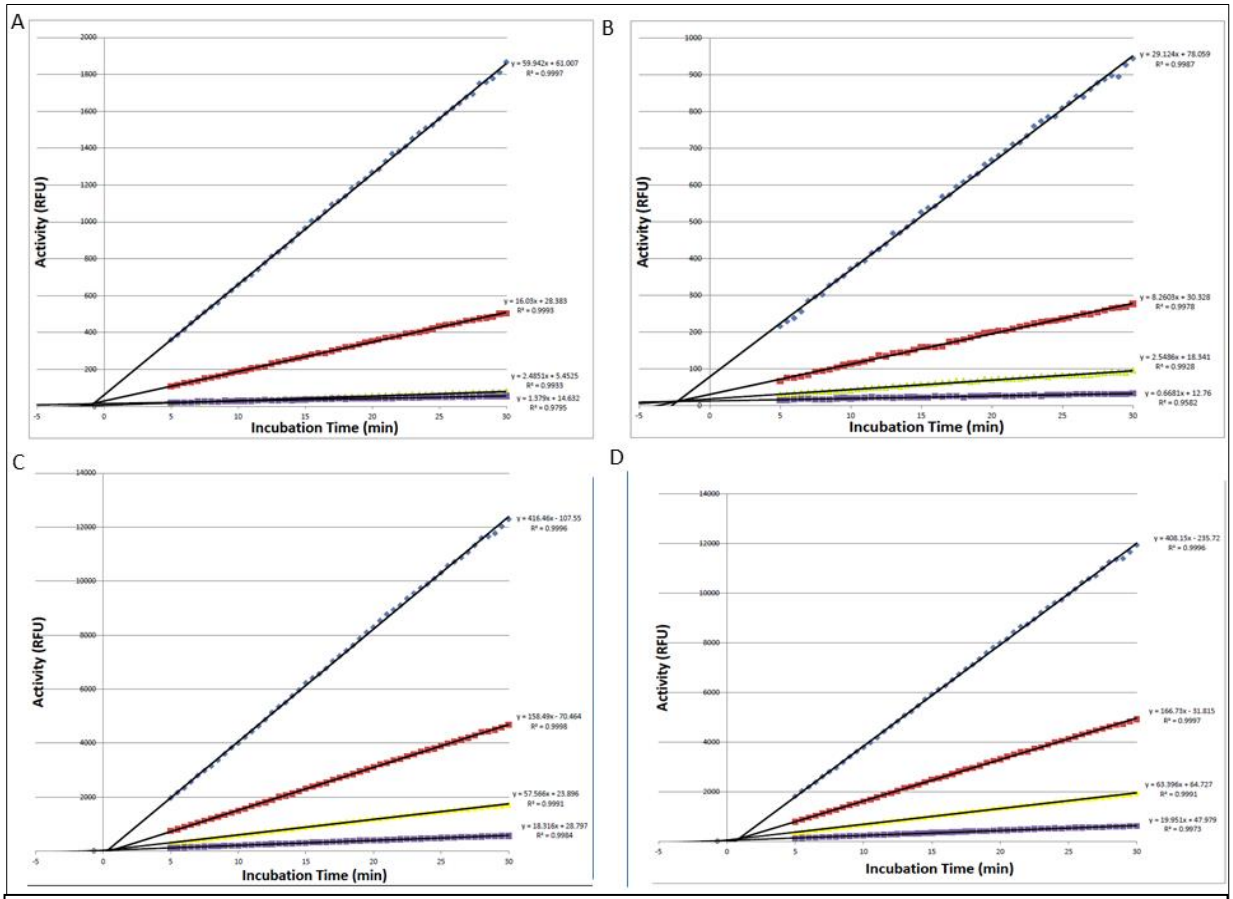

Time course for diethoxyfluorescein metabolism. Panel A: BENCYP6P9a; panel B: MALCYP6P9a; panel C: MOZCYP6P9b and panel D: UGANCY6P9b. Blue line: 90pmol; red line: 30pmol; yellow line: 10pmol and purple lines: 3.33pmol.

APPENDIX 3.5

Summary of IC_{50} by time for insecticides with recombinant CYP6P9a and CYP6P9b

	Time (min)													
	6.0	**7.5**	**9.0**	**10.5**	**12.0**	**13.5**	**15.0**	**16.5**	**18.0**	**19.5**	**21.0**	**22.5**	**24.0**	**25.5**
MOZCYP6P9b														
Miconazole	0.028	0.025	0.023	0.022	0.022	0.021	0.021	0.020	0.020	0.021	0.022	0.021	0.023	0.024
Cypermethrin	0.080	0.089	0.093	0.100	0.110	0.110	0.140	0.150	0.160	0.180	0.190	0.20	0.230	0.270
Cyhalothrin	0.080	0.096	0.100	0.110	0.120	0.130	0.150	0.170	0.180	0.230	0.250	0.270	0.300	0.300
Chlorpyrifos	0.690	0.810	0.920	0.970	0.950	1.100	1.200	1.300	1.400	1.500	1.600	1.600	1.800	1.800
Bendiocarb	>25	>25	>25	>25	>25	>25	>25	>25	>25	>25	>25	>25	>25	>25
Bifenthrin	1.800	2.200	2.400	2.400	2.300	2.400	2.500	2.500	2.700	2.900	2.900	2.800	3.000	3.000
Etofenprox	0.360	0.460	0.560	0.600	0.670	0.720	0.750	0.760	0.830	0.920	0.970	1.000	1.100	1.100
Propoxur	>25	>25	>25	>25	>25	>25	>25	>25	>25	>25	>25	>25	>25	>25
Deltamethrin	0.065	0.079	0.090	0.100	0.120	0.130	0.150	0.170	0.190	0.210	0.230	0.240	0.280	0.300
4,4′-DDT	7.100	8.200	9.400	11.00	11.00	13.00	15.00	11.00	8.400	8.000	8.400	9.800	13.00	24.00
Permethrin	2.400	2.500	2.500	2.500	2.400	2.300	2.500	2.60	2.600	2.800	2.800	2.600	2.700	3.000
UGANCYP6P9b														
Miconazole	0.020	0.020	0.020	0.020	0.021	0.021	0.021	0.023	0.022	0.022	0.022	0.021	0.020	0.020
Cypermethrin	0.110	0.120	0.130	0.140	0.160	0.180	0.200	0.230	0.250	0.280	0.280	0.280	0.310	0.310
Cyhalothrin	0.120	0.130	0.140	0.160	0.170	0.180	0.200	0.220	0.220	0.240	0.250	0.250	0.260	0.260
Chlorpyrifos	1.100	1.200	1.200	1.200	1.300	1.400	1.700	1.800	2.000	2.000	2.100	2.100	2.000	2.200
Bendiocarb	>25	>25	>25	>25	>25	>25	>25	>25	>25	>25	>25	>25	>25	>25
Bifenthrin	3.200	3.100	2.400	2.500	2.800	3.000	4.000	4.000	3.800	3.700	3.900	3.900	4.100	3.900
Etofenprox	0.710	0.750	0.810	0.860	0.760	0.850	0.920	1.100	1.100	1.300	1.400	1.500	1.500	1.400
Propoxur	>25	>25	>25	>25	>25	>25	>25	>25	>25	>25	>25	>25	>25	>25
Deltamethrin	0.120	0.120	0.130	0.150	0.170	0.210	0.210	0.220	0.240	0.270	0.290	0.270	0.280	0.290
4,4′-DDT	>25	>25	>25	>25	>25	>25	>25	>25	>25	>25	>25	>25	>25	>25
Permethrin	3.000	3.000	2.800	2.700	2.800	3.000	3.000	3.100	3.100	3.000	3.000	3.200	3.400	3.600
MALCYP6P9a														
Miconazole	0.013	0.021	0.013	0.023	0.029	0.011	0.026	0.013	0.025	0.022	0.017	0.018	0.013	0.016
Cypermethrin	0.024	0.066	0.140	0.110	0.140	0.150	0.190	0.160	0.091	0.160	0.170	0.130	0.280	0.330
Cyhalothrin	0.087	0.140	0.160	0.097	0.130	0.360	0.550	0.460	0.270	0.170	0.150	0.240	0.350	0.410
Chlorpyrifos	0.670	0.250	1.600	3.700	4.400	1.500	2.700	1.700	2.500	3.600	2.200	1.700	1.200	3.000
Bendiocarb	>25	>25	>25	>25	>25	>25	>25	>25	>25	>25	>25	>25	>25	>25

Bifenthrin	0.230	0.320	0.820	1.500	2.100	1.300	2.000	1.300	1.800	1.200	1.700	0.490	1.000	1.600
Etofenprox	0.330	0.420	0.660	1.400	1.200	1.700	2.300	2.500	3.000	2.700	2.000	1.600	0.800	2.500
Propoxur	>25	>25	>25	>25	>25	>25	>25	>25	>25	>25	>25	>25	>25	>25
Deltamethrin	0.05	0.040	0.063	0.099	0.140	0.380	0.520	0.880	1.000	1.100	0.680	0.400	0.310	0.210
4,4'-DDT	0.450	2.500	>25	>25	>25	>25	>25	>25	20.00	6.600	6.800	8.700	9.300	>25
Permethrin	2.200	2.800	3.800	6.700	4.200	4.000	5.800	4.900	7.400	3.600	6.800	4.200	4.000	4.600
BENCYP6P9a														
Miconazole	0.023	0.024	0.021	0.021	0.019	0.023	0.022	0.024	0.024	0.024	0.029	0.026	0.023	0.029
Cypermethrin	0.064	0.099	0.130	0.140	0.150	0.160	0.160	0.130	0.180	0.210	0.230	0.260	0.270	0.330
Cyhalothrin	0.097	0.110	0.150	0.160	0.160	0.150	0.160	0.230	0.280	0.320	0.320	0.290	0.220	0.230
Chlorpyrifos	1.400	1.700	2.100	2.300	2.100	2.300	3.800	3.800	3.800	3.500	3.600	3.100	2.500	3.100
Bendiocarb	>25	>25	>25	>25	>25	>25	>25	>25	>25	>25	>25	>25	>25	>25
Bifenthrin	1.200	2.000	2.000	2.000	2.400	2.300	3.900	3.600	4.400	3.600	3.500	3.700	3.000	3.500
Etofenprox	0.850	1.100	1.300	1.500	1.900	2.400	2.500	2.700	3.000	3.000	2.500	2.200	2.300	2.300
Propoxur	>25	>25	>25	>25	>25	>25	>25	>25	>25	>25	>25	>25	>25	>25
Deltamethrin	0.085	0.130	0.180	0.230	0.290	0.380	0.470	0.530	0.670	0.530	0.360	0.460	0.380	0.430
4,4'-DDT	0.540	0.650	0.800	0.830	1.200	5.900	10.00	7.100	4.700	3.700	23.00	14.00	15.00	22.00
Permethrin	3.100	4.200	4.700	4.100	3.500	3.400	3.600	3.400	3.700	5.000	4.500	3.800	4.500	4.900

APPENDIX 3.6

Kinetic Parameters of CYP6P9b Mutants Recombinant Proteins With DEF and Pyrethroids

(A):

Table 1: Kinetic Constants for mutant CYP6P9b-mediated metabolism of DEF

Recombinant Proteins	K_{cat} (min^{-1})	K_M (µM)	K_{cat}/K_M (min^{-1} $µM^{-1}$)
Val^{109}IleCYP6P9b	7.32±0.13***	0.10±0.007	72.47±5.18$^{\$\$}$
Asp^{335}GluCYP6P9b	21.82±3.13**	0.23±0.10†	94.86±43.43$^{\$\$}$
Asn^{384}SerCYP6P9b	5.46±0.32***	0.10±0.023	54.05±12.71$^{\$\$}$
Pro^{401}AlaCYP6P9b	88.32±7.57	0.25±0.07†	353.28±103.44$^{\$}$
MOZCYP6P9b	103.4±5.86	0.13±0.003	820.63±49.72

Values are as mean ± S.E.M. of three independent replicates
Apparent K_{cat} given as disappearance of pmol DEF/min/pmol P450. Catalytic efficiency was calculated as K_{cat}/K_M
** and *** statistically significant K_{cat} values at p<0.01 and p<0.001 respectively compared with MOZCYP6P9b
$^{\$}$ and $^{\$\$}$ statistically significant K_{cat} values at p<0.05 and p<0.01 respectively compared with MOZCYP6P9b

(B):

Table 2: Percentage depletion of pyrethroid insecticides by mutant CYP6P9b recombinant proteins

Recombinant Proteins	Deltamethrin	Permethrin
Val^{109}IleCYP6P9b	17.88±1.00**	46.03±1.43*
Asp^{335}GluCYP6P9b	4.15±1.41***	35.65±1.55*
Asn^{384}SerCYP6P9b	18.15±0.42**	18.33±0.63**
Pro^{401}AlaCYP6P9b	81.25±0.17	80.45±0.28
MOZCYP6P9b	92.04±0.34	82.59±3.15

Values are mean ± S.D. of three replicates compared with negative control (-NADPH);
* and ** and ***Significantly different from FANGCYP6P9a or FANGCYP6Pb at p<0.05, p<0.01 or p<0.001, respectively.

(C) Table 3: Kinetic constants for mutant CYP6P9b-mediated permethrin metabolism

Recombinant Proteins	K_{cat} (min^{-1})	K_M (µM)	K_{cat}/K_M (min^{-1} $µM^{-1}$)
Val^{109}Ile_CYP6P9b	1.35±0.57**	20.5±1.35†	0.06±0.03$^{\$\$\$}$
Asp^{335}Glu_CYP6P9b	0.98±0.12***	5.19±1.89†	0.19±0.07$^{\$\$}$
Asn^{384}Ser_CYP6P9b	0.87±0.08***	17.85±0.87†	0.04±0.005$^{\$\$\$}$
Pro^{401}Ala_CYP6P9b	4.21±0.96*	15.38±6.50	0.27±0.13$^{\$}$
MOZCYP6P9b(Wild Type)	7.902±0.83	10.33±2.38	0.76±0.19

Values are as mean ± S.E.M. of three independent replicates. Significantly different from negative control (-NADPH).
*, ** and *** K_{cat} significantly different from MOZCYP6P9b at p<0.05, 0.01 and 0.001, respectively.
$^{\dagger}K_M$ significantly different from MOZCYP6P9b at p<0.05.
$^{\$}$, $^{\$\$}$ and $^{\$\$\$}$ Catalytic efficiency significantly different from MOZCYP6P9b at p<0.05, 0.01 and 0.001, respectively.

APPENDIX 4.1

Kinetic Constants of Recombinant P450s CYP6M7, CYP6Z1, CYP9J11 and CYP6AA4 With Pyrethroids, Bendiocarb and DDT

A. Kinetic Constants for Recombinant CYP6M7, CYP6Z1, CYP9J11 and CYP6AA4 Metabolism of Permethrin and Deltamethrin

Recombinant Proteins	K_{cat} (min^{-1})	K_M (μM)	K_{cat}/K_M (min^{-1} μM^{-1})
		Permethrin	
CYP6M7	6.06±0.24	13.81±7.08	0.45±0.03
CYP6Z1	1.90±0.08	4.37±0.62	0.44±0.06
CYP9J11	5.39±0.69	31.04±5.79	0.17±0.04
CYP6AA4	11.99±2.17	33.62±9.18	0.36±0.12
		Deltamethrin	
CYP6M7	7.04±0.24	19.64±10.65	0.36±0.04
CYP6Z1	1.74±0.07	2.89±0.52	0.60±0.11
CYP9J11	1.94±0.45	6.08±2.01	0.32±0.13
CYP6AA4	15.65±2.64	30.01±7.92	0.52±0.16

Values are mean ±S.D. of three replicates

Apparent K_{cat} was calculated as pmol/min/pmol P450; Catalytic efficiency was calculated as K_{cat}/K_M

B. Kinetic Constants for Recombinant CYP6Z1 and CYP9J11 Metabolism of Bendiocarb and DDT

Recombinant Proteins	*Vmax* (min^{-1})	K_{half} (μM)	*h*	$Vmax/K_{half}$ (min^{-1} μM^{-1})
		Bendiocarb		
CYP6Z1	0.46±0.009	6.22±0.17	5.82	0.074±0.0025
CYP9J11	0.53±0.044	8.30±0.83	2.29	0.06±0.0084
		DDT		
CYP6Z1	101.7±25.5	13.38±2.99	2.60	7.60±2.55

C. Kinetic Constants for Recombinant CYP6Z1 Metabolism of DEF, RBE and RME

Recombinant Proteins	K_{cat} (min^{-1})	K_M (μM)	K_{cat}/K_M (min^{-1} μM^{-1})
Diethoxyfluorescein (DEF)	390.3±21.21	0.13±0.03	2983.94±630.32
Resorufin benzylether (RBE)	980.2±32.27	1.99±0.11	491.57±32.43
Resorufin methylether (RME)	395.7±19.90	0.19±0.03	2056.65±367.63

APPENDIX 4.2

Binding parameters of the productive mode of permethrin, deltamethrin and bendiocarb docked to the active sites of CYP6Z1 model

	Rank	ChemScore (kJ/mol)	ΔG (kJ/mol)	S(hbond)	S(metal)	S(lipo)	ΔE(clash)
Permethrin	2nd	39.19	-41.12	1.00	0.00	307.87	0.22
Deltamethrin	3rd	36.14	-37.15	0.97	0.00	278.77	0.01
Bendiocarb	1st	24.69	-24.32	1.93	0.00	135.46	0.07
DDT	1st	36.81	-38.01	0.00	0.00	299.93	0.91

APPENDIX 5.0

List of publications produced from this study and/or during research activities, and manuscripts in preparation

1. Sulaiman S. Ibrahim, Jacob M. Riveron, Bibby Jaclyn, Helen Irving, Mark J.I. Paine, and Charles S. Wondji. **Allelic variation of cytochrome P450 genes drives the resistance to bednet insecticides in a major African malaria vector.** 2015. (Manuscript in preparation).
2. Kayla G. Barnes, Sulaiman S. Ibrahim, Jacob Riveron, Helen Irving, Martin Chiumia, Barnett Mbewe , Themba Mzihalowa' Mike Coleman, Janet Hemingway and Charles S. Wondji. **The Cytochrome P450 gene CYP6AA4 confers pyrethroid resistance in the Malaria vector *Anopheles funestus* amidst a South/North shift in the role of key resistance genes across Malawi.** 2015. (Manuscript in preparation).
3. Sulaiman S. Ibrahim., Yayo A. Manu., Zainab Tukur., Helen Irving and Charles S. Wondji. **High frequency of *kdr* L1014F is associated with pyrethroid resistance in *Anopheles coluzzii* in Sudan savannah of northern Nigeria.** *BMC Infectious Diseases* 2014, **14**:441.
4. Jacob M Riveron†, Sulaiman S Ibrahim†, Emmanuel Chanda, Themba Mzilahowa, Nelson Cuamba, Helen Irving, Kayla G Barnes, Miranda Ndula and Charles S Wondji. **The highly polymorphic *CYP6M7* cytochrome P450 gene partners with the directionally selected *CYP6P9a* and *CYP6P9b* genes to expand the pyrethroid resistance front in the malaria vector *Anopheles funestus* in Africa**. *BMC Genomics* 2014, **15**:817. † equal contribution authors.
5. Jacob M Riveron, Cristina Yunta, Sulaiman S Ibrahim, Rousseau Djouaka, Helen Irving, Benjamin Menze, Hanafy M Ismail, Janet Hemingway, Hilary Ranson, Armando Albert and Charles S Wondji. **A single mutation in the *GSTe2* gene allows for tracking of metabolically based insecticide resistance in a major malaria vector.** *Genome Biology* 2014, **15**:R27.
6. Charles Mulamba, Jacob M. Riveron, Sulaiman S. Ibrahim, Helen Irving, Kayla G. Barnes, Louis G. Mukwaya, Josephine Birungi and Charles S. Wondji. **Widespread pyrethroid and DDT**

resistance in the major malaria vector Anopheles funestus in East Africa is driven by metabolic resistance mechanisms. *PLoS ONE*, **9**(10):e110058.

7. Jacob M Riveron, Helen Irving, Miranda Ndula, Kayla G Barnes, Sulaiman S Ibrahim, Mark J.I. Paine, and Charles S. Wondji. **Directionally selected P450 alleles are driving the spread of pyrethroid resistance in the major malaria vector *Anopheles funestus*.** *PNAS*, 2013. **110** (1): 252-257.
8. H Irving, JM Riveron, SS Ibrahim, NF Lobo and CS Wondji. **Positional cloning of *rp2* QTL associates the P450 genes *CYP6Z1*, *CYP6Z3* and *CYP6M7* with pyrethroid resistance in the malaria vector *Anopheles funestus*.** *Heredity,* 2012. 1-10.